

Synthetic Coelenterazine Derivatives  
for Bioluminescent Imaging

August 2017

NISHIHARA, Ryo

A Thesis for the Degree of Ph.D. in Engineering

Synthetic Coelenterazine Derivatives  
for Bioluminescent Imaging

August 2017

Graduate School of Science and Technology

Keio University

NISHIHARA, Ryo

## Table of Contents

Chapter 1 General introduction	1
1.1. Molecular imaging	1
1.2. Bioluminescence	1
1.3. Are bioluminescent reporter proteins applicable to highly sensitive imaging techniques?	2
1.4. Typical bioluminescent reporter	3
1.5. Bright bioluminescent system derived from nature	4
1.6. Typical applications of coelenterazine-utilizing luciferase	6
1.7. Objective of this research	8
References	11
Chapter 2 Fabrication of Blue-shifted Coelenterazine Derivatives for Bioluminescent Applications	13
2.1. Introduction	14
2.2. Experimental section	16
2.2.1. Materials and instruments	16
2.2.2. Synthesis of CTZ derivatives	17
2.2.3. Chemiluminescence assays	25
2.2.4. pH-Dependent chemiluminescence	25
2.2.5. Bioluminescence assay	25
2.2.6. Bioluminescence intensities	26
2.2.7. Kinetic profiles of bioluminescence	26
2.2.8. Bioluminescence spectra	26
2.2.9. Solubility test of DeepBlueC <sup>TM</sup> and 6-pi-Ph-CTZ	26
2.3. Results and discussion	27
2.3.1. Development of C-6 modified CTZ derivatives	27
2.3.2. Comparison of bioluminescence properties	35
2.3.3. Summary of luminescence properties	37
2.4. Conclusions	37
2.5. Appendix	38
2.5.1. pH-Dependent chemiluminescence	38
2.5.2. pH-Dependent bioluminescence with several marine luciferases	39
References	42

Chapter 3 Luciferase-Specific Coelenterazine Analogues for Optical Contamination-Free Bioassays	45
3.1. Introduction	46
3.2. Experimental section	47
3.2.1. Design and synthesis of luciferase-specific novel CTZ analogues	47
3.2.2. Luciferase specificity of newly synthesized CTZ analogues	61
3.2.3. Luciferase-selective property of CTZ analogues in lysates and living mammalian cells	64
3.2.4. Highly specific illumination of hormonal activities of a ligand with mixed single-chain probes emitting almost superimposed optical spectra	64
3.2.5. pH-Driven optical specificity of CTZ analogues to marine luciferases	66
3.3. Results	67
3.3.1. Structural analysis on the marine luciferase-luciferin interactions	67
3.3.2. Determination of luciferase specificity of newly synthesized CTZ analogues	68
3.3.3. Evaluation of the spectral overlaps among marine and beetle luciferases	73
3.3.4. Multiplex assays system for specific illumination of hormonal activities of steroid hormones	74
3.3.5. Prolonged bioluminescence stability of CTZ analogues in living mammalian cells	75
3.3.6. The CTZ analogues exert distinctive luciferase selectivity according to pH ranges	77
3.4. Discussion	80
3.5. Conclusions	83
3.6. Appendix	84
3.6.1. Discussion on the pH-driven optical intensities of CTZ analogues	84
3.6.2. Characteristics of molecular strain probe (TP2.4)	85
3.6.3. Effects of molecular tension on bioluminescent kinetic profile	88
References	89
 Chapter 4 Fabrication of a New Lineage of Artificial Luciferase from Databases	 91
4.1. Introduction	92
4.2. Experimental section	93
4.2.1. Artificial design of a new lineage of Alucs by extracting frequently occurring amino acids from the alignment of copepod luciferases	93
4.2.2. Synthesis of cDNA constructs encoding the new lineage of artificial luciferases	94
4.2.3. Determination of the sequential identity ranking and phylogenetic trees	95

of the new lineage of artificial luciferases	
4.2.4. Determination of the absolute optical intensities of the new ALucs and comparison with conventional luciferases	95
4.2.5. Substrate specificity of the new lineage of ALucs	96
4.2.6. Live cell bioluminescence imaging with marine luciferases	97
4.2.7. Determination of photon fluxes	97
4.2.8. Construction of single-chain bioluminescent probes with ALucs	100
4.3. Results	101
4.3.1. Artificial luciferases can be fabricated by extracting frequently occurring amino acids from the alignment of copepod luciferases	101
4.3.2. ALuc40s survive in mammalian cells and emit strong bioluminescence	102
4.3.3. The C-terminal end of ALuc41 dominates the optical intensities	103
4.3.4. The new lineage of ALucs shows unique substrate selectivity without significant colorshifts in the spectra	104
4.3.5. Live cell bioluminescence imaging with conventional and newly established ALucs	106
4.3.6. Determination of the overall photon fluxes	108
4.3.7. Molecular tension probes	109
4.4. Discussion	110
4.5. Conclusions	111
References	112
Chapter 5 Blue Coelenterazine Derivatives for Highly Sensitive Bioluminescence Imaging	115
5.1. Introduction	116
5.2. Experimental section	117
5.2.1. Synthesis of novel CTZ derivatives	117
5.2.2. Chemiluminescence assay	140
5.2.3. Initial bioluminescence intensities in cell lysate	140
5.2.4. Kinetic profiles in combination with RLuc8.6-535	140
5.2.5. Molecular dynamic simulations for free energy calculations of ligand binding	141
5.2.6. Bioluminescence spectra in cell lysate	143
5.2.7. Bioluminescence intensities in living cells	143
5.2.8. Cell membrane permeability assay of luciferins	144
5.2.9. Bioluminescence single cell imaging	144
5.2.10. Bioluminescence <i>in vivo</i> imaging	144
5.3. Results and discussion	145
5.3.1. Design of novel alkylated CTZ derivatives	145

5.3.2. Chemiluminescence assays	148
5.3.3. Initial bioluminescence intensities	150
5.3.4. Bioluminescence kinetic profiles with RLuc8.6-535	155
5.3.5. Luminescence spectra of CTZ derivatives	157
5.3.6. Docking simulation study	160
5.3.7. Bioluminescence intensities in living mammalian cells	165
5.3.8. Novel CTZ derivatives for highly sensitive bioluminescence imaging	168
5.3.8.1. Single cell imaging	168
5.3.8.2. <i>in vivo</i> imaging of cancer cells	168
5.4. Conclusions	171
References	172
Chapter 6 Fabrication of Red-shifted Coelenterazine Analogues for Bioluminescent Applications	177
6.1. Introduction	178
6.2. Experimental section	181
6.2.1. Synthesis of novel CTZ derivatives	181
6.2.2. Determination of relative bioluminescence intensities of dye-bridged CTZ analogues with existing marine luciferases	188
6.2.3. Determination of the optical spectra of azide-bridged CTZ analogues	190
6.2.4. Fabrication of new ALucs for selected CTZ analogues	190
6.2.5. Relative bioluminescence intensity matrix of selected CTZ analogues with new Aluc variants	192
6.2.6. Cell-based assays on the basis of the new ALuc-luciferin systems	193
6.2.7. Measurement of the BRET and CRET spectra of azide- or dye-bridged CTZ analogues	193
6.2.8. Plasmid-driven optical intensity and stability of selected CTZ analogues with ALuc30	195
6.3. Results and discussion	195
6.3.1. Azide-bridged CTZ analogues showed greatly improved optical intensities and red-shifted bioluminescence spectra	196
6.3.2. Selected coelenterazine analogues showed unique luciferase preference	199
6.3.3. 6-N3-CTZ selectively luminesces with ALuc26 in living mammalian cells	202
6.3.4. CRET and BRET spectra of dye-bridged CTZ analogues	203
6.3.5. Expression vector-driven optical intensity and stabilities of ALuc30	206
6.4. Conclusions	207

6.5. Appendix	208
6.5.1. BL investigation of C-2 or C-6 modified CTZ analogues with RLuc8.6-535	208
References	209
Chapter 7 General conclusions and perspective	213
List of publications	217
Acknowledgement	218

## Chapter 1

### General Introduction

#### 1.1 Molecular imaging

Molecular imaging techniques are utilized as methods for visualization and quantification of complicated *in vivo* cellular processes to accelerate the understanding of life phenomena in living subjects. Until present, several molecular imaging techniques have been developed (e.g. positron emission tomography (PET), single photon emission computed tomography (SPECT), magnetic resonance imaging (MRI) and computed tomography (CT) imaging). Nowadays, novel luminescence imaging techniques based on fluorescence (FL) and bioluminescence (BL) are getting a lot of attention, because of their inexpensiveness and relatively easy operation<sup>1</sup>.

#### 1.2 Bioluminescence

Bioluminescence is an attractive emitted light from luminous organisms. The luminous phenomenon is triggered by an enzymatic oxidation reaction involving a bioluminescent substrate (luciferin) and an enzyme (luciferase) (Figure 1-1). The light from luminous creatures is so-called “cold light”, because the luciferase maintains and fixes the chemical conformation of its luciferin in the excited state to reduce energy loss via heat. Recently, many researchers have paid attention to these highly efficient luminescent systems as bioanalytical sensors for various applications<sup>2-4</sup>.

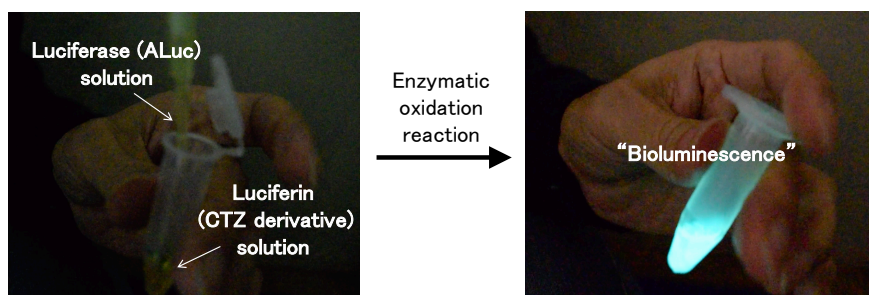


**Figure 1-1** Bioluminescence from synthetic novel luciferin derivative (6-N3-CTZ: Chapter6) and artificial luciferase. Bioluminescence emission is easily obtained by mixing luciferin and luciferase solution in the presence of oxygen. (These pictures were taken by the author with an iPhone4s)

### **1.3 Are bioluminescent reporter proteins applicable to highly sensitive imaging techniques?**

Luminescent proteins such as green fluorescence protein (GFP)<sup>5</sup> identified by Dr. Osamu Shimomura are widely used for optical readout in the life science field and involved in even the recent development of iPS cells<sup>6</sup>. Therefore, the development of novel optical imaging tools is of high interest to scientists in many (bio)chemistry-oriented fields, such as chemical biology, cell biology and others.

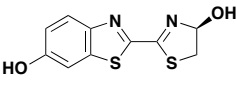
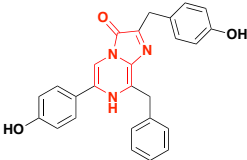
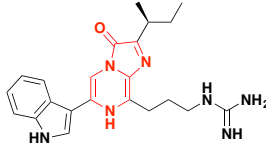
Recently, compared to fluorescence (FL), bioluminescence (BL) is considered a better optical readout method in bioassays by virtue of its sensitivity and non-invasiveness, because the luminescence phenomenon occurs through an enzymatic reaction with no interference from excitation light. As a result, BL-based optical imaging provides significant advantages of high signal-to-noise (S/N) ratio arising as a consequence of lower background signal and wider dynamic measurement range<sup>7</sup>. However, because the lower turn-over number of bioluminescent protein luciferases range from 10/min for firefly luciferase (photinus) to 111/min for *renilla reniformis* luciferase<sup>8</sup>, the BL signals obtained from luciferases inside living cells were extremely low compared to FL imaging. For example, according to a previous publication, the versatile bioluminescent reporter protein, RLuc8, can generate only  $1/10^3$  of the power density of light emission required for FL imaging<sup>8</sup>. For that reason,

more sensitive signal readers, CCD cameras (high quantum efficiency), are increasingly being utilized as imaging equipment for BL imaging, which extends the possible application of BL proteins in the field of life science<sup>9</sup>. Therefore, many researchers are eager to develop artificial BL probes with high quantum yield or to discover novel BL systems for highly sensitive BL imaging and assembled BL-based assays (e.g. protein-protein interaction imaging, reporter gene assay and optical imaging of tumors in living animal etc.)<sup>10</sup>

## 1.4 Typical bioluminescent reporter

Although approximately 30 BL systems were confirmed in nature so far<sup>10</sup>, the chemical structure of natural luciferins is identified only in 9 species. Among those, several luciferins were applied in bioanalytical methods. The typical bioluminescent reporters are summarized as follows.

**Table 1-1** Typical luciferin-luciferase systems utilized in BL imaging. The chemical structure of the imidazopyrazinone backbone is highlighted in red<sup>3,11</sup>.

	D-Luciferin	Coelenterazine	<i>Cypridina</i> Luciferin	Furimazine
Bioluminescent substrate				
Luciferase	Firefly (FLuc) Click beetle	<i>Renilla</i> (RLuc) <i>Gaussia</i> (GLuc) Artificial (ALuc)	<i>Cypridina</i> (CLuc)	<i>Gaussia gracilirostris</i> (NanoLuc)
Wavelength	560 nm	480-500 nm	465 nm	460 nm
Co-factor	ATP, Mg <sup>2+</sup> , O <sub>2</sub>	O <sub>2</sub>	O <sub>2</sub>	O <sub>2</sub>

D-Luciferin, which emits light at a relatively long wavelength ( $\lambda_{\max}$ =560 nm) in the presence of Mg<sup>2+</sup> and ATP as cofactors, is widely used in bioassays. Especially the relatively longer emission wavelength enables the application of D-luciferin-utilizing luciferase for *in vivo* imaging. However, the cofactors potentially lead to

complex assay protocols in bioanalysis and the use of the D-luciferin-luciferase pair is confined to the observation of intracellular processes. In contrast, marine luciferases such as *Renilla* luciferase (RLuc) and *Gaussia* luciferase (GLuc) generate cofactor-free bioluminescence with native coelenterazine (nCTZ), which enable monitoring intracellular and extracellular life phenomena such as exocytosis in synaptic bouton<sup>12</sup>. Interestingly, most of the investigated marine luciferases catalyze luciferins having an imidazopyrazinone backbone, resulting in oxygen dependent luminescence. However, the BL quantum yield of firefly luciferase (FLuc) (0.4)<sup>13</sup> is still larger than of marine luciferases. Therefore, to improve brightness, some novel synthesized marine luciferases with improved light output intensity such as NanoLuc in combination with furimazine as luciferin have recently been developed<sup>11</sup>, which show approximately 150-fold stronger optical signals than FLuc in a particular assay condition, because of their relative high turn-over number.

In general, a luciferase oxidizes its specific luciferin, thereby most of the chemical modifications of luciferin prevent enzymatic recognition. But, taking NanoLuc as an example, the optimization of the luciferin structure for its artificial luciferase may lead to the development of high brightness BL systems.

## 1.5 Bright bioluminescent system derived from nature

In nature, *Aqueous Victoria* jelly fish and sea pansy *Renilla reniformis* brighten their respective green fluorescent protein (GFP) via the phenomenon of bioluminescence resonance energy transfer (BRET). As shown in Figure 1-2, in the presence of *Renilla* GFP, a radiationless energy transfer from RLuc to *Renilla* GFP is occurred, resulting in 3-fold increased light output<sup>8</sup>. The increased emission is due to the high fluorescence quantum yield of *Renilla* GFP (0.3), which is significantly larger than that of the RLuc bioluminescent system (0.05)<sup>14</sup>. In addition, using the BRET mechanism<sup>14</sup>, not only the increased quantum yields, but red-shift of the emission are promising perspectives.

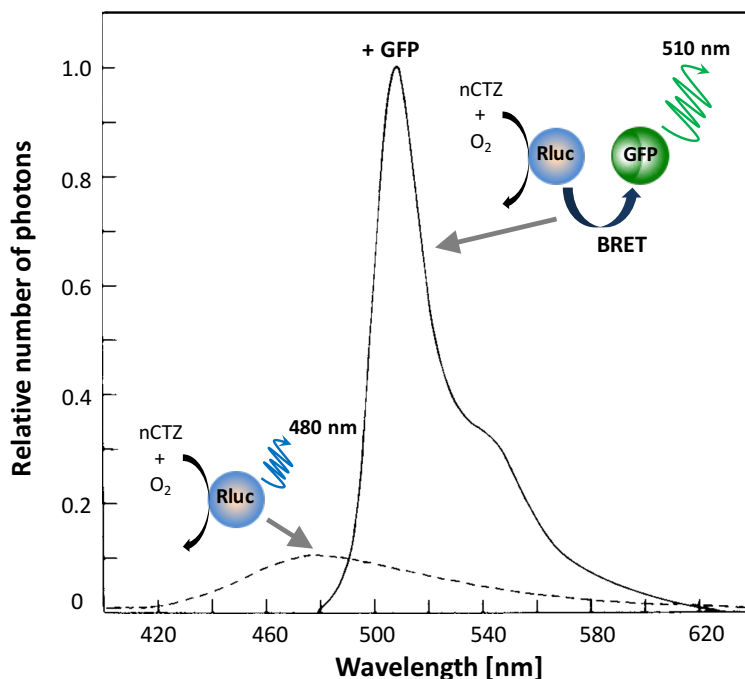


**Figure 1-2** Bioluminescence spectra of CTZ with RLuc in the absence and presence of 1 eq. *Renilla* GFP.

According to the results of an intermolecular BRET study (Figure 1-2), an efficient intramolecular BRET protein consisting of EYFP and RLuc (BAF-Y) has been developed<sup>15</sup>. Fabrication of BRET proteins having a luciferase and a fluorescent protein connected by an appropriate amino acid linker is a quite an efficient strategy towards high energy transfer efficiency and quantum yield, because the linker maintains the BRET-permissive distance between the two proteins and has little effect on BL kinetic profiles of the luciferase moiety. In addition, by fusion of a bright RLuc mutant and a yellow fluorescent protein (YFP) (QY = 0.57), real-time monitoring of intracellular structures in mammalian cells and tumor detection in a living mouse with high resolution was recently achieved and named Nano-lantern<sup>8</sup>. More recently, the extension of color variants by using other fluorescent proteins as BRET acceptor was also achieved by the same research group (Figure 1-3)<sup>16</sup>.

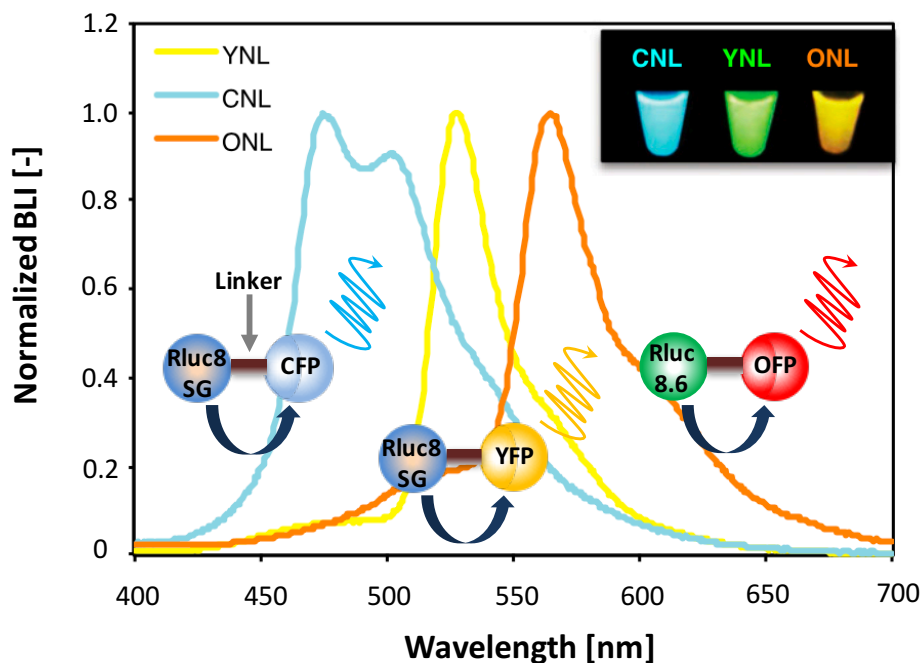


**Figure 1-3** Bioluminescence spectra of multicolor Nano-lanterns

## 1.6 Typical applications of coelenterazine-utilizing luciferase

Proteins fill most of the mass of a cell and play a predominant part in most biological processes.<sup>16</sup> Optical imaging of protein–protein interactions (PPIs) facilitates comprehensive elucidation of intracellular molecular events.<sup>17</sup> To date, PPIs have been visualized with various strategies using fluorescent proteins and luciferases, which include bioluminescence resonance energy transfer (BRET) (Figure 1-4(A)),<sup>15</sup> and protein complementation assay (PCA) (Figure 1-4(B)).<sup>18,19</sup>

One of the reported CTZ derivatives, DeepBlueC<sup>TM</sup> is used as a donor BL luciferin in BRET-based PPI studies with green fluorescent protein (GFP<sup>2</sup>) as the acceptor, because its emission peak at around 400 nm minimally interferes with the emission (510 nm) of the GFP<sup>2</sup> acceptor<sup>10</sup>. Although the large spectral gap between the emissions of donor and acceptor improves the sensitivity of analysis, the BLI of DeepBlueC<sup>TM</sup> is negligibly low compared to that of native-CTZ, because of its structural modification<sup>20</sup>.

PCA is an emerging technology for determining the occurrence of PPIs in mammalian cell lines, where a

monomeric luciferase is split into two fragments (C-terminal and N-terminal fragments) for a temporal loss and conditional reconstitution of the activities only upon PPI.<sup>21,22</sup> To date, many luciferases including FLuc,<sup>18,19</sup> RLuc,<sup>23</sup> and artificial luciferase (ALuc)<sup>24</sup> have been utilized for PCA. However, this methodology requires a complex probe design and a tedious optimization process for seeking a suitable dissection site and restores merely 0.5–5% of the original optical intensity after complementation.<sup>19,25</sup> The sophisticated molecular design limits the general applicability of an optimized PPI model to other bioassays.

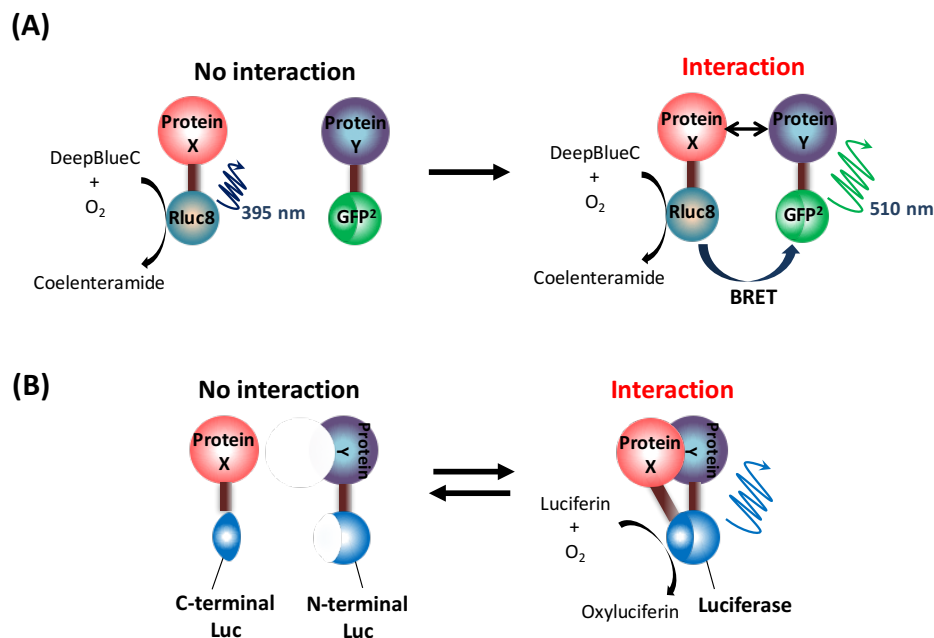


**Figure 1-4** Protein-protein interactions (PPIs) analysis based on (A) BRET and (B) PCA

Kim introduced a unique strategy for illuminating PPIs called “molecular strain probes”, where a full-length RLuc8 or ALuc23 was sandwiched between two proteins of interest.<sup>26</sup> The full-length luciferases in the strain probe allow greater absolute bioluminescence than split-luciferases in PCAs. Although the basic concept of a molecular strain probe is unique and broadly applicable for bioluminescence imaging (BLI) and PPI, no follow-up studies have been elucidated to date. We hypothesized that a full-length luciferase basically has the ability to vary its enzymatic activity even by molecular tension physically induced by PPIs, besides conventionally

recited factors such as ions, temperature, and pH. Therefore, (i) luciferases may have the intrinsic nature to modulate their enzymatic activity in response to molecular tension induced by PPIs although the extent of optical variation might be trivial, and (ii) the sensitivity of the probes to molecular tension is dominated by the molecular designs including the flexible region of the luciferase and the length of the flexible linkers.

For these reason, beetle luciferases such as FLuc were excluded in this evaluation because they are said to be generally darker than marine luciferases and comprise a long flexible region, naturally easing molecular tension.<sup>13,14</sup>

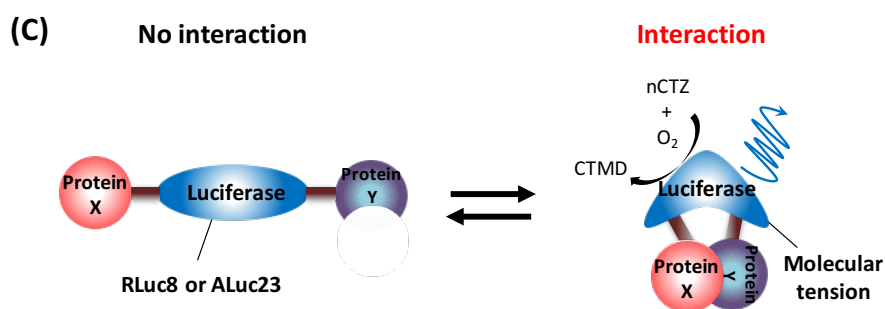


Figure 1-5 Protein-protein interactions (PPIs) analysis based on molecular strain probe

## 1.7 Objective of this research

BL applied to imaging techniques commonly has the drawbacks of poor optical emission intensity and limited emission color variety, especially when it comes to the near-infrared (NIR) spectral region (600-900 nm) favorable for *in vivo* imaging.

To address these drawbacks, this research work tackled the development of novel bioluminescent luciferins based on the coelenterazine (CTZ) structure and engineered variants of luciferases.

However, the modification of bioluminescent substrate and enzyme is quite difficult due to 1) the fact that the enzymatic recognition mechanism of CTZ from marine luciferases is unknown because of no existing x-ray crystal structure of *renilla* luciferase (RLuc) including its substrate, CTZ; 2) the high substrate specificity of

marine luciferases; and 3) little to no homology with other bioluminescent luciferases.

This dissertation is mainly divided into 4 chapters and each research objective differs in the type of chemical modification of CTZ derivatives. The research abstract of each chapter is mentioned below.

**Chapter 2:** I demonstrate for the first time that an extension of the imidazopyrazinone core of native coelenterazine (CTZ) by comparably large substituents can result in *renilla* luciferase (RLuc) variant substrates with significant bioluminescence emission. CTZ in combination with RLuc has gained significant attention in bioluminescence-based assays, since in contrast to the firefly luciferin/luciferase combination, it does not require the presence of co-factors, which potentially lead to complex assay protocols. Unfortunately, however, the bioluminescence intensities of CTZs are commonly lower compared to other bioluminescent systems. For this purpose, there is a high interest in the development of new CTZ derivatives. While a number of such compounds has been presented in previously, only few of them show significant levels of bioluminescence emission. In particular, reports on the derivatization of CTZ by the introduction of substituents at the C-6 position of the imidazopyrazinone core are rare. They have been mostly out of focus, since C-6 substitution has been considered as detrimental to enzyme recognition. In this chapter, I introduce the creation of efficient C-6 modified CTZ derivatives optimized for RLuc and its derivatives, which is the most widely used marine luciferase.

**Chapters 3 and 4:** Bioluminescence is a popular technique used in reporter assays for gene expression, and labeling of cells or proteins in order to track biological mechanisms or metastasis *in vivo*. However, the emission spectra of luciferases are broad and overlap, preventing optical readouts of multiple luciferases due to optical contamination or spectral overlap. Therefore, there is great interest in developing luciferase-specific coelenterazine analogues for use in high-throughput bioassays requiring multiple optical readouts (e.g. multiple

luciferases in the reaction mixture). This chapter introduces the first ever luciferase RLuc8.6-535- or artificial luciferase (ALuc)-specific CTZ derivatives. This allows overcoming a general disadvantage of known luciferases, which emission spectra are broad and overlap, preventing optical readouts of multiple luciferases. Furthermore, in Chapter 4, I describe a new lineage of artificial luciferases (ALucs) with unique optical properties for bioassays and molecular imaging.

**Chapter 5:** I successfully developed novel blue-shifted CTZ derivatives, wherein the (p-hydroxy)-phenyl group in the C-6 position was alkylated to investigate the flexibility and limitations of substitution at the C-6 position on enzyme recognition. With 50-fold stronger emission at comparable wavelength, C-6 alkylated CTZ derivatives are useful bright blue-shifted alternatives to commercially available blue-shifted derivative DeepBlueC<sup>TM</sup>, which enable single cell analysis with high-resolution and *in vivo* imaging of cancer cells in combination with NIR fluorescent protein (iRFP) fused RLuc8.6-535 variant.

**Chapter 6:** Ten novel fluorescent dye modified CTZ derivatives were successfully synthesized to expand the bioluminescent color palette. The aim of this molecular design is that 1) it does not inhibit the recognition by RLuc, because the fluorescent dye is connected at a position of CTZ not exposed to the enzyme recognition pocket; and 2) the energy from CTZ is transferred to dye moiety, which emits light due to the BRET mechanism. Furthermore, with the unique CTZ derivatives, I accomplished 1) improved optical intensity and sustainability; 2) a greatly biased luciferase specificity by bulkiness-driven steric hindrance; and/or 3) red-shifted emission by an intramolecular energy transfer mechanism (CRET and BRET).

## References

- (1) Smith, B. S. and Gambhir, S. S., *Chem. Rev.*, **2017**, *117*, 901-986.
- (2) Close, D. M., Xu, T., Sayler, G. S. and Ripp S., *Sensors.*, **2011**, *11*, 180-206.
- (3) Thorne N., Inglese J. and Auld, D. S., *Chemistry and Biology.*, **2010**, *17*, 646-657.
- (4) Prescher, J. A. and Contag, C. H., *Curr. Opin in Chem. Bio.*, **2010**, *14*, 80-89.
- (5) Shimomura, O., Chalfie, M. and Tsien, R. Y., *Angew. Chem., Int. Ed.*, **2009**, *48*, 5555.
- (6) Luo, Y, Rao, M and Zou, J, *Curr. Opin in Chem. Bio.*, **2014**, *7*, 1-18.
- (7) Shimomura, O, *Bioluminescence Chemical Principles and Methods, Revised Edition*, World Scientific Publishing, Singapore, **2012**.
- (8) Saito, K., Chang, Y. F., Horikawa, K., Hatsugai, N., Higuchi, Y., Hashida, M., Yoshida, Y., Matsuda, T., Arai, Y. and Nagai, T., *Nat. Commun.*, **2012**, *3*, 1-9.
- (9) Xu, H., L, C. M., He, Y., T, H. W. and Wu, Q. S., *J. Luminesc.*, **2010**, *130*, 1872-1879.
- (10) Kaskova, Z. M., Tsarkova, A. S. and Yampolsky, I. V., *Chem. Soc. Rev.*, **2016**, *21*, 6048-6077.
- (11) Hall, M. P., Unch, J., Binkowski, B. F., Valley, M. P., Butler, B. L., Wood, M. G., Otto, P., Zimmerman, K., Vidugiris, G., Machleidt, T., Robers, M. B., Benink, H. A., Eggers, C. T., Slater, M. R., Meisenheimer, P. L., Klaubert, D. H., Fan, F., Encell, L. P., and Wood, K. V., *ACS Chem. Biol.*, **2012**, *7*, 1848-1857.
- (12) Lindberg, E., Mizukami, S., Ibata, K., Fukano, T., Miyawaki, A., and Kikuchi, K., *Chem Sci.*, **2013**, *4*, 4395-4400.
- (13) Ando, Y., Niwa, K., Yamada, N., Enomoto, T, Irie, T., Kubota, H., Ohmiya, Y. and Akiyama, H., *Nature Photonics*, **2007**, *2*, 44-47.
- (14) Loening, A. M., Fenn, T. D., Wu, A. M., and Gambhir, S. S. *Protein Eng. Des. Sel.*, **2006**, *19*, 391-400.
- (15) Hoshino, H., Nakajima, Y. and Ohmiya, Y., *Nature Method.*, **2007**, *4*, 637-639.

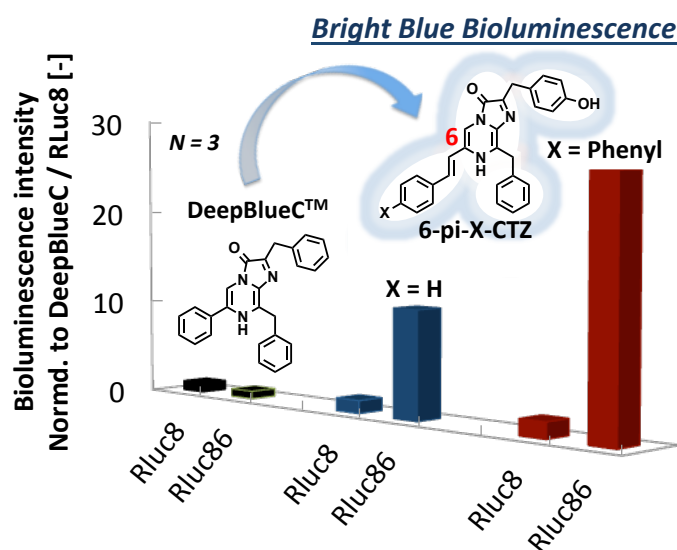
- (16) Takai, A., Nakano, M., Saito, K., Haruno, R., Watanabe, T. M., Ohyanagi, T., Jin, T., Okada, Y. and Nagai, T., *PNAS*, **2015**, *112*, 4352-4356.
- (17) Ozawa, T., Yoshimura, H. and Kim, S. B., *Anal. Chem.*, **2013**, *85*, 590-609.
- (18) Luker, K. E., Smith, M. C., Luker, G. D., Gammon, S. T., PiwnicaWorms, H. and PiwnicaWorms, D., *Proc. Natl. Acad. Sci. U.S.A.*, **2004**, *101*, 12288-12293.
- (19) Kim, S. B., Awais, M., Sato, M., Umezawa, Y. and Tao, H., *Anal. Chem.*, **2007**, *79*, 1874-1880.
- (20) Nishihara, R., Suzuki, H., Hoshino, E., Suganuma, S., Sato, M., Nishiyama, S., Iwasawa, N., Citterio, D. and Suzuki, K., *Chem. Commun.*, **2015**, *51*, 391-394.
- (21) Tarassov, K., Messier, V., Landry, C. R., Radinovic, S., Serna Molina, M. M., Shames, I., Malitskaya, Y., Vogel, J., Bussey, H., and Michnick, S. W., *Science*, **2008**, *320*, 1465-1470.
- (22) Kim, S. B., Umezawa, Y., Kanno, K. A., and Tao, H., *ACS Chem. Biol.*, **2008**, *3*, 359-372.
- (23) Kaihara, A., and Umezawa, Y., *Asian J.*, **2008**, *3*, 38-45.
- (24) Kim, S. B., Torimura, M., and Tao, H., *Bioconjugate Chem.*, **2013**, *24*, 2067-2075.
- (25) Paulmurugan, R., and Gambhir, S. S., *Anal. Chem*, **2005**, *77*, 1295-1302.
- (26) Kim, S. B., Sato, M., and Tao, H., *Bioconjugate Chem.*, **2009**, *20*, 2324-2330.

## Chapter 2

### Fabrication of Blue-Shifted Coelenterazine Derivatives for Bioluminescent Applications

#### Summary

Three novel coelenterazine (CTZ) derivatives with extension at the C-6 position of the imidazopyrazinone structure show significant bioluminescence emission with known *renilla* luciferase variants, indicating a promising method to develop CTZ derivatives with superior optical properties compared to hitherto reported compounds.



## 2.1 Introduction

Bioluminescence-based assays such as gene reporter assays in cell cultures and *in vivo* imaging are known for their low background signals and high sensitivity.<sup>1</sup> The mechanism relies on an enzymatic oxidation reaction involving a bioluminescent substrate (luciferin) and an enzyme (luciferase).

The luciferin most widely applied in imaging assays is the firefly luciferin, which emits light at a relatively long wavelength (560 nm).<sup>2-5</sup> Unfortunately however, the process leading to light emission of firefly luciferin requires the presence of  $Mg^{2+}$  ions and ATP as co-factors, which potentially leads to complex assay protocols in bioanalysis. For this reason, the  $Mg^{2+}$  and ATP independent *renilla* luciferase (Rluc) enzyme in combination with coelenterazine (CTZ) (Figure 2-1 and 2-2a) as the substrate has recently been used as a versatile reporter protein.<sup>6</sup> However, the Rluc/CTZ pair results in relatively short wavelength emission in the blue spectral region (480 nm) with a low intensity compared to other bioluminescent systems.<sup>7,8</sup> To overcome these limitations, there is a lot of interest in developing new CTZ derivatives.<sup>9-14</sup> But the design of novel CTZ derivatives resulting in better optical characteristics is challenging, since the detailed enzymatic recognition mechanism of the Rluc system is still mostly unknown.<sup>15-17</sup> In fact, most of the reported CTZ derivatives fail to emit bioluminescence, since their structural modifications prevent their enzymatic recognition.<sup>5-9</sup> The luminescence capacity of CTZ is due to its imidazopyrazinone structure. In previously published work, the effects on the bioluminescence properties of substitution at the C-2, C-5, C-6 and C-8 positions of the imidazopyrazinone core have been investigated (Figure 2-1).<sup>9,10,14,18,19</sup>

Although it is generally said that the effect of substitution at the C-2 position on enzymatic recognition is relatively low, the benzyl group at the C-2 position is a prerequisite for the luminescence of imidazopyrazinone derivatives.<sup>19</sup> Few C-2 CTZ derivatives show luminescence properties superior to those of native CTZ, except in combination with aequorin. CTZ derivatives modified at the C-8 position have also been reported.<sup>9</sup> A compound having a styryl group at the C-8 position (Figure 2-1 and 2-2b) showed approximately 120 nm red-

shifted chemiluminescence emission compared to that of the native CTZ, but this structural change resulted in negligibly low bioluminescence in combination with RLuc.<sup>20</sup>

Different types of CTZ derivatives (e-CTZ and v-CTZ) have been obtained by forming a bridge between the C-5 carbon and the (p-hydroxy)-phenyl substituent at the C-6 position of the native CTZ (Figure 2-1).<sup>14,21</sup> This modification leads to more planar and rigid molecular structures with increased bioluminescence emission, however at the cost of molecular stability.<sup>21</sup>

As mentioned above, native CTZ has a (p-hydroxy)-phenyl group in the C-6 position. Some CTZ derivatives with alternative substituents at this position have also been reported.<sup>12,13,22,23</sup> However, most of these studies have focused on the chemiluminescence properties.

There are only a few studies on the C-6 substituent effects on enzymatic recognition and on the bioluminescence properties of the resultant CTZ derivatives.<sup>14</sup> To fill this gap, I have decided to further investigate the influence of substituents at the C-6 position of native CTZ on the chemiluminescence (CL) and bioluminescence properties (BL). Compared to BL, the measurement of CL allows us to study the structure-related basic luminescence properties independent of any possible luciferin-luciferase mismatch.<sup>24-26</sup>

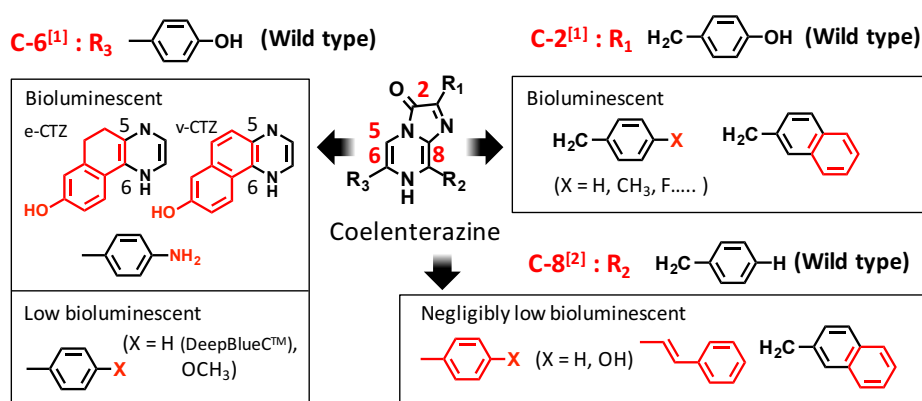


**Figure 2-1** The chemical structure of native CTZ and reported CTZ derivatives from RLuc

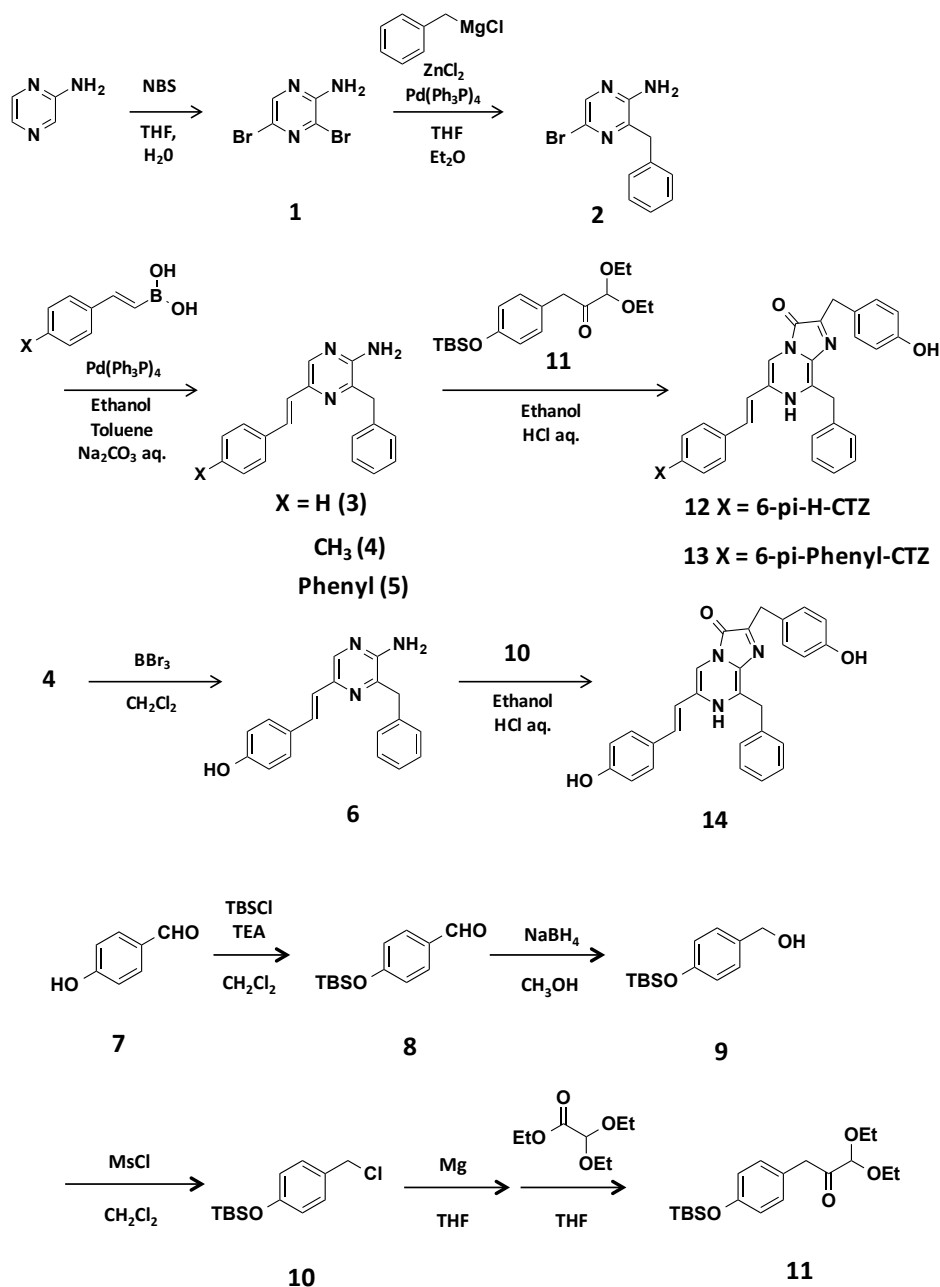
## 2.2 Experimental section

### 2.2.1 Materials and Instruments

All reagents and solvents for organic synthesis were purchased from commercial suppliers (Tokyo Kasei, Aldrich Chemical, Wako Pure Chemical and Biotium) and were used without further purification. All moisture-sensitive reactions were carried out under an atmosphere of argon. The composition of mixed solvents is given by the volume ratio (v/v).  $^1\text{H-NMR}$  and  $^{13}\text{C-NMR}$  spectra were recorded on an ECA-500 (JEOL Ltd.) or ECA-600 (JEOL Ltd.) spectrometer at room temperature. The measurements for  $^1\text{H-NMR}$  was performed at 500 MHz. The measurement of  $^{13}\text{C-NMR}$  was performed at 125 MHz or 150 MHz. All chemical shifts are relative to an internal standard of tetramethylsilane ( $\delta = 0.0$  ppm) or solvent residual peaks ( $\text{CDCl}_3$ :  $\delta = 7.26$  ppm,  $\text{CD}_3\text{OD}$ :  $\delta = 3.31$  ppm,  $\text{DMSO-}d_6$ :  $\delta = 2.50$  ppm for  $^1\text{H}$ ;  $\text{CDCl}_3$ :  $\delta = 77.16$  ppm,  $\text{CD}_3\text{OD}$ :  $\delta = 49.00$  ppm,  $\text{DMSO-}d_6$ :  $\delta = 39.52$  ppm for  $^{13}\text{C}$ ), and coupling constants are given in Hz. Flash chromatography separation was conducted using a YFLC-A1-560 chromatograph (Yamazen Co. Ltd.). HPLC purification was performed on a reversed-phase column, Intersil ODS-3 (30  $\times$  50 mm) (GL Sciences Inc.), fitted on an LC-918 recycling preparative HPLC system (Japan Analytical Industry Co. Ltd.). High-resolution MS spectra (HR-MS) were recorded on a Waters LCT premier XE with MeOH as the eluent.

All solvents for spectrometry were purchased from Kanto Chemical. Native CTZ and DeepBlueC<sup>TM</sup> were purchased from Biotium. CTZ and CTZ derivatives were stored at  $-34^\circ\text{C}$ .

Chemiluminescence spectra was measured using a SREX Fluorolog-3 fluorescence spectrophotometer (Model FL-3-11, Horiba Jobin Yvon, Kyoto, Japan). For bioluminescence assays, A plasmid encoding wild-type *renilla* luciferase (pGL4.75) was purchased from Promega (Madison, WI, USA). Plasmids encoding Rluc variants (Rluc8 and Rluc8.6-535) were generously gifted by Dr. Sanjiv S. Gambhir (Stanford Univ.).



Synthetic scheme for 6-pi-H-CTZ, 6-pi-OH-CTZ and 6-pi-Ph-CTZ Compound 2, 3, 8, 9, 10 and 11 were

synthesized according to reported procedure<sup>27-30</sup>.

## 2.2.2 Synthesis of CTZ derivatives

### 3-Benzyl-5-bromopyrazin-2-amine (2)

Zinc chloride (1.62 g, 11.9 mmol, 3 eq.) was dissolved in Et<sub>2</sub>O (12 mL) and THF (27 mL) and stirred at room

temperature. 2.0 M Benzylmagnesium chloride solution in THF (4.4 mL, 8.94 mmol, 2.2 eq.) and 3,5-dibromopyrazin-2-amine (**1**) (1.0 g, 3.96 mmol, 1eq.) dissolved in THF (5 mL) were slowly added into the solution at room temperatures under argon. After vacuum deaeration, a catalytic amount of tetrakis(triphenylphosphine)palladium(0) was added into the solution and the mixture was deaerated again and stirred for 23 hours at room temperature. The solution was filtered through a Celite pad to remove the palladium catalyst. The solution was extracted with ethyl acetate, and the brown organic phase was washed with water and brine, dried over Na<sub>2</sub>SO<sub>4</sub> and evaporated. The resulting residue was purified by flash chromatography (silica gel, eluent composition: n-hexane / ethyl acetate = 80/20 to 70/30), affording 3-benzyl-5-bromopyrazin-2-amine (**2**) as yellow liquid (0.73 g, 69%).

<sup>1</sup>H-NMR (500 MHz, CDCl<sub>3</sub>): δ (ppm) = 8.04 (s, 1H), 7.21-7.38 (m, 5H), 4.37 (s, 2H), 4.08 (s, 2H).

#### **(E)-3-Benzyl-5-styrylpyrazin-2-amine (**3**)<sup>4</sup>**

3-Benzyl-5-bromopyrazine-2-amine (**2**) (200 mg, 0.76 mmol, 1 eq.) and (*E*)-styrylboronic acid (180.52 mg, 1.22 mmol, 1.6 eq.) were dissolved in toluene (16 ml) and stirred at room temperature. Ethanol (2.4 ml) and 1 M Na<sub>2</sub>CO<sub>3</sub> aq. (6 ml) were added into the reaction mixture. After vacuum deaeration, a catalytic amount of tetrakis(triphenylphosphine)palladium(0) was added into the solution and the mixture was deaerated again and stirred for 12 hours at 100 °C. After cooling to room temperature, the solution was filtered through a Celite pad to remove the palladium catalyst. The solution was extracted with ethyl acetate, and the brown organic phase was washed with water and brine, dried over Na<sub>2</sub>SO<sub>4</sub> and evaporated. The resulting residue was purified by flash chromatography (silica gel, eluent composition: n-hexane / ethyl acetate = 67/33 to 50/50), affording (*E*)-3-benzyl-5-styrylpyrazine-2-amine (**3**) as a yellow solid (194.9 mg, 67%).

<sup>1</sup>H-NMR (500 MHz, CDCl<sub>3</sub>): δ (ppm) = 7.94 (s, 1H), 7.53 (d, *J* = 7.7 Hz, 2H), 7.47 (d, *J* = 16.0 Hz, 1H), 7.23-7.36 (m, 8H), 7.06 (d, *J* = 16.0 Hz, 1H), 4.49 (s, 2H), 4.12 (s, 2H). <sup>13</sup>C-NMR (125 MHz, CDCl<sub>3</sub>): δ (ppm) =

41.5, 124.9, 126.8, 127.2, 127.9, 128.6, 128.7, 129.1, 136.7, 137.2, 139.6, 141.1, 141.3, 151.8. HR-MS: calcd for C<sub>19</sub>H<sub>17</sub>N<sub>3</sub>: 287.1422 [M+H]<sup>+</sup>, found: *m/z* 288.1501.

**(E)-3-Benzyl-5-(4-methoxystyryl)pyrazin-2-amine (4)**

3-Benzyl-5-bromopyrazine-2-amine (**2**) (217.83 mg, 0.83 mmol, 1 eq.) and (*E*)-(4-methoxystyryl)boronic acid (235.74 mg, 1.32 mmol, 1.6 eq.) were dissolved in toluene (16 ml) and stirred at room temperature. Ethanol (2.4 ml) and 1 M Na<sub>2</sub>CO<sub>3</sub> aq. (6 ml) were added into the reaction mixture. After vacuum deaeration, a catalytic amount of tetrakis(triphenylphosphine)palladium(0) was added into the solution and the mixture was deaerated again and stirred for 18 hours at 100 °C. After cooling to room temperature, the solution was filtered through a Celite pad to remove the palladium catalyst. The solution was extracted with ethyl acetate, and the brown organic phase was washed with water and brine, dried over Na<sub>2</sub>SO<sub>4</sub> and evaporated. The resulting residue was purified by flash chromatography (silica gel, eluent composition: n-hexane / ethyl acetate = 80/20 to 50/50), affording (*E*)-3-benzyl-5-(4-methoxystyryl)pyrazin-2-amine (**4**) as a yellow solid (131.5 mg, 50%). <sup>1</sup>H-NMR (500 MHz, CDCl<sub>3</sub>): δ (ppm) = 7.99 (s, 1H), 7.47 (dd, *J* = 8.6 Hz, 16.0 Hz, 2H), 7.24-7.33 (m, 5H), 6.96 (d, *J* = 16.0 Hz, 1H), 6.90 (d, *J* = 14.6 Hz, 2H), 4.42 (s, 2H), 4.15 (s, 2H), 3.82 (s, 3H). <sup>13</sup>C-NMR (125 MHz, CDCl<sub>3</sub>): δ (ppm) = 41.4, 55.4, 114.2, 122.8, 127.1, 128.1, 128.6, 129.1, 129.3, 130.0, 136.8, 139.2, 141.0, 141.7, 151.6, 159.5. HR-MS: calcd for C<sub>20</sub>H<sub>19</sub>N<sub>3</sub>O: 317.1528 [M+H]<sup>+</sup>, found: *m/z* 318.1606.

**(E)-5-(2-([1,1'-Biphenyl]-4-yl)vinyl)-3-benzylpyrazin-2-amine (5)**

3-Benzyl-5-bromopyrazine-2-amine (**2**) (150 mg, 0.57 mmol, 1 eq.) and (*E*)-(2-([1,1'-biphenyl]-4-yl)vinyl)boronic acid (203.9 mg, 0.91 mmol, 1.6 eq.) were dissolved in toluene (12 ml) and stirred at room temperature. Ethanol (2 ml) and 1 M Na<sub>2</sub>CO<sub>3</sub> aq. (4.6 ml) were added into the reaction mixture. After vacuum deaeration, a catalytic amount of tetrakis(triphenylphosphine)palladium(0) was added into the solution and the

mixture was deaerated again and stirred for 15 hours at 100 °C. After cooling to room temperature, the solution was filtered through a Celite pad to remove the palladium catalyst. The solution was extracted with ethyl acetate, and the brown organic phase was washed with water and brine, dried over Na<sub>2</sub>SO<sub>4</sub> and evaporated. The resulting residue was purified by flash chromatography (silica gel, eluent composition: n-hexane / ethyl acetate = 80/20 to 50/50), affording (*E*)-5-(2-([1,1'-biphenyl]-4-yl)vinyl)-3-benzylpyrazin-2-amine (**5**) as a yellow solid (49.7 mg, 24%).

<sup>1</sup>H-NMR (500 MHz, CDCl<sub>3</sub>): δ (ppm) = 8.03 (s, 1H), 7.63-7.59 (m, 7H), 7.54 (d, *J* = 16.0 Hz, 1H), 7.43 (t, *J* = 15.5, 2H), 7.34-7.31 (m, 3H), 7.27-7.24 (m, 3H), 7.14 (d, *J* = 16.0 Hz, 1H), 4.45 (s, 2H), 4.16 (s, 2H). <sup>13</sup>C-NMR (125 MHz, CDCl<sub>3</sub>): δ (ppm) = 41.4, 124.8, 127.0, 127.2, 127.3, 127.4, 128.6, 128.9, 129.1, 136.3, 136.6, 139.6, 140.5, 140.7, 141.1, 141.3, 151.8. HR-MS: calcd for C<sub>25</sub>H<sub>21</sub>N<sub>3</sub>: 363.1735 [M+H]<sup>+</sup>, found: *m/z* 364.1814.

#### **(*E*)-4-(2-(5-Amino-6-benzylpyrazin-2-yl)vinyl)phenol (6)**

(*E*)-3-Benzyl-5-(4-methoxystyryl)pyrazin-2-amine (**4**) (202 mg, 0.64 mmol, 1 eq.) was dissolved in dichloromethane (12 ml). 1.0 M Boron tribromide dichloromethane solution (12 ml) was added slowly into the solution at 0 °C, followed by stirring for 13 hours at 40 °C. After cooling to room temperature, saturated NaHCO<sub>3</sub> aq. was added into the reaction mixture to neutralize and then evaporated to remove most of the solvent. The residue was extracted with ethyl acetate, and the yellow organic phase was washed with water and brine, dried over Na<sub>2</sub>SO<sub>4</sub> and evaporated. The resulting residue was purified by flash chromatography (silica gel, eluent composition: n-hexane / ethyl acetate = 50/50), affording (*E*)-4-(2-(5-amino-6-benzylpyrazin-2-yl)vinyl)phenol (**6**) as a yellow solid (42.7 mg, 22%).

<sup>1</sup>H-NMR (500 MHz, CD<sub>3</sub>OD): δ (ppm) = 7.93 (s, 1H), 7.37 (d, *J* = 8.6 Hz, 2H), 7.38-7.21 (m, 6H), 6.93 (d, *J* = 16.0 Hz, 1H), 6.77 (d, *J* = 8.6 Hz, 2H), 4.11 (s, 2H). <sup>13</sup>C-NMR (125 MHz, DMSO-d<sub>6</sub>): δ (ppm) = 39.2, 116.1, 122.6, 126.7, 127.7, 128.3, 128.7, 128.8, 129.3, 138.7, 139.3, 139.5, 141.1, 152.9, 157.7

HR-MS: calcd for C<sub>19</sub>H<sub>17</sub>N<sub>3</sub>O: 303.1372 [M+H]<sup>+</sup>, found: *m/z* 304.1450.

#### 4-((*tert*-Butyldimethylsilyl)oxy)benzaldehyde (**8**)

4-Hydroxybenzaldehyde (**7**) (10.0 g, 82.3 mmol, 1 eq.) and *tert*-butyldimethylsilyl chloride (13.6 g, 90.8 mmol, 1.1 eq.) were dissolved in dichloromethane (400 mL). Triethylamine (15 mL) was added into the reaction mixture at 0 °C, followed by stirring for 18 hours at room temperature. A part of the solvent was evaporated and washed with water and brine, dried over Na<sub>2</sub>SO<sub>4</sub> and evaporated. The resulting residue was purified by flash chromatography (silica gel, eluent composition: n-hexane / ethyl acetate = 90/10), affording 4-((*tert*-butyldimethylsilyl)oxy)benzaldehyde (**8**) as a water-clear viscous oil (18.5 mg, 95%).

<sup>1</sup>H-NMR (500 MHz, CDCl<sub>3</sub>): δ (ppm) = 9.89 (s, 1H), 7.99 (d, *J* = 8.7 Hz, 2H), 6.95 (d, *J* = 8.7 Hz, 2H), 1.00 (s, 9H), 0.25 (s, 6H).

#### 4-((*tert*-Butyldimethylsilyl)oxy)phenyl)methanol (**9**)

4-((*tert*-Butyldimethylsilyl)oxy)benzaldehyde (**8**) (18.9 g, 79.9 mmol, 1 eq.) was dissolved in methanol (300 mL) and stirred at room temperature. Sodium borohydride (3.7 g, 97.5 mmol, 1.2 eq.) was added into the reaction mixture at 0 °C, followed by stirring for 30 min at room temperature. The solvent was evaporated and the residue was extracted with dichloromethane, and the transparent organic phase was washed with water and brine, dried over Na<sub>2</sub>SO<sub>4</sub> and evaporated, affording 4-((*tert*-butyldimethylsilyl)oxy)phenyl)methanol (**9**) as a water-clear viscous oil (21.1 g, 99%).

<sup>1</sup>H-NMR (500 MHz, CDCl<sub>3</sub>): δ (ppm) = 7.24 (d, *J* = 8.4 Hz, 2H), 6.83 (d, *J* = 8.4 Hz, 2H), 4.61 (s, 2H), 0.95 (s, 9H), 0.20 (s, 6H).

***tert*-Butyl(4-(chloromethyl)phenoxy)dimethylsilane (10)**

(4-((*tert*-Butyldimethylsilyloxy)phenyl)methanol (**9**) (7.0 g, 29.3 mmol, 1.0 eq.) and triethylamine (8.0 ml, 58.6 mmol, 2.0 eq.) were dissolved in dichloromethane (150 mL). Methylsulfonyl chloride (3.4 g, 44.6 mmol, 1.5 eq.) in dichloromethane (50 mL) was added into the reaction mixture at 0 °C, followed by stirring for 3 hours at room temperature. The solvent was evaporated and the residue was extracted with dichloromethane, and the transparent organic phase was washed with water and brine, dried over Na<sub>2</sub>SO<sub>4</sub> and evaporated. The resulting residue was purified by flash chromatography (silica gel, eluent composition: n-hexane / ethyl acetate = 95/5), affording *tert*-butyl(4-(chloromethyl)phenoxy)dimethylsilane (**10**) as a water-clear viscous oil (5.09 g, 68%).

<sup>1</sup>H-NMR (500 MHz, CDCl<sub>3</sub>): δ (ppm) = 7.24 (d, *J* = 8.6 Hz, 2H), 6.81 (d, *J* = 8.6 Hz, 2H), 4.55 (s, 2H), 0.98 (s, 9H), 0.20 (s, 6H).

**3-(4-((*tert*-Butyldimethylsilyloxy)phenyl)-1,1-diethoxypropane-2-one (11)**

Magnesium turnings (774.5 mg, 31.9 mmol, 2 eq.) was added into THF (10 mL), followed by additional THF (10 mL) and a catalytic amount of 1,2-dibromoethane (0.4 mL, 0.004 mmol) under argon to activate magnesium turnings. *tert*-Butyl(4-(chloromethyl)phenoxy)dimethylsilane (**10**) (4.0 g, 15.6 mmol, 1.0 eq.) in THF (40 mL) was slowly added into the solution, followed by stirring for 1 hours at 50°C. After cooling to room temperature, the Grignard reagent is obtained as dark gray solution. Ethyl diethoxyacetate (3.2 mL, 17.9 mmol, 0.9 eq.) and THF (30 mL) were added into a separate reaction flask, followed by stirring at -78°C (acetone / dry ice). The Grignard reagent was slowly added into the solution under argon, followed by stirring for 2 hours at -78°C. Water was added into the solution to quench, followed by warming to room temperature. The solvent was evaporated and the residue was extracted with ethyl acetate, and the transparent organic phase was washed with water and brine, dried over Na<sub>2</sub>SO<sub>4</sub> and evaporated. The resulting residue was purified by silica gel

chromatography (eluent composition: n-hexane / ethyl acetate = 95/5 to 90/10), affording 3-(4-((*tert*-butyldimethylsilyl)oxy)phenyl)-1,1-diethoxypropane-2-one (**11**) as a water-clear viscous oil (2.5 g, 47%).

<sup>1</sup>H-NMR (500 MHz, CDCl<sub>3</sub>): δ (ppm) = 7.08-7.06 (m, 2H), 6.79-6.76 (m, 2H), 4.62 (s, 1H), 3.80 (s, 2H), 3.73-3.63 (m, 2H), 3.58-3.48 (m, 2H), 1.24 (t, *J* = 7.1 Hz, 6H), 0.97 (s, 9H), 0.18 (s, 6H).

**(*E*)-8-Benzyl-2-(4-hydroxybenzyl)-6-styrylimidazo[1,2-*a*]pyrazin-3(7H)-one (12) (6-*pi*-H-CTZ)**

(*E*)-3-Benzyl-5-styrylpyrazin-2-amine (**3**) (31.32 mg, 0.10 mmol, 1 eq.) and ketoacetal (**11**) (76.62 mg, 0.21 mmol, 2 eq.) were dissolved in ethanol (2.0 ml) and H<sub>2</sub>O (0.2 ml) and stirred at room temperature. After vacuum deaeration, the solution was cooled to 0 °C and HCl was added under nitrogen flow. Once the solution reached room temperature, it was heated and stirred for 10 hours at 70 °C. The solvent was evaporated under vacuum and the crude compound was purified by semipreparative reversed-phase HPLC (eluent composition: MeCN / H<sub>2</sub>O = 50/50 with 0.1% formic acid), affording (*E*)-8-benzyl-2-(4-hydroxybenzyl)-6-styrylimidazo[1,2-*a*]pyrazin-3(7H)-one (**12**) as a yellow solid (10.2 mg, 22%).

<sup>1</sup>H-NMR (500 MHz, CD<sub>3</sub>OD, CDCl<sub>3</sub>): δ (ppm) = 7.59 (s, 1H), 7.37-7.21 (m, 10H), 7.15 (d, *J* = 8.6 Hz, 2H), 6.96 (t, *J* = 16.3 Hz, 1H), 6.69 (d, *J* = 8.6 Hz, 2H), 4.40 (s, 2H), 4.04 (s, 2H). <sup>13</sup>C-NMR (125 MHz, CD<sub>3</sub>OD, CDCl<sub>3</sub>): δ (ppm) = 33.8, 115.9, 127.4, 127.9, 129.3, 129.3, 129.4, 129.5, 130.5, 156.3. HR-MS: calcd for C<sub>28</sub>H<sub>23</sub>N<sub>3</sub>O<sub>2</sub>: 433.1790 [M-H]<sup>-</sup>, found: *m/z* 432.1712.

**(*E*)-6-(2-([1,1'-Biphenyl]-4-yl)vinyl)-8-benzyl-2-(4-hydroxybenzyl)imidazo[1,2-*a*]pyrazin-3(7H)-one (13) (6-*pi*-Ph-CTZ)**

(*E*)-5-(2-([1,1'-Biphenyl]-4-yl)vinyl)-3-benzylpyrazin-2-amine (**5**) (30.0 mg, 0.08 mmol, 1 eq.) and ketoacetal (**11**) (75.26 mg, 0.16 mmol, 2 eq.) were dissolved in ethanol (2.0 ml) and H<sub>2</sub>O (0.2 ml) and stirred at room temperature. After vacuum deaeration, the solution was cooled to 0 °C and HCl was added under nitrogen

flow. Once the solution reached room temperature, it was heated and stirred for 10 hours at 70 °C. The solvent was evaporated under vacuum and the crude compound was purified by semipreparative reversed-phase HPLC (eluent composition: CH<sub>3</sub>OH / H<sub>2</sub>O = 100/5 with 0.1% formic acid), affording (*E*)-6-(2-([1,1'-biphenyl]-4-yl)vinyl)-8-benzyl-2-(4-hydroxybenzyl)imidazo[1,2-*a*]pyrazin-3(7*H*)-one (**13**) as a yellow solid (2.0 mg, 5%).

<sup>1</sup>H-NMR (600 MHz, CD<sub>3</sub>OD): δ (ppm) = 7.62-7.57 (m, 7H), 7.43-7.22 (m, 9H), 7.15 (d, *J* = 8.59 Hz, 2H), 7.15 (d, *J* = 15.4 Hz, 1H), 6.69 (d, *J* = 8.59 Hz, 2H), 4.39 (s, 2H), 4.03 (s, 2H)

<sup>13</sup>C-NMR (150 MHz, CD<sub>3</sub>OD, CDCl<sub>3</sub>): δ (ppm) = 21.4, 116.2, 127.8, 128.3, 128.5, 129.7, 129.7, 129.9, 130.7, 130.8, 131.3, 136.6, 138.2, 141.7, 142.4, 156.9. HR-MS: calcd for C<sub>34</sub>H<sub>27</sub>N<sub>3</sub>O<sub>2</sub>: 509.2103 [M-H]<sup>-</sup>, found: *m/z* 508.2025.

#### **(*E*)-8-Benzyl-2-(4-hydroxybenzyl)-6-(4-hydroxystyryl)imidazo[1,2-*a*]pyrazin-3(7*H*)-one**

#### **(14) (6-*pi*-OH-CTZ)**

(*E*)-4-(2-(5-Amino-6-benzylpyrazin-2-yl)vinyl)phenol (**6**) (30 mg, 0.08 mmol, 1 eq.) and ketoacetal (**11**) (75.26 mg, 0.16 mmol, 2 eq.) were dissolved in ethanol (2.0 ml) and H<sub>2</sub>O (0.2 ml) and stirred at room temperature. After vacuum deaeration, the solution was cooled to 0 °C and HCl (0.1 ml) was added under nitrogen flow. Once the solution reached room temperature, it was heated and stirred for 10 hours at 70 °C. The solvent was evaporated under vacuum and the crude compound was purified by semipreparative reversed-phase HPLC (eluent composition: MeCN / H<sub>2</sub>O = 33/67 with 0.1% formic acid), affording (*E*)-8-benzyl-2-(4-hydroxybenzyl)-6-

(4-hydroxystyryl)imidazo[1,2-*a*]pyrazin-3(7*H*)-one (**14**) as a yellow solid (10.3 mg, 23%). <sup>1</sup>H-NMR (500 MHz, CD<sub>3</sub>OD, CDCl<sub>3</sub>): δ (ppm) = 7.52 (s, 1H), 7.41-7.21 (m, 10H), 6.82 (d, *J* = 8.6 Hz, 2H), 6.82 (d, *J* = 8.6 Hz, 2H), 6.75 (d, *J* = 8.6 Hz, 2H), 6.62 (d, *J* = 16.90 Hz, 1H), 4.37 (s, 2H), 4.09 (s, 2H) <sup>13</sup>C-NMR (125 MHz, CD<sub>3</sub>OD, CDCl<sub>3</sub>): δ (ppm) = 33.6, 33.8, 108.6, 115.9, 116.4, 127.9, 128.9, 129.3, 129.4, 130.5, 137.3, 149.9, 153.7, 156.2,

158.8. HR-MS: calcd for  $C_{28}H_{23}N_3O_3$ : 449.1739 [M-H]<sup>-</sup>, found:  $m/z$  448.1661.

### 2.2.3. Chemiluminescence assay

A CH<sub>3</sub>OH solution of the respective CTZ derivative (1 mM, 200  $\mu$ l) was added to a quartz cell and set in a SREX Fluorolog-3 fluorescence spectrophotometer (Model FL-3-11, Horiba Jobin Yvon, Kyoto, Japan). The chemiluminescence spectra were measured at a scan rate of 1200 nm/min after injecting 2 ml of DMSO. Figure 2-4(A) shows the chemiluminescence spectra of native CTZ and the CTZ derivatives.

### 2.2.4. pH-Dependent chemiluminescence

The wavelength of chemiluminescence emission of coelenterazines depends on their protonation states. An experiment performed according to a procedure described in reference 18 of the main text demonstrates the influence of a trace amount of base on the chemiluminescence emission spectra of CTZ and its derivatives in DMSO (Figure 2-4(B), Table 2-1). The chemiluminescence spectra were measured after injecting 2 ml of DMSO containing 0.5% (v/v) of 1 M aqueous sodium hydroxide into a CH<sub>3</sub>OH solution of the respective CTZ derivative (1 mM, 200  $\mu$ l).

### 2.2.5. Bioluminescence assay

To determine the bioluminescence properties of the novel CTZ derivatives, plasmids encoding wild-type *renilla* luciferase (Rluc), and variants Rluc8 and Rluc8.6 were separately transfected into COS-7 cells cultured in a 24-well plate using a TransIT-LT1 transfection reagent (Takara, Osaka, Japan). The cells were incubated for 48 h and then treated with a lysis buffer (E291A) (Promega, Madison, WI, USA) according to the manufacturer's protocol.

### 2.2.6. Bioluminescence intensities

To measure bioluminescence intensities, an aliquot of the cell lysate including luciferase (1  $\mu\text{L}$ ) was mixed with Hanks' balanced salt solution (HBSS) (50  $\mu\text{L}$ ) containing 2  $\mu\text{M}$  native CTZ or the respective CTZ derivative in Röhren polystyrene tubes (Sarstedt, Nümbrecht, Germany). Bioluminescence intensities of native CTZ and the derivatives were immediately measured for the first 1 s with a Lumat LB 9507 luminometer (Berthold Technologies, Bad Wildbad, Germany).

### 2.2.7. Kinetic profiles of bioluminescence

To measure the kinetic profiles of bioluminescence, signal monitoring was continued for 600 s after mixing. The reaction conditions are identical to those described in the previous section. The results are shown in Figure 2-9(A)-(E).

### 2.2.8. Bioluminescence spectra

For the recording of bioluminescence spectra, an aliquot of the lysate (100  $\mu\text{L}$ ) was mixed with HBSS (400  $\mu\text{L}$ ) containing 20  $\mu\text{M}$  native CTZ or CTZ derivative in a quartz cell, and the mixture was then measured with a F-7000 spectrophotometer (Hitachi, Tokyo, Japan) at a scan rate of 2400 nm/min. The wavelengths of maximal bioluminescence intensities ( $\lambda_{\text{max}}$ ) were determined using the instrument software (FL Solutions ver. 2.1). Figure 2-3(B), 2-6(B), 2-7(B) and 2-9 shows the bioluminescence spectra obtained with Rluc8 and Rluc8.6-535.

### 2.2.9. Solubility test of DeepBlueC<sup>TM</sup> and 6-pi-Ph-CTZ

DeepBlueC<sup>TM</sup> is hardly soluble in water, but it is soluble in organic solvents such as ethanol and methanol. The solubility of DeepBlueC<sup>TM</sup> in these solvents is approximately 0.5 mg/ml (Product information from Cyman Chemical). As for 6-pi-Ph-CTZ, the experimentally determined solubility in methanol is 0.51 mg/ml. As for the

aqueous solubility, it is similar to that of DeepBlueC™.

## 2.3. Results and discussion

### 2.3.1. Development of C-6 modified CTZ derivatives

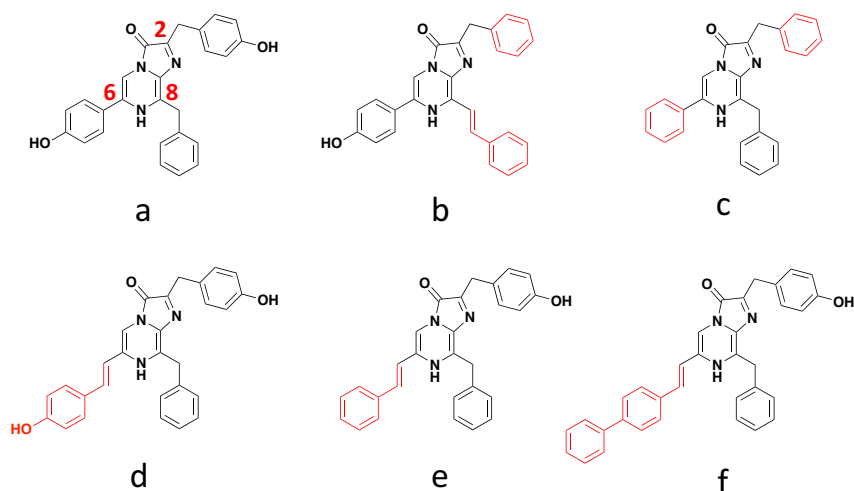


**Figure 2-2** The chemical structure of novel CTZ derivatives. The characteristic functional groups in the chemical structures are highlighted in red. (a: native CTZ, b: C-8 styryl-substituted compound, c: DeepBlueC™, d: 6-pi-OH-CTZ, e: 6-pi-H-CTZ and f: 6-pi-Phenyl-CTZ)

As the first new derivative, the styryl-substituted compound 6-pi-OH-CTZ was successfully synthesized (Figure 2-2d). Its CL spectrum is shown in Figure 2-4. In contrast to the significantly red-shifted C-8 styryl-substituted compound (Figure 2-2b),<sup>20</sup> the spectral similarity between 6-pi-OH-CTZ and native CTZ shows that the C-6 substituent has little influence on the CL emission wavelength. This result is not really surprising, since it has been previously reported that even the complete absence of a substituent at C-6 still results in a CL emission peak at around 450 nm.<sup>31</sup> This finding has been generally attributed to a dihedral angle twist between the imidazopyrazinone core and the substituent at the C-6 position in various CTZ derivatives, which prevents an effective extension of  $\pi$ -electron conjugation from the imidazopyrazinone core.<sup>32</sup>

Next, the enzymatic recognition-dependent BL properties of 6-*pi*-OH-CTZ were investigated using native *renilla* luciferase (Rluc) and the widely known Rluc8 and Rluc8.6-535 variants.<sup>15</sup> Figure 2-3 shows a comparison of the BL intensities and spectra of 6-*pi*-OH-CTZ and native CTZ. Figure 2-3(A) indicates that 6-*pi*-OH-CTZ is recognized by Rluc8 and Rluc8.6-535, but not by Rluc. The BL intensity of the 6-*pi*-OH-CTZ/Rluc8 pair is 44% of that of the native CTZ/Rluc combination. On the other hand, the intensity of 6-*pi*-OH-CTZ with Rluc8.6-535 is 123% of that of the CTZ/Rluc pair and therefore it is a relatively bright derivative. As for the BL spectra with Rluc8.6, the emission wavelengths of 6-*pi*-OH-CTZ and native CTZ are very similar (Figure 2-3(B)). However, with Rluc8, 6-*pi*-OH-CTZ shows approximately 50 nm red-shifted emission compared to that of CTZ (Figure 2-3(B)). As a result, it can be concluded that CTZ derivatives with a  $\pi$ -conjugated substituent at the C-6 position can show significant BL emission with the known Rluc variants, Rluc8 and Rluc8.6-535.

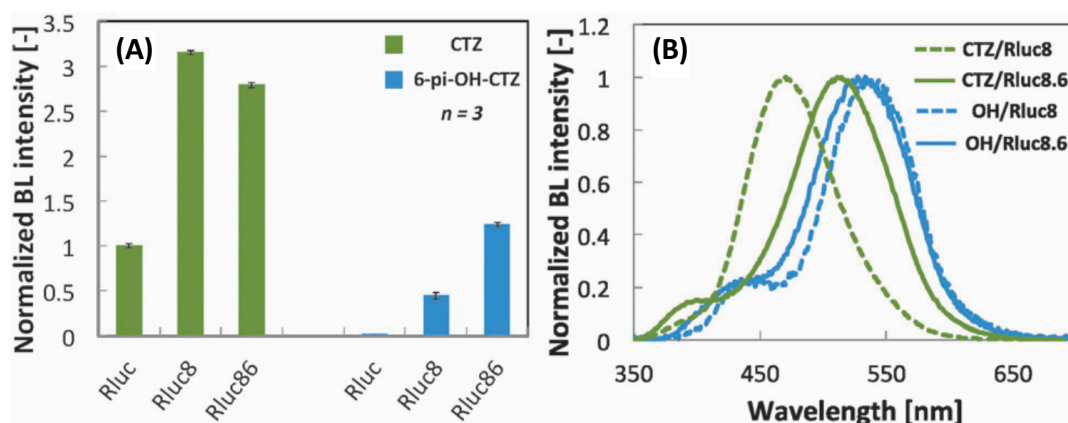


**Figure 2-3** The luminescence properties of 6-*pi*-OH-CTZ: (A) BL intensities; (B) BL spectra with RLuc8 and RLuc8.6-535

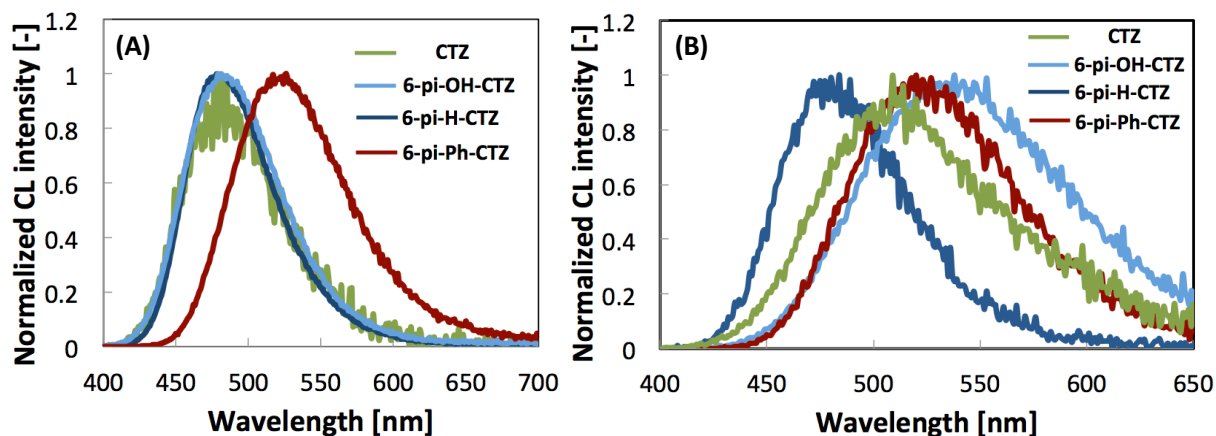


**Figure 2-4** The chemiluminescence spectra of CTZs: (A) in the DMSO; (B) in the DMSO containing 0.5% (v/v) of 1 M aqueous sodium hydroxide

**Table 2-1** Chemiluminescence emission wavelengths of native-CTZ and C-6 modified CTZ derivatives (6-pi-X-CTZ: X = OH, H, Phenyl)

	Native CTZ	OH	H	Phenyl
<b>Emission max. (nm)</b>				
<b>DMSO only</b>	465	479	478	526
<b>Emission max. (nm)</b>				
<b>DMSO plus base</b>	509	538	484	520

In the case of BL, the spectral location of the emission band depends not only on the chemical structure of the CTZ derivative, but to a large extent on its interactions with proximal amino acid residues in the luciferase enzyme,<sup>16</sup> which remain to a large degree still unknown. Upon oxidation in the presence of Rluc, native CTZ is converted into the light emitting excited state coelenteramide, with its emission wavelength depending on the protonation state (Figure 2-5). It is hypothesized that the red-shifted emission of native CTZ and 6-pi-OH-CTZ with Rluc8.6-535 can be attributed to the excited state coelenteramide (CTMD) existing in its deprotonated pyrazine anion form inside the enzymatic pocket. This assumption is supported by the fact that CTZs having a hydroxyl group on the C-6 substituent (native CTZ, 6-pi-OH-CTZ) show a red-shift in their CL emissions upon

addition of a base to the sample solution (Figure 2-4(B) and Table 2-2). Based on a previous report, the spectral shoulders near 400 nm observed in Figure 2-3(B) are assumed to originate from the neutral species of coelenteramide<sup>15</sup> due to incomplete deprotonation of the hydroxyl group on the C-6 substituent.

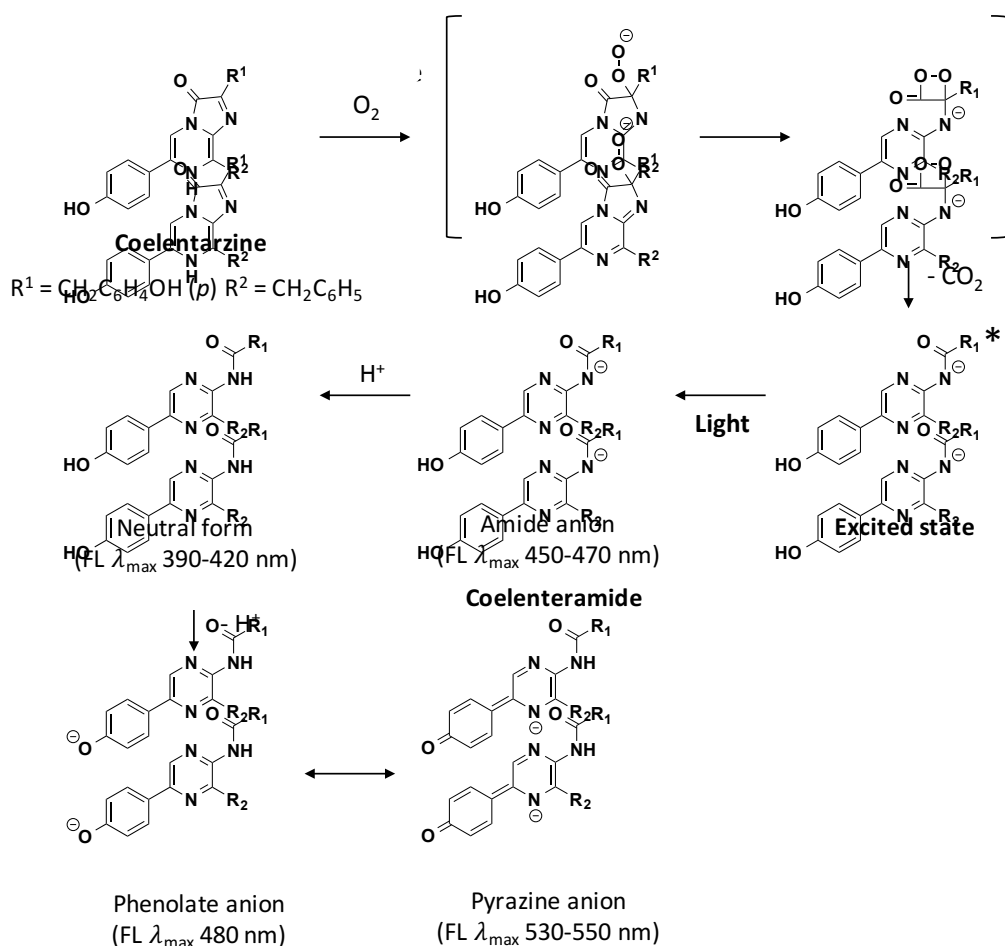


**Figure 2-5** Chemical reaction mechanism of CTZ luminescence

As the next compound, 6-pi-H-CTZ (Figure 2-2e) was designed and synthesized to evaluate the effect of the absence of the hydroxyl group in the C-6 substituent on the CL and BL properties. The measurement of the CL spectrum of 6-pi-H-CTZ (Figure 2-4(A)) was carried out under the same conditions as in the case of 6-pi-OH-CTZ. Also for this substitution pattern, the emission peak of 6-pi-H-CTZ was found at 478 nm, almost identical to the native CTZ.

It has been reported that the replacement of the p-hydroxyl group on the 6-phenyl substituent of native CTZ can drastically decrease the capacity of BL emission.<sup>11</sup> Figure 2-6 shows the results of BL measurements with 6-pi-H-CTZ. Emission was observed in combination with the Rluc8 and Rluc8.6-535 luciferases (Figure 2-6(A)). The intensity of 6-pi-H-CTZ with Rluc8.6-535 is approximately 41% of that of native CTZ/Rluc. The BL spectra recorded in the presence of Rluc8 and Rluc8.6-535 are both significantly blue-shifted compared to those of native CTZ (Figure 2-6(B)). This different BL spectral behavior in comparison with 6-pi-OH-CTZ clearly indicates that the p-hydroxyl group of the C-6 substituent is involved in the enzymatic interaction of CTZs with the RLuc series luciferases. The absence of that hydroxyl group prevents the formation of the pyrazine anion upon enzymatic oxidation, most reasonably resulting in the neutral coelenteramide, which emits at a short wavelength. With the two CTZ derivatives 6-pi-OH-CTZ and 6-pi-H-CTZ, it has been demonstrated that compounds having a styryl group at the C-6 position show significant BL emission in combination with the known RLuc variants, RLuc8 and RLuc8.6-535. This is a clear indication that CTZ derivatives obtained by replacing the original (p-hydroxy)-phenyl substituent at the C-6 position undergo enzymatic recognition by Rluc8 and Rluc8.6-535. To the best of our knowledge, the styryl-groups are the largest examples of C-6 substituents reported so far, with the resulting CTZ derivatives still showing significant BL emission.

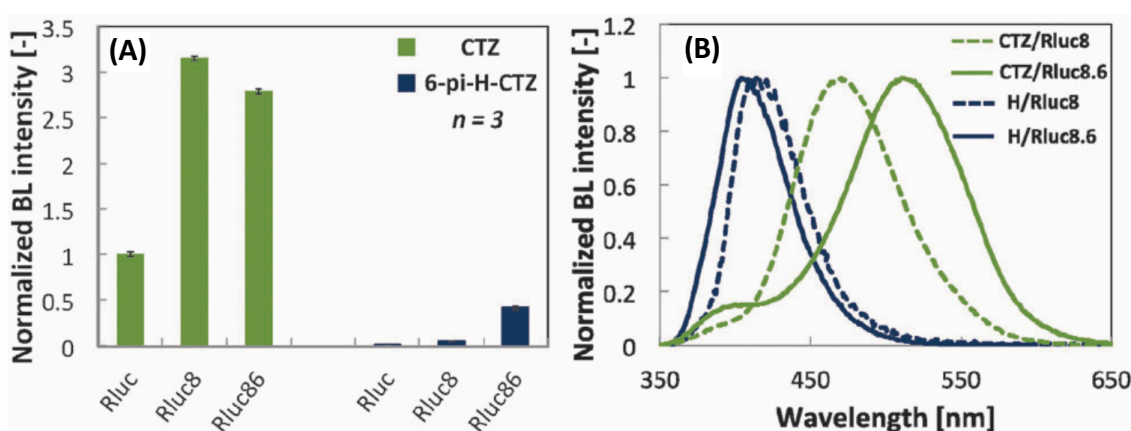


**Figure 2-6** The luminescence properties of 6-pi-H-CTZ: (A) BL intensities; (B) BL spectra with RLuc8 and RLuc8.6-535

To further evaluate the possibility of extending the substituent at the C-6 position, 6-pi-Ph-CTZ having a bulky phenyl group in the para position of the 6-styryl group was designed and synthesized (Figure 2-2f). Interestingly, the CL spectrum of 6-pi-Ph-CTZ (Figure 2-4) showed a 50 nm red-shifted emission compared to that of native CTZ. This seems to be in contradiction to the dihedral angle twist mentioned earlier. At this time, it is only possible to assume that the electronic properties of the additional phenyl group (e.g. its weak inductive electron withdrawing effect) result in an extension of the conjugated  $\pi$ -electron system by a reduction of the dihedral twisting at the C-6 position. The results of bioluminescence measurements are shown in Figure 2-7.

A comparison of BL intensities (Figure 2-7(A)) shows that 6-pi-Ph-CTZ is recognized by Rluc8 and Rluc8.6-535, and in combination with Rluc8.6-535 its intensity reaches 94% of that of the native CTZ/Rluc pair. This result indicates that the structural modification at the C-6 position has little influence on the enzymatic recognition by Rluc8 and Rluc8.6-535. The corresponding bioluminescence spectra (Figure 2-7(B)) show the emission peak of 6-pi-Ph-CTZ at 418 nm with Rluc8.6. This is again significantly blue-shifted in comparison to native CTZ, presumably because of the absence of a deprotonatable hydroxyl group. As a result, 6-pi-Ph-CTZ is the brightest short wavelength emitting CTZ derivative reported so far.

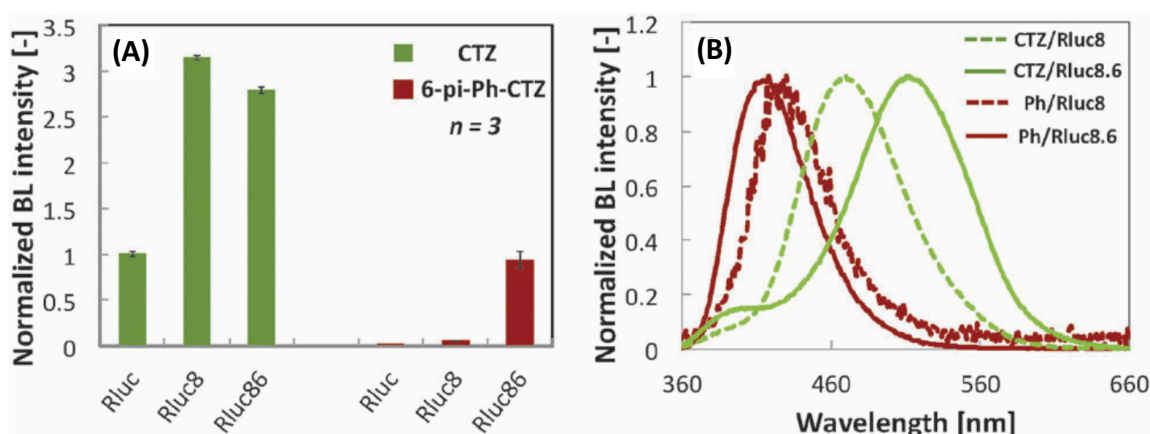


**Figure 2-7** The luminescence properties of 6-pi-Ph-CTZ: (A) BL intensities; (B) BL spectra with RLuc8 and RLuc8.6-535

All of the three CTZ derivatives evaluated in this study having a styryl group on the C-6 position of the imidazopyrazinone core showed weak BL emission with Rluc8, but significantly stronger emission with Rluc8.6-535. In contrast to native CTZ (480 nm in Rluc8 and 526 nm in Rluc8.6-535), the three new derivatives show no differences in the BL emission wavelength between Rluc8 and Rluc8.6-535. Therefore, it can be assumed that C-6 styryl-substituted CTZ derivatives interact with different amino acid residues compared to native CTZ. A further hint in this direction is the fact that native CTZ also emits BL in combination with other related enzymes, such as *Gaussia* luciferase, whereas 6-pi-H-CTZ and 6-pi-OH-CTZ are selectively recognized by the Rluc8 and Rluc8.6-535 variants only (Figure 2-8).

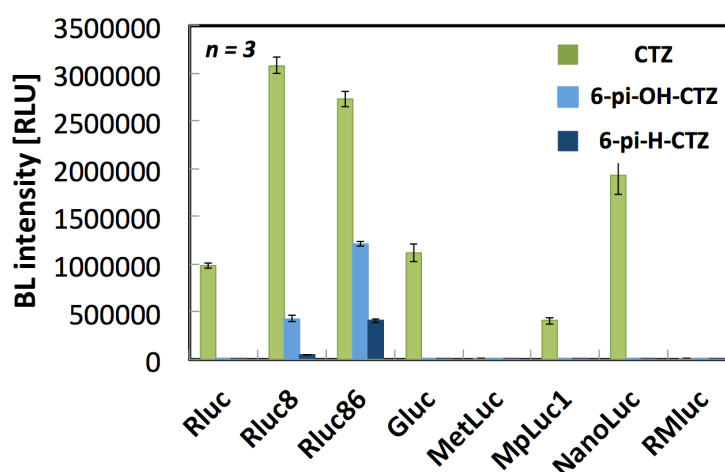


**Figure 2-8** Bioluminescence intensities of CTZs with various marine luciferases

Measurements of the bioluminescence emission time profiles revealed that all three CTZ derivatives show flash-type luminescence with emission kinetics and half-life times of an order similar to native CTZ (Figure 2-9(A)-(E)).

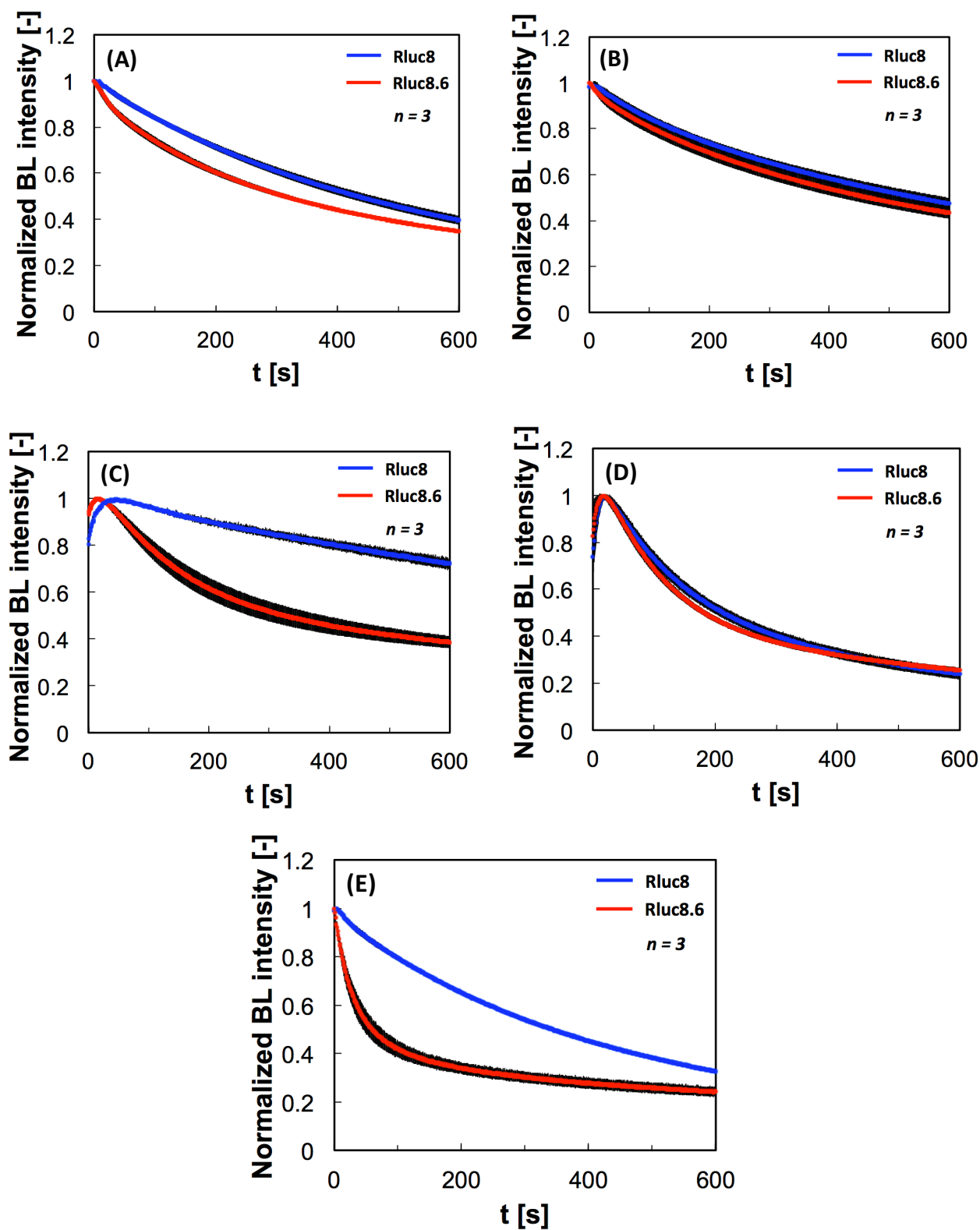


**Figure 2-9** Kinetic profile of bioluminescence with RLuc8 and RLuc8.6-535: (A) Native-CTZ; (B) 6-pi-OH-CTZ; (C) 6-pi-H-CTZ; (D) 6-pi-Ph-CTZ; (E) DeepBlueC™

**Table 2-2** Kinetic profile of native-CTZ, C-6 modified CTZ derivatives (6-pi-X-CTZ: X = OH, H, Phenyl) and DeepBlueC™

	Native CTZ	OH	H	Phenyl	DeepBlueC™
<b>BL half-life time (RLuc8) [s]</b>	433	544	>600	213	342
<b>BL half-life time (RLuc8-535) [s]</b>	313	463	325	182	59

### 2.3.2. Comparison of bioluminescence properties

An example of a commercially available CTZ derivative, emerging from structural modifications at both C-2 and C-6 (missing hydroxyl substituent) positions of the imidazopyrazinone core, is the emission wavelength blue-shifted DeepBlueC™ (Figure 2-2c).<sup>33</sup> DeepBlueC™ is used as a donor in BL resonance energy transfer (BRET)-based applications with green fluorescent protein (GFP) as the acceptor, because its emission peak at around 400 nm minimally interferes with the emission of the GFP acceptor. Typical applications are BRET studies to image protein–protein interactions.<sup>34</sup> However, the BL emission intensity of DeepBlueC™ is only 3.7% compared to that of native CTZ. Since the BL emission of 6-pi-H-CTZ and of DeepBlueC™ is in a similarly short wavelength range, a comparison of the BL properties of the two compounds was performed (Figure 2-10). In terms of BL intensities, 6-pi-H-CTZ and 6-pi-Ph-CTZ with RLuc8.6-535 showed approximately 11-fold and 25-fold stronger emission than DeepBlueC™ with RLuc8 (Figure 2-10). Therefore, 6-pi-H-CTZ and 6-pi-Ph-CTZ are promising bright blue-shifted CTZ derivatives.

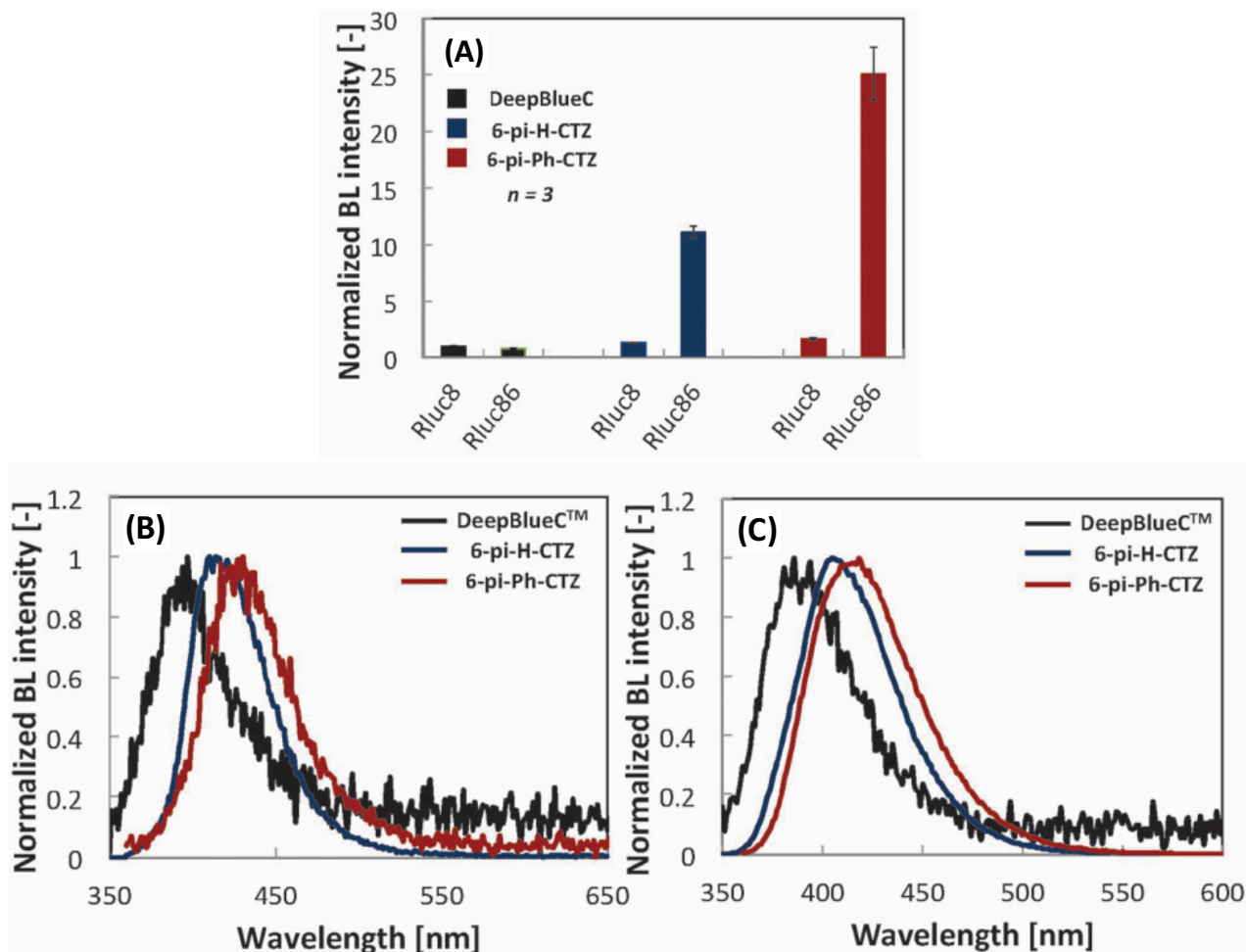


**Figure 2-10** Comparison of BL properties: (A) BL intensities (B) BL spectra with RLuc8 and (C) BL spectra with RLuc8.6-535.

In BL, the environmental effects of the enzyme active site on the light emitting species are very high. Although many details still remain unknown, the emission wavelength of native CTZ with various luciferases is significantly altered by the surrounding environment determined by amino acid residues due to factors such as hydrophobicity and pH changes.

### 2.3.3. Summary of luminescence properties

**Table 2-3** Luminescence properties of native-CTZ, C-6 modified CTZ derivatives (6-pi-X-CTZ: X = OH, H, Phenyl) and DeepBlueC™

	Native CTZ	OH	H	Phenyl	DeepBlueC™
<b>Renilla luciferase</b>					
<b>Initial intensity (%)</b>	100	0.19	0.01	N.D.	N.D.
<b>Emission max. (nm)</b>	478	N.D.	N.D.	N.D.	N.D.
<b>Rluc8</b>					
<b>Initial intensity (%)</b>	314	44	5	6	3.75
<b>Emission max. (nm)</b>	480	527	410	430	397
<b>Rluc8.6-535</b>					
<b>Initial intensity (%)</b>	278	123	41	94	3.04
<b>Emission max. (nm)</b>	526	527	405	418	386
<b>Chemiluminescence</b>					
<b>Emission max. (nm)</b>	465	479	478	526	456 <sup>a</sup>

N.D.: not detected due to low luminescent intensity

<sup>a</sup>Data from Ref19

## 2.4. Conclusions

In this work, three types of novel CTZ derivatives with styryl substituents at the C-6 position have been successfully developed. All of them showed strong BL emission in combination with the Rluc8 and Rluc8.6-535 *renilla* luciferase variants, with brightest emission observed in the case of the 6-pi-Ph-CTZ/Rluc8.6-535 pair. With 11-fold and 25-fold stronger emission at comparable wavelengths and similar bioluminescence emission half-life times (Figure 2-9(A)-(E), Table 2-2), 6-pi-H-CTZ and 6-pi-Ph-CTZ are useful bright blue-shifted alternatives to DeepBlueC™, which is commonly applied in BRET-based assays in combination with GFP.

It has been demonstrated for the first time that an extension of the imidazopyrazinone core of native CTZ by comparably large substituents can result in Rluc variant substrates with significant BL emission.

## 2.5. Appendix

### 2.5.1. pH-Dependent chemiluminescence

The pKa value of the NH unit in the imidazopyrazinone structure has been reported as 8.3. It has been suggested that the NH of the pyrazine group dissociates to give an anion, which is oxidized by molecular oxygen and transforms via an amino dioxetanone intermediate into the coelenteramide anion in a singlet excited state. Therefore, it can be expected that under acidic condition the oxidation of coelenterazine is difficult to occur, resulting in low emission intensities. Figure 2-11(A)-(C) below show the pH-dependent chemiluminescence emission spectra for 6-pi-OH-CTZ, 6-pi-H-CTZ and 6-pi-Ph-CTZ in disodium hydrogenphosphate citric acid buffer solutions (pH3-8). Measurements have been performed under the following conditions: A CH<sub>3</sub>OH solution of the respective CTZ derivative (1 mM, 100  $\mu$ l) and the buffer solution (100  $\mu$ l) were mixed in a quartz cell and set in a fluorescence spectrophotometer. The chemiluminescence spectra were measured at a scan rate of 1200 nm/min after injecting 2 ml of DMSO. It should be noted that due to these experimental conditions, there is a time lag caused during the measurement. However, the results clearly demonstrate that chemiluminescence occurs at shorter wavelength and is weakened under acidic conditions. Only upon the addition of base, required to create the pyrazine anion, the red-shifted emission can be observed. The red-shift emission is assigned to the pyrazine anion, because only coelenterazines having a phenolic hydroxyl group on the C-6 substituent can form the pyrazine anion.

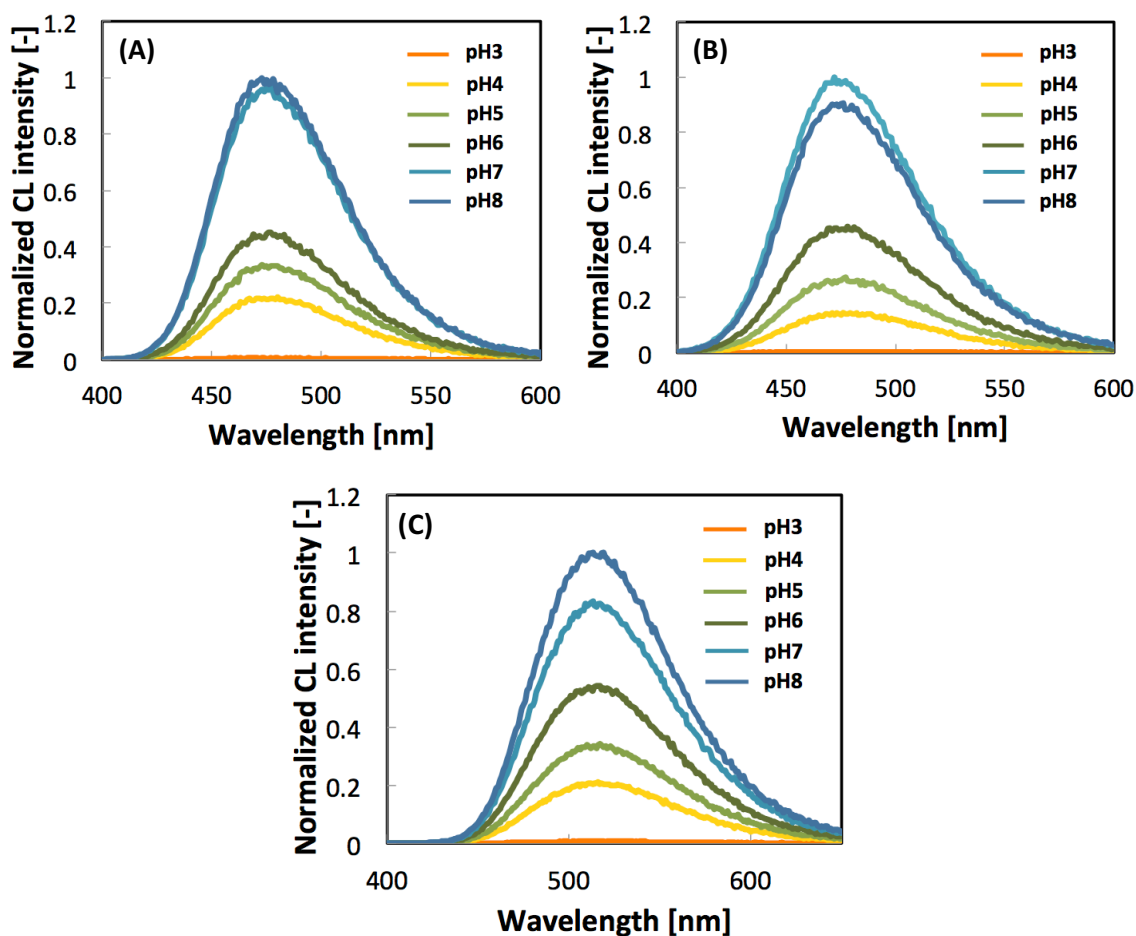


**Figure 2-11** pH dependent chemiluminescence: (A) 6-pi-OH-CTZ; (B) 6-pi-H-CTZ; (C) 6-pi-Ph-CTZ

### 2.5.2 pH-Dependent bioluminescence with several marine luciferases

The proton-driven optical intensities of marine luciferases were calculated to help elucidate the pH-bioluminescence relationship (Figure 2-12). African green monkey kidney-derived COS-7 cells were raised in a 96-well plate, and transfected with a pcDNA3.1(+) vector (Invitrogen) encoding GLuc, RLuc8.6-535, ALuc23, or ALuc34 with a lipofection reagent, TransIT-LT (Mirus). 16 h after transfection, the cells were lysed with a lysis buffer (Promega) and an aliquot of the lysates (10  $\mu$ L) in the plate were simultaneously mixed with 40  $\mu$ L of the substrate solution, which was prepared by mixing a native coelenterazine (nCTZ) or the analog (6-pi-OH-CTZ) stock (Figure 2-12(B)) with an aliquot of the universal buffer with the pH ranging from 4 to 9 (final concentration of the substrate: 0.1 mg/mL). Immediately after the substrate injection, the plate was moved into

an image analyzer (LAS-4000, FujiFilm), and the corresponding optical intensities were integrated for 30 s. The time course of the intensities was estimated every 5 min for 20 min (Figure 2-12 (D)).

The optical intensities according to the proton concentrations (pH) were determined so as to elucidate the smallest cation ( $H^+$ )-driven feature of ALuc activity (Figure 2-12). In the lower pH region, such as pH 4 and 5 (acidic condition), the optical intensities were suppressed to the background level. In contrast, the optical intensities of ALuc23 and ALuc34 were dramatically elevated at pH 7 up to *ca.* 5-fold, compared to pH 6 (Figure 2-12(C)). The ALucs sustained 51–53% of the initial optical intensities, even after 20 min at pH 9, whereas GLuc and RLuc8.6-535 showed poor optical stability and retained less than 30% of the initial intensities after 20 min (Figure 2-12(D)).

The corresponding feature of ALucs was observed even with a coelenterazine analog, 6-pi-OH-CTZ (Figure 2-12(A)). The maximal optical intensities were obtained at pH 9 and the intensities were prolonged up to 41% (ALuc23) and 60% (ALuc34) of the initial intensities, even 20 min after the substrate injection (Figure 2-13). This pH-driven elevation of ALuc activities is highly distinctive from those of other marine luciferases, such as OLuc, GLuc, *Cypridina* luciferase (CLuc) and *Periphylla* luciferase (PLuc), whose maximal optical intensities are generally found at *ca.* pH 7.5, quickly decrease at a pH higher than 8, and lose much of the intensity at *ca.* pH 9.8,<sup>35,36</sup>

Since the pKa value of the hydroxyl groups of nCTZ is *ca.* 7.6 in an aqueous phase,<sup>37</sup> nCTZ is considered to be in a deprotonated, anionic form at *ca.* pH 9 (Figure 2-12). The highest optical intensities of ALucs at pH 9 strongly suggest that ALucs provide an optical platform for accommodating anionic nCTZ and its analogs, compared to other luciferases. Because 6-pi-OH-CTZ has a double bond at C-6 position (Figure 2-12(B)), the anionic 6-pi-OH-CTZ is much more stable than the anionic nCTZ owing to the unique double bond, and optimally interacts with ALucs at the higher pH region. Actually, 6-pi-OH-CTZ added ALucs emitted the maximal intensities only at pH 9, whereas nCTZ-added ALucs showed a similar optical intensity at both pH 8

and 9 (Figure 2-12(A)).

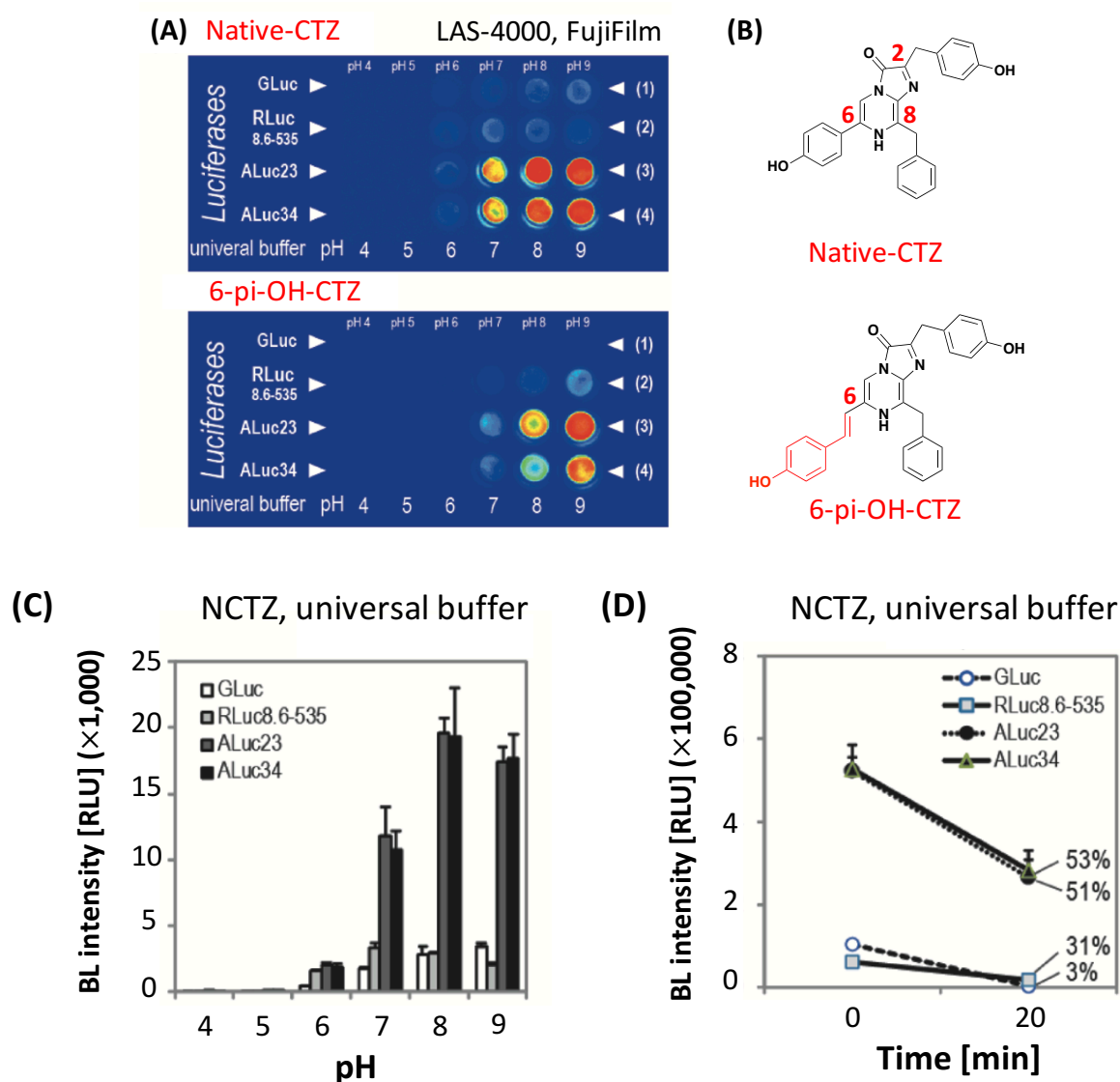


**Figure 2-12** Proton-driven optical properties of ALucs. (A) Proton-dependent elevation of the optical intensities of ALucs with native CTZ or 6-pi-OH-CTZ, imaged in pseudo-colors ( $n=3$ ; standard deviation). The images in panels are one of the results in triplicate. (B) The chemical structures of native CTZ or 6-pi-OH-CTZ. (C) Proton-dependent elevation of the optical intensities of ALucs ( $n=3$ ; standard deviation). The maximal optical intensities were found in the higher pH region. (D) The relative optical stability of ALuca and marine luciferases at pH9 ( $n=3$ ; standard deviation). The percentages indicate the sustained optical intensities in ratio 20 minutes after native-CTZ injection.

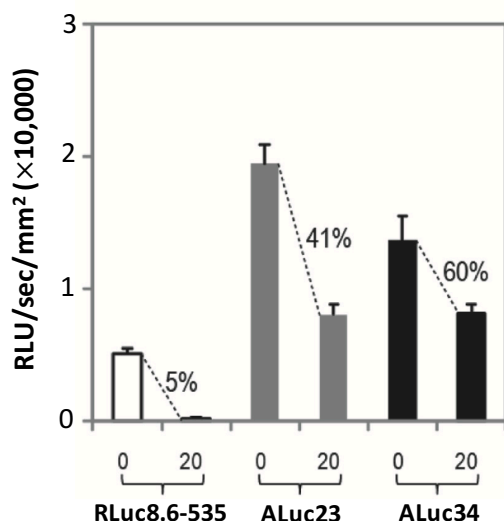


**Figure 2-13** Optical stability of luciferases with 6-pi-OH-CTZ. The percentages show the remained optical intensities after 20 minutes, compared to the initial intensities.

## References

- (1) Naylor, L. H., *Biochem. Pharmacol.*, **1999**, *58*, 749–757.
- (2) Shao, Q., Jiang, T., Ren, G., Cheng, Z. and Xing, B., *Chem. Commun.*, **2009**, 4028–4030.
- (3) Kojima, R., Takakura, H., Ozawa, T., Tada, Y., Nagano, T. and Urano, Y., *Angew. Chem., Int. Ed.*, **2013**, *52*, 1175–1179.
- (4) Sun, Y.-Q., Liu, J., Wang, P., Zhang, J. and Guo, W., *Angew. Chem., Int. Ed.*, **2012**, *51*, 8428–8430.
- (5) Yang, Y., Shao, Q., Deng, R., Wang, C., Teng, X., Cheng, K., Cheng, Z., Huang, L., Liu, Z., Liu, X. and Xing, B., *Angew. Chem., Int. Ed.*, **2012**, *51*, 3125–3129.
- (6) Lorenz, W. W., Cormier, M. L., O’Kane, D. J., Hua, D., Escher, A. A. and Szalay, A. A., *J. Biolumin. Chemilumin.*, **1996**, *11*, 31–37.
- (7) Newton, H. E., *Bioluminescence*, Academic Press, New York, **1952**.
- (8) Kim, S. B., Suzuki, H., Sato, M. and Tao, H., *Anal. Chem.*, **2011**, *83*, 8732–8740.
- (9) Goto, T., *Pure Appl. Chem.*, **1968**, *17*, 421–442.
- (10) Teranishi, K., Hisamatsu, M. and Yamada, T., *Luminescence*, **1999**, *14*, 297–302.

- (11) Nakamura, H., Wu, C., Murai, A., Inouye, S. and Shimomura, O., *Tetrahedron Lett.*, **1997**, 38, 6405–6406.
- (12) Saito, R., Hirano, T., Maki, S., Niwa, H. and Ohashi, M., *Bull. Chem. Soc. Jpn.*, **2011**, 84, 90–99.
- (13) Saito, R., Hirano, T., Niwa, H. and Ohashi, M., *Chem. Lett.*, **1998**, 27, 95–96.
- (14) Inouye, S. and Shimomura, O., *Biochem. Biophys. Res. Commun.*, **1997**, 233, 349–353.
- (15) Loening, A. M., Wu, A. M. and Gambhir, S. S., *Nat. Methods*, **2007**, 4, 641–643.
- (16) Woo, J., Howell, M. H. and von Arnim, A. G., *Protein Sci.*, **2008**, 17, 725–735.
- (17) Loening, A. M., Fenn, T. D. and Gambhir, S. S., *J. Mol. Biol.*, **2007**, 374, 1017–1028.
- (18) Qi, C. F., Gomi, Y., Hirano, T., Ohashi, M., Ohmiya, Y. and Tsuji, F. I., *J. Chem. Soc., Perkin Trans.*, **1992**, 1, 1607–1611.
- (19) De, A. and Gambhir, S. S., *FASEB J.*, **2005**, 19, 2017–2019.
- (20) Wu, C., Nakamura, H., Murai, A. and Shimomura, O., *Tetrahedron Lett.*, **2001**, 42, 2997–3000.
- (21) Vysotski, E. S., *Anal. Bioanal. Chem.*, **2010**, 398, 1809–1817.
- (22) Imai, Y., Shibata, T., Maki, S., Niwa, H., Ohashi, M. and Hirano, T., *J. Photochem. Photobiol.*, **2001**, 146, 95–107.
- (23) Shimomura, O. and Teranishi, K., *Luminescence*, **2000**, 15, 51–58.
- (24) Teranishi, K. and Shimomura, O., *Anal. Biochem.*, **1997**, 249, 37–43.
- (25) Teranishi, K., *Luminescence*, **2001**, 16, 367–374.
- (26) Teranishi, K. and Goto, T., *Bull. Chem. Soc. Jpn.*, **1990**, 63, 3132–3140.
- (27) Jiang, B., Yang, C. G., Xiong, W. N. and Wang, J., *Bioorganic & Medicinal Chemistry*, **2009**, 9, 1149.
- (28) Adamczyk, M., Akireddy, S. R., Johnson, D. D., Mattingly, P. G., Pan, Y. and Reddy, R. E., *Tetrahedron*, **2003**, 59, 8131
- (29) Adamczyk, M., Johnson, D. D., Mattingly, P. G., Pan, Y. and Reddy, R. E. *Organic Preparations and*

*Procedures International*, **2001**, 33, 477

(30) Phakhodee, W., Toyoda, M., Chou, C. M., Khunnawutmanotham, N. and Isobe, M., *Tetrahedron*, **2011**, 67, 1150-1157

(31) Shimomura, O., *Bioluminescence Chemical Principles and Methods, Revised Edition*, World Scientific Publishing, Singapore, **2012**.

(32) Fujio, S., Hashizume, D., Takamuki, Y., Yasui, M., Iwasaki, F., Maki, S., Niwa, H., Ikeda, H. and Hirano, T., *Tetrahedron Lett.*, **2004**, 45, 8531–8534.

(33) Hart, R. C., Matthews, J. C., Hori, K. and Cormier, M. J., *Biochemistry*, **1979**, 18, 2204–2210.

(34) Carriba, P., Navarro, G., Ciruela, F., Ferre, S., Casado, V. Agnati, L., Cortes, A., Mallol, J., Fuxe, K., Canela, E. I., Lluís, C. and Franco, R., *Nat. Methods*, **2008**, 5, 727–733.

(35) Ruecker, O., Zillner, K., Groebner-Ferreira, R. and Heitzer, M., *Mol. Genet. Genomics*, **2008**, 280, 153.

(36) Shimomura, O., “*Bioluminescence*”, 2006, World Scientific Publishing Co., Pte. Ltd., Singapore.

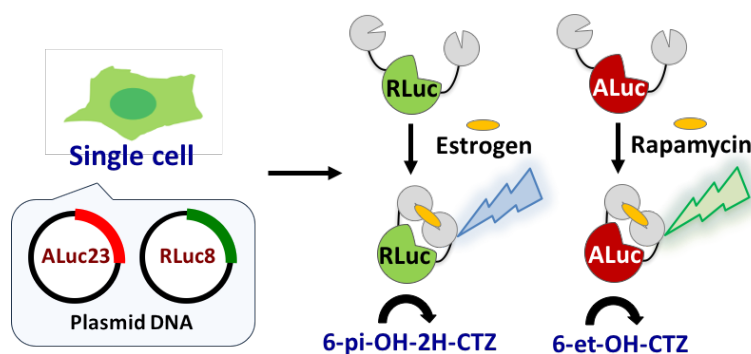
(37) Ohmiya, Y. and Hirano, T., *Chem. Biol.*, **1996**, 3, 337.

## Chapter3

# Luciferase-Specific Coelenterazine Analogues for Optical Contamination-Free Bioassays

### Summary

Spectral overlaps among the multiple optical readouts are commonly occurring optical contamination in fluorescence and bioluminescence. To fabricate optical contamination-free bioassays, I created five-different lineages of coelenterazine (CTZ) analogues designed to selectively illuminate a specific luciferase with unique luciferase selectivity. In the attempt, I found that CTZ analogues with ethynyl or styryl groups display dramatically biased bioluminescence to specific luciferases and pHs by modifying the functional groups at the C-2 and C-6 positions of the imidazopyradinone backbone of CTZ. The CTZ analogues specifically illuminate anti-estrogenic and rapamycin activities in a mixture of optical probes, although the optical spectra are almost superimposed. This unique bioluminescence platform has great potential for simultaneously imaging all optical readouts in bioassays without optical contamination.



### 3.1. Introduction

Luciferases are a family of light-generating proteins found in a large variety of insects, marine organisms and prokaryotes<sup>1</sup>. Beetle luciferases, including firefly luciferase (FLuc), mediate oxidative decarboxylation of D-luciferin in the presence of ATP, Mg<sup>2+</sup>, and O<sub>2</sub>, whereas many marine luciferases, from deep-sea organisms, utilize coelenterazine (CTZ), and require only O<sub>2</sub> for catalysis<sup>2</sup>. Luciferases have broad emission bandwidths ca. 400-620 nm with peak emission mostly in the green and yellow-green spectral region<sup>3</sup>, which creates spectral overlap when multiple marine luciferases are incorporated into the same reaction condition and concurrently activated by the same coelenterazine substrate.

Overlapping emissions from luciferases impair multiplex imaging of *in vivo* reporter assays, resulting in optical signal contamination. In contrast, fluorescent proteins have a broader color palette, but suffer from strong background due to autofluorescence. Tactical algorithms for unmixing overlapping multiple optical spectra, by a process of spectral unmixing calculations and deconvolution, have been developed<sup>4,5</sup>; however, they have not provided a fundamental solution to this problem. In addition, near-infrared fluorescent proteins (iRFPs)<sup>6</sup>, several variants of beetle and marine luciferases<sup>7,8</sup>, and red- and blue-shifted analogues of CTZ<sup>3,9</sup> have been studied, but so far have been ineffective in eliminating signal contamination in multiplex assays due to insufficient spectral shift, and/or low intensity light emission.

In order to take advantage of the high sensitivity and low background of marine luciferases, our objective was to find a solution to spectral overlap by synthesizing new CTZ analogues with isotype specificity. Here I studied 20 CTZ analogues, including 15 newly synthesized analogues, with modifications to the C-2 and C-6 functional groups (Figure 3-3), which enabled me to develop luciferase-specific analogues. In addition, I integrated this substrate-specific activation of luciferases into a two-switch assay system that further increased specificity by utilizing two single-chain probes, previously reported by our group<sup>10,11</sup>. The application of this system enabled me to selectively activate a specific luciferase, thereby preventing spectral overlap that is usually

caused by the concurrent activation of more than one luciferase. The system was designed to carry *Renilla reniformis* luciferase 8 (RLuc8) and artificial luciferases (ALucs), where ALucs were previously fabricated by 3 steps: (i) formation of an artificial sequence by extracting frequently occurring amino acid sequences from the aligned sequences of copepod luciferases, (ii) single-sequence alignment (SSA) of the artificial sequence for highlighting the repeated catalytic domains, and (iii) increase of the sequential homology between the repeated catalytic domains. The brief process was illustrated in Figure 3-1<sup>12</sup>. The maximal sequential identities of ALuc16 and ALuc25 for instance are 81% and 72% of that of *Metridia pacifica* luciferase, according to NCBI Blast Alignment Search, ver. BLASTP 2.2.27+. Their crystallographic structures are not determined yet. This method provides a breakthrough for overcoming spectral overlap by specifically determining multiple optical readouts in mixture with high throughput, and facilitates contamination-free bioassays and molecular imaging.

## 3.2. Experimental section

### 3.2.1. Design and synthesis of luciferase-specific novel CTZ analogues

RLuc and *Oplophorus* Luciferase (OLase) are reported to exert broad substrate specificities with the C-2 position-modified CTZ analogues<sup>14</sup>. Separately, I showed that RLuc8 and RLuc8.6-535 emit significant bioluminescence with C-6 position-modified CTZ analogues in Chapter 1<sup>9</sup>. This precedent study inspired me to synthesize unique CTZ analogues modified at the C-2 and/or C-6 positions.

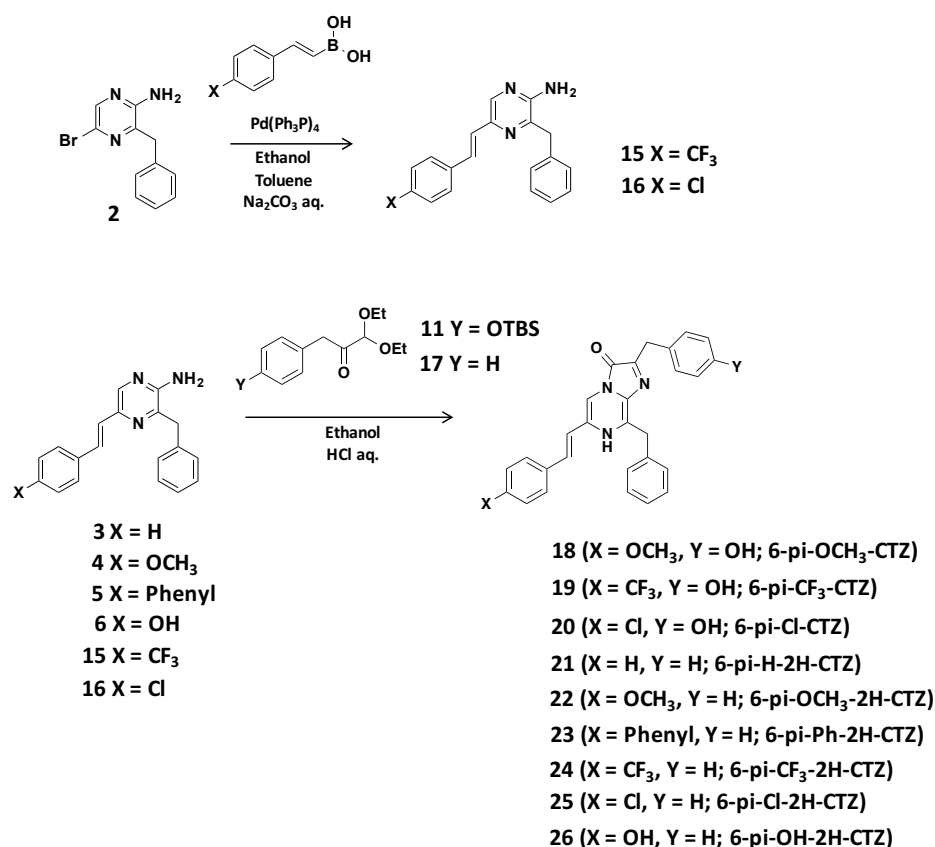
In this report, in order to fabricate CTZ analogues allowing a unique optical specificity to a marine luciferase, I synthesized a series of C2- and/or C-6-substituted CTZ analogues (Figure 3-3). The new CTZ derivatives besides conventional CTZ analogues are categorized into five groups according to the chemical structure, for convenience (Figure 3-3). The CTZ analogues are designated hereafter with the abbreviated names.

The chemical structural characteristics of the groups are as follows: compounds of Group 1 share a common

ethynyl group at the C-6 position, and a phenol group at the C-2 position. Compounds of Group 2 commonly carry a styryl group at the C-6 position, and a benzyl group at the C-2 position. Compounds of Group 3 comprise a common styryl group at the C-6 position, and a phenol group at the C-2 position. In the case of compounds of Groups 4 and 5, their chemical structures are very close to the nCTZ. The only difference of Group 4 from nCTZ is whether the OH groups at the C-6 and/or C-2 positions exist or not. The structure of Group 5 is different from nCTZ in the point that the C-8 position has a phenol group.

The newly synthesized CTZ analogues are stable when stored at -34°C, in darkness and nitrogen atmosphere.

The CTZ analogues are unstable in DMSO.



Synthetic scheme for the synthetic coelenterazine analogues (6-pi-CTZ series). Compounds **2**, **3**, **4**, **5**, **6**, **11** and **17** were synthesized based on reported procedures<sup>9,1-3</sup>.

**(E)-3-Benzyl-5-(4-(trifluoromethyl)styryl)pyrazin-2-amine (15)**

3-Benzyl-5-bromopyrazine-2-amine (**2**) (250 mg, 0.95 mmol, 1 eq.) and (*E*)-(4-trifluoromethylstyryl)boronic acid (328.3 mg, 1.52 mmol, 1.6 eq.) were dissolved in toluene (13.9 ml) and stirred at room temperature. Ethanol (2.1 ml) and 1 M Na<sub>2</sub>CO<sub>3</sub> aq. (5 ml) were added into the reaction mixture. After vacuum deaeration, a catalytic amount of tetrakis(triphenylphosphine)palladium(0) was added into the solution and the mixture was deaerated again and stirred for 11 hours at 100 °C. After cooling to room temperature, the solution was filtered through a Celite pad to remove the palladium catalyst. The solution was extracted with ethyl acetate, and the brown organic phase was washed with water and brine, dried over Na<sub>2</sub>SO<sub>4</sub> and evaporated. The resulting residue was purified by flash chromatography (silica gel, eluent composition: n-hexane / ethyl acetate = 80/20 to 50/50), affording (*E*)-3-benzyl-5-(4-trifluoromethylstyryl)pyrazine-2-amine (**15**) as a yellow solid (179.0 mg, 53%).

<sup>1</sup>H-NMR (500 MHz, CDCl<sub>3</sub>): δ (ppm) = 7.96 (s, 1H), 7.22-7.46 (m, 10H), 7.27 (d, *J* = 15.9 Hz, 1H), 4.59 (s, 2H), 4.13 (s, 2H). <sup>13</sup>C-NMR (125 MHz, CDCl<sub>3</sub>): δ (ppm) = 41.49, 125.74, 125.77, 126.87, 127.22, 127.34, 127.99, 128.64, 129.22, 136.53, 140.18, 140.51, 140.77, 141.39, 152.21. HR-MS: calcd for C<sub>20</sub>H<sub>16</sub>F<sub>3</sub>N<sub>3</sub>: 356.1375 [M+H]<sup>+</sup>, found: *m/z* 356.1357.

**(E)-3-Benzyl-5-(4-chlorostyryl)pyrazin-2-amine (16)**

3-Benzyl-5-bromopyrazine-2-amine (**2**) (155 mg, 0.57 mmol, 1 eq.) and (*E*)-(4-chlorostyryl)boronic acid (165.75 mg, 0.91 mmol, 1.6 eq.) were dissolved in toluene (10.7 ml) and stirred at room temperature. Ethanol (1.5 ml) and 1 M Na<sub>2</sub>CO<sub>3</sub> aq. (3.6 ml) were added into the reaction mixture. After vacuum deaeration, a catalytic amount of tetrakis(triphenylphosphine)palladium(0) was added into the solution and the mixture was deaerated again and stirred for 13 hours at 100 °C. After cooling to room temperature, the solution was filtered through a Celite pad to remove the palladium catalyst. The solution was extracted with ethyl acetate, and the brown

organic phase was washed with water and brine, dried over Na<sub>2</sub>SO<sub>4</sub> and evaporated. The resulting residue was purified by flash chromatography (silica gel, eluent composition: n-hexane / ethyl acetate = 50/50), affording (*E*)-3-benzyl-5-(4-chlorostyryl)pyrazine-2-amine (**16**) as a yellow solid (151.6 mg, 82%).

<sup>1</sup>H-NMR (500 MHz, CDCl<sub>3</sub>): δ (ppm) = 8.01 (s, 1H), 7.49-7.25 (m, 11H), 7.06 (d, *J* = 16.04 Hz, 1H), 4.43 (s, 2H), 4.16 (s, 2H). <sup>13</sup>C-NMR (125 MHz, CDCl<sub>3</sub>): δ (ppm) = 41.45, 125.39, 127.27, 127.97, 128.31, 128.62, 128.96, 129.17, 133.37, 135.78, 136.61, 139.74, 140.90, 141.25, 151.96. HR-MS: calcd for C<sub>19</sub>H<sub>16</sub>ClN<sub>3</sub>: 322.1111 [M+H]<sup>+</sup>, found: *m/z* 322.1096.

**(*E*)-8-Benzyl-2-(4-hydroxybenzyl)-6-(4-methoxystyryl)imidazo[1,2-*a*]pyrazin-3(7*H*)-one (**18**; 6piOMe-CTZ)**

(*E*)-3-Benzyl-5-(4-methoxystyryl)pyrazin-2-amine (**4**) (30 mg, 0.09 mmol, 1 eq.) and ketoacetal (**11**) (66.64 mg, 0.18 mmol, 2 eq.) were dissolved in ethanol (2.0 ml) and H<sub>2</sub>O (0.2 ml) and stirred at room temperature. After vacuum deaeration, the solution was cooled to 0 °C and HCl (0.1 ml) was added under nitrogen flow. Once the solution reached room temperature, it was heated and stirred for 14 hours at 80 °C. The solvent was evaporated under vacuum and the crude compound was purified by semipreparative reversed-phase HPLC (eluent composition: MeOH / H<sub>2</sub>O = 25/75 with 0.1% formic acid), affording (*E*)-8-benzyl-2-(4-hydroxybenzyl)-6-(4-methoxystyryl)imidazo[1,2-*a*]pyrazin-3(7*H*)-one (**18**) as a yellow solid (7.34 mg, 16%).

<sup>1</sup>H-NMR (500 MHz, CD<sub>3</sub>OD, CDCl<sub>3</sub>): δ (ppm) = 7.51 (s, 1H), 7.42-7.14 (m, 11H), 6.88 (d, *J* = 7.16 Hz, 2H), 6.77 (s, 1H), 6.69 (d, *J* = 6.87 Hz, 2H), 4.37 (s, 2H), 4.03 (s, 2H), 3.78 (s, 3H). <sup>13</sup>C-NMR (125 MHz, CDCl<sub>3</sub>): δ (ppm) = 54.42, 113.93, 114.88, 126.87, 127.87, 128.35, 128.46, 128.72, 129.51, 136.68, 155.68, 160.311. HR-MS: calcd for C<sub>29</sub>H<sub>26</sub>N<sub>3</sub>O<sub>3</sub>: 464.1974 [M+H]<sup>+</sup>, found: *m/z* 468.1977.

**(E)-8-Benzyl-2-(4-hydroxybenzyl)-6-(4-(trifluoromethyl)styryl)imidazo[1,2-*a*]pyrazin-3(7*H*)-one (19; 6piCF<sub>3</sub>-CTZ)**

(*E*)-3-Benzyl-5-(4-(trifluoromethyl)styryl)pyrazin-2-amine (**15**) (34.2 mg, 0.09 mmol, 1 eq.) and ketoacetal (**11**) (67.85 mg, 0.19 mmol, 2 eq.) were dissolved in ethanol (2.0 ml) and H<sub>2</sub>O (0.2 ml) and stirred at room temperature. After vacuum deaeration, the solution was cooled to 0 °C and HCl (0.1 ml) was added under nitrogen flow. Once the solution reached room temperature, it was heated and stirred for 6 hours at 80 °C. The solvent was evaporated under vacuum and the crude compound was purified by silica column chromatography (eluent composition: n-hexane / ethyl acetate = 50/50 to ethyl acetate to ethyl acetate / methanol = 20 /1), affording (*E*)-8-benzyl-2-(4-hydroxybenzyl)-6-(4-(trifluoromethyl)styryl)imidazo[1,2-*a*]pyrazin-3(7*H*)-one (**19**) as a yellow solid (11.99 mg, 29%).

<sup>1</sup>H-NMR (500 MHz, CD<sub>3</sub>OD): δ (ppm) = 7.66-7.61 (m, 5H), 7.37-7.19 (m, 6H), 7.13 (d, *J* = 8.59 Hz, 2H), 7.06 (d, *J* = 16.32 Hz, 1H), 6.68 (d, *J* = 8.59 Hz, 2H), 4.37 (s, 2H), 4.02 (s, 2H). <sup>13</sup>C-NMR (125 MHz, CD<sub>3</sub>OD): δ (ppm) = 33.35, 34.99, 111.55, 116.21, 123.57, 124.56, 126.71, 126.74, 127.96, 128.15, 129.48, 129.58, 129.71, 129.75, 129.92, 130.51, 130.69, 130.80, 130.95, 138.05, 141.44, 157.00. HR-MS: calcd for C<sub>29</sub>H<sub>23</sub>F<sub>3</sub>N<sub>3</sub>O<sub>2</sub>: 502.1742 [M+H]<sup>+</sup>, found: *m/z* 502.1767.

**(E)-8-Benzyl-6-(4-chlorostyryl)-2-(4-hydroxybenzyl)imidazo[1,2-*a*]pyrazin-3(7*H*)-one (20; 6piCl-CTZ)**

(*E*)-3-Benzyl-5-(4-chlorostyryl)pyrazin-2-amine (**16**) (40 mg, 0.12 mmol, 1 eq.) and ketoacetal (**11**) (87.63 mg, 0.24 mmol, 2 eq.) were dissolved in ethanol (3.0 ml) and H<sub>2</sub>O (0.3 ml) and stirred at room temperature. After vacuum deaeration, the solution was cooled to 0 °C and HCl (0.2 ml) was added under nitrogen flow. Once the solution reached room temperature, it was heated and stirred for 4 hours at 80 °C. The solvent was evaporated under vacuum and the crude compound was purified by silica column chromatography (eluent composition: dichloromethane / methanol = 20/1), affording (*E*)-8-benzyl-6-(4-chlorostyryl)-2-(4-

hydroxybenzyl)imidazo[1,2-*a*]pyrazin-3(7*H*)-one (**20**) as a yellow solid (22.97 mg, 39%).

<sup>1</sup>H-NMR (500 MHz, CD<sub>3</sub>OD, CDCl<sub>3</sub>): δ (ppm) = 7.48 (s, 1H), 7.42 (d, *J* = 8.59 Hz, 2H), 7.38-7.22 (m, 7H), 7.20 (d, *J* = 8.59 Hz, 2H), 7.12 (d, 1H), 6.79 (d, *J* = 16.32 Hz, 1H), 6.74 (d, *J* = 8.59 Hz, 2H), 4.36 (s, 2H), 4.08 (s, 2H). <sup>13</sup>C-NMR (125 MHz, CD<sub>3</sub>OD, CDCl<sub>3</sub>): δ (ppm) = 33.18, 109.75, 109.84, 115.70, 127.64, 128.32, 129.09, 129.17, 129.41, 129.65, 130.29, 134.60, 136.84, 155.83. HR-MS: calcd for C<sub>28</sub>H<sub>23</sub>ClN<sub>3</sub>O<sub>2</sub>: 468.1479 [M+H]<sup>+</sup>, found: *m/z* 468.1458.

**(*E*)-2,8-Dibenzyl-6-styrylimidazo[1,2-*a*]pyrazin-3(7*H*)-one (21; 6piH-2H-CTZ)**

(*E*)-3-Benzyl-5-styrylpyrazin-2-amine (**3**) (40.00 mg, 0.13 mmol, 1 eq.) and ketoacetal (**17**) (61.88 mg, 0.27 mmol, 2 eq.) were dissolved in ethanol (3.0 ml) and H<sub>2</sub>O (0.3 ml) and stirred at room temperature. After vacuum deaeration, the solution was cooled to 0 °C and HCl (0.2 ml) was added under nitrogen flow. Once the solution reached room temperature, it was heated and stirred for 3.5 hours at 80 °C. The solvent was evaporated under vacuum and the crude compound was purified by silica column chromatography (eluent composition: dichloromethane / methanol = 20/1), affording (*E*)-2,8-dibenzyl-6-styrylimidazo[1,2-*a*]pyrazin-3(7*H*)-one (**21**) as a yellow solid (32.06 mg, 44%)

<sup>1</sup>H-NMR (500 MHz, CD<sub>3</sub>OD): δ (ppm) = 7.48-7.15 (m, 17H), 6.80 (d, *J* = 16.61 Hz, 1H), 4.36 (s, 2H), 4.17 (s, 2H). <sup>13</sup>C-NMR (125 MHz, CD<sub>3</sub>OD, CDCl<sub>3</sub>): δ (ppm) = 33.92, 34.17, 109.50, 109.68, 119.02, 119.50, 126.90, 127.20, 127.55, 127.76, 128.96, 129.12, 129.22, 129.28, 129.35, 129.38, 131.41, 136.55, 136.99, 138.88, 153.24. HR-MS: calcd for C<sub>28</sub>H<sub>24</sub>N<sub>3</sub>O: 418.1919 [M+H]<sup>+</sup>, found: *m/z* 418.1910.

**(*E*)-2,8-Dibenzyl-6-(4-methoxystyryl)imidazo[1,2-*a*]pyrazin-3(7*H*)-one (22; 6piOMe-2H-CTZ)**

(*E*)-3-Benzyl-5-(4-methoxystyryl)pyrazin-2-amine (**4**) (42.85 mg, 0.13 mmol, 1 eq.) and ketoacetal (**17**) (60.01 mg, 0.27 mmol, 2 eq.) were dissolved in ethanol (3.0 ml) and H<sub>2</sub>O (0.3 ml) and stirred at room

temperature. After vacuum deaeration, the solution was cooled to 0 °C and HCl (0.2 ml) was added under nitrogen flow. Once the solution reached room temperature, it was heated and stirred for 15 hours at 80 °C. The solvent was evaporated under vacuum and the crude compound was purified by silica column chromatography (eluent composition: dichloromethane / methanol = 20/1), affording (*E*)-2,8-dibenzyl-6-(4-methoxystyryl)imidazo[1,2-*a*]pyrazin-3(7*H*)-one (**22**) as a yellow solid (31.4 mg, 51%).

<sup>1</sup>H-NMR (500 MHz, CD<sub>3</sub>OD, CDCl<sub>3</sub>): δ (ppm) = 7.50 (s, 1H), 7.43 (d, *J* = 8.59 Hz, 2H), 7.39-7.15 (m, 11H), 6.90 (d, *J* = 8.88 Hz, 2H), 6.72 (d, *J* = 16.32 Hz, 1H), 4.38 (s, 2H), 4.17 (s, 2H), 3.33 (s, 3H). <sup>13</sup>C-NMR (125 MHz, CD<sub>3</sub>OD, CDCl<sub>3</sub>): δ (ppm) = 30.35, 34.22, 55.66, 109.20, 114.97, 127.04, 127.90, 128.73, 128.81, 129.03, 129.12, 129.36, 129.44, 129.52, 129.58, 131.39, 131.97, 137.28, 139.18. HR-MS: calcd for C<sub>29</sub>H<sub>26</sub>N<sub>3</sub>O<sub>2</sub>: 448.2025 [M+H]<sup>+</sup>, found: *m/z* 448.2035.

**(*E*)-6-(2-([1,1'-Biphenyl]-4-yl)vinyl)-2,8-dibenzylimidazo[1,2-*a*]pyrazin-3(7*H*)-one (23; 6piPh-2H-CTZ)**

(*E*)-5-(2-([1,1'-Biphenyl]-4-yl)vinyl)-3-benzylpyrazin-2-amine (**5**) (30.00 mg, 0.11 mmol, 1 eq.) and ketoacetal (**17**) (50.49 mg, 0.22 mmol, 2 eq.) were dissolved in ethanol (2.0 ml) and H<sub>2</sub>O (0.2 ml) and stirred at room temperature. After vacuum deaeration, the solution was cooled to 0 °C and HCl (0.1 ml) was added under nitrogen flow. Once the solution reached room temperature, it was heated and stirred for 6 hours at 80 °C. The solvent was evaporated under vacuum and the crude compound was purified by silica column chromatography (eluent composition: ethyl acetate), affording (*E*)-6-(2-([1,1'-biphenyl]-4-yl)vinyl)-2,8-dibenzylimidazo[1,2-*a*]pyrazin-3(7*H*)-one (**23**) as yellow solid (13.36 mg, 24%)

<sup>1</sup>H-NMR (500 MHz, CD<sub>3</sub>OD, CDCl<sub>3</sub>): δ (ppm) = 7.61-7.16 (m, 21H), 6.89 (d, *J* = 16.32 Hz, 1H), 4.39 (s, 2H), 4.16 (s, 2H). <sup>13</sup>C-NMR (125 MHz, CD<sub>3</sub>OD, CDCl<sub>3</sub>): δ (ppm) = 34.17, 110.02, 127.08, 127.48, 127.93, 128.06, 128.24, 129.14, 129.39, 129.47, 129.53, 131.16, 135.88, 137.25, 139.11, 141.12, 142.13. HR-MS: calcd for C<sub>34</sub>H<sub>27</sub>N<sub>3</sub>O: 494.2232 [M+H]<sup>+</sup>, found: *m/z* 494.2220.

**(E)-2,8-Dibenzyl-6-(4-(trifluoromethyl)styryl)imidazo[1,2-*a*]pyrazin-3(7*H*)-one (24; 6piCF<sub>3</sub>-2H-CTZ)**

(*E*)-3-Benzyl-5-(4-(trifluoromethyl)styryl)pyrazin-2-amine (**15**) (30.00 mg, 0.08 mmol, 1 eq.) and ketoacetal (**17**) (35.56 mg, 0.16 mmol, 2 eq.) were dissolved in ethanol (2.0 ml) and H<sub>2</sub>O (0.2 ml) and stirred at room temperature. After vacuum deaeration, the solution was cooled to 0 °C and HCl (0.1 ml) was added under nitrogen flow. Once the solution reached room temperature, it was heated and stirred for 4 hours at 80 °C. The solvent was evaporated under vacuum and the crude compound was purified by silica column chromatography (eluent composition: chloroform / methanol = 20/1), affording (*E*)-2,8-dibenzyl-6-(4-(trifluoromethyl)styryl)imidazo[1,2-*a*]pyrazin-3(7*H*)-one (**24**) as yellow solid (22.58 mg, 58%)

<sup>1</sup>H-NMR (500 MHz, CDCl<sub>3</sub>): δ (ppm) = 7.62-6.95 (m, 17H), 6.57 (s, 1H), 4.38 (s, 2H), 4.10 (s, 2H). <sup>13</sup>C-NMR (125 MHz, CDCl<sub>3</sub>): δ (ppm) = 34.45, 109/96, 123.01, 125.17, 125.81, 126.49, 126.72, 127.22, 127.33, 127.48, 128.28, 128.49, 128.64, 128.91, 129.14, 129.28, 129.91, 130.17, 136.18, 138.16, 139.22. HR-MS: calcd for C<sub>29</sub>H<sub>23</sub>F<sub>3</sub>N<sub>3</sub>O: 486.1793 [M+H]<sup>+</sup>, found: *m/z* 486.1764.

**(E)-2,8-Dibenzyl-6-(4-chlorostyryl)imidazo[1,2-*a*]pyrazin-3(7*H*)-one (25; 6piCl-2H-CTZ)**

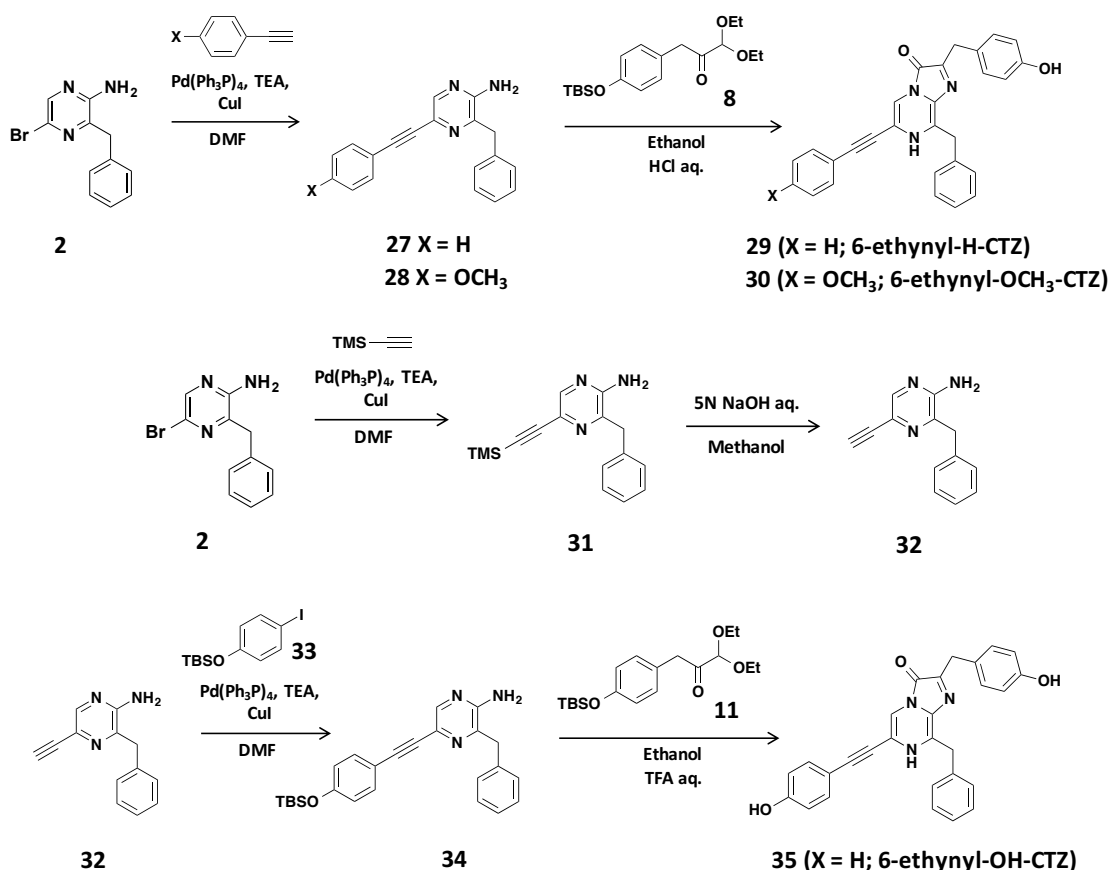
(*E*)-3-Benzyl-5-(4-chlorostyryl)pyrazin-2-amine (**16**) (40.21 mg, 0.12 mmol, 1 eq.) and ketoacetal (**9**) (55.54 mg, 0.24 mmol, 2 eq.) were dissolved in ethanol (3.0 ml) and H<sub>2</sub>O (0.3 ml) and stirred at room temperature. After vacuum deaeration, the solution was cooled to 0 °C and HCl (0.2 ml) was added under nitrogen flow. Once the solution reached room temperature, it was heated and stirred for 3.5 hours at 80 °C. The solvent was evaporated under vacuum and the crude compound was purified by silica column chromatography (eluent composition: dichloromethane / methanol = 20/1), affording (*E*)-2,8-dibenzyl-6-(4-chlorostyryl)imidazo[1,2-*a*]pyrazin-3(7*H*)-one (**25**) as yellow solid (15.32 mg, 27 %)

<sup>1</sup>H-NMR (500 MHz, CD<sub>3</sub>OD, CDCl<sub>3</sub>): δ (ppm) = 7.54 (s, 1H), 7.44 (d, *J* = 8.31 Hz, 2H), 7.39-7.16 (m, 13H), 6.85 (d, *J* = 16.32 Hz, 1H), 4.38 (s, 2H), 4.17 (s, 2H). <sup>13</sup>C-NMR (125 MHz, CD<sub>3</sub>OD, CDCl<sub>3</sub>): δ (ppm)

= 14.35, 34.23, 110.20, 120.32, 127.00, 127.43, 127.85, 128.61, 129.07, 129.31, 129.38, 129.47, 129.61, 130.10, 134.83, 135.47, 137.15, 139.02. HR-MS: calcd for C<sub>28</sub>H<sub>22</sub>ClN<sub>3</sub>O: 452.1530 [M+H]<sup>+</sup>, found: *m/z* 452.1510.

**(*E*)-2,8-Dibenzyl-6-(4-hydroxystyryl)imidazo[1,2-*a*]pyrazin-3(7*H*)-one (26; 6piOH-2H-CTZ)**

(*E*)-4-(2-(5-Amino-6-benzylpyrazin-2-yl)vinyl)phenol (**6**) (40 mg, 0.13 mmol, 1 eq.) and ketoacetal (**17**) (58 mg, 0.26 mmol, 2 eq.) were dissolved in ethanol (2.0 ml) and H<sub>2</sub>O (0.2 ml) and stirred at room temperature. After vacuum deaeration, the solution was cooled to 0 °C and HCl (0.1 ml) was added under nitrogen flow. Once the solution reached room temperature, it was heated and stirred for 5 hours at 80 °C. The solvent was evaporated under vacuum and the crude compound was purified by silica column chromatography (eluent composition: n-hexane / ethyl acetate = 50/50 to ethyl acetate to ethyl acetate / methanol = 20 /1), affording (*E*)-2,8-dibenzyl-6-(4-hydroxystyryl)imidazo[1,2-*a*]pyrazin-3(7*H*)-one (**26**) as a yellow solid (27.83 mg, 49%).  
<sup>1</sup>H-NMR (500 MHz, CD<sub>3</sub>OD): δ (ppm) = 7.42 (s, 1H), 7.35-7.10 (m, 12H), 7.05 (d, *J* = 16.6 Hz, 1H), 6.73 (d, *J* = 8.6 Hz, 2H), 6.56 (d, *J* = 16.6 Hz, 2H), 4.31 (s, 2H), 4.08 (s, 2H) <sup>13</sup>C-NMR (125 MHz, CD<sub>3</sub>OD): δ (ppm) = 34.3, 34.5, 109.3, 116.6, 127.3, 128.1, 128.8, 129.2, 129.4, 129.6, 129.7, 129.8, 132.0, 137.9, 139.7, 159.3. HR-MS: calcd for C<sub>28</sub>H<sub>24</sub>N<sub>3</sub>O<sub>2</sub>: 434.1869 [M+H]<sup>+</sup>, found: *m/z* 434.1857.



Synthetic scheme for the synthetic coelenterazine analogues (6-ethyl-CTZ series). Compounds **27**, **28** and **33**

were synthesized based on reported procedures<sup>20, 21</sup>.

### 3-Benzyl-5-(phenylethynyl)pyrazin-2-amine (**27**)

3-Benzyl-5-bromopyrazin-2-amine (**2**) (160.00 mg, 0.60 mmol, 1 eq.) was dissolved in DMF (12.8 ml) and TEA (1.0 ml) and stirred at room temperature. Phenylacetylene (0.20 ml, 1.82 mmol, 3 eq.) was added into the reaction mixture. After vacuum deaeration, a catalytic amount of tetrakis(triphenylphosphine)palladium(0) and CuI was added into the solution and the mixture was deaerated again and stirred for 18 hours at 120 °C. After cooling to room temperature, the solution was filtered through a Celite pad to remove the catalysts. The solution was extracted with ethyl acetate, and the organic phase was washed with water and brine, dried over Na<sub>2</sub>SO<sub>4</sub> and evaporated. The resulting residue was purified by flash chromatography (silica gel, eluent composition: n-hexane / ethyl acetate = 67/33), affording 3-benzyl-5-(phenylethynyl)pyrazin-2-amine (**27**) as a yellow solid

(163.0 mg, 94%).

<sup>1</sup>H-NMR (500 MHz, CDCl<sub>3</sub>): δ (ppm) = 8.21 (s, 1H), 7.56-7.62 (m, 2H), 7.33-7.37 (m, 2H), 4.54 (s, 2H), 4.17 (s, 2H). <sup>13</sup>C-NMR (125 MHz, CDCl<sub>3</sub>): δ (ppm) = 41.24, 86.54, 89.90, 122.54, 127.22, 128.36, 128.39, 128.55, 129.09, 131.73, 136.03, 141.17, 144.36, 151.68. HR-MS: calcd for C<sub>19</sub>H<sub>15</sub>N<sub>3</sub>: 286.1344 [M+H]<sup>+</sup>, found: *m/z* 286.1331.

### 3-Benzyl-5-((4-methoxyphenyl)ethynyl)pyrazin-2-amine (28)

3-Benzyl-5-bromopyrazine-2-amine (**2**) (154.00 mg, 0.58 mmol, 1 eq.) was dissolved in DMF (12.0 ml) and TEA (1.0 ml) and stirred at room temperature. p-Ethynylanisole (0.23 ml, 1.72 mmol, 3 eq.) was added into the reaction mixture. After vacuum deaeration, a catalytic amount of tetrakis(triphenylphosphine)palladium(0) and CuI was added into the solution and the mixture was deaerated again and stirred for 14 hours at 120 °C. After cooling to room temperature, the solution was filtered through a Celite pad to remove the catalysts. The solution was extracted with ethyl acetate, and the organic phase was washed with water and brine, dried over Na<sub>2</sub>SO<sub>4</sub> and evaporated. The resulting residue was purified by flash chromatography (silica gel, eluent composition: n-hexane / ethyl acetate = 67/33), affording 3-benzyl-5-((4-methoxyphenyl)ethynyl)pyrazin-2-amine (**28**) as a yellow solid (181.0 mg, 98%).

<sup>1</sup>H-NMR (500 MHz, CDCl<sub>3</sub>): δ (ppm) = 8.18 (s, 1H), 7.53 (d, *J* = 8.4 Hz, 2H), 7.24-7.35 (m, 5H), 6.89 (d, *J* = 8.4 Hz, 2H), 4.50 (s, 2H), 4.16 (s, 2H), 3.84 (s, 3H). <sup>13</sup>C-NMR (125 MHz, CDCl<sub>3</sub>): δ (ppm) = 41.27, 55.25, 85.29, 90.00, 113.90, 113.97, 114.61, 127.20, 128.42, 129.08, 133.26, 136.12, 141.10, 141.14, 151.48, 159.83. HR-MS: calcd for C<sub>20</sub>H<sub>17</sub>N<sub>3</sub>O: 316.1450 [M+H]<sup>+</sup>, found: *m/z* 316.1442.

### 8-Benzyl-2-(4-hydroxybenzyl)-6-(phenylethynyl)imidazo[1,2-*a*]pyrazin-3(7*H*)-one (29, 6etH-CTZ)

3-Benzyl-5-(phenylethynyl)pyrazin-2-amine (**27**) (49.9 mg, 0.17 mmol, 1 eq.) and ketoacetal (**11**) (128.0 mg,

0.36 mmol, 2.1 eq.) were dissolved in ethanol (3.3 ml) and H<sub>2</sub>O (0.3 ml) and stirred at room temperature. After vacuum deaeration, the solution was cooled to 0 °C and TFA (0.2 ml) was added under nitrogen flow. Once the solution reached room temperature, it was heated and stirred for 4 hours at 70 °C. The solvent was evaporated under vacuum and the crude compound was purified by silica column chromatography (eluent composition: dichloromethane / methanol = 30/1 to 15/1) and chromatograph on a ODS plate (eluent composition: acetonitrile / H<sub>2</sub>O = 50/50), affording 8-benzyl-2-(4-hydroxybenzyl)-6-(phenylethynyl)imidazo[1,2-*a*]pyrazin-3(7*H*)-one (**29**) as yellow solid (11.9 mg, 16%).

<sup>1</sup>H-NMR (500 MHz, CD<sub>3</sub>OD): δ (ppm) = 7.69 (s, 1H), 7.23-7.31 (m, 5H), 7.36-7.55 (m, 5H), 7.16 (d, *J* = 8.2 Hz, 2H), 6.69 (d, *J* = 8.2 Hz, 2H), 4.31 (s, 2H), 4.06 (s, 2H). <sup>13</sup>C-NMR (125 MHz, CD<sub>3</sub>OD, CDCl<sub>3</sub>): δ (ppm) = 33.45, 35.17, 82.07, 93.55, 115.50, 116.04, 122.64, 127.41, 128.00, 129.37, 129.50, 129.53, 129.70, 130.27, 130.27, 130.68, 132.49, 137.73, 156.55. HR-MS: calcd for C<sub>28</sub>H<sub>21</sub>N<sub>3</sub>O<sub>2</sub>: 430.1556 [M-H]<sup>-</sup>, found: *m/z* 430.1557.

**8-Benzyl-2-(4-hydroxybenzyl)-6-((4-methoxyphenyl)ethynyl)imidazo[1,2-*a*]pyrazin- 3(7*H*)-one (30, 6etOMe-CTZ)**

3-Benzyl-5-((4-methoxyphenyl)ethynyl)pyrazin-2-amine (**28**) (29.7 mg, 0.09 mmol, 1 eq.) and ketoacetal (**11**) (67.1 mg, 0.19 mmol, 2.1 eq.) were dissolved in ethanol (2.0 ml) and H<sub>2</sub>O (0.1 ml) and stirred at room temperature. After vacuum deaeration, the solution was cooled to 0 °C and TFA (0.2 ml) was added under nitrogen flow. Once the solution reached room temperature, it was heated and stirred for 4.5 hours at 70 °C. The solvent was evaporated under vacuum and the crude compound was purified by silica column chromatography (eluent composition: dichloromethane / methanol = 30/1 to 20/1) and reversed phase PLC (eluent composition: acetonitrile / H<sub>2</sub>O = 50/50), affording 8-benzyl-2-(4-hydroxybenzyl)-6-((4-methoxyphenyl)ethynyl)imidazo[1,2-*a*]pyrazin-3(7*H*)-one (**30**) as yellow solid (7.96 mg, 18%).

$^1\text{H-NMR}$  (500 MHz,  $\text{CD}_3\text{OD}$ ):  $\delta$  (ppm) = 7.63 (s, 1H), 7.48 (d,  $J$  = 8.8 Hz, 2H), 7.23-7.37 (m, 5H), 7.15 (d,  $J$  = 8.5 Hz, 2H), 6.94 (d,  $J$  = 8.8 Hz, 2H), 6.69 (d,  $J$  = 8.5 Hz, 2H), 4.31 (s, 2H), 4.06 (s, 2H), 3.82 (s, 3H).  $^{13}\text{C-NMR}$  (125 MHz,  $\text{CD}_3\text{OD}$ ):  $\delta$  (ppm) = 33.63, 34.86, 80.27, 94.45, 114.48, 114.91, 115.33, 115.61, 116.19, 127.48, 128.23, 129.75, 129.81, 130.64, 130.85, 132.73, 134.31, 137.83, 156.97, 162.13. HR-MS: calcd for  $\text{C}_{29}\text{H}_{23}\text{N}_3\text{O}_3$ : 460.1661 [M-H] $^-$ , found:  $m/z$  460.1673.

### 3-Benzyl-5-((trimethylsilyl)ethynyl)pyrazin-2-amine (31)

3-Benzyl-5-bromopyrazine-2-amine (**2**) (267.00 mg, 1.01 mmol, 1 eq.) was dissolved in DMF (12.0 ml) and TEA (1.5 ml) and stirred at room temperature. Ethynyltrimethylsilane (0.57 ml, 4.03 mmol, 4 eq.) was added into the reaction mixture. After vacuum deaeration, a catalytic amount of tetrakis(triphenylphosphine)palladium(0) and CuI was added into the solution and the mixture was deaerated again and stirred for 20.5 hours at 120 °C. After cooling to room temperature, the solution was filtered through a Celite pad to remove the catalysts. The solution was extracted with ethyl acetate, and the organic phase was washed with water and brine, dried over  $\text{Na}_2\text{SO}_4$  and evaporated. The resulting residue was purified by flash chromatography (silica gel, eluent composition: n-hexane / ethyl acetate = 67/33), affording 3-benzyl-5-((trimethylsilyl)ethynyl)pyrazin-2-amine (**31**) as a yellow solid (188.7 mg, 66%).  $^1\text{H-NMR}$  (400 MHz,  $\text{CDCl}_3$ ):  $\delta$  (ppm) = 8.13 (s, 1H), 7.20-7.32 (m, 5H), 4.54 (s, 2H), 4.13 (s, 2H), 0.28 (s, 9H).

### 3-Benzyl-5-ethynylpyrazin-2-amine (32)

3-Benzyl-5-((trimethylsilyl)ethynyl)pyrazin-2-amine (**31**) (99.9 mg, 0.35 mmol, 1 eq.) was dissolved in methanol (5.0 ml) and stirred at room temperature. 5N NaOH aq. (0.25 ml, 1.00 mmol, 2.81 eq.) was added into the reaction mixture and stirred at room temperature for 3 hours. 1N HCl aq. was added into the reaction to quench and evaporated to dryness. The residue was dissolved and extracted with ethyl acetate, and the organic

layer was washed with water and brine, dried over Na<sub>2</sub>SO<sub>4</sub>, and evaporated. The resulting residue was purified by flash chromatography (silica gel, eluent composition: n-hexane / ethyl acetate = 67/33), affording 3-benzyl-5-ethynylpyrazin-2-amine (**32**) as a yellow solid (66.8 mg, 90%).

<sup>1</sup>H-NMR (400 MHz, CDCl<sub>3</sub>): δ (ppm) = 8.14 (s, 1H), 7.22-7.33 (m, 5H), 4.56 (s, 2H), 4.13 (s, 2H), 3.21 (s, 1H). HR-MS: calcd for C<sub>13</sub>H<sub>11</sub>N<sub>3</sub>: 210.1031 [M+H]<sup>+</sup>, found: *m/z* 210.1029.

### 3-Benzyl-5-((4-((*tert*-butyldimethylsilyl)oxy)phenyl)ethynyl)pyrazin-2-amine (**34**)

3-Benzyl-5-ethynylpyrazin-2-amine (**32**) (91.00 mg, 0.27 mmol, 1 eq.) and *tert*-butyl(4-iodophenoxy)dimethylsilane (**33**) (56.9 mg, 0.27 mmol, 1 eq.) were dissolved in DMF (10.0 ml) and TEA (3.0 ml) and stirred at room temperature. After vacuum deaeration, a catalytic amount of tetrakis(triphenylphosphine)palladium(0) and CuI was added into the solution and the mixture was deaerated again and stirred for 2 hours at room temperature. The solution was filtered through a Celite pad to remove the catalysts. The solution was extracted with ethyl acetate, and the organic phase was washed with water and brine, dried over Na<sub>2</sub>SO<sub>4</sub> and evaporated. The resulting residue was purified by flash chromatography (silica gel, eluent composition: n-hexane / ethyl acetate = 70/30 to 60/40 to 55/45), affording 3-benzyl-5-((4-((*tert*-butyldimethylsilyl)oxy)phenyl)ethynyl)pyrazin-2-amine (**34**) as a yellow solid (65.1 mg, 58%).

<sup>1</sup>H-NMR (400 MHz, CDCl<sub>3</sub>): δ (ppm) = 8.17 (s, 1H), 7.48 (d, *J* = 8.8 Hz, 2H), 7.26-7.49 (m, 5H), 6.82 (d, *J* = 8.8 Hz, 2H), 4.50 (s, 2H), 4.16 (s, 2H), 0.99 (s, 9H), 0.22 (s, 6H). <sup>13</sup>C-NMR (100 MHz, CDCl<sub>3</sub>): δ (ppm) = 4.43, 18.19, 25.60, 41.30, 85.40, 90.10, 115.25, 120.17, 127.23, 128.43, 128.82, 129.11, 133.26, 136.10, 114.16, 144.14, 151.45, 156.25. HR-MS: calcd for C<sub>25</sub>H<sub>29</sub>N<sub>3</sub>OSi: 416.2158 [M+H]<sup>+</sup>, found: *m/z* 416.2131.

**8-Benzyl-2-(4-hydroxybenzyl)-6-((4-hydroxyphenyl)ethynyl)imidazo[1,2-*a*]pyrazin-3(7*H*)-one (35, 6etOH-CTZ)**

3-Benzyl-5-((4-((*tert*-butyldimethylsilyl)oxy)phenyl)ethynyl)pyrazin-2-amine (**34**) (33.0 mg, 0.07 mmol, 1 eq.) and ketoacetal (**11**) (30.8 mg, 0.07 mmol, 2.1 eq.) were dissolved in ethanol (2.0 ml) and H<sub>2</sub>O (0.2 ml) and stirred at room temperature. After vacuum deaeration, the solution was cooled to 0 °C and TFA (0.3 ml) was added under nitrogen flow. Once the solution reached room temperature, it was heated and stirred for 3 hours at 80 °C. The solvent was evaporated under vacuum and the crude compound was purified by silica column chromatography (eluent composition: chloroform / methanol = 20/1 to 10/1) and chromatograph on a ODS plate (eluent composition: methanol / H<sub>2</sub>O = 80/20), affording 8-benzyl-2-(4-hydroxybenzyl)-6-((4-hydroxyphenyl)ethynyl)imidazo[1,2-*a*]pyrazin-3(7*H*)-one (**35**) as yellow solid (6.5 mg, 20%)

<sup>1</sup>H-NMR (400 MHz, CD<sub>3</sub>OD):  $\delta$  (ppm) = 7.65 (s, 1H), 7.20-7.36 (m, 7H), 7.14 (d, *J* = 8.4 Hz, 2H), 6.78 (d, *J* = 8.8 Hz, 2H), 6.69 (d, *J* = 8.4 Hz, 2H), 4.30 (s, 2H), 4.05 (s, 2H). <sup>13</sup>C-NMR (150 MHz, CD<sub>3</sub>OD):  $\delta$  (ppm) = 33.71, 34.72, 79.47, 95.19, 113.09, 114.65, 116.24, 116.61, 116.76, 127.49, 128.30, 129.66, 129.81, 130.59, 130.89, 134.50, 137.78, 157.01, 160.32. HR-MS: calcd for C<sub>28</sub>H<sub>21</sub>N<sub>3</sub>O<sub>3</sub>: 448.1661 [M-H]<sup>-</sup>, found: *m/z* 448.1678.

### 3.2.2. Luciferase specificity of newly synthesized CTZ analogues.

The bioluminescence intensities of the 20 CTZ analogues were determined with various marine luciferases (Figure 3-3).

African green monkey kidney fibroblast-derived COS-7 cells were grown in a 96-well optical bottom plate (Thermo Scientific). The cells were transiently transfected with pcDNA 3.1(+) vector encoding GLuc, RLuc8.6-535, or a series of ALucs, and incubated in a CO<sub>2</sub> incubator (Sanyo). 16 hours after transfection, the cells were lysed with a lysis buffer (Promega) for 20 minutes according to the manufacturer's instructions. Aliquots of the lysates (10  $\mu$ L), on a fresh 96-well plate, were mixed with an assay solution dissolving 50  $\mu$ L of a CTZ analogue

( $10^{-4}$  M, final concentration) and immediately inserted into a dark chamber (LAS-4000 (FujiFilm)) equipped with a cooled charge coupled device (CCD) camera system. The optical intensities were determined with an image acquisition software (Image Reader v2.0) and analyzed with a specific image analysis software (Multi Gauge v3.1).

The applied protein amounts of the luciferases were gauged via a Western blotting analysis (Figure 3-3(A) inset *a*). COS-7 cells transiently transfected with pcDNA3.1(+) vectors encoding luciferases were washed once with PBS and lysed with an aliquot of a sample buffer carrying 10% 2-mercaptoethanol (Wako). An aliquot of each sample was electrophoresed in a pre-casted acrylamide gel (Bio-Rad), transferred to a nitrocellulose membrane (Millipore), and incubated with a mouse anti- $\beta$ -actin antibody (Sigma) (primary antibodies). The membrane blots were further treated with horseradish peroxidase (HRP)-conjugated secondary antibody (GE Healthcare) and finally visualized with a chemiluminescence substrate kit (Wako).

The bioluminescence spectra of various luciferases were determined in order to measure the superimposed area (Figure 3-5(b) inset *a*). The COS-7 cells were transfected with pcDNA 3.1(+) encoding GLuc, RLuc8, RLuc8.6-535, CBgreen, FLuc, ALuc16, and ALuc23. The cells were incubated for 16 h and lysed with a lysis buffer (Promega) for marine luciferases (GLuc, RLuc8, RLuc8.6-535, ALuc16, and ALuc23), or with a Bright-Glo assay solution (Promega) containing D-luciferin for beetle luciferases (CBgreen and FLuc). An aliquot of the lysates in a microtube (10  $\mu$ L) was mixed with an assay buffer carrying  $10^{-4}$  M of native CTZ for marine luciferases, whereas all the lysates prepared for beetle luciferases were transferred to a microtube without any treatment. The microtubes were immediately transferred to the dark chamber of a precision spectrophotometer (AB-1850, ATTO), which simultaneously acquires the full visible and near infrared ranges of emitted photons (i.e., 391–789 nm). The corresponding optical spectra were determined in a 20-second integration mode. The spectra were normalized in percentages for peak emission. The design of ALucs was listed on Figure 3-1.

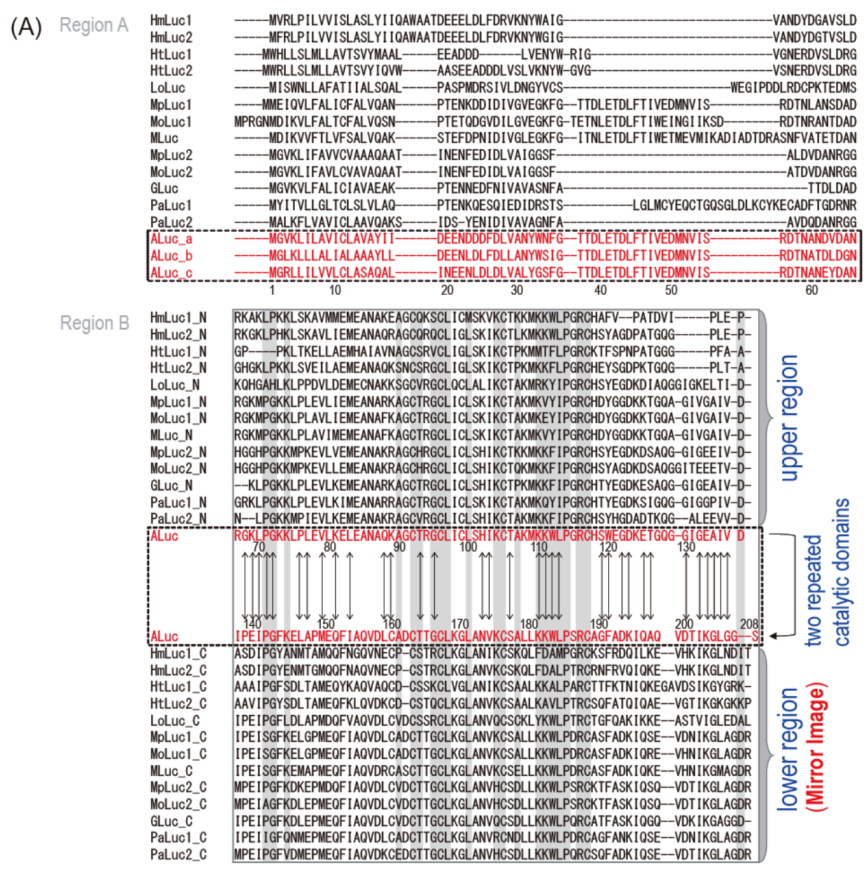


**Figure 3-1** Basic scheme for the fabrication of artificial luciferases (ALucs). The sequence was fabricated by extracting frequently occurring amino acids from the alignment of copepod luciferases in public databases. (A) The prototype sequence of ALucs, which was highlighted in box and red. In case of Region B, I tried to increase the homology between the upper and lower region. This was modified from our previous study<sup>6</sup>. (B) Sequential structures of the artificial luciferases used in the present study: i.e., ALuc16, ALuc23, and ALuc30. The sequence of each ALuc is exactly folded in three. The sequential homology between second and third lines is high.

### 3.2.3. Luciferase-selective property of CTZ analogues in lysates and living mammalian cells

Luciferase specificity and kinetics of the key CTZ analogues from Figure 3-3 were further investigated in living mammalian cells (Figure 3-4).

Figure 3-4(A) highlights the high luciferase selectivity of the CTZ analogues selected from Figure 3-3. The percentages (%) indicate the relative optical intensities of each substrate to the maximal value according to luciferases.

The live-cell images and time-course of bioluminescence developed by the key CTZ analogues were determined with COS-7 cells expressing various marine or beetle luciferases (Figure 3-4(B)).

COS-7 cells grown in 6-channel microslides ( $\mu$ -Slide VI0.4, ibidi) were transiently transfected with pcDNA 3.1(+) vector encoding GLuc, RLuc8.6-535, ALuc16, FLuc, CLuc, and CBgreen. 48 hours after incubation, the cells in each channel were rinsed once with PBS and simultaneously bathed with 60  $\mu$ L of native coelenterazine (nCTZ), 6etOH-CTZ, 6piOH-2H-CTZ, or 6piOH-CTZ dissolved in an assay buffer (final concentration:  $10^{-4}$  M, Promega), using a multichannel pipet (Gilson). The microslides were immediately transferred to the dark chamber of the LAS-4000 (FujiFilm) and the corresponding optical intensities from the microslides were monitored every 5 minutes with a 4-minute integration mode after the substrate injection. The time-courses of the optical intensities from living COS-7 cells were: (i) measured time and area, i.e., the unit is RLU/sec/mm<sup>2</sup>, and (ii) normalized by the percentage of the maximal intensity (%) (Figure 3-4(B)) using the specific image analyzing software, Multi Gauge v3.1 (Figure 3-7(A)).

### 3.2.4. Highly specific illumination of hormonal activities of a ligand with mixed single-chain probes emitting almost superimposed optical spectra.

The advantages of the luciferase-specific CTZ analogues were demonstrated with a unique multiplex assay system comprising two single-chain probes with almost superimposed optical spectra (Figure 3-6).

For the experiment, I coexpressed two independent “molecular strain” probes, “TP2.4”<sup>11</sup> and “ERS”<sup>10</sup>, which carry full-length ALuc23 and RLuc8, respectively (Figure 3-6(A)). The full-length ALuc23 and RLuc8 are sandwiched between FRB and FKBP or between the ER LBD and the SH2 domain of  $\nu$ -Src, respectively. If the pair of proteins engage in an intramolecular protein–protein interaction (PPI) via a ligand, the PPI applies molecular strain to the sandwiched full-length luciferase. The tensed luciferase is designed to enhance the optical intensities in a ligand-dependent manner.

pcDNA 3.1(+) vectors encoding TP2.4 and ERS were cotransfected into COS-7 cells in a 96-well optical bottom plate and incubated in a CO<sub>2</sub> incubator for 16 h. The cotransfected cells in the microplate were partly stimulated with 10<sup>-5</sup> M of dihydrotestosterone (DHT), cortisol, 17 $\beta$ -estradiol (E2), 4-hydroxytamoxifen (OHT), vehicle (0.1% DMSO) for 20 minutes, or partly with 10<sup>-5</sup> M of rapamycin or vehicle (0.1% ethyl alcohol) for 4 h. It is considered that the 4 h of incubation time to reach the optical plateau comprise all the periods for (i) plasma membrane (PM) permeation of rapamycin, (ii) rapamycin-induced intramolecular binding between FRB and FKBP, and (iii) the tensed ALuc–substrate interaction and corresponding emission of bioluminescence. Steps (ii) and (iii) are unlikely to be a rate-determining step because molecular interaction between FRB and FKBP or between FKBP and rapamycin generally reaches a plateau within 2 min, according to surface plasmon resonance (SPR) studies.<sup>22,23</sup> Thus, the remaining step (i) should be the rate-determining step. The PM permeability of chemicals greatly depends on the hydrophobicity. Variance of the stimulation times between steroid and rapamycin, i.e., 20 min vs 4 h, is considered to reflect the PM permeability of the chemicals. After careful decantation of the medium, the cells were washed once with a PBS buffer and lysed with a lysis buffer (Promega) for 20 minutes. An aliquot of the lysates (10  $\mu$ L) was transferred into a 1.6 mL microtube and mixed with 50  $\mu$ L of 6etOH-CTZ, 6piOH-2H-CTZ, or D-luciferin, dissolved in Promega’s assay buffer. The corresponding optical intensities were immediately determined for 5 s with a luminometer (GloMax 20/20n, Promega).

### 3.2.5. pH-Driven optical specificity of CTZ analogues to marine luciferases

Further, a pH-driven feature of the synthesized CTZ analogues was investigated with a universal buffer. I first determined the optical intensities of luciferases in the full pH range to see the optical profile according to pH (Figure 3-8) and then focused on a narrow range from pH 7 to 10 (Figure 3-9).

For the experiment of Figure 3-8, COS-7 cells grown in the 96-well plate were transiently transfected with pcDNA 3.1(+) vector encoding GLuc, RLuc8.6-535, ALuc23 or ALuc34, and incubated in a CO<sub>2</sub> incubator (Sanyo). 16 hours after incubation, the cells were lysed with a lysis buffer (Promega) for 20 minutes according to the manufacturer's instructions. Separately, aqueous universal buffer solutions pH = 4-10 were prepared by mixing the acidic and basic buffer components: i.e., 0.2 M boric acid (H<sub>3</sub>BO<sub>3</sub>), 0.05 M citric acid, and 0.1 M Na<sub>3</sub>PO<sub>4</sub>, and the pHs were adjusted with NaOH. 10<sup>-3</sup> M of nCTZ, 6piOH-CTZ, 6etOH-CTZ, 6H-2OH-CTZ, and CTZ<sub>h</sub> were 10-fold diluted with the prepared universal buffer solutions with varying pH 4-10 (final concentration: 10<sup>-4</sup> M), respectively, immediately before the experiments. For the optical measurement, an aliquot of each lysate (10 μL) on a fresh 96-well plate was simultaneously mixed with 100 μL universal buffer solutions pH 4-10 dissolving 10<sup>-4</sup> M of nCTZ or 6piOH-CTZ (final concentration) using a multichannel micropipette (Gilson). The plate was then quickly moved to the dark chamber of the LAS-4000 (FujiFilm), and the corresponding optical intensities were determined and analyzed with the specific softwares, Image Reader v2.0 and Multi Gauge v3.1 (Figure 3-8).

The column-purified ALuc16 in Figure 3-9 was obtained from our previous study<sup>16</sup>. Briefly, a pOPTHM vector encoding ALuc16 (providing a cleavable N-terminal His6-MBP tag) was expressed in the bacterial strain SHuffle T7 Express *lysS* (New England Biolabs) with 0.3 mM IPTG induction at 16°C. The supernatant of the lysate was purified with an ÄKTA Purifier system (GE Healthcare), and was dialyzed to a metal-cation-free Tris-HCl buffer (0.05 M, pH 8.2) at 4°C for 24 h, and finally adjusted to a concentration of 1 mg/mL by dilution. The purified ALuc16 stock was diluted 500-fold to 2 μg/mL with pure water before the experiments. The

measurement of the optical intensities from the column-purified ALuc16 was conducted as follows. An aliquot of the column-purified ALuc16 (5  $\mu\text{L}$ ) was simultaneously mixed with 100  $\mu\text{L}$  universal buffer solutions pH 7-10, dissolving  $10^{-4}$  M of nCTZ, 6etOH-CTZ, 6H2OH-CTZ, or CTZ*h* using a multichannel micropipette (Gilson) on a 96-well optical bottom microplate (Nunc), and the developed optical intensities were determined and analyzed with the image analyzer, LAS-4000 (FujiFilm).

### 3.3 Results

#### 3.3.1. Structural analysis on the marine luciferase–luciferin interactions

In order to elucidate the mechanisms of substrate specificity of RLuc and ALucs, I initially inspected the interactions between RLuc8 and coelenteramide in the crystal structure<sup>3</sup>. The bound coelenteramide (oxidized product of CTZ) differs in structure to native CTZ (Figure 3-2); however, the functional groups at the C-2 and C-6 positions of the imidazopyrazine backbone are unchanged. The C-6 hydroxyphenyl inserts into the active site pocket, and the *para*-hydroxyl (the hydroxy group at the 4 position of the phenyl ring) interacts with His285 and Glu144 at the base of the pocket, which are reported to act as a catalytic triad in conjunction with Asp120<sup>12</sup>. Residues Trp156, Val185, Lys189, Phe261, and Phe262 form a hydrophobic annulus around the C-6 phenyl group. By increasing the steric bulk at the C-6 position, I predicted that steric hindrance would inhibit binding to RLuc, and that, due to the low sequence identity between RLuc and ALucs, ca. 17%, ALucs might be able to accommodate a bulkier moiety if they contain variant residues in their active site pockets. In contrast, the C-2 hydroxyphenyl group of the bound coelenteramide protrudes from the active site pocket, and forms hydrophobic interactions with Leu165, and Phe180.

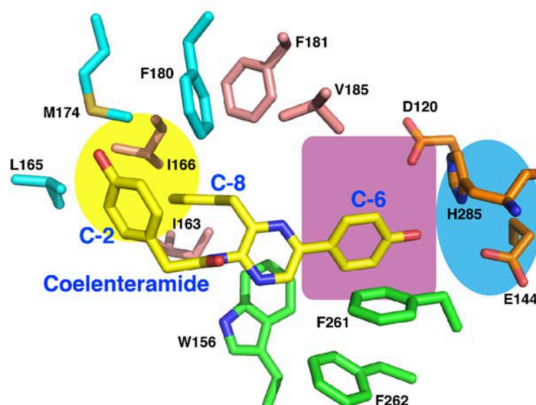


**Figure 3-2** Coelenteramide product (yellow) bound to the active site of RLuc8 (PDB ID: 2PSJ).

### 3.3.2. Determination of luciferase specificity of newly synthesized CTZ analogues

Five-different lineages of CTZ analogues were synthesized to make a new breakthrough for specific imaging of intracellular molecular events in mammalian cells (Figure 3-3).

To date, most research has focused on the synthesis of C-2, C-6 and C-8 substituents of CTZ in combination with analyses utilizing marine luciferases<sup>14,15</sup>. However, most of these reported CTZ analogues failed to induce bright bioluminescence with RLuc, whereas I successfully reported that C-6 position-modified CTZ analogues exerted significantly increased bioluminescence with RLuc8 and RLuc8.6-535<sup>9</sup>. On the basis of the structural analysis above, I attempted to modify both C-2 and C-6 positions in the hope of rationally altering the luciferase selectivity.

Among synthesized CTZ analogues, high ALuc specificity was found with Group 1 (i.e., 6et-X-CTZ analogues, where “6et” means an ethynyl group at the C-6 position and “X” symbols any functional group), which is characteristics in the ethynyl group at the C-6 position, compared to the other analogues (Figure 3-3). In contrast, the same CTZ analogues of Group 1 did not produce notable bioluminescence with the other conventional marine luciferases, GLuc and RLuc8.6-535: e.g., ALuc16 and ALuc23 exerted 1530-fold ( $\pm 185$ ) and 3378-fold ( $\pm 382$ ) stronger bioluminescence intensity than GLuc with 6etOMe-CTZ. Similarly, RLuc8.6-

535 did not show any considerable optical intensity with the CTZ analogues in Group 1.

6etOMe-CTZ and 6etOH-CTZ in Group 1 show high selectivity only to ALucs, whereas 6piOMe-CTZ and 6piOH-CTZ in Group 2 are accommodated into both RLuc8.6-535 and ALucs. It is considered that the double bond extension and orientation at the C-6 position determines the structural preference for both RLuc8.6-535 and ALucs.

CTZ analogues of Group 2 are characterized by a styryl group at the C-6 position and an OH group at the C-2 position (i.e., 6pi-X-CTZ, where “6pi” means a styryl group and “X” indicates any functional group). In this group, 6piCl-CTZ and 6piCF<sub>3</sub>-CTZ show high selectivity to ALuc only. 6piOH-CTZ of Group 2 interestingly exhibited biased selectivity to both ALucs and RLuc8.6-535, but not to GLuc. The structural comparison between 6piOH-CTZ of Group 2 and 6H-2OH-CTZ of Group 4 reveals that RLuc8.6-535 is strongly influenced by not only the presence or absence of the OH group at the C-6 position, but also the length of the functional group at the C-6 position. In contrast to RLuc8.6-535, ALucs can easily accommodate bulky and extended chemical structures of the sidechain at the C-6 position, which is considered to be located at the loose moiety of ALucs.

Group 3 is unique in the point that all derivatives share a styryl group at the C-6 position of the imidazopyrazinone backbone and lack the hydroxyl (OH) group at the C-2 position (the phenol group). Group 3 may be abbreviated 6pi-X-2H-CTZ, where “6pi” means a styryl group at the C-6 position and “X” indicates any functional group. Furthermore, “2H” shows a benzyl group at the C-2 position. All the CTZ analogues of this group, except 6piOH-2H-CTZ, failed to develop bioluminescence with all the examined marine luciferases. 6piOH-2H-CTZ of Group 3 interestingly luminesced selectively with RLuc8.6-535. 6piOH-2H-CTZ with RLuc8.6-535 efficiently emitted 1014-fold ( $\pm 149$ ) and 38-fold ( $\pm 5$ ) stronger bioluminescence intensity than with GLuc and ALuc16, respectively.

The comparison of the chemical structure of 6piOH-2H-CTZ with that of 6piOH-CTZ reveals that the OH

group at the C-2 position is a key functional group in binding to ALucs, but is not essential for interaction with RLuc8.6-535. It is interpreted in a way that the C-2 position is located at the loose moiety of RLuc8.6-535 and thus less influential, different from the case of ALuc (Figure 3-2).

A comparison of the chemical structures between 6piOH-2H-CTZ and 6piH-2H-CTZ of Group 3 shows that the OH group at the C-6 position of 6piOH-2H-CTZ is essential for interacting with the residues in the active site of RLuc8.6-535. Furthermore, upon review of the chemical structures between 6piOH-2H-CTZ and 6piOH-CTZ, it shows that the OH group at the C-2 position is a key functional group only for ALucs, but not for RLuc8.6-535. The greatly biased optical intensities were highlighted in Figure 3-3 (relative) and Table 3-1 (absolute).

CTZ derivatives of Group 4 have no OH group at the benzene rings of C-2 and/or C-6. DeepBlueC (6H-2H-CTZ in our nomenclature) developed no considerable bioluminescence with all the tested luciferases. 6H-2OH-CTZ and CTZ*h* (6OH-2H-CTZ in our nomenclature) showed ALuc-biased optical intensities.

The 8OH-CTZ of Group 5 showed no optical intensities with the applied luciferases.

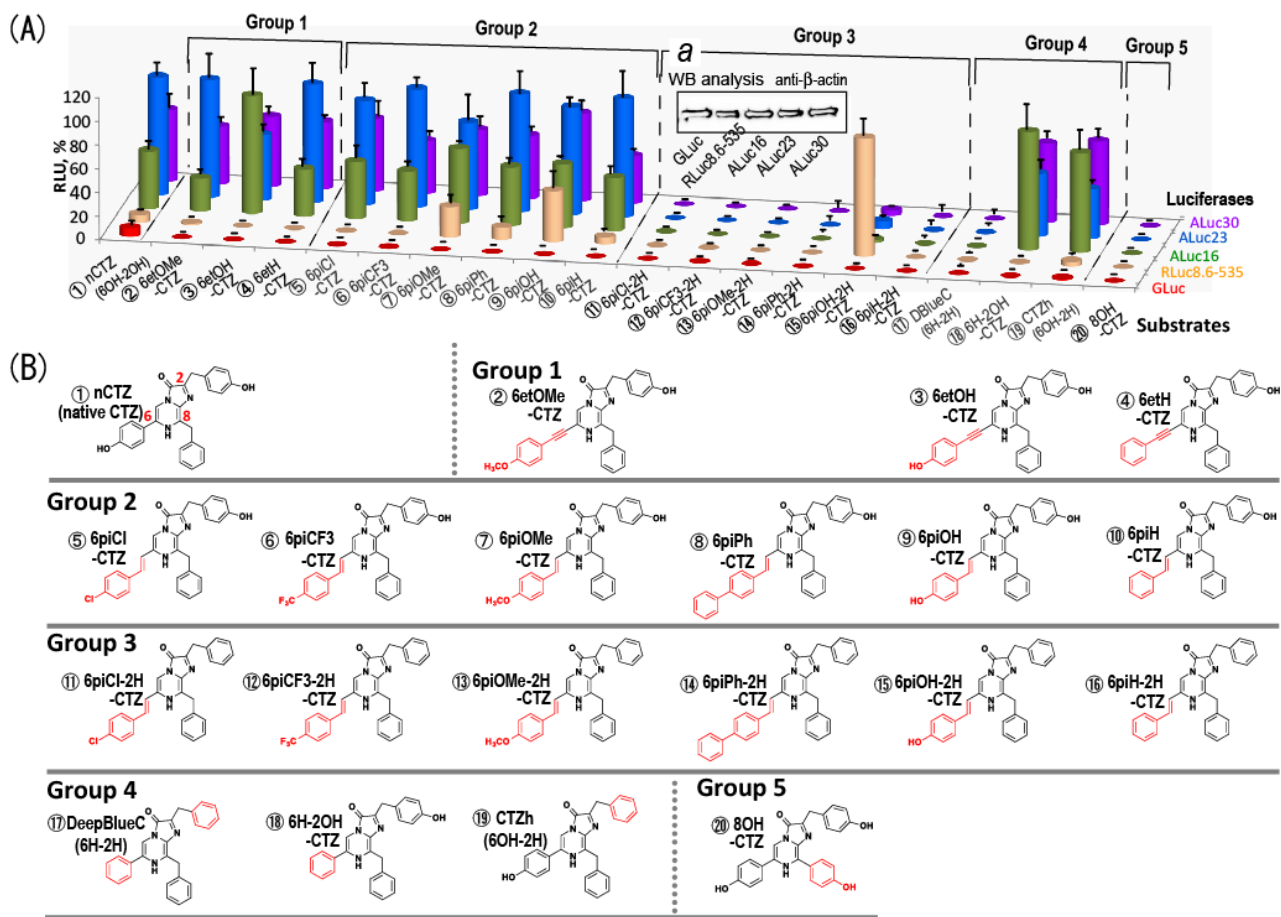


**Figure 3-3** (A) Relative optical intensities of marine luciferases to the synthetic luciferins. The optical intensities of five marine luciferases to each luciferin were normalized to the maximal intensity. The synthetic luciferins were grouped into five categories according to their chemical structures. Inset *a* shows a Western blot analysis indicating relative protein amounts between the marine luciferases. The house-keeping protein,  $\beta$ -actin, was stained with a specific antibody. (B) The detailed chemical structures of synthetic coelenterazine analogues. Compound **1** (native CTZ; nCTZ) and its derivatives are categorized into 5 groups: Group 1 contains an ethynyl group at the C-6 position. A distinctive feature between groups 2 and 3 is the presence or absence of the hydroxyl (OH) group at the C-2 phenyl ring. Both groups 2 and 3 share extension of the double bond conjugated system at the C-6 position. Group 4 analogues lack the OH group at the C-2 and/or C-6 positions, upon comparison with nCTZ. Group 5 has an OH group at the C8 position. The characteristic functional groups in the chemical structures are highlighted in red.

**Table 3-1** The absolute optical intensities of selected CTZ analogues according to luciferases ( $n=3$ ). The optical intensities (RLU) as primary data were divided by integration time (sec) and area ( $\text{mm}^2$ ). Therefore, the unit is  $\text{RLU}/\text{sec}/\text{mm}^2$ . The standard deviation ( $\pm$ s.d.) was specified in parenthesis.

$\text{RLU}/\text{sec}/\text{mm}^2$			
	③6etOH-CTZ	6pi-OH-2H-CTZ	⑨6piOH-CTZ
<b>GLuc</b>	2 ( $\pm$ 2)	4 ( $\pm$ 2)	8 ( $\pm$ 1)
<b>RLuc8.6-535</b>	1 ( $\pm$ 1)	1014 ( $\pm$ 149)	6340 ( $\pm$ 215)
<b>ALuc16</b>	510 ( $\pm$ 116)	27 ( $\pm$ 6)	6680 ( $\pm$ 148)

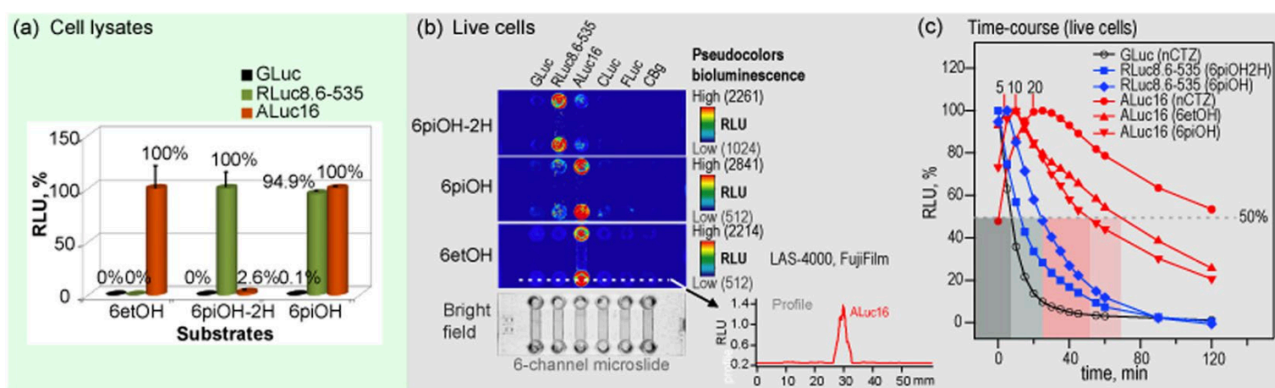


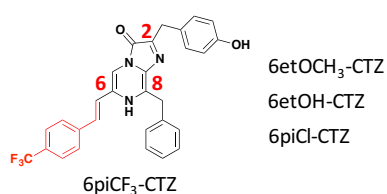
**Figure 3-4** Biased selectivity of the synthetic luciferins to marine luciferases. **(a)** The relative selectivity of representative synthetic luciferins according to luciferases in cell lysates. **(b)** The corresponding live-cell images on a 6-channel microslide, demonstrating the relative luciferase-selectivity of the selected coelenterazine (CTZ) analogues in living mammalian cells. The optical intensity ranges of 6piOH-2H-CTZ, 6etOH-CTZ, and 6piOH-CTZ were 1024–2261, 512–2214, 512–2841 RLU, respectively. **(c)** The time course of the optical intensities after substrate injection to the microslide channels growing live cells. The bioluminescence exhibited clearly distinctive time courses according to the chemical structures of the synthetic luciferins and the kinds of marine luciferases. The blue- and red-marked lines indicate the intensity profiles of RLuc8.6-535 and ALuc16 by time, respectively. Greatly enhancing features in the optical intensity by time were observed with ALuc16. Abbreviations: GLuc, *Gaussia princeps* luciferase; RLuc8.6-535, *Renilla reniformis* luciferase 8.6-535; ALuc16, artificial luciferase 16; CLuc, Cypridina luciferase; FLuc, firefly luciferase; CBgreen, click beetle luciferase green.

### 3.3.3. Evaluation of the spectral overlaps among marine and beetle luciferases

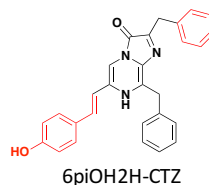
The spectral overlaps among marine and beetle luciferases was briefly demonstrated (Figure 3-5). The spectral peaks were found in the range from 480 to 560 nm. The bioluminescence spectra have broad full width at half maximum (FWHM) and thus the major portion of the spectra overlapped each other. The spectrum of RLuc8.6-535 overlaps ca. 75% and 82% with that of GLuc and ALuc16, respectively. Further, the spectrum of RLuc8.6-535 is superimposed with ca. 96% and 89% of click beetle green (CBgreen) and FLuc, respectively.

(A)

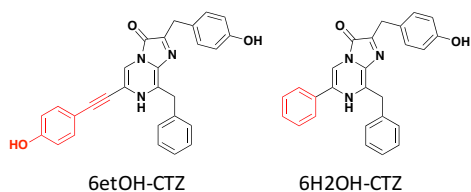
1 ) ALuc-selective



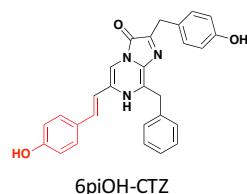
2 ) RLuc-selective



4 ) CBLuc and FLuc-selective



3 ) ALuc and RLuc-selective



5 ) CLuc-selective



(B)

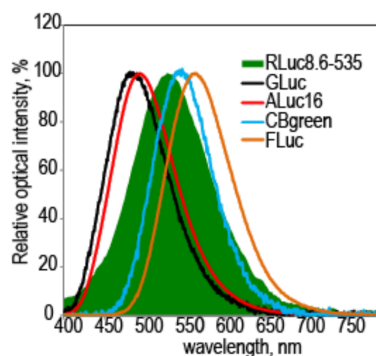


**Figure 3-5** (A) Various chemical structures of beetle and marine luciferins, including those newly synthesized in this study, are illustrated in groups <sup>1-5</sup>. (B) shows the bioluminescence spectra of representative beetle and marine luciferases. The green-filled area shows the spectrum of RLuc8.6-535.

### 3.3.4. Multiplex assay system for specific illumination of hormonal activities of steroid hormones

A multiplex assay system was fabricated for specifically illuminating hormonal activities of a ligand (Figure 3-6). The optical intensities from COS-7 cells expressing ERS and TP2.4 were developed with D-Luciferin, 6etOH-CTZ, or 6piOH-2H-CTZ. Among the substrates, 6etOH-CTZ selectively elevated the luminescence intensity 9-fold, compared to that of the negative control (0.1% ethyl alcohol) only with the cell lysates stimulated by  $10^{-5}$  M rapamycin, whereas 6piOH-2H-CTZ pinpoint-illuminated 6-fold stronger bioluminescence only with the cell lysates stimulated by  $10^{-5}$  M OHT.

In contrast, D-luciferin did not exhibit any elevation of the optical intensities from the cell lysates. The above results demonstrate that (i) the newly synthesized substrates, 6etOH-CTZ and 6piOH-2H-CTZ, allow to pinpoint-illuminate rapamycin and ER antagonist (OHT) activities, respectively, and (ii) the ligand specificity is derived from the unique selectivity of 6etOH-CTZ and 6piOH-2H-CTZ to ALuc23 of TP2.4, and to RLuc8.6-535 of ERS, respectively.

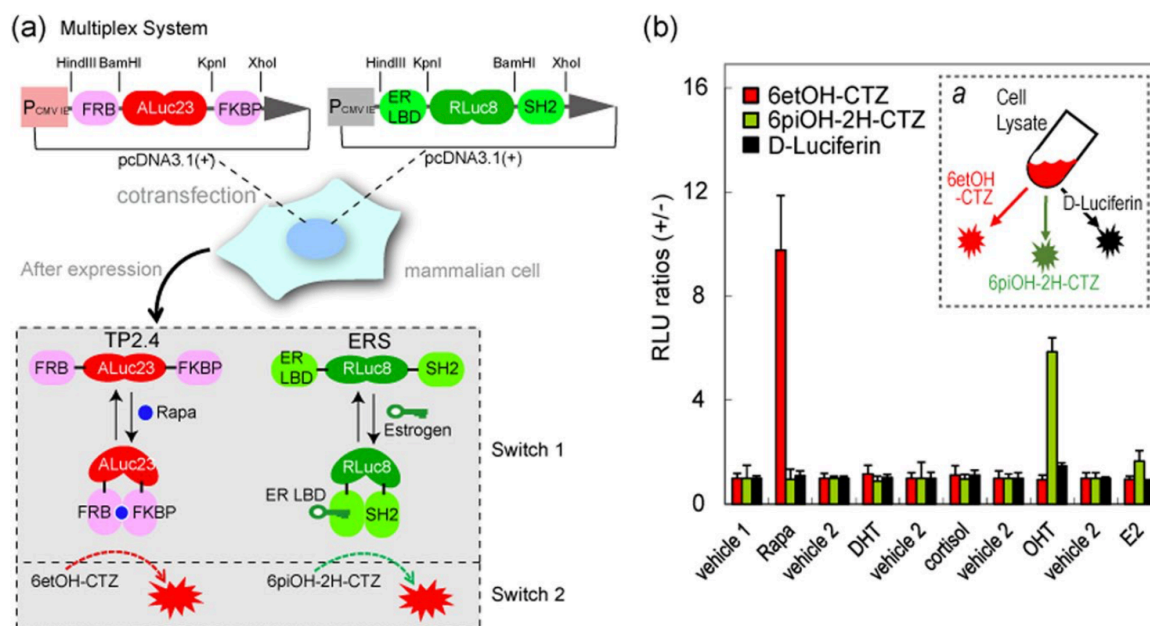


**Figure 3-6** (a) Schematic diagram of a multiplex assay system with two pcDNA3.1(+) vectors encoding molecular tension probe 2.4 (TP2.4) and ER LBD-RLuc8-SH2 (ERS), respectively. After expression, TP2.4 and ERS coexist in mammalian cells, which are ready to illuminate ligand activity. The working mechanisms of TP2.4 and ERS are briefly illustrated in the box-highlighted Switches 1 and 2. Upon stimulation by a ligand, TP2.4 or ERS exerts an intramolecular protein-to-protein interaction (PPI) (Switch 1). This PPI enhances the sandwiched luciferase's activity. The enhanced activities are pinpoint visualized with specific coelenterazine (CTZ) analogues (Switch 2). (b) Specific optical intensities of the substrates in the multiplex assay system carrying two luciferase-based probes. Conventional assays are unable to discriminate the two optical signals. However, the present multiplex system pinpoint-illuminated the rapamycin or estrogen antagonist (OHT) activities without any signal contamination. Vehicles 1 and 2 are negative controls with 0.1% alcohol and 0.1% DMSO, respectively. Inset *a* briefly illustrates the experimental procedure with the specific substrates. The live cells were firstly stimulated with rapamycin and estrogen, lysed, and pinpoint-illuminated with a specific luciferin. Abbreviations: FRB, the rapamycin-binding domain of mTOR; FKBP, FK506-binding protein; ER LBD, the ligand binding domain of human estrogen receptor; SH2, the SH2 domain of  $\nu$ -Src; Rapa, rapamycin; DHT, 5 $\alpha$ -dihydrotestosterone; OHT, 4-hydroxytamoxifen; E2, 17 $\beta$ -estradiol.

### 3.3.5. Prolonged bioluminescence stability of CTZ analogues in living mammalian cells

The time-course of bioluminescence intensities of the key CTZ analogues was determined with live COS-7 cells expressing GLuc, RLuc8.6-535, or ALuc16 (Figure 3-4 and Figure 3-7).

The excellent luciferase specificity of the synthesized CTZ analogues, 6etOH-CTZ and 6piOH-2H-CTZ was observed even in living mammalian cells, grown in a 6-channel microslide (Figure 3-4(B)). The selectivity features in live cells almost corresponded with those of the cell lysates shown in Figure 3-3. Meanwhile, discordance in the results between the lysates and the live cells was also observed with 6piOH-CTZ: i.e., the 6piOH-CTZ-RLuc8.6-535 combination emitted ca. 80% of the optical intensity of the 6piOH-CTZ-ALuc16 combination in the lysate, but the same combination in the lysate showed only 20% emission of the 6piOH-CTZ-ALuc16 mixture in living mammalian cells. This difference in emission in the lysates and in the live cells, along with the pH environment, is explained in the discussion section.

The bioluminescence emission half-lives of RLuc8.6-535 with 6piOH-2H-CTZ and 6piOH-CTZ in living COS-7 cells are found to be ca. 12.6 and 24.2 minutes, respectively. On the other hand, 6piOH-CTZ and 6etOH-CTZ showed greatly prolonged half-lives with ALuc16, which took 50.7 and 69.5 minutes to drop to half-maximal intensity during decay (Figure 3-7(B)).

GLuc in living COS-7 cells quickly decreased its optical intensity by the addition of nCTZ and reached half-maximal optical intensity within 7.4 minutes, whereas ALuc16 showed a greatly prolonged and growing bioluminescence over time. The ALuc16-nCTZ combination reached the maximal optical intensity at ca. 20 minutes and then gradually decayed to the half-maximal intensity in ca. 140 minutes, which is approximately 18-fold longer than the GLuc-nCTZ combination, and ca. 10.5-fold more sustained than the RLuc8.6-535-6piOH-2H-CTZ combination. A growing optical profile over time was also found with ALuc16-6etOH and ALuc16-6piOH-CTZ pairs, whose intensities reached the maximal values in 5 and 10 minutes, respectively.

The above results are summarized by the following: (i) the key CTZ analogues with ethynyl and styryl groups exert excellent luciferase specificity in both lysates and living mammalian cells, (ii) the key CTZ analogues with ethynyl or styryl groups allow greatly prolonged and growing profile of bioluminescence with RLuc8.6-535 and ALuc16 in living mammalian cells, and (iii) the growing profile of bioluminescence reflects the relative

plasma membrane permeability of the CTZ analogues in living mammalian cells, considering that the intracellular localization of ALuc16 and RLuc8.6-535 differs in the cells and the growing profile is not observed in the cell lysates.

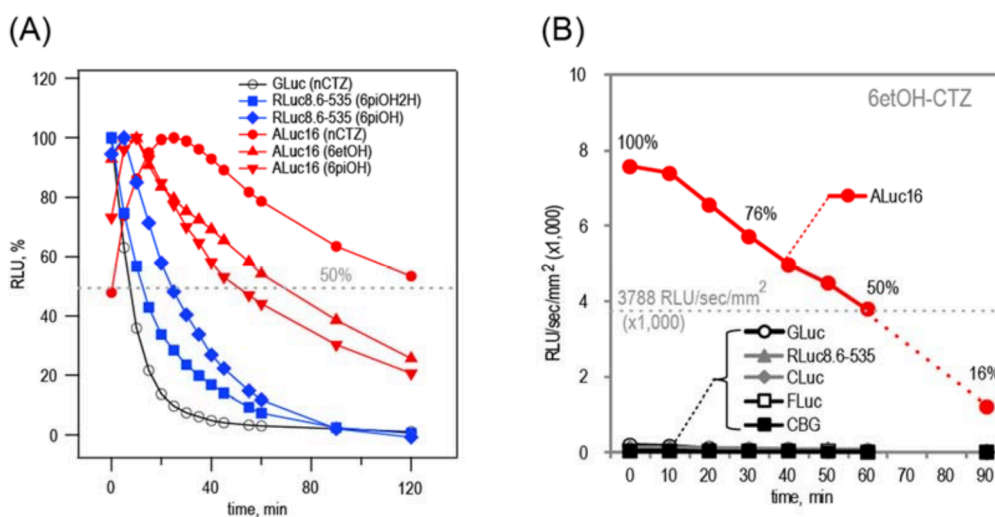


**Figure 3-7** Half-lives of the bioluminescence intensities of marine luciferases according to luciferins in living cells. (A) Time-course of the decay of the relative optical intensities of various luciferase-luciferin pairs. (B) Time course of the decay of the absolute optical intensities (RLU/sec/mm<sup>2</sup>) of the 6etOH-CTZ-ALuc16 pair.

### 3.3.6. The CTZ analogues exert distinctive luciferase selectivity according to pH ranges

The optical intensities of ALuc23 and ALuc34 in lysates were heavily suppressed to the background intensity in an acidic pH span lower than pH 5 (Figure 3-8), and in the highly basic pH range above pH 11 (data not shown). The maximal optical intensities of nCTZ and 6piOH-CTZ with ALucs were found at pH 8 and 9, respectively.

For determining the precise pH-driven feature of ALucs, ALuc16 was expressed in *E. coli* and was column-purified (Figure 3-9), and the pH-driven optical feature was highlighted in the pH 7–10 range. The optical intensities of ALuc16 with 6etOH-CTZ and 6H-2OH-CTZ were found to be greatly influenced by varying pH, whereas the intensities of nCTZ and CTZh were relatively stable and unaffected by varying pH. Interestingly,

the optical intensity of ALuc16 with 6etOH-CTZ was suppressed almost to the background at pH 10 (ca. 3% of the maximal intensity at pH 8): i.e., at pH 10, ALuc16 selectively luminesces with nCTZ, 6H-2OH-CTZ, CTZh, but not with 6etOH-CTZ. The result indicates that the pH can act as a key ingredient for postulating a luciferase-specific assay scheme with minimized optical contamination by combining the pH environment with a specific luciferase-CTZ analogue pair.

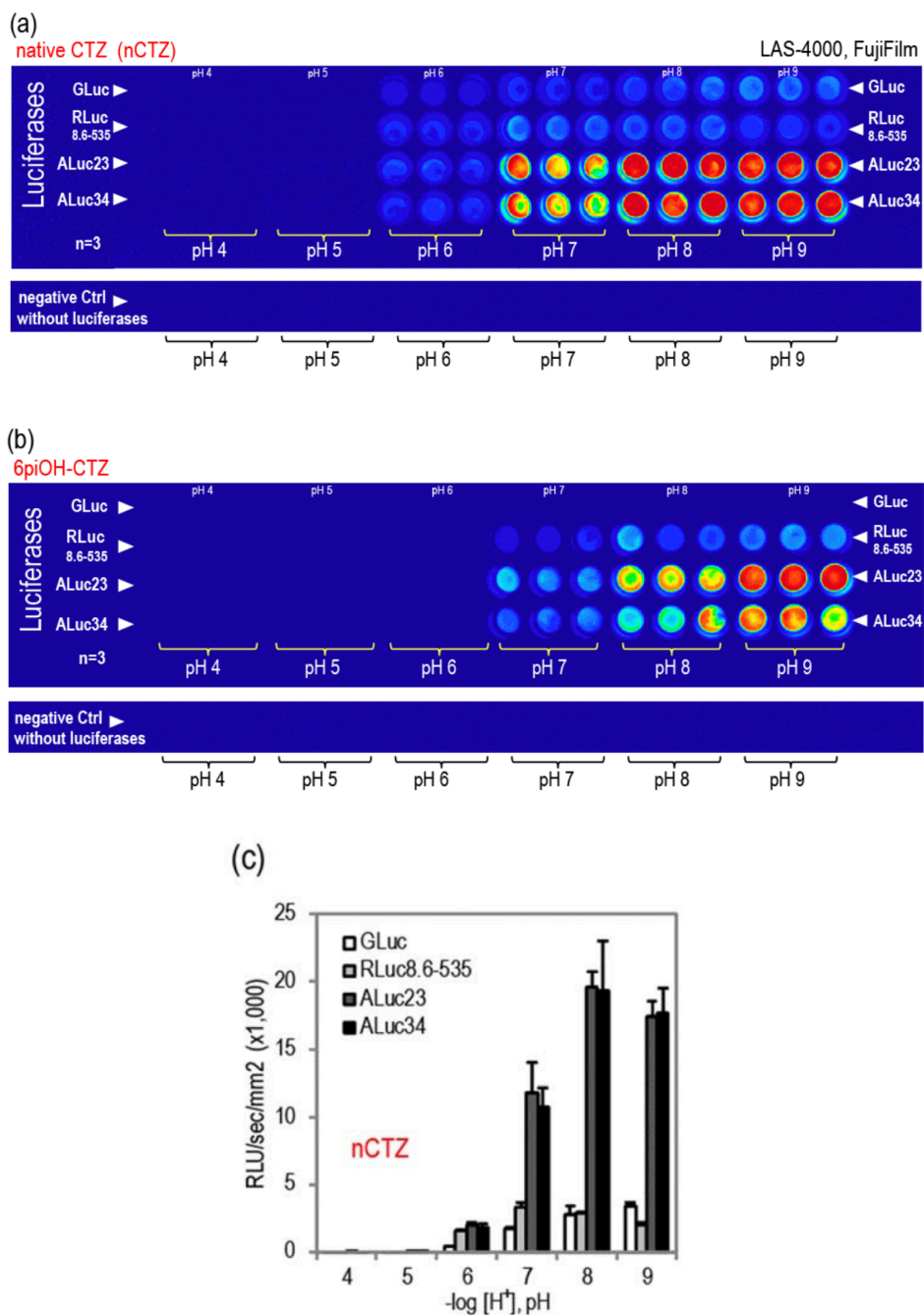


**Figure 3-8** pH-driven features of CTZ-luciferase activity. (a) pH-dominated optical variance of nCTZ with marine luciferases (b) pH-driven optical variance of 6piOH-CTZ with marine luciferase. (c) The absolute optical intensities of (a) showing nCTZ-luciferase activities according to pH (RLU/sec/mm<sup>2</sup>) (*n*=3)

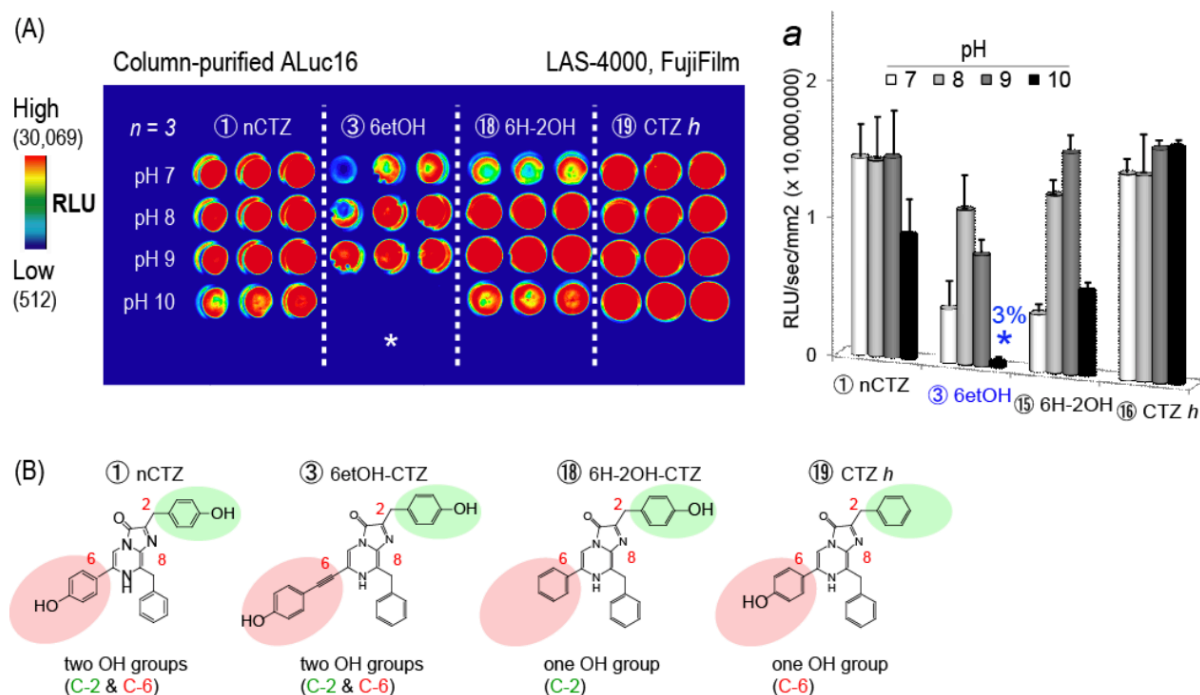


**Figure 3-9** pH-driven optical intensities of CTZ analogues with purified ALuc16. (A) The optical image of bioluminescence driven by varying pHs. Each CTZ analogue exhibited a distinctive pH preference with purified ALuc16. Inset *a* highlights the absolute optical intensities of the selected CTZ analogues according to pHs. The asterisks highlight the suppressed optical intensities by pH. (B) Chemical structures of the CTZ analogues, which were chosen for their characteristic structural differences. As shown in the model, CTZ analogues bearing a hydroxyl (OH) group at the C-2 position (nCTZ, 6etOH-CTZ and 6H-2OH-CTZ) are heavily suppressed in a high pH range (green circles), whereas a CTZ analogue without an OH group (CTZ *h*) at the C-2 position was relatively unaffected by pHs.

### 3.4. Discussion

Multiplex imaging of intracellular molecular events is expected to show a key breakthrough for bioassays and molecular imaging, considering the potential efficiency and high sample throughput. However, most emission spectra of conventional reporter luciferases are superimposed on each other in the green and yellow-green regions, resulting in spectral overlaps (Figure 3-5(B)). Spectral unmixing algorithms, optical filters, and quenching reagents have not provided a fundamental solution to overcome the spectral crosstalk and signal leakage.

To tackle this issue, I examined 20 kinds of CTZ analogues (15 of which were newly synthesized), designed to selectively access the active site cavity of a luciferase, and pinpoint-illuminate bioluminescence even in a multiplex assay system. The synthesized CTZ analogues were divided into five groups according to their chemical structures, and discussed in the context of the quantitative chemical structure-bioluminescence intensity relationship (QSIR). The unique design of CTZ analogues was inspired by our review of the luciferin-binding chemistry between RLuc8 and CTZ in the crystallographic information showing the contribution of the C-2 and C-6 positions to the luciferase selectivity: e.g., by increasing the steric bulkiness at the C-6 position of CTZ, the steric hindrance would inhibit the binding to RLuc8. According to Figure 3-2, the C-2 hydroxyphenyl forms hydrophobic interactions with Leu165 and Phe180 (cyan). Removal of the C-2 *para*-hydroxy group in the G3 analogue 6pi-OH-2H selectively activated RLuc8.6-535 perhaps by enabling an additional hydrophobic interaction with Met174 (yellow circle). However, the C-2 group is likely to possess more conformational freedom in the product than the substrate, and this structure may not represent a biologically relevant conformation. ALucs have very low sequence identity to RLuc (ca. 17%), and therefore most likely contain variant residues that interact with the C-2 group making ALucs sensitive to C-2 group substitutions. The C-8 phenylmethyl group is buried in a hydrophobic pocket consisting of Trp156 (green), Asp162 C (not shown), Ile163, Ile166, Phe181, Val185 (salmon), Met174 and Phe180 (cyan). Chemical modifications to this group are likely cause charge repulsion and steric hindrance. I suspect this hydrophobic pocket is highly conserved due to the abrogation of catalytic activity in all tested luciferases with the G5 analogue containing a C-8 *para*-hydroxy group (8phenol-CTZ). Increases in steric bulk to the C-6 hydroxyphenyl that produce a kink (G2 and G3 analogues) appear to be accommodated via orientation into free space deep in the active site pocket (magenta rectangle). The rigid increase in steric bulk associated with an ethynyl moiety (G1 analogues) might cause a steric clash with the putative catalytic triad (Asp120, Glu144 and His285) (blue ellipse). It should be noted that the putative catalytic triad is not in the immediate proximity of the imadazopyrazine backbone, so it is not clear

if catalysis could occur in this conformation. It is possible that the substrate inserts deeper into the active site pocket, and that the 2PSJ crystal structure captured the coelenteramide product during its exit from the pocket.

The experimental results with 5 lineages of CTZ analogues revealed that 6etOH-CTZ and 6piOH-2H-CTZ pinpoint-illuminated the activities of ALuc16 and RLuc8.6-535, respectively, while 6piOH-CTZ luminesced with both ALuc16 and RLuc8.6-535. The overall results allow us to conclude that the OH groups and the length at the C-2 and C-6 positions of CTZ analogues are critical determinants for the selectivity to ALuc and RLuc, respectively.

The dominant role of the C-6 position of CTZ to RLuc8 activity was previously reported<sup>12</sup>. The study revealed that the OH group at the C-6 position forms conserved triad binding with the residues of RLuc8, and has a key role in the activity. I independently showed that CTZ*i* carrying iodine at the C-2 position is highly selective to ALuc30. I hypothesized it is because the iodine is accommodated into a room in the active site pocket of ALuc30<sup>16</sup>. The above views support that the present luciferase-luciferin reactions adhere a typical host–guest chemistry.

The time course of bioluminescence in Figure 3-4(C) may be discussed with the relative membrane permeability of CTZ analogues in living mammalian cells. Different from other marine luciferases, ALuc16 showed a gradually increasing bioluminescence after substrate injection with 6piOH-CTZ, 6etOH-CTZ, and nCTZ, which were found to reach the optical maxima at ca. 5, 10, and 20 minutes, respectively. In living mammalian cells, ALuc16 is sequestered into the endoplasmic reticulum (ER), which the substrates have to gain access (meaning passing two membrane barriers). The results are interpreted as (i) the substrates reach delayed equilibrium with ALuc16 in the ER, (ii) the order of 6piOH-CTZ, 6etOH-CTZ, and nCTZ should reflect the relative plasma membrane permeability of the substrates in living mammalian cells, and (iii) ALuc16 sequestered in the ER generally reaches slower equilibrium than RLuc8.6-535 localizing in the cytosol.

RLuc8.6-535 reaches more delayed equilibrium with 6piOH-CTZ than with 6piOH- 2H-CTZ, whose only

structural difference is the number of the hydrophilic OH groups (Figure 3-3(B)). 6piOH-CTZ comprising two OH groups should permeate the lipophilic plasma membrane with a delayed time course, compared to 6piOH-2H-CTZ carrying a single OH group.

Discrepancy in the relative optical intensities of 6-pi-OH-CTZ in the lysates (Figure 3-4(A)) and the live cells (Figure 3-4(B)) may be explained by the distinctive pH environments in the lysates and the cytosol of the living cells: i.e., the pHs of the lysis buffer (Promega) and the cytosol of living mammalian cells are ca. 5.6 and neutral (pH 7.0–7.4)<sup>17</sup>, respectively. As shown in Figure 3-8, the optical intensity gaps between ALuc8.6-535 and RLuc8.6-535 are larger in the neutral range than the acidic region. Thus, it is natural that the relative intensity gap between ALuc16 and RLuc8.6-535 in living mammalian cells is larger than in the light emission-suppressive acidic condition (pH 5.6) in the lysates.

There is great merit to be had in specific and high throughput determination of multiple optical readouts in bioassays and molecular imaging. Figure 3-6 showed that the luciferase specificity of synthetic CTZ analogues allows the simultaneous determination of two distinct ligand activities in a mixture of single-chain probes without optical signal crosstalk. This means that two distinctive “on-off” switches work in the present multiplex assay system: i.e., the first switch is the ligand binding of the probe set, ERS and TP2.4, and the second switch is the substrate binding of the probe set (Figure 3-6(a)). The multiplex system is designed to luminesce only in the case that the two switches are “on”: i.e., the probe in the system luminesces only in the coexistence of both the agonist and the specific substrate.

### **3.5. Conclusions**

Taken together, the newly synthesized CTZ analogues presented here show that selective activation of luciferases can be achieved, and that this selectivity can be exploited to pinpoint-illuminate specific luciferase activity among multiple optical readouts. In addition, I tailored the specific activation of luciferases by utilizing

two distinct molecular probe proteins, only able to luminesce in the combined presence of a specific CTZ analogue and a specific bioactive small molecule in a two-switch system. Although my system was unable to change the emission spectra of the luciferases, its application prevented spectral overlap, enabling high throughput screening of signal contamination-free bioassays and molecular imaging. Co-crystal structures of ALucs and RLuc8 with bound CTZ analogues would facilitate the development of even more specific analogues, and further optimization of our system. In addition, elucidation of the binding interactions between substrates and residues in the active site pockets of luciferases, could potentially be exploited by protein engineering to change the wavelength of light emission, and provide improved applications amenable to bioassays, *in vivo* imaging, and analyses of live animal models with more efficient penetration of light through tissues.

## 3.6. Appendix

### 3.6.1. Discussion on the pH-driven optical intensities of CTZ analogues.

It is intriguing to interpret the dramatic pH-driven feature in the luciferase–CTZ activities (Figure 3-8). It is noted that CTZ analogues bearing multiple OH groups should be more strongly influenced by pH variations than those bearing single or no OH groups. Furthermore, it should be noted that the OH group on the C-2 of CTZ analogues plays a key role for interacting with ALucs, in contrast to the OH group at the C-6 position (Figure 3-9(A)). Hence, as a rule for the ALuc-CTZ activity, it was determined that CTZ analogues bearing an OH group at the C-2 position (e.g. nCTZ, 6etOH-CTZ, 6H-2OH-CTZ), were more influenced by pH than other analogues that did not contain an OH group at the C-2 position, for example CTZ*h* as shown in (Figure 3-9(A)).

The optical intensity profile in Figure 8 reveals that ALuc-CTZ activity is completely suppressed in the acidic pH range, sharply enhanced in the neutral range (pH 7), and reaches a plateau at a weak basic pH range from pH 8 to 9. In the neutral and basic pH ranges, the OH group of CTZ analogues is considered to be deprotonated, and interacting with the residues in the active site of marine luciferases, as the pK<sub>a</sub> value of phenols in nCTZ is

around  $10^{17}$ . This view is supported by a previous study, where the deprotonated OH group forms a triad bond with the active site residues of luciferase, and acts as an activity center for marine luciferase<sup>13</sup>. Thus, the dramatic pH-driven features of ALuc-CTZ activity may be explained by the pH susceptibility of the OH groups of CTZs deprotonated at each pKa value.

### **3.6.2. Characteristics of molecular strain probe (TP2.4)<sup>11</sup>**

The ligand-driven feature of the optical intensities of TP2.4 was determined with varying concentrations of rapamycin (Figure 3-10). Stimulation with vehicle (0.1% ethanol) resulted in a basic optical intensity, whereas the presence of rapamycin increased the optical intensities even at low concentrations, with the signal reaching a plateau at  $10^{-5}$  M. The detectable concentration of rapamycin was as low as  $10^{-9}$  M. In contrast to my expectation, rapamycin at  $10^{-4}$  M resulted in only a basic level of optical intensities, close to those observed upon treatment with vehicle alone (0.1% ethanol). The poor optical intensity is interpreted as being caused by cell death induced by the excess amount of rapamycin.

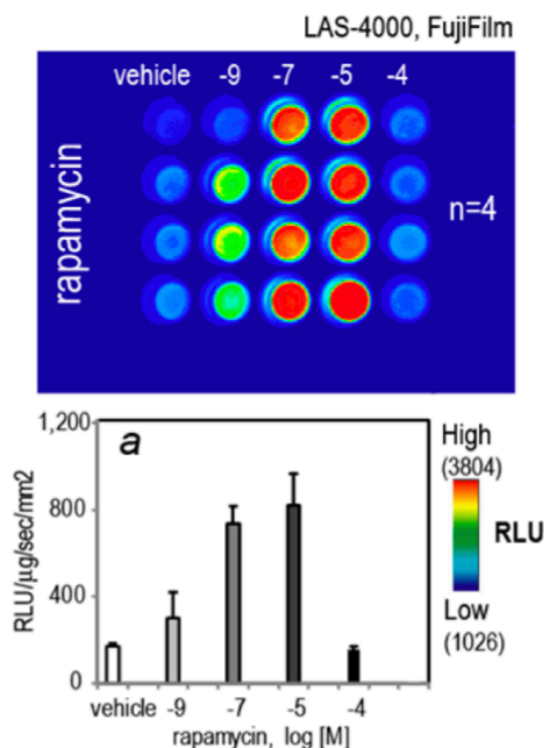


**Figure 3-10** Optical intensities of TP2.4 in response to varying concentrations of rapamycin ( $n = 4$ ). Inset *a* indicates the absolute optical intensities adjusted by protein amount ( $\mu\text{g}$ ), integration time (s), and light-emitting area ( $\text{mm}^2$ )

I also confirmed that optical intensities of TP2.4 are solely enhanced by intramolecular tension induced by ligand-activated FRB-FKBP interactions. The presence of  $10^{-6}$  M of rapamycin failed to increase or decrease the optical intensities of the cells carrying (i) TP0.1 alone, (ii) TP0.2 alone, or (iii) both TP0.1 and TP0.2, whereas the same stimulation enhanced the optical intensities up to 5.4-fold in the case of cells expressing TP2.4 (Figure 3-10(A)).

An apparent variance in the expression levels of TP2.4 was examined with Western blot analysis (Figure 3-10(B)). Anti-FKBP and anti- $\beta$ -actin antibodies recognized specific proteins at 45 kDa, which are the same as the expected molecular weight of TP2.4 and  $\beta$ -actin (housekeeping protein) after expression. Apparently biased variance in the protein amounts at 45 kDa was not observed by stimulation of rapamycin.

This negative control study revealed that (i) molecular tension induced by rapamycin-driven FRB–FKBP interaction is the only factor contributing to the enhancement of ALuc activities, (ii) intermolecular PPIs do not enhance the ALuc activities, (iii) the presence of  $10^{-6}$  M of rapamycin itself does not boost or inhibit the ALuc activities, and (iv) the Western blot analysis showed that TP2.4 is properly expressed at the expected size and the expression levels are not greatly affected by stimulation of rapamycin for 4 h.

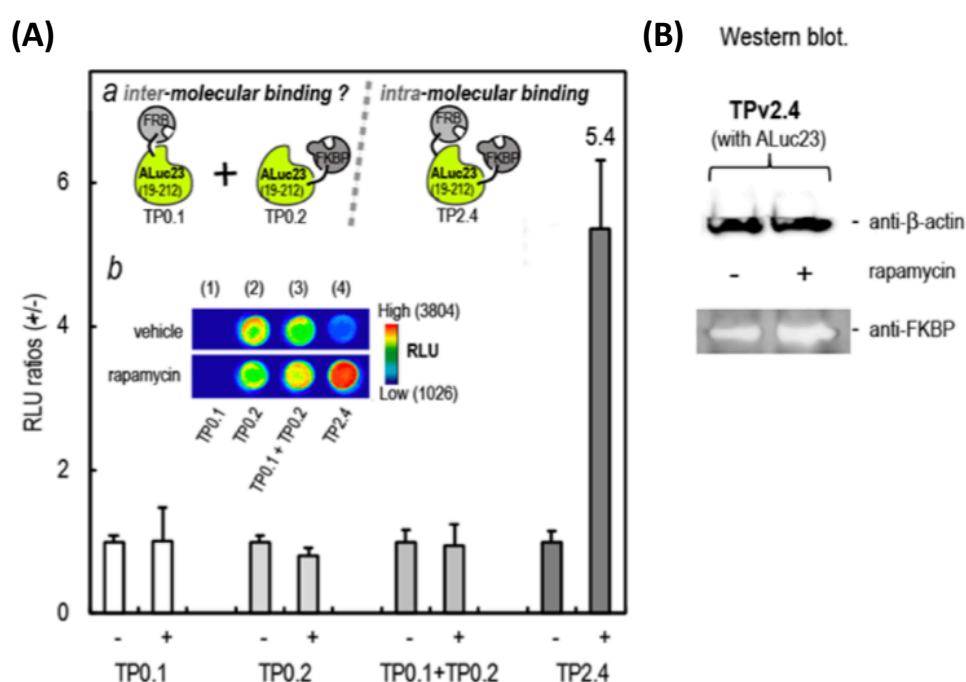


**Figure 3-11** (A) Relative optical intensities of TP2.4 and its negative control probes (tension-free; TP0.1 and/or TP0.2) before and after rapamycin stimulation ( $n = 3$ ). Inset *a* illustrates the molecular binding models of the tension probes. Upon stimulation with  $10^{-6}$  M of rapamycin, no tension is applied to ALuc23 in the probes, (i) TP0.1, (ii) TP0.2, or (iii) cotransfection of TP0.1 and TP0.2, whereas tension is induced to ALuc23 in the case of TP2.4. An intermolecular binding between TP0.1 and TP0.2 do not vary the optical intensity. Inset *b* shows the optical images. (C) Western blot analysis to show protein amounts of lysates of TP2.4. The lysates were electrophoresed and blotted with rabbit anti-FKBP antibody (abcam) or anti- $\beta$ -actin antibody (Sigma). Both  $\beta$ -actin and TP2.4 are found at approximately 45 kDa.

### 3.6.3. Effects of molecular tension on bioluminescent kinetic profile<sup>10</sup>

The kinetic profile (bioluminescence quantum yield: QY, turn-over rates and Michael-Menten constant:  $K_m$ ) of ERS (RLuc8 based molecular strain probe) in the presence or absence of OHT ligand is previously determined<sup>10</sup>. The comparison of kinetic characteristics between RLuc8 and ERS is summarized as Table 3-2. The QY value of ERS ( $6.3 \pm 1.1\%$ ) is similar to that of RLuc8. In contrast, the  $K_m$  value of ERS is  $94.3 \pm 37.1 \mu\text{M}$ , which is 58-fold higher than RLuc8. In addition, the turn-over number of ERS ( $(6.1 \pm 0.5) \times 10^{19}$  photon/s/mol) is much slower than RLuc8 ( $(4.3 \pm 0.2) \times 10^{22}$  photon/s/mol). Therefore, these comparisons indicated the molecular strain probe controls its bioluminescence activities by changing catalytic turn-over number. The difference between RLuc8 and ERS is the modification of RLuc8 with ER LBD (28 kDa) and SH2 (12 kDa) at N- or C-terminal. Given that some amino acid configuring the active sites are close to the N- and C-terminals of RLuc8, the modification of RLuc8 with ER LBD and SH2 is considered to influence the turnover rate rather than QY.

**Table 3-2** Bioluminescence activities variance of RLuc8 and ERS in the presence or absence of ligand

probe	substrate	ligand	quantum yield (%)	$K_m$ ( $\mu\text{M}$ )	turnover number (photons/s/mol)
<b>RLuc8</b>	CTZ	-	$6.9 \pm 0.1$	$1.6 \pm 0.2$	$(4.3 \pm 0.2) \times 10^{22}$
<b>ERS</b>	CTZ	-	$6.3 \pm 1.1$	$94.3 \pm 37.1$	$(6.1 \pm 0.5) \times 10^{19}$
<b>ERS</b>	CTZ	Vehicle*	$5.6 \pm 0.9$	-	-
<b>ERS</b>	CTZ	OHT	$5.0 \pm 0.7$	-	-
<b>ERS</b>	CTZ	E <sub>2</sub>	$5.0 \pm 0.6$	-	-

\*Vehicle represents 0.1% dimethyl sulfoxide (DMSO). OHT and E<sub>2</sub> are dissolved in 0.1 DMSO (final concentration 1  $\mu\text{M}$ ) The luminescence increase of ERS is observed upon treatment of 1nM OHT and reached a plateau at 1  $\mu\text{M}$  OHT.

## References

- (1) Hastings, J. W., *Gene.*, **1996**, *173*, 5–11.
- (2) Shimomura, O. *Bioluminescence*, World Scientific Publishing, Singapore, **2006**.
- (3) Loening, A. M., Wu, A. M. and Gambhir, S. S., *Nat. Methods.*, **2007**, *4*, 641–643.
- (4) Yuan, J., Peng, L. L., Bouma, B. E. and Tearney, G. J., *Optics Express.*, **2010**, *18*, 18839–18851.
- (5) Gammon, S. T. M., Leevy, W. M., Gross, S., Gokel, G. W. and Piwnica-Worms, D., *Anal. Chem.*, **2006**, *78*, 1520–1527.
- (6) Shcherbakova, D. M. and Verkhusha, V. V., *Nat. Methods*, **2013**, *10*, 751–754.
- (7) Jathoul, A. P., Grounds, H., Anderson, J. C. and Pule, M. A., *Angew. Chem., Int. Ed.*, **2014**, *53*, 13059–13063.
- (8) Loening, A. M., Dragulescu-Andrasi, A. and Gambhir, S. S., *Nat. Methods*, **2010**, *7*, 5–6.
- (9) Nishihara, R., Suzuki, H., Hoshino, E., Suganuma, S., Sato, M., Nishiyama, S., Iwasawa, N., Citterio, D. and Suzuki, K., *Chem. Commun.*, **2015**, *51*, 391–394.
- (10) Kim, S. B., Sato, M. and Tao, H., *Bioconjugate Chem.*, **2009**, *20*, 2324–2330.
- (11) Kim, S. B., Nishihara, R., Citterio, D. and Suzuki, K. *Bioconjugate Chem.*, **2016**, *27*, 354–362.
- (12) Kim, S. B., Torimura, M. and Tao, H., *Bioconjugate Chem.*, **2013**, *24*, 2067–2075.
- (13) Woo, J. C., Howell, M. H. and Von Arnim, A. G., *Protein Sci.*, **2008**, *17*, 725–735.
- (14) Gealageas, R., Malikova, N. P., Picaud, S., Borgdor , A. J., Burakova, L. P., Brûlet, P., Vysotski, E. S. and Dodd, R. H., *Anal Bioanal Chem.*, **2014**, *406*, 2695–2707.
- (15) Inouye, S., Sato, J., Sahara-miura, Y., Yoshida, S., Kurakata, H. and Hosoya, T., *Biochem. Biophys. Res. Comm.*, **2013**, *437*, 23–28.
- (16) Kim, S. B. and Izumi, H., *Biochem. Biophys. Res. Comm.*, **2014**, *448*, 418–423.
- (17) Bright, G.R., Fisher, G.W., Rogowska, J. and Taylor, D.L., *J Cell Biol.*, **1987**, *104*, 1019–1033.

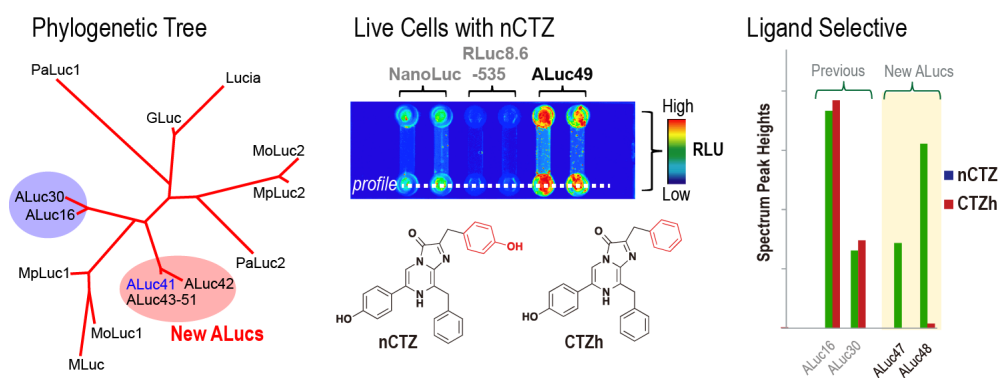


## Chapter4

# Fabrication of a New Lineage of Artificial Luciferases from Databases

## Summary

The intelligent fabrication of artificial luciferases (ALucs) with unique optical properties has a fundamental impact on bioassays and molecular imaging. In this study, we accomplished a new lineage of ALucs with unique substrate preferences by extracting consensus amino acids from the alignment of copepod luciferase sequences in public databases. The spine sequence was made first, created from a frequency analysis of the amino acids in the aligned 25 copepod luciferase sequences in public databases with a sequence logo generator. A total of 11 sibling sequences of ALucs were created by modifying the spine sequence. The phylogenetic tree shows that the newly fabricated ALucs form an independent branch, which is isolated even from our precedent series of ALucs. The new lineage of ALucs were found to survive and was strongly luminescent in living mammalian cells with unique substrate selectivity to native coelenterazine. The total photon fluxes were determined with custom-synthesized native coelenterazine and coelenterazine *h*. The precedent approach to creating *de novo* luciferases with designed optical properties and functionalities is an important addition to the standard optical toolbox, which is dependent on Darwinian natural selection or random mutagenesis.



## 4.1. Introduction

Natural beetle and marine luciferases have been established from a large variety of insects, marine organisms, and prokaryotes<sup>1,2</sup>. The discovery of new reporter proteins for molecular imaging has expanded the frontier region of molecular imaging studies<sup>3</sup>. Conventionally, the establishment of new luciferases from light-emitting organisms in nature has been considered as the only method to expand the reporter pool. Such crude luciferases from light-emitting organisms are the result of Darwinian natural selection<sup>4</sup> and are generally poor in optical intensities and stability; thus, attempts to improve their optical properties by random mutagenesis have been done<sup>5</sup>. However, such random mutagenesis-driven approaches are generally slow and tedious and consume a considerable amount of time and labor. Further, crystallographic information on natural beetle and marine luciferases, which is essential for site-directed mutagenesis, is very rare<sup>6</sup>.

As an alternative approach, we recently showed a new method of creating artificial luciferases (ALucs) by extracting the consensus amino acids from a public database of copepod luciferases, such as the National Center for Biotechnology Information (NCBI) database<sup>7</sup>. This strategy is based on the premise that the frequently occurring amino acids (consensus amino acids) at a given position have a larger thermostabilizing effect compared with less frequent amino acids. This approach was originally developed for finding effective mutation sites and thus is called “*consensus sequence-driven mutagenesis strategy*” (CSMS)<sup>8,9</sup>. We applied the basic concept to the fabrication of whole sequences of consensus amino acids. Although the elucidated approach is unique and empirically successful, no follow-up studies have been done by other research groups thus far. Meanwhile, the database of copepod luciferases has further increased to 25 kinds<sup>10</sup>.

In this study, two prototypical sequences (ALuc41 and ALuc42) of new ALucs were fabricated from frequently occurring amino acids, which were sequentially extracted from the alignment of 25 copepod luciferase sequences with the help of the Web software WebLogo version 2.8.2 (<http://weblogo.berkeley.edu/logo.cgi>). The artificially fabricated spine sequences, i.e., ALuc41 and its sibling

sequences (ALuc42–51), were found to survive and strongly luminesce in mammalian cells. An analysis of the phylogenetic tree showed that the sequences made formed a new lineage and were clearly distinctive from any existing luciferases (CLUSTALW version 2.1). The new lineage of ALucs showed strong bioluminescence in living mammalian cells with unique substrate specificity to coelenterazine (CTZ) analogues. The corresponding total photon fluxes of the luciferases were determined with the use of custom-synthesized nCTZ and CTZ $h$ , the purity of which were confirmed by the NMR peaks and HPLC spectra.

The present study provides guidance on how to make a new lineage of artificial luciferases from public databases and shows their utility as an optical readout by determining the optical properties.

## **4.2. Experimental section**

### **4.2.1. Artificial design of a new lineage of ALucs by extracting frequently occurring amino acids from the alignment of copepod luciferases**

A new lineage of copepod luciferases was created by extracting frequently occurring amino acids from 25 aligned sequences of marine planktonic copepod luciferases (Figure 4-3). The extraction from the alignment was done with the use of the Web software WebLogo version 2.8.2 (<http://weblogo.berkeley.edu/logo.cgi>)<sup>11</sup>, which highlighted a consensus amino acid sequence, the first spine sequence of which was named “ALuc41.” Some consecutive amino acids in the sequence of ALuc41 were further modified by embedding a His-tag and elongating the highly variable region in the N-terminal side, which was named “ALuc42.” The sequence, ALuc41, was aligned in three rows to determine two repeated catalytic domains, which are commonly found among copepod luciferases (Figure 4-3(A)). A series of sibling sequences of ALucs was further fabricated from the prototypical sequence by substituting several amino acids in the C-terminal region with new ones (Figure 4-1).

In addition, an endoplasmic reticulum (ER) retention signal, i.e., KDEL, was added at the C-terminal end of

the created sequence for retention in the ER. This was done because copepod luciferases are supposed to have a secretion peptide at the N-terminal end. The average length and molecular weight (MW) of the newly made artificial sequences were 195.7 ( $\pm 5.7$  s.d.) AAs and 21.2 ( $\pm 0.7$  s.d.) kD, respectively. The average theoretical isoelectric point (pI) was 5.7 ( $\pm 0.5$  s.d.).

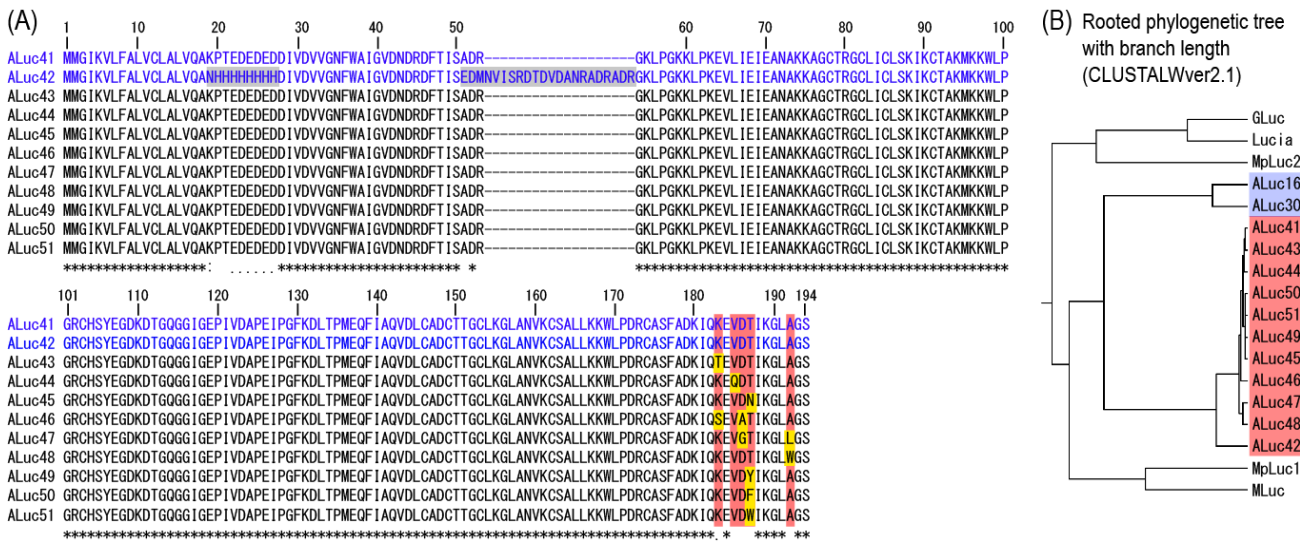


**Figure 4-1** (A) A specified alignment of the sequences of the newly created ALucs. ALuc41 (blue) is extracted from an alignment of copepod luciferases in the public database NCBI with a sequence logo generator (WebLogo version 2.8.2). Its sequence is further modified by the addition of a His-tag epitope and an extended sequence in the N-terminal region. The sequences of ALuc43–51 were created by altering the C-terminal amino acids (red and yellow). (B) A rooted phylogenetic tree of the newly created ALucs and existing marine luciferases according to CLUSTALW version 2.1. The red shaded area indicates the newly created ALucs; the blue shaded area denotes the previous ALucs.

#### 4.2.2. Synthesis of cDNA constructs encoding the new lineage of artificial luciferases

The murine codon-optimized cDNA constructs encoding the artificially designed amino acid sequences (ALuc41-51) were custom-synthesized on order by Eurofins Genomics (Tokyo, Japan) (Figure 4-1(A)). The synthesized cDNAs were subcloned into pcDNA3.1(+) (Invitrogen) by using the specific restriction sites

*HindIII* and *XhoI* for expression in mammalian cells. The overall sequence fidelity was confirmed with the use of a sequencing service provided by Eurofins Genomics (Tokyo, Japan).

#### **4.2.3. Determination of the sequential identity ranking and phylogenetic trees of the new lineage of artificial luciferases**

The rooted and unrooted phylogenetic trees of the artificially designed ALucs and existing marine luciferases were determined by using CLUSTALW version 2.1 (Figure 4-1(B); Figure 4-3(B)). The maximal identities and similarity rankings of the new ALucs were also compared with those of existing marine luciferases by using an alignment search tool provided by the NCBI BLAST (BLASTP 2.5.1+; <http://www.ncbi.nlm.nih.gov/>). Figure 4-3(B), inset *a*, shows the maximal sequential identity rankings.

#### **4.2.4 Determination of the absolute optical intensities of the new ALucs and comparison with conventional luciferases**

The relative optical properties of ALuc41–45 were examined in COS-7 cells derived from African green monkey kidney fibroblasts. COS-7 cells were grown in Dulbecco's minimal essential medium (DMEM; high glucose) (Gibco) supplemented with 10% heat-inactivated fetal bovine serum (FBS) (Gibco) and 1% penicillin/streptomycin (P/S) (Gibco) (Figure 4-3(C)).

The COS-7 cells, grown in a 96-well microplate (Nunc), were transiently transfected with the pcDNA3.1(+) plasmids encoding each ALuc (Figure 4-1) or the existing marine luciferases, i.e., *Gaussia princeps* luciferase (Gluc; GenBank AAG54095.1)<sup>16</sup> or *Renilla reniformis* luciferase 8.6-535 (RLuc8.6-535)<sup>5</sup>, as internal references by using the lipofection reagent TransIT-LT1 (Mirus). 16 hours after the transfection, the cells in each well were lysed with 50  $\mu$ L lysis buffer (E291A; Promega). An aliquot of the lysates (10  $\mu$ L) was transferred into a fresh 96-well optical bottom microplate (Nunc) by using an 8-channel micropipette. The relative optical intensities

in the plate were also determined with the use of an image analyzer (LAS-4000; Fujifilm) immediately after simultaneous injection of 40  $\mu\text{L}$  of the RLuc assay buffer carrying nCTZ by using a multichannel micropipette (Figure 4-3(C)).

The absolute optical intensities shown in Figure 4-4(B) were determined by applying the same protocol as that in Figure 4-3(C). The bioluminescence intensities were normalized by integration time (sec) and light-emitting area ( $\text{mm}^2$ ). The normalized bioluminescence intensities were subsequently expressed in relative luminescence units per second–area ( $\text{RLU}/\text{sec}/\text{mm}^2$ ).

#### 4.2.5 Substrate specificity of the new lineage of ALucs

The substrate-specific bioluminescence of the new lineage of ALucs was examined with the use of various coelenterazine analogues (Figure 4-5 and Figure 4-7). The COS-7 cells grown in a 96-well microplate were transiently transfected with a pcDNA3.1(+) vector encoding one of the following marine luciferases: GLuc, RLuc8.6-535, ALuc16, ALuc30, and ALuc41–48. 16 hours after the transfection, the cells were lysed, and an aliquot of the lysates (20  $\mu\text{L}$ ) was carefully transferred to a 200- $\mu\text{L}$ -volume microtube. The lysate in the microtube was mixed with 60  $\mu\text{L}$  of the substrate solution dissolving nCTZ or CTZh and then was immediately transferred into the dark chamber of a precision spectrophotometer (AB-1850; ATTO), which can simultaneously acquire all emitted photons ranging from 391 to 789 nm.

Similarly, the substrate specificity of the new lineage of ALucs was examined with the use of a larger number of CTZ analogues (Figure 4-7). COS-7 cells expressing ALucs were prepared by applying the same protocol as that in Figure 4-3. The cells were lysed, and then an aliquot of the lysates (10  $\mu\text{L}$ ) was carefully transferred to a 96-well optical bottom microplate, simultaneously mixed with 40  $\mu\text{L}$  of each coelenterazine variant (nCTZ, CTZ400, CTZh, CTZn, CTZi, CTZf, CTZcp, CTZhcp, CTZ fcp, and CTZip) by using a multichannel micropipette, and placed in an image analyzer (LAS-4000; Fujifilm). The relative optical intensities were

immediately integrated for 30 seconds.

#### 4.2.6. Live cell bioluminescence imaging with marine luciferases

The live cell images and optical profiles of NanoLuc (Promega), RLuc8.6-535, and ALuc49 were determined with the use of the COS-7 cells grown in 6-channel microslides ( $\mu$ -Slide VI<sup>0.4</sup>; ibidi) (Figure 4-6).

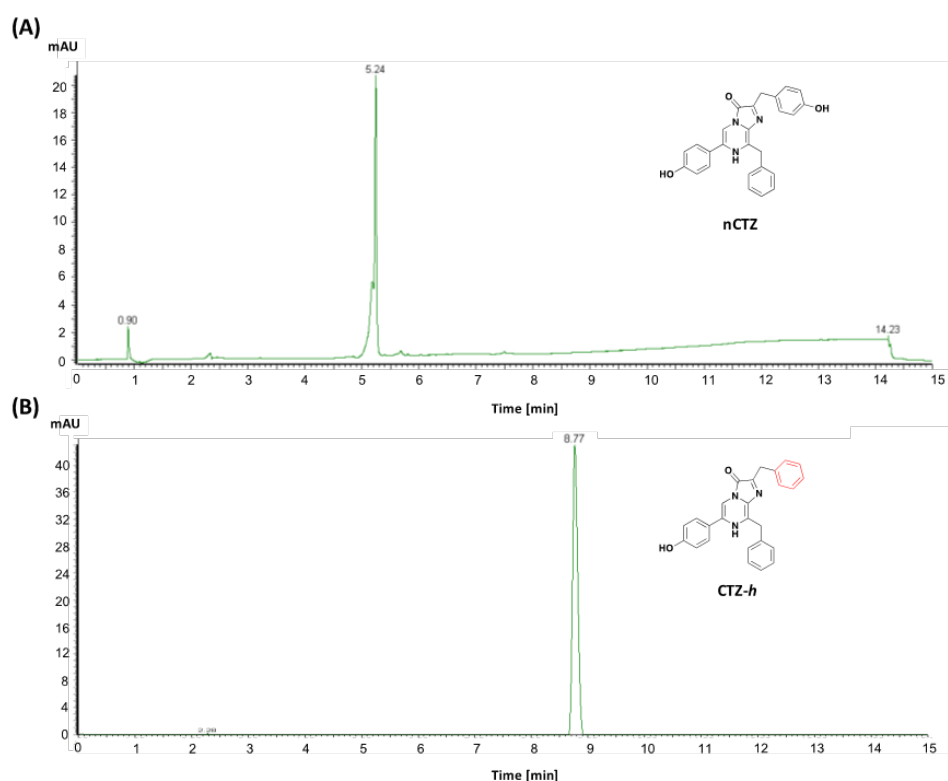
The COS-7 cells in 6-channel microslides were transiently transfected with the pcDNA 3.1(+) vector encoding NanoLuc, RLuc8.6-535, or ALuc49. 16 hours after the incubation, the cells in each channel were rinsed once with HBSS buffer (Gibco) and simultaneously bathed with 60  $\mu$ L of furimazine, 6piOH-CTZ, or nCTZ dissolved in HBSS buffer (final concentration:  $10^{-4}$  M) by using a multichannel micropipette (Gilson). The microslides were immediately set in the dark chamber of the LAS-4000 image analyzer (Fujifilm), and the corresponding optical intensities from the microslides were integrated for 20 sec. The optical intensities and profiles from the living COS-7 cells in the microslide were normalized by measured time (sec) and area ( $\text{mm}^2$ ); the unit was RLU/sec/ $\text{mm}^2$ , and the specific image analysis software Multi Gauge version 3.1 (Fujifilm) was used.

#### 4.2.7 Determination of photon fluxes

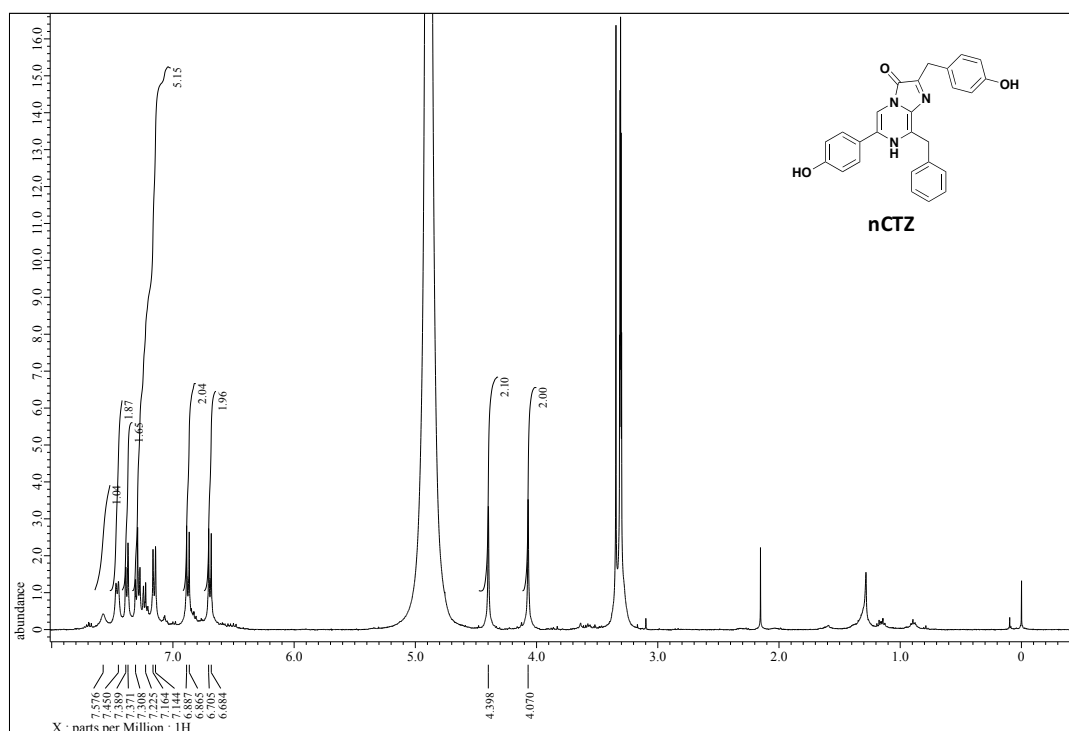
The total amount of photon fluxes of the existing marine luciferases and newly fabricated ALucs were determined with the use of the substrates nCTZ and CTZh (Figure 4-8 and Table 4-1).

For the measurement, we referred to a previous methodology for the quantum yields (QYs)<sup>17</sup>. In brief, in the presence of an excess level of enzymes, the quantum yields (QYs) are defined by  $N_{\text{tot}}/S_{\text{tot}}$ , where  $N_{\text{tot}}$  and  $S_{\text{tot}}$  denote the total amounts of emitted photons and consumed substrate, respectively. If the luciferase level is in excess compared with luciferins ( $E \gg S$ ), all the luciferins should be consumed. In this case, the initial amount of luciferin ( $S_{\text{ini}}$ ) is equivalent to the total consumed luciferin ( $S_{\text{tot}}$ ).

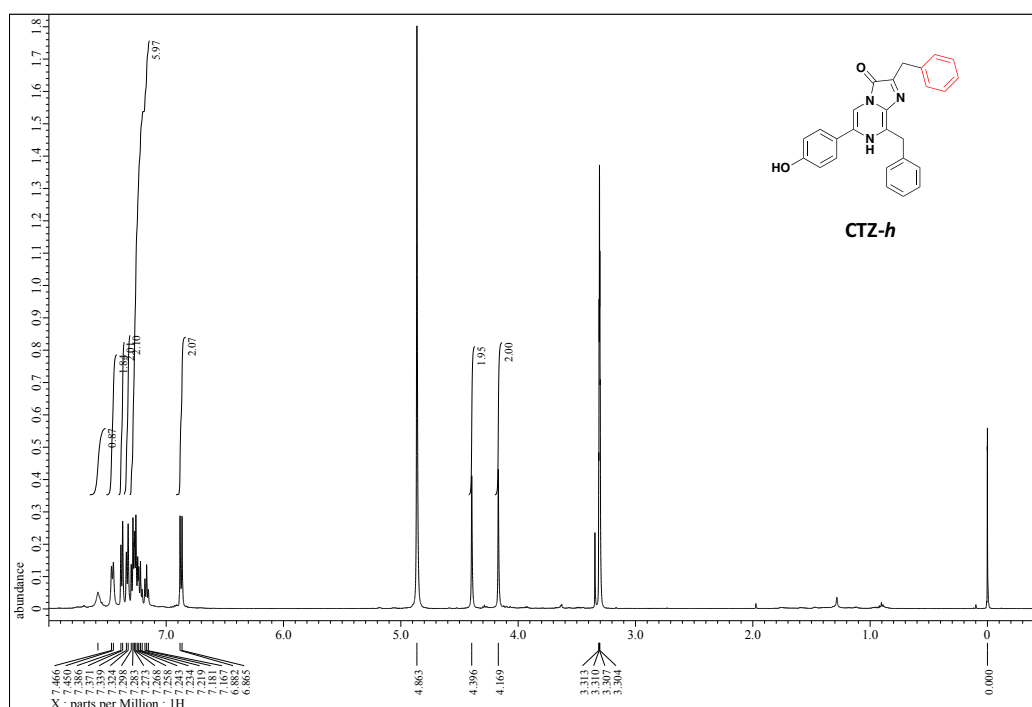
For exact measurement of the total amount of photon fluxes, I custom-synthesized nCTZ and CTZ*h* and carefully determined the purity beforehand based on the NMR peaks and HPLC spectra (Figure 4-2). Detailed procedure of the organic synthesis of nCTZ and CTZ*h*. nCTZ and CTZ*h* were synthesized as described in a previous research<sup>18</sup>. The purity of each compound was confirmed by the <sup>1</sup>H-NMR and HPLC spectra. The <sup>1</sup>H-NMR spectra were recorded on an ECA-500 or ECS-400 spectrometer (JEOL Ltd.). The chemical shifts were determined with the use of tetramethylsilane as an internal standard material. HPLC measurements were carried out with an Acquity UPLC system (Waters Ltd.) under the following conditions: eluent A (H<sub>2</sub>O + 0.1% CH<sub>2</sub>O<sub>2</sub>) and eluent B (CH<sub>3</sub>CN + 0.1% CH<sub>2</sub>O<sub>2</sub>) (A/B = 1/0 to 0/1). The absorbance at 254 nm was monitored.



**Figure 4-2** HPLC spectra showing the purity of the substrates nCTZ (A) and CTZ*h* (B). Unique single peaks were found at 5.24 and 8.77 minutes without any other peaks showing impurity.

<sup>1</sup>H-NMR spectra

<sup>1</sup>H-NMR (400 MHz, CD<sub>3</sub>OD):  $\delta$  (ppm) = 7.57 (s, 1H), 7.46 (d,  $J = 7.8$  Hz, 2H), 7.38 (d,  $J = 7.3$  Hz, 2H), 7.30-7.14 (m, 5H), 6.87 (d,  $J = 9.0$  Hz, 2H), 6.69 (d,  $J = 8.7$  Hz, 2H), 4.39 (s, 2H), 4.07 (s, 2H).



<sup>1</sup>H-NMR (500 MHz, CD<sub>3</sub>OD):  $\delta$  (ppm) = 7.58 (s, 1H), 7.45 (d,  $J = 8.0$  Hz, 2H), 7.37 (d,  $J = 7.4$  Hz, 2H), 7.33 (t,  $J = 7.4$  Hz, 2H), 7.29-7.15 (m, 6H), 6.87 (d,  $J = 8.5$  Hz, 2H), 4.39 (s, 2H), 4.16 (s, 2H).

For this measurement, the COS-7 cells grown in a 6-well microplate were transiently transfected with the mammalian expression plasmid pcDNA3.1(+) encoding one of the following luciferases: GLuc, RLuc8.6-535, ALuc16, ALuc30, ALuc47, and ALuc49, by using the lipofection reagent TransIT-LT1 (Mirus). The cells were incubated for 2 days for overexpression of the luciferases, followed by lysing with a lysis buffer (Promega).

An aliquot of the lysates (20  $\mu$ L) was set in each well of a 96-well optical bottom microplate and simultaneously mixed with 60  $\mu$ L of low-concentration substrates (2 nmole) by using a 12-channel micropipette (Gilson). The microplate was immediately set in the dark chamber of the LAS-4000 image analyzer (Fujifilm), and the total light emission was integrated until the reaction approached completion (about 10 min) at room temperature (22.5  $^{\circ}$ C); a few seconds of delay occurred between the substrate injection and measurement. In parallel, the photons from a standard LED light source (L11494-525; Hamamatsu) (1 pW) were measured as an internal standard. Thus, the photon counts were easily calculated from the optical intensities.

#### **4.2.8. Construction of single-chain bioluminescent probes with ALucs**

The advantages of using the newly fabricated ALucs in bioassays were determined with the use of single-chain bioluminescent probes (“bioluminescent capsules”) carrying full-length ALuc47 or ALuc49 (Figure 4-9). The corresponding probes were named P47 and P49, respectively.

The working mechanism of bioluminescent capsules has been previously shown by the authors<sup>18</sup>. Briefly, the capsule is designed to carry a full-length ALuc, the C-terminal end of which is linked to a membrane localization signal (MLS) through a known substrate sequence of caspases (“DEVD”). The luciferase fixed in the capsule is dissected by active caspase 3 and is eventually diffused freely to the cytosol. The free luciferase has higher optical activities than the fixed one to the plasma membrane.

## 4.3. Results

### 4.3.1. Artificial luciferases can be fabricated by extracting frequently occurring amino acids from the alignment of copepod luciferases

As shown in Figure 4-3, two spine sequences were created by extracting frequently occurring amino acids from the alignment of 25 copepod luciferase sequences with the help of the Web software WebLogo version 2.8.2 (<http://weblogo.berkeley.edu/logo.cgi>)<sup>11</sup>. The sequential identity of the artificial sequences was found to be highly distinctive from that of any existing marine luciferases according to the program BLASTP 2.5.1+ (NCBI BLAST). For example, the closest sequence was that of *Pleuromamma xiphias*, the maximal identity of which was only 77% of ALuc41 according to the program BLASTP 2.5.1+ in the NCBI BLAST (Figure 4-3(B), inset *a*). The phylogenetic tree showed that the newly fabricated ALuc40 series formed an independent branch, which was isolated even from precedent ALuc series (Figure 4-3(B)).

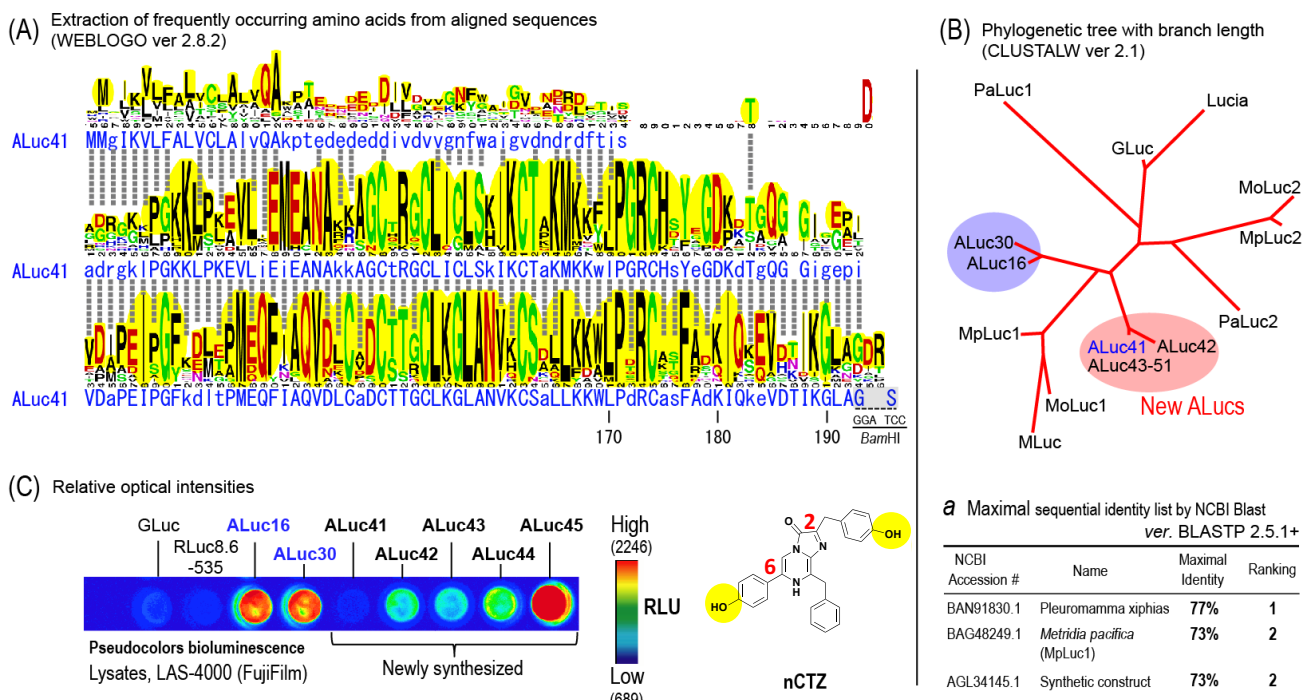


**Figure 4-3** Fabrication of a spine sequence of new artificial luciferases from an alignment of copepod luciferases in public databases (NCBI BLAST and SIB BLAST). (A) The frequently occurring amino acids were extracted from the alignment with the help of the Web software WebLogo version 2.8.2 (<http://weblogo.berkeley.edu/logo.cgi>)<sup>11</sup>. (B) An unrooted phylogenetic tree according to CLUSTALW version 2.1. The blue and red circles mark the relative positions of existing and new artificial luciferases, respectively. Inset **a** shows the identity ranking of existing marine luciferases compared with ALuc41. The identity ranking was determined with the program BLASTP 2.5.1+ in the NCBI BLAST. (C) The relative optical intensities of ALuc41–48 compared with conventional luciferases ( $n=5$ ). The optical image in pseudo-color was developed with nCTZ.

### 4.3.2. ALuc40s survive in mammalian cells and emit strong bioluminescence

The relative optical intensities of the new ALucs and conventional marine luciferases were determined (Figure 4-3(C)). The results showed that the new ALucs were successfully expressed in mammalian cells and emitted strong bioluminescence with nCTZ (Figure 4-3(C)). The optical intensities of ALuc45 were the strongest among the initially tested marine luciferases, whereas those of conventional marine luciferases, GLuc and RLuc8.6-535, were comparably weak; for example, the optical intensities of ALuc45 were 6.2-fold ( $\pm 1.2$  s.d.) stronger than those of GLuc.

As shown in Figure 4-3(C), ALuc43 and ALuc45 generally showed 7.4- and 14.6-fold stronger bioluminescence than ALuc41, respectively, in the optical intensities. However, the only sequential difference of ALuc41 with ALuc45 was whether the amino acid at position 187 was T or N. Similarly, the only sequential differences of ALuc43 and ALuc44 with ALuc41 were T183 and Q185, respectively. This sequence–intensity correlation indicates that the amino acids at positions 183, 185, and 187 at the C-terminal end of ALuc41 are key sites for enzymatic activities. The result suggests that the C-terminal end of ALuc41 may form the active site or may be close to that site.

### 4.3.3 The C-terminal end of ALuc41 dominates the optical intensities

We previously anticipated a supersecondary structure of ALuc30 with respect to the X-ray crystallographic information of the coelenterazine-binding protein (CBP; PDB accession number: 2hps and 2hq8)<sup>12</sup>, where the amino acids at the C-terminal end were close to the C6 position of nCTZ (Figure 4-4(A)).

Motivated by the results presented in Figure 4-3(C), which show the role of the amino acids at the C-terminal end, we further modified the key amino acids at the C-terminal end to ensure the sequence–intensity correlation (Figure 4-4).

As shown in Figure 4-3(C), because ALuc45 had the strongest intensity, we further synthesized ALucs 49, 50, and 51 by substituting N187 of ALuc45 with Y, F, and W, respectively. ALuc46 and ALuc47, which were variants of ALuc45, carried the mutation sites K183S/D186A and D186G/A192L, respectively.

The comparison of optical intensities showed that ALuc49 and ALuc50 were as bright as or brighter than ALuc45 (Figure 4-4(B)). The optical stabilities of the new ALucs were examined by comparing the optical intensities at 5 minutes after nCTZ injection with those at 0 minutes after nCTZ injection (Figure 4-4(B), inset a). ALuc51 and ALuc48 maintained 49% and 40% of their initial optical intensities after 5 minutes. GLuc showed the poorest optical stability of 16% in the same experimental conditions.

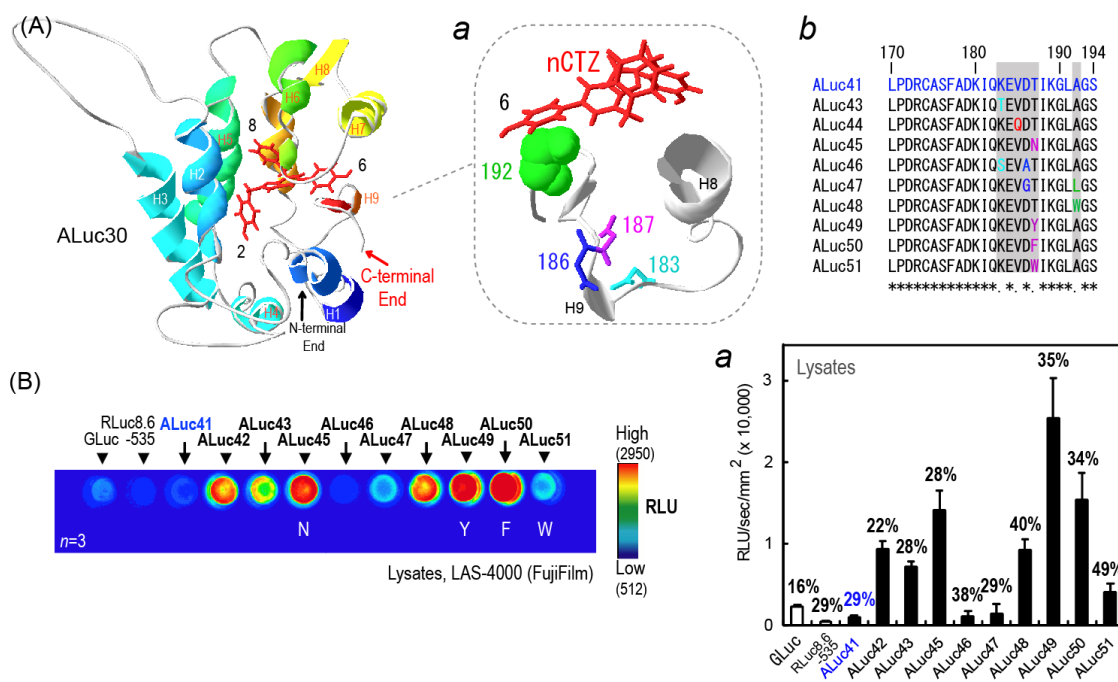


**Figure 4-4** The significance of the C-terminal end of ALuc41–51, promoted by the super 2-dimensional molecular structure of ALuc30. (A) A super 2-dimensional molecular structure of ALuc30. Inset *a* shows the C-terminal end of ALuc30; inset *b* aligns the C-terminal sequences of ALuc41–51. (B) The bioluminescence image of ALuc41–51 compared with conventional marine luciferases. Inset *a* shows the absolute optical intensities normalized by integration time (sec) and light-emitting area (mm<sup>2</sup>). The percentages in the bar graphs indicate the remaining optical intensities after 5 minutes ( $n=3$ ).

#### 4.3.4 The new lineage of ALucs shows unique substrate selectivity without significant colorshifts in the spectra

The relative substrate preference of the new lineage of ALucs was determined with the use of various coelenterazine analogues (Figure 4-5 and Figure 4-7).

The optical intensities of the new lineage of ALucs were generally dark with coelenterazine analogues, except nCTZ (Figure 4-7). The comparison of nCTZ and CTZ*h* showed that the previously reported ALuc16 and ALuc30 were bright with both nCTZ and CTZ*h*, whereas the new lineage of ALucs presented a high preference only for nCTZ (Figure 4-5). The mostly biased optical intensities were observed with ALuc47; i.e., the intensity

of the nCTZ–ALuc47 pair was found to be 217-fold brighter than that of CTZh–ALuc47. This distinctive substrate preference between the old and new lineages of ALucs suggests that the two groups may have a distinctive substrate–luciferase binding chemistry (e.g., turnover rate and quantum yields).

The spectrum peaks ( $\lambda_{\max}$ ) of the new ALucs were generally found in the green region of 487–500 nm with the substrates nCTZ and CTZh (Figure 4-5(B)). The spectrum peak heights of ALuc16 were almost invariant with the addition of nCTZ or CTZh. In contrast, the new ALucs (ALuc42 and 47) greatly preferred nCTZ for better optical intensities. In the case of ALuc42, the red light longer than 600 nm to the total was approximately 4%.

The T187 at the C-terminal end of ALuc41 was substituted by N (ALuc45), Y (ALuc49), F (ALuc50), and W (ALuc51) to obtain possible redshifts in the spectra by the formation of  $\pi$ – $\pi$  stacking or hydrogen bonds between the substrate and side chains of the active site of ALucs. However, no considerable red- or blue-shifts were observed in the spectra of the new lineage of ALucs after the addition of either nCTZ or CTZh.

The substrate-specific bioluminescence of the new lineage of ALucs was further examined with the use of a series of coelenterazine analogues (Figure 4-7). The analogues were categorized into three groups: the first group either had or did not have hydroxyl groups at both the C2 and C6 positions of the imidazopyradinone backbone (Group 1), the second group had no hydroxyl group or modification at the C2 position (Group 2), and the third group commonly had a cyclopropyl (CP) or an isopropyl (IP) group at the C8 position (Group 3). The maximal optical intensities were found with the nCTZ in Group 1, whereas no considerable optical intensities were observed with Group 3, which carried CP or IP. Very poor optical intensities were observed with Group 2.

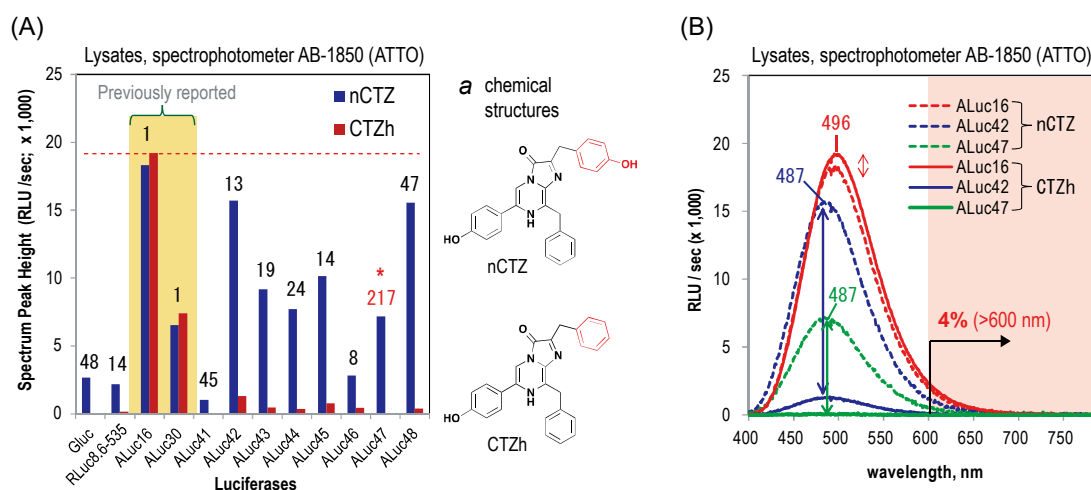


**Figure 4-5** Substrate-driven properties of the bioluminescence spectra of ALucs. (A) The peak heights of the bioluminescence spectra of various luciferases according to nCTZ (blue bars) and CTZh (red bars). The numbers on the bars indicate the fold intensities of each luciferase with nCTZ compared with CTZh. The red asterisk “\*” denotes the maximal fold intensity variance with nCTZ and CTZh. The yellow shaded area shows the spectrum heights of previously reported ALucs. Inset *a* presents a comparison of the chemical structures of nCTZ and CTZh. (B) Comparison of the bioluminescence spectra of ALuc16, 42, and ALuc47 according to nCTZ (dotted line) and CTZh (solid line). The pink shaded area indicates wavelengths longer than 600 nm.

#### 4.3.5 Live cell bioluminescence imaging with conventional and newly established ALucs

The live cell images of conventional and newly established ALucs were determined in living COS-7 cells grown in 6-channel microslides (Figure 4-6).

NanoLuc and RLuc8.6-535 have been previously reported as the brightest among marine luciferases<sup>9, 13, 14</sup>. Thus their live cell images were compared with those of ALuc49 (Figure 4-6(A)). The results showed that the applied substrates pinpoint illuminated the specific luciferases in the live cells of the microslides; i.e., furimazine and 6piOH-CTZ selectively illuminated NanoLuc and RLuc8.6-535, respectively. Meanwhile, nCTZ showed the brightest optical image with ALuc49. The comparison of absolute intensities indicated that the NanoLuc–furimazine pair (102,347 RLU/sec/mm<sup>2</sup> (±1,727 s.d.)) was approximately 2-fold brighter than the ALuc49–nCTZ pair (50,867 RLU/sec/mm<sup>2</sup> (±1,600 s.d.)) in the live cells (Figure 4-6(B)). The poorest absolute optical intensities of the luciferases in live cells were found with 6piOH-CTZ (1,937 RLU/sec/mm<sup>2</sup> (±71 s.d.)).

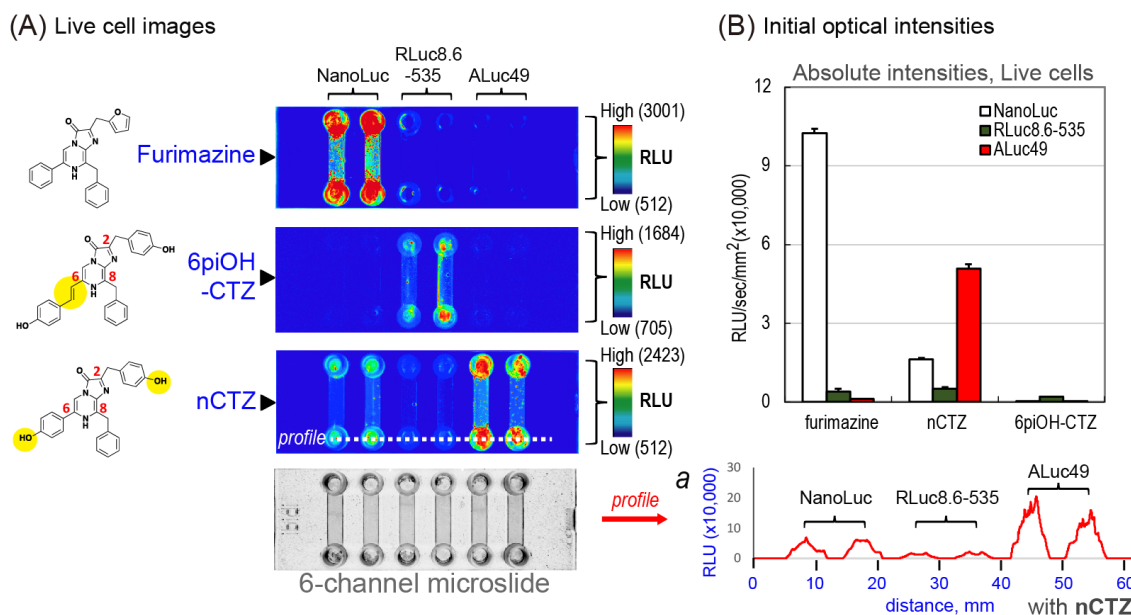


**Figure 4-6** (A) Live cell bioluminescence imaging with conventional and newly established ALucs. The optical image was taken with a CCD camera equipped with the LAS-4000 system (Fujifilm) after simultaneous injection of furimazine, nCTZ, or 6piOH-CTZ with the use of a multichannel micropipette. Inset *a* shows the optical profile of the microslide containing COS-7 cells after the addition of nCTZ. (B) The absolute optical intensities of the live cells on the microslides after the addition of furimazine, nCTZ, or 6piOH-CTZ.

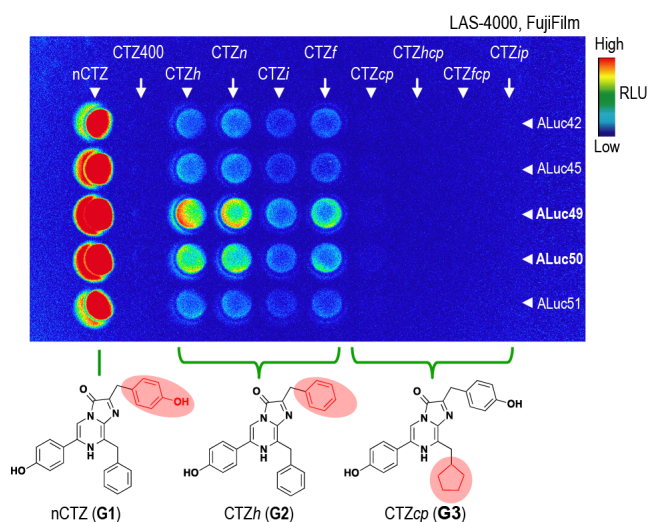


**Figure 4-7** Substrate-specific bioluminescence intensities of the new lineage of ALucs. The substrate-driven optical intensities were determined with the use of various coelenterazine analogues. The new ALucs showed a greatly biased optical intensity with nCTZ (Group 1). The CTZh and CTZcp represent Groups 2 and 3, respectively.

### **4.3.6 Determination of the overall photon fluxes**

The overall photon fluxes of the luciferases were determined by long-term integration of the photons, which were generated by complete consumption of a low concentration of luciferins with overexpressed luciferases (Figure 4-8 and Table 4-1).

With respect to the substrate-binding chemistry, the old lineage of ALucs may be close to RLuc8.6-535, whereas the new lineage of ALucs (ALuc47 and ALuc49) should be categorized into a different group, considering the greatly biased optical preference only for nCTZ. The overall trend of the total photon fluxes indicates that the new lineage of ALuc47 and ALuc49 may have poorer optical efficiency compared with the previously reported ALuc16 and ALuc30, but a greatly biased optical preference only for nCTZ as a unique optical property. Considering the sum of photon fluxes of RLuc8.6-535 is slightly smaller than the previously reported QYs for RLuc and RLuc8 (5.3% and 6.9%, respectively, with nCTZ)<sup>9</sup>, the sum of photon fluxes may be close to the absolute QYs and reflect the trend of the QYs of the luciferases.

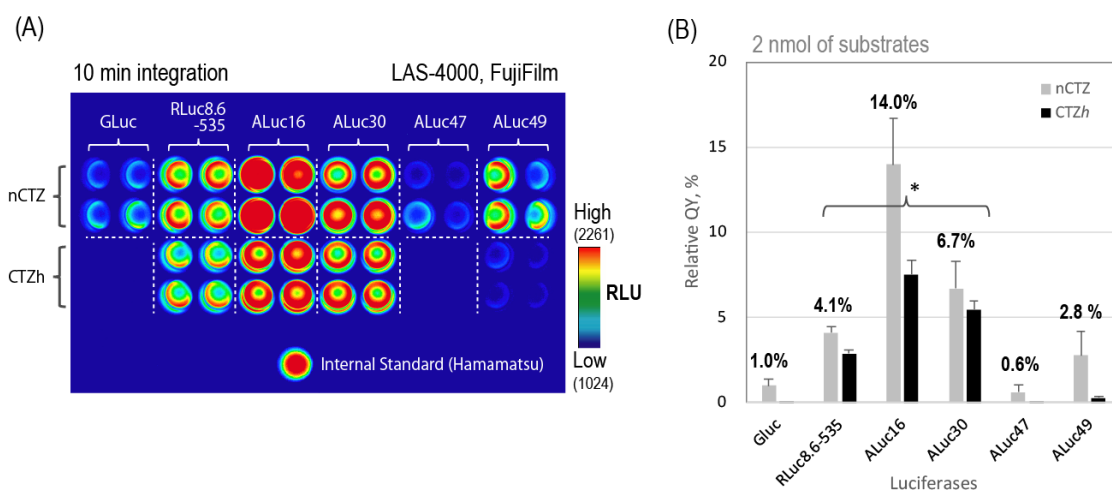


**Figure 4-8** Determination of the relative quantum yields (QYs). (A) The optical image after long-term integration (10 minutes) of the emitted photons. The diluted substrates (2 nmole) were set for complete consumption by overexpressed luciferases ( $n=4$ ). (B) The sum of photon fluxes of the luciferases according to the substrates. The specific values are shown in Table 4-1. The percentages on the bars denote the sum of photon fluxes of luciferases with nCTZ. The asterisk “\*” indicates a group of luciferases that emit relatively unbiased bioluminescence with CTZ analogues.

**Table 4-1** The specific values of the QYs of the marine luciferases with nCTZ and CTZh. The QY values are presented in the bar graphs in Figure 4-8.

	(Photons/mm <sup>2</sup> /sec)				
	nCTZ		CTZh		
	Ave	SD	Ave	SD	
<b>GLuc</b>	10,840	± 3,874	353	± 58	
<b>RLuc8.6-535</b>	44,499	± 3,864	31,298	± 2,350	
<b>ALuc16</b>	151,312	± 29,485	81,471	± 8,802	
<b>ALuc30</b>	72,429	± 17,696	59,087	± 5,879	
<b>ALuc47</b>	6,772	± 4,811	250	± 87	
<b>ALuc49</b>	29,956	± 15,357	2,987	± 1,286	

### 4.3.7 Molecular tension probes

The useful features of the new lineage of ALucs were shown by applying the ALucs to a single-chain bioluminescent probe, referred to as a “bioluminescent capsule” (Figure 4-9).

The addition of an apoptosis inducer, staurosporine (STS), increased the optical intensities of P47 and P49 by 50% and 28%, respectively. These enhanced optical intensities were attributed to the activated caspases provoking the release of the full-length ALucs from the capsules, allowing enhanced optical intensities.

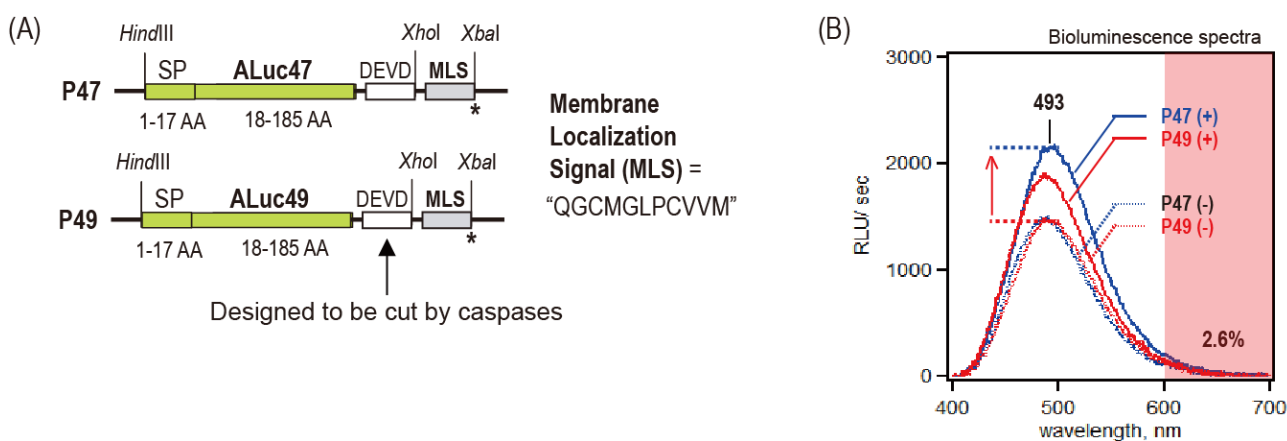


**Figure 4-9** Illumination of caspase activities with ALuc47- and ALuc49-based bioluminescent probes, referred to as “bioluminescent capsules,” in living mammalian cells. (A) The cDNA constructs encoding the created bioluminescent capsules, P47 and P49. The capsules were made by linking the newly fabricated ALuc47 or ALuc49 with the membrane localization signal (MLS) through flexible linkers. (B) The optical spectra of the capsules with and without an apoptosis inducer staurosporine (STS). The capsules are designed to be initially anchored in the PM. The (+) and (-) signs indicate the addition of the apoptosis inducer staurosporine (STS) and the vehicle, respectively.

#### 4.4. Discussion

We previously created a series of artificial luciferases by extracting the frequently occurring amino acids in a bundle of aligned copepod luciferase sequences<sup>7</sup>. Although the approach was unique and experimentally successful, no follow-up studies by other research groups have been reported thus far. Meanwhile, the copepod luciferase sequences in public databases have further increased to 25 kinds<sup>10</sup>. Based on the increased data pool, we created a new lineage of ALucs that is phylogenetically distinctive from any existing luciferases, including previously reported ALucs, as shown in Figure 4-3(B).

It is interesting to discuss the biased substrate selectivity of the previously and the newly created lineages of ALucs (Figure 4-5). The only difference between nCTZ and CTZ*h* is the hydroxyl group (OH) at the C-2 position. This therefore shows that the OH group at the C-2 position works as a determinant of the substrate selectivity of the old and new lineages of ALucs; i.e., the OH group at the C-2 position is essential for the new lineage of ALucs (ALuc41-51) and cannot be substituted by iodine or fluorine, as shown in Figure 4-7. In contrast, the active site of the old lineage of ALucs (ALuc16-34) is considered to have a very loose moiety on accommodation of the functional groups at the C-2 position of the substrate, because ALuc30 activates CTZ*h*, CTZ*f*, and CTZ*i* with high selectivity<sup>12</sup>. This clear variance in substrate preference between the two lineages of ALucs suggests that their respective substrate-binding chemistries may be distinctive from each other. The distinctive substrate selectivity of the new ALucs may be taken for granted, because the new ALucs form a new lineage in the phylogenetic tree (Figure 4-3(B)).

The creation of *de novo* proteins is generally regarded to consume a large amount of time and effort. In this study, the following success factors are considered: (i) information on copepod luciferases has been recently accumulated in public databases<sup>15</sup>; (ii) the sequences of copepod luciferases are highly conserved, making it easy to identify consensus amino acids; and (iii) the authors empirically know that the high homology between the two-repeated catalytic domains of a copepod luciferase is proportional to the optical intensity and sustainability. Thus, the authors consider this new lineage of ALucs as a rare successful example with copepod luciferases, which may not be generally applicable to other marine luciferase cases.

## 4.5. Conclusions

Taken together, the present study provides a unique approach to creating *de novo* enzymes and encourages researchers to fabricate their own artificial enzymes of interest with designed optical properties and functionalities for bioassays, where (i) The luciferase sequence–activity comparison revealed that the C-

terminal end of ALucs dominates the enzymatic activities; (ii) The substrate study revealed that the OH group at the C-2 position of the substrate is essential for the new lineage of ALucs, and cannot be substituted by other functional groups or atoms; (iii) The total photon fluxes of old and new lineages of luciferases were determined and compared for the first time. For the exact determination, I synthesized nCTZ and CTZh. Considering that the modification of the enzymatic activities of luciferases has been mostly dependent on Darwinian natural selection or random mutagenesis, the present approach to creating *de novo* enzymes with designed optical properties and functionalities may be an important addition to the standard optical toolbox for bioassays and molecular imaging.

## References

- (1) Hastings, J. W., *Gene*, **1996**, *173*, 5-11.
- (2) Viviani, V. R., Uchida, A., Viviani, W., and Ohmiya, Y., *Photochem. Photobiol.*, **2002**, *76*, 538-544.
- (3) Badr, C. E., *Methods Mol. Biol.*, **2014**, *1098*, 1-18.
- (4) Stolz, U., Velez, S., Wood, K. V., Wood, M., and Feder, J. L., *Proc. Natl. Acad. Sci. U. S. A.*, **2003**, *100*, 14955-14959.
- (5) Loening, A. M., Wu, A. M., and Gambhir, S. S., *Nat. Methods*, **2007**, *4*, 641-643.
- (6) Kim, S. B., *Protein Eng. Des. Sel.*, **2012**, *25*, 261-269.
- (7) Kim, S. B., Torimura, M., and Tao, H., *Bioconjugate Chem.*, **2013**, *24*, 2067-2075.
- (8) Lehmann, M., Loch, C., Middendorf, A., Studer, D., Lassen, S. F., Pasamontes, L., van Loon, A. P. G. M., and Wyss, M. *Protein Eng.*, **2002**, *15*, 403-411.
- (9) Loening, A. M., Fenn, T. D., Wu, A. M., and Gambhir, S. S. *Protein Eng. Des. Sel.*, **2006**, *19*, 391-400.
- (10) Takenaka, Y., Noda-Ogura, A., Imanishi, T., Yamaguchi, A., Gojobori, T., and Shigeri, Y. *Gene*, **2013**, *528*, 201-205.

- (11) Crooks, G. E., Hon, G., Chandonia, J. M., and Brenner, S. E., *Genome Res*, **2004**, *14*, 1188-1190.
- (12) Kim, S. B., and Izumi, H., *Biochem. Biophys. Res. Comm.*, **2014**, *448*, 418-423.
- (13) Hall, M. P., Unch, J., Binkowski, B. F., Valley, M. P., Butler, B. L., Wood, M. G., Otto, P., Zimmerman, K., Vidugiris, G., Machleidt, T., Robers, M. B., Benink, H. A., Eggers, C. T., Slater, M. R., Meisenheimer, P. L., Klaubert, D. H., Fan, F., Encell, L. P., and Wood, K. V., *ACS Chem. Biol.*, **2012**, *7*, 1848-1857.
- (14) Loening, A. M., Dragulescu-Andrasi, A., and Gambhir, S. S., *Nat. Methods.*, **2010**, *7*, 5-6.
- (15) Takenaka, Y., Yamaguchi, A., Tsuruoka, N., Torimura, M., Gojobori, T., and Shigeri, Y., *Mol. Biol. Evol.*, **2010**, *29*, 1669-1681.
- (16) Tannous, B. A., Kim, D. E., Fernandez, J. L., Weissleder, R., and Breakefield, X. O., *Mol. Ther.*, **2005**, *11*, 435-443.
- (17) Seliger, H. H., and Mc, E. W., *Arch. Biochem. Biophys.*, **1960**, *88*, 136-141.
- (18) Kim, S. B., Ito, Y., and Torimura, M., *Bioconjugate Chem.*, **2012**, *23*, 2221-2228.

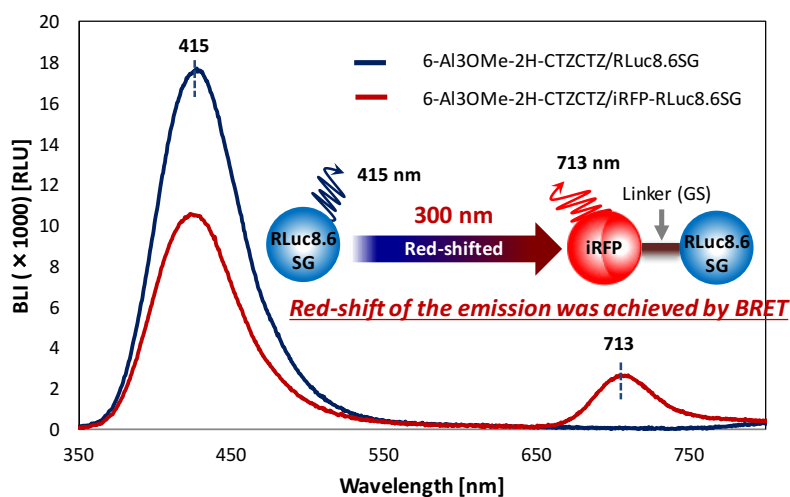


## Chapter5

# Blue Coelenterazine Derivatives for Highly Sensitive Bioluminescence Imaging

### Summary

Bioluminescence imaging has been suffering from light absorption by biological molecules such as water, hemoglobin, melanin and light scattering in mammalian tissue, due to its short-wavelength luminescence spectra. Here, I report a near-infrared (NIR) BRET protein consisting of light output enhanced *Renilla* luciferase (RLuc) mutants and near-infrared fluorescent protein (iRFP), which is illuminated by a blue-shifted CTZ derivative. To achieve highly sensitive bioluminescence imaging, I conduct structure-activity-related studies between 18 novel coelenterazine (CTZ) derivatives and RLuc mutants. Therefore, in this chapter, I achieve luminescence enhancement and red-shift of the emission of marine luciferase by bioluminescence resonance energy transfer (BRET) from the bright RLuc system to the fluorescent protein.



## 5.1. Introduction

Bioluminescence (BL) imaging is becoming a standard optical technique for selectively visualizing target biological molecules or organs to understand life phenomena<sup>1-4</sup>. Most bioluminescence occurs through an enzymatic reaction between the bioluminescent substrate (luciferin) and an enzyme (luciferase). The advantages of bioluminescence over fluorescence are lower background signals due to the absence of an excitation light source. Therefore, the highly sensitive analysis by BL is mostly due to negligibly small background signals, which result in higher signal-to-noise (S/N) ratio<sup>5</sup>. However, as described in Chapter 1, the signal of BL is also lower than that of fluorescence, which causes low spatio- and/or temporal-resolution. In addition, the color variation of BL is relatively sparse compared to that of fluorescence. Recently, to overcome these drawbacks, some research groups reported luciferase mutants emitting light through bioluminescence resonance energy transfer (BRET)<sup>6-9</sup>, in which the excited energy of an enzymatic reaction is transferred intermolecularly to a fluorescent protein (FPs). For example, BAF-Y<sup>6</sup> and Nano-lantern<sup>7</sup> achieve an improvement of the bioluminescence output compared to that of one of the most versatile luciferases, the mutant of *Renilla reniformis* (RLuc) called RLuc8. In addition, the color variants of Nano-lantern are also expanded by changing FPs (see Chapter 1.5)<sup>9</sup>. The fabrication of a BRET protein is recognized as an efficient strategy to extend the emission color palette and to improve BL signals. Recently, enhanced Nano-lantern (eNL) with its optimal luciferin called furimazine allows real time monitoring of multiplex cellular events with high spectral resolution<sup>8</sup>. However, the emission color range of the reported FPs fused marine luciferases is limited to the range from 460 nm to 600 nm (Figure 5-1). In this chapter, by developing novel blue-shifted CTZ derivatives and a phytochrome-based red fluorescent protein (iRFP)<sup>10</sup> fused BRET probe, I extend the emission color palette of CTZ-utilizing BL systems, particularly for the blue-region (emission maximum 410 nm) and near-infrared (NIR) region (emission maximum 713 nm; emission over 700 nm is the most appropriate range for *in vivo* imaging of deep physiological tissue<sup>11</sup>).

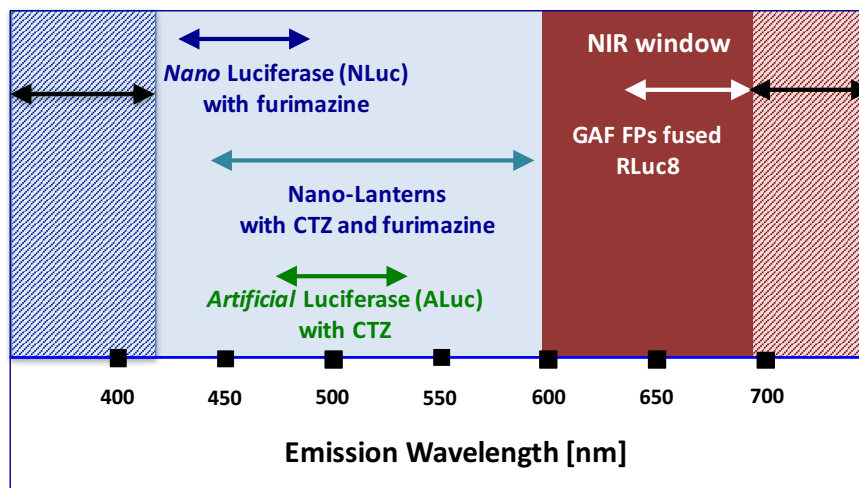
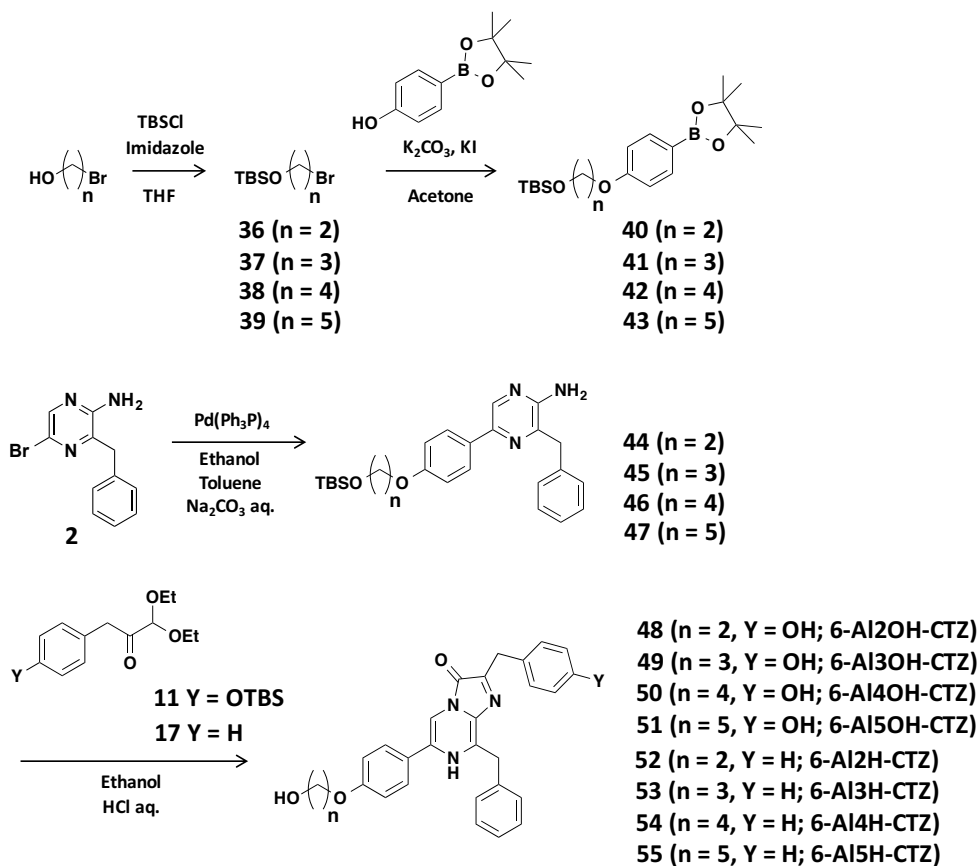


Figure 5-1 Recent development of marine luciferases for BL imaging

## 5.2. Experimental section

### 5.2.1. Synthesis of novel CTZ derivatives



Synthetic scheme for 6-alkylated CTZ derivatives

***tert*-Butyldimethyl(2-(4-(4,4,5,5-tetramethyl-1,3,2-dioxaborolan-2-yl)phenoxy)ethoxy)silane (40)**

4-(4,4,5,5-Tetramethyl-1,3,2-dioxaborolan-2-yl)phenol (500.0 mg, 2.2 mmol, 1 eq.) and K<sub>2</sub>CO<sub>3</sub> (410.0 mg, 2.9 mmol, 1.3 eq.) were dissolved in acetone (20 ml) and stirred at room temperature. (2-Bromoethoxy)(*tert*-butyl)dimethylsilane (**36**) (812.0 mg, 3.4 mmol, 1.5 eq.) and potassium iodide (20.0 mg, 0.1 mmol, 0.05 eq.) were dissolved in acetone (20 ml) and added into the reaction mixture and stirred for 24 hours at 70 °C. After cooling to room temperature, the solution was extracted with ethyl acetate, and the clear organic phase was washed with water and brine, dried over Na<sub>2</sub>SO<sub>4</sub> and evaporated. The resulting residue was purified by flash chromatography (silica gel, eluent composition: n-hexane / ethyl acetate = 80/20), affording *tert*-butyldimethyl(2-(4-(4,4,5,5-tetramethyl-1,3,2-dioxaborolan-2-yl)phenoxy)ethoxy)silane (**40**) as a white solid (307 mg, 36%)

<sup>1</sup>H-NMR (500 MHz, CD<sub>3</sub>OD): δ (ppm) = 7.73 (d, *J* = 8.5 Hz, 2H), 6.89 (d, *J* = 8.5 Hz, 2H), 4.05 (t, *J* = 5.1 Hz, 2H), 3.97 (t, *J* = 5.4 Hz, 2H), 1.33(m, 12H), 0.90 (s, 9H), 0.09 (s, 6H). <sup>13</sup>C-NMR (125 MHz, CDCl<sub>3</sub>): δ (ppm) = -5.05, 18.54, 24.99, 26.05, 62.07, 69.18, 83.66, 114.02, 136.61, 161.64. HR-MS: calcd for C<sub>20</sub>H<sub>35</sub>BO<sub>4</sub>Si: 379.2476 [M+H]<sup>+</sup>, found: *m/z* 379.2477.

***tert*-Butyldimethyl(3-(4-(4,4,5,5-tetramethyl-1,3,2-dioxaborolan-2-yl)phenoxy)propoxy)silane (41)**

4-(4,4,5,5-Tetramethyl-1,3,2-dioxaborolan-2-yl)phenol (500.0 mg, 2.2 mmol, 1 eq.) and K<sub>2</sub>CO<sub>3</sub> (410.0 mg, 2.9 mmol, 1.3 eq.) were dissolved in acetone (20 ml) and stirred at room temperature. (3-Bromopropoxy)(*tert*-butyl)dimethylsilane (**37**) (690.0 mg, 2.7 mmol, 1.2 eq.) and potassium iodide (20.0 mg, 0.1 mmol, 0.05 eq.) were dissolved in acetone (20 ml) and added into the reaction mixture and stirred for 13 hours at 70 °C. After cooling to room temperature, the solution was extracted with ethyl acetate, and the clear organic phase was washed with water and brine, dried over Na<sub>2</sub>SO<sub>4</sub> and evaporated. The resulting residue was purified by flash chromatography (silica gel, eluent composition: n-hexane / ethyl acetate = 80/20), affording *tert*-

butyldimethyl(3-(4-(4,4,5,5-tetramethyl-1,3,2-dioxaborolan-2-yl)phenoxy)propoxy)silane (**41**) as a white solid (489.3 mg, 63%)

$^1\text{H-NMR}$  (500 MHz,  $\text{CD}_3\text{OD}$ ):  $\delta$  (ppm) = 7.73 (d,  $J$  = 8.5 Hz, 2H), 6.89 (d,  $J$  = 8.5 Hz, 2H), 4.08 (t,  $J$  = 6.3 Hz, 2H), 3.79 (t,  $J$  = 6.3 Hz, 2H), 1.97 (m, 2H), 1.32 (s, 12H), 0.88 (s, 9H), 0.03 (s, 6H).  $^{13}\text{C-NMR}$  (125 MHz,  $\text{CDCl}_3$ ):  $\delta$  (ppm) = -5.24, 18.45, 25.00, 26.05, 32.45, 59.57, 64.33, 83.67, 113.97, 136.60, 161.79. HR-MS: calcd for  $\text{C}_{21}\text{H}_{37}\text{BO}_4\text{Si}$ : 393.2632  $[\text{M}+\text{H}]^+$ , found:  $m/z$  393.2609.

***tert*-Butyldimethyl(4-(4-(4,4,5,5-tetramethyl-1,3,2-dioxaborolan-2-yl)phenoxy)butoxy)silane (42)**

4-(4,4,5,5-Tetramethyl-1,3,2-dioxaborolan-2-yl)phenol (500.0 mg, 2.2 mmol, 1 eq.) and  $\text{K}_2\text{CO}_3$  (410.0 mg, 2.9 mmol, 1.3 eq.) were dissolved in acetone (20 ml) and stirred at room temperature. (4-Bromobutoxy)(*tert*-butyl)dimethylsilane (**38**) (721.6 mg, 2.7 mmol, 1.2 eq.) and potassium iodide (20.0 mg, 0.1 mmol, 0.05 eq.) were dissolved in acetone (20 ml) and added into the reaction mixture and stirred for 13 hours at 70 °C. After cooling to room temperature, the solution was extracted with ethyl acetate, and the clear organic phase was washed with water and brine, dried over  $\text{Na}_2\text{SO}_4$  and evaporated. The resulting residue was purified by flash chromatography (silica gel, eluent composition: n-hexane / ethyl acetate = 80/20), affording *tert*-butyldimethyl(4-(4-(4,4,5,5-tetramethyl-1,3,2-dioxaborolan-2-yl)phenoxy)butoxy)silane (**42**) as a white solid (881 mg, 95%)

$^1\text{H-NMR}$  (500 MHz,  $\text{CD}_3\text{OD}$ ):  $\delta$  (ppm) = 7.73 (d,  $J$  = 7.4 Hz, 2H), 6.87 (d,  $J$  = 7.4 Hz, 2H), 4.00 (t,  $J$  = 6.0 Hz, 2H), 3.68-3.63 (m, 2H), 1.86-1.81 (m, 2H), 1.70-1.65 (m, 2H), 1.32 (s, 12H), 0.89 (s, 9H), 0.05 (s, 6H).  $^{13}\text{C-NMR}$  (125 MHz,  $\text{CDCl}_3$ ):  $\delta$  (ppm) = -5.16, 18.46, 24.98, 25.97, 26.09, 29.44, 62.91, 67.70, 83.63, 113.95, 136.60, 161.81. HR-MS: calcd for  $\text{C}_{22}\text{H}_{39}\text{BO}_4\text{Si}$ : 407.2789  $[\text{M}+\text{H}]^+$ , found:  $m/z$  407.2779.

***tert*-Butyldimethyl((5-(4-(4,4,5,5-tetramethyl-1,3,2-dioxaborolan-2-yl)phenoxy)pentyl)oxy)silane (43)**

4-(4,4,5,5-Tetramethyl-1,3,2-dioxaborolan-2-yl)phenol (500.0 mg, 2.2 mmol, 1 eq.) and K<sub>2</sub>CO<sub>3</sub> (410.0 mg, 2.9 mmol, 1.3 eq.) were dissolved in acetone (20 ml) and stirred at room temperature. ((5-Bromopentyl)oxy)(*tert*-butyl)dimethylsilane (**39**) (759.5 mg, 2.7 mmol, 1.2 eq.) and potassium iodide (20.0 mg, 0.1 mmol, 0.05 eq.) were dissolved in acetone (20 ml) and added into the reaction mixture and stirred for 7 hours at 70 °C. After cooling to room temperature, the solution was extracted with ethyl acetate, and the clear organic phase was washed with water and brine, dried over Na<sub>2</sub>SO<sub>4</sub> and evaporated. The resulting residue was purified by flash chromatography (silica gel, eluent composition: n-hexane / ethyl acetate = 90/10 to 80/20), affording *tert*-butyldimethyl((5-(4-(4,4,5,5-tetramethyl-1,3,2-dioxaborolan-2-yl)phenoxy)pentyl)oxy)silane (**43**) as a white solid (916 mg, 96%)

<sup>1</sup>H-NMR (500 MHz, CD<sub>3</sub>OD): δ (ppm) = 7.73 (d, *J* = 8.5 Hz, 2H), 6.87 (d, *J* = 8.5 Hz, 2H), 3.98 (t, *J* = 6.5 Hz, 2H), 3.64-3.60 (m, 2H), 1.81-1.78 (m, 2H), 1.59-1.48 (m, 4H), 1.33 (s, 12H), 0.89 (s, 9H), 0.04 (s, 6H). <sup>13</sup>C-NMR (125 MHz, CDCl<sub>3</sub>): δ (ppm) = -5.13, 18.50, 22.47, 24.99, 26.11, 29.13, 32.66, 63.15, 67.79, 83.64, 113.97, 136.61, 161.84. HR-MS: calcd for C<sub>23</sub>H<sub>41</sub>BO<sub>4</sub>Si: 421.2945 [M+H]<sup>+</sup>, found: *m/z* 421.2927.

**3-Benzyl-5-(4-(2-((*tert*-butyldimethylsilyl)oxy)ethoxy)phenyl)pyrazin-2-amine (44)**

3-Benzyl-5-bromopyrazine-2-amine (**2**) (150 mg, 0.56 mmol, 1 eq.) and *tert*-butyldimethyl(2-(4-(4,4,5,5-tetramethyl-1,3,2-dioxaborolan-2-yl)phenoxy)ethoxy)silane (**40**) (307 mg, 0.81 mmol, 1.4 eq.) were dissolved in toluene (15 ml) and stirred at room temperature. Ethanol (3 ml) and 1 M Na<sub>2</sub>CO<sub>3</sub> aq. (4.5 ml) were added into the reaction mixture. After vacuum deaeration, a catalytic amount of tetrakis(triphenylphosphine)palladium(0) was added into the solution and the mixture was deaerated again and stirred for 12 hours at 100 °C. After cooling to room temperature, the solution was filtered through a Celite pad to remove the palladium catalyst. The solution was extracted with ethyl acetate, and the brown organic phase

was washed with water and brine, dried over Na<sub>2</sub>SO<sub>4</sub> and evaporated. The resulting residue was purified by flash chromatography (silica gel, eluent composition: n-hexane / ethyl acetate = 80/20 to 70/30), affording 3-benzyl-5-(4-(2-((*tert*-butyldimethylsilyl)oxy)ethoxy)phenyl)pyrazin-2-amine (**44**) as a yellow solid (225 mg, 92%).

<sup>1</sup>H-NMR (500 MHz, CDCl<sub>3</sub>): δ (ppm) = 8.33 (s, 1H), 7.86 (d, *J* = 8.5 Hz, 2H), 7.33-7.24 (m, 5H), 6.99 (d, *J* = 8.5 Hz, 2H), 4.33 (s, 2H), 4.17 (s, 2H), 4.09 (t, *J* = 5.1 Hz, 2H), 4.00 (t, *J* = 5.1 Hz, 2H), 0.92 (s, 12H), 0.11 (s, 6H). <sup>13</sup>C-NMR (125 MHz, CDCl<sub>3</sub>): δ (ppm) = -5.02, 18.56, 26.07, 41.40, 62.13, 69.52, 115.00, 127.11, 127.15, 128.70, 129.10, 130.14, 136.99, 140.58, 142.77, 151.38, 159.26. HR-MS: calcd for C<sub>25</sub>H<sub>33</sub>N<sub>3</sub>O<sub>2</sub>Si: 436.2420 [M+H]<sup>+</sup>, found: *m/z* 436.2426.

### 3-Benzyl-5-(4-(3-((*tert*-butyldimethylsilyl)oxy)propoxy)phenyl)pyrazin-2-amine (**45**)

3-Benzyl-5-bromopyrazine-2-amine (**2**) (308 mg, 1.16 mmol, 1 eq.) and *tert*-butyldimethyl(3-(4-(4,4,5,5-tetramethyl-1,3,2-dioxaborolan-2-yl)phenoxy)propoxy)silane (**41**) (702.29 mg, 1.85 mmol, 1.6 eq.) were dissolved in toluene (15 ml) and stirred at room temperature. Ethanol (3 ml) and 1 M Na<sub>2</sub>CO<sub>3</sub> aq. (4.5 ml) were added into the reaction mixture. After vacuum deaeration, a catalytic amount of tetrakis(triphenylphosphine)palladium(0) was added into the solution and the mixture was deaerated again and stirred for 18 hours at 100 °C. After cooling to room temperature, the solution was filtered through a Celite pad to remove the palladium catalyst. The solution was extracted with ethyl acetate, and the brown organic phase was washed with water and brine, dried over Na<sub>2</sub>SO<sub>4</sub> and evaporated. The resulting residue was purified by flash chromatography (silica gel, eluent composition: n-hexane / ethyl acetate = 80/20 to 70/30), affording 3-benzyl-5-(4-(3-((*tert*-butyldimethylsilyl)oxy)propoxy)phenyl)pyrazin-2-amine (**45**) as a yellow solid (478.9 mg, 91%).

<sup>1</sup>H-NMR (500 MHz, CDCl<sub>3</sub>): δ (ppm) = 8.33 (s, 1H), 7.86 (d, *J* = 8.5 Hz, 2H), 7.33-7.25 (m, 5H), 6.98 (d, *J*

= 8.5 Hz, 2H), 4.34 (s, 2H), 4.17 (s, 2H), 4.11 (t,  $J = 6.3$  Hz, 2H), 3.82 (t,  $J = 5.7$  Hz, 2H), 2.00 (quin,  $J = 6.0$  Hz, 2H), 0.89 (s, 12H), 0.05 (s, 6H).  $^{13}\text{C}$ -NMR (125 MHz,  $\text{CDCl}_3$ ):  $\delta$  (ppm) = -5.21, 18.47, 26.07, 32.50, 41.42, 59.60, 64.67, 114.93, 127.11, 127.15, 128.71, 129.10, 129.93, 137.00, 140.58, 142.86, 151.34, 159.40. HR-MS: calcd for  $\text{C}_{26}\text{H}_{35}\text{N}_3\text{O}_2\text{Si}$ : 450.2577  $[\text{M}+\text{H}]^+$ , found:  $m/z$  450.2557.

### 3-Benzyl-5-(4-(4-((*tert*-butyldimethylsilyl)oxy)butoxy)phenyl)pyrazin-2-amine (46)

3-Benzyl-5-bromopyrazine-2-amine (**2**) (180 mg, 0.68 mmol, 1 eq.) and *tert*-butyldimethyl(4-(4-(4,4,5,5-tetramethyl-1,3,2-dioxaborolan-2-yl)phenoxy)butoxy)silane (**42**) (443 mg, 1.09 mmol, 1.6 eq.) were dissolved in toluene (10 ml) and stirred at room temperature. Ethanol (2 ml) and 1 M  $\text{Na}_2\text{CO}_3$  aq. (3 ml) were added into the reaction mixture. After vacuum deaeration, a catalytic amount of tetrakis(triphenylphosphine)palladium(0) was added into the solution and the mixture was deaerated again and stirred for 15 hours at 100 °C. After cooling to room temperature, the solution was filtered through a Celite pad to remove the palladium catalyst. The solution was extracted with ethyl acetate, and the brown organic phase was washed with water and brine, dried over  $\text{Na}_2\text{SO}_4$  and evaporated. The resulting residue was purified by flash chromatography (silica gel, eluent composition: n-hexane / ethyl acetate = 80/20 to 67/33), affording 3-benzyl-5-(4-(4-((*tert*-butyldimethylsilyl)oxy)butoxy)phenyl)pyrazin-2-amine (**46**) as a yellow solid (303.5 mg, 96%).

$^1\text{H}$ -NMR (500 MHz,  $\text{CDCl}_3$ ):  $\delta$  (ppm) = 8.32 (s, 1H), 7.86 (d,  $J = 8.8$  Hz, 2H), 7.30-7.25 (m, 5H), 6.97 (d,  $J = 8.5$  Hz, 2H), 4.34 (s, 2H), 4.17 (s, 2H), 4.03 (t,  $J = 6.5$  Hz, 2H), 3.69 (t,  $J = 6.3$  Hz, 2H), 1.89-1.84 (m, 2H), 1.73-1.69 (m, 2H), 0.90 (s, 12H), 0.06 (s, 6H).  $^{13}\text{C}$ -NMR (125 MHz,  $\text{CDCl}_3$ ):  $\delta$  (ppm) = -5.13, 18.49, 26.02, 26.11, 29.48, 41.42, 62.95, 68.04, 114.94, 127.12, 127.16, 128.71, 129.11, 129.94, 136.99, 140.58, 142.87, 151.34, 159.42. HR-MS: calcd for  $\text{C}_{27}\text{H}_{37}\text{N}_3\text{O}_2\text{Si}$ : 467.2733  $[\text{M}+\text{H}]^+$ , found:  $m/z$  464.2724.

**3-Benzyl-5-(4-((5-((*tert*-butyldimethylsilyl)oxy)pentyl)oxy)phenyl)pyrazin-2-amine (47)**

3-Benzyl-5-bromopyrazine-2-amine (**2**) (180 mg, 0.68 mmol, 1 eq.) and *tert*-butyldimethyl((5-(4-(4,4,5,5-tetramethyl-1,3,2-dioxaborolan-2-yl)phenoxy)pentyl)oxy)silane (**43**) (458 mg, 1.09 mmol, 1.6 eq.) were dissolved in toluene (10 ml) and stirred at room temperature. Ethanol (2 ml) and 1 M Na<sub>2</sub>CO<sub>3</sub> aq. (3 ml) were added into the reaction mixture. After vacuum deaeration, a catalytic amount of tetrakis(triphenylphosphine)palladium(0) was added into the solution and the mixture was deaerated again and stirred for 12 hours at 100 °C. After cooling to room temperature, the solution was filtered through a Celite pad to remove the palladium catalyst. The solution was extracted with ethyl acetate, and the brown organic phase was washed with water and brine, dried over Na<sub>2</sub>SO<sub>4</sub> and evaporated. The resulting residue was purified by flash chromatography (silica gel, eluent composition: n-hexane / ethyl acetate = 80/20 to 67/33), affording 3-benzyl-5-(4-((5-((*tert*-butyldimethylsilyl)oxy)pentyl)oxy)phenyl)pyrazin-2-amine (**47**) as a yellow solid (253 mg, 52%).

<sup>1</sup>H-NMR (500 MHz, CDCl<sub>3</sub>): δ (ppm) = 8.32 (s, 1H), 7.86 (d, *J* = 8.5 Hz, 2H), 7.30-7.25 (m, 5H), 6.97 (d, *J* = 8.8 Hz, 2H), 4.34 (s, 2H), 4.17 (s, 2H), 4.01 (t, *J* = 6.5 Hz, 2H), 3.64 (t, *J* = 6.3 Hz, 2H), 1.84-1.81 (m, 2H), 1.61-1.57 (m, 2H), 1.54-1.51 (m, 2H), 0.90 (s, 12H), 0.06 (s, 6H). <sup>13</sup>C-NMR (125 MHz, CDCl<sub>3</sub>): δ (ppm) = 5.11, 18.51, 22.51, 26.13, 29.20, 32.70, 41.42, 63.17, 68.13, 114.95, 127.12, 128.61, 128.71, 129.10, 129.93, 136.98, 140.58, 142.87, 151.34, 159.45. (the signal for one carbon could not be assigned due to broadening) HR-MS: calcd for C<sub>28</sub>H<sub>39</sub>N<sub>3</sub>O<sub>2</sub>Si: 478.2890 [M+H]<sup>+</sup>, found: *m/z* 478.2876.

**8-Benzyl-2-(4-hydroxybenzyl)-6-(4-(2-hydroxyethoxy)phenyl)imidazo[1,2-*a*]pyrazin-3(7*H*)-one (48) (6-AI2OH-CTZ)**

3-Benzyl-5-(4-(2-((*tert*-butyldimethylsilyl)oxy)ethoxy)phenyl)pyrazin-2-amine (**44**) (30 mg, 0.06 mmol, 1 eq.) and 3-(4-((*tert*-butyldimethylsilyl)oxy)phenyl)-1,1-diethoxypropan-2-one (**11**) (47.9 mg, 0.13 mmol, 2 eq.)

were dissolved in ethanol (2.0 ml) and H<sub>2</sub>O (0.2 ml) and stirred at room temperature. After vacuum deaeration, the solution was cooled to 0 °C and HCl (0.1 ml) was added under nitrogen flow. Once the solution reached room temperature, it was heated and stirred for 5 hours at 80 °C. The solvent was evaporated under vacuum and the crude compound was purified by semipreparative reversed-phase HPLC (eluent composition: CH<sub>3</sub>OH / H<sub>2</sub>O = 60/40 with 0.1% formic acid), affording 8-benzyl-2-(4-hydroxybenzyl)-6-(4-(2-hydroxyethoxy)phenyl)imidazo[1,2-*a*]pyrazin-3(7*H*)-one (**48**) as a yellow solid (12.8 mg, 45%).

<sup>1</sup>H-NMR (500 MHz, CD<sub>3</sub>OD): δ (ppm) = 7.63 (s, 1H), 7.56 (d, *J* = 8.3 Hz, 2H), 7.39-7.21 (m, 5H), 7.15 (d, *J* = 8.3 Hz, 2H), 7.03 (d, *J* = 8.3 Hz, 2H), 6.69 (d, *J* = 8.5 Hz, 2H), 4.39 (s, 2H), 4.08-4.06 (m, 4H), 3.88 (t, *J* = 4.8 Hz, 2H). <sup>13</sup>C-NMR (125 MHz, CD<sub>3</sub>OD, CDCl<sub>3</sub>): δ (ppm) = 33.20, 61.60, 70.74, 108.17, 116.07, 116.19, 128.13, 129.30, 129.74, 129.78, 130.78, 138.16, 156.97, 161.57. HR-MS: calcd for C<sub>28</sub>H<sub>25</sub>N<sub>3</sub>O<sub>4</sub>: 468.1923 [M+H]<sup>+</sup>, found: *m/z* 468.1923.

#### **8-Benzyl-2-(4-hydroxybenzyl)-6-(4-(3-hydroxypropoxy)phenyl)imidazo[1,2-*a*]pyrazin-3(7*H*)-one (49) (6-**Al3OH-CTZ**)**

3-Benzyl-5-(4-(3-((*tert*-butyldimethylsilyl)oxy)propoxy)phenyl)pyrazin-2-amine (**45**) (30 mg, 0.06 mmol, 1 eq.) and 3-(4-((*tert*-butyldimethylsilyl)oxy)phenyl)-1,1-diethoxypropan-2-one (**11**) (48.2 mg, 0.13 mmol, 2 eq.) were dissolved in ethanol (2.0 ml) and H<sub>2</sub>O (0.2 ml) and stirred at room temperature. After vacuum deaeration, the solution was cooled to 0 °C and HCl (0.1 ml) was added under nitrogen flow. Once the solution reached room temperature, it was heated and stirred for 5.5 hours at 80 °C. The solvent was evaporated under vacuum and the crude compound was purified by semipreparative reversed-phase HPLC (eluent composition: CH<sub>3</sub>OH / H<sub>2</sub>O = 60/40 with 0.1% formic acid), affording 8-benzyl-2-(4-hydroxybenzyl)-6-(4-(3-hydroxypropoxy)phenyl)imidazo[1,2-*a*]pyrazin-3(7*H*)-one (**49**) as a yellow solid (6.55 mg, 20%).

<sup>1</sup>H-NMR (500 MHz, CD<sub>3</sub>OD): δ (ppm) = 7.61 (s, 1H), 7.54 (d, *J* = 8.0 Hz, 2H), 7.38-7.20 (m, 5H), 7.14 (d, *J*

= 8.5 Hz, 2H), 7.00 (d,  $J = 8.8$  Hz, 2H), 6.69 (d,  $J = 8.5$  Hz, 2H), 4.39 (s, 2H), 4.10 (t,  $J = 6.3$  Hz, 2H), 4.06 (s, 2H), 3.73 (t,  $J = 6.3$  Hz, 2H), 1.98 (q,  $J = 6.3$  Hz, 2H).  $^{13}\text{C}$ -NMR (125 MHz,  $\text{CD}_3\text{OD}$ ,  $\text{CDCl}_3$ ):  $\delta$  (ppm) = 33.27, 59.44, 65.90, 108.10, 115.99, 116.20, 128.15, 129.27, 129.75, 130.67, 130.79, 138.13, 156.99, 161.65. HR-MS: calcd for  $\text{C}_{29}\text{H}_{27}\text{N}_3\text{O}_4$ : 482.2080  $[\text{M}+\text{H}]^+$ , found:  $m/z$  482.2051.

**8-Benzyl-2-(4-hydroxybenzyl)-6-(4-(4-hydroxybutoxy)phenyl)imidazo[1,2-*a*]pyrazin-3(7*H*)-one (50) (6-AI4OH-CTZ)**

3-Benzyl-5-(4-(4-((*tert*-butyldimethylsilyl)oxy)butoxy)phenyl)pyrazin-2-amine (**46**) (30 mg, 0.06 mmol, 1 eq.) and 3-(4-((*tert*-butyldimethylsilyl)oxy)phenyl)-1,1-diethoxypropan-2-one (**11**) (48.5 mg, 0.13 mmol, 2 eq.) were dissolved in ethanol (2.0 ml) and  $\text{H}_2\text{O}$  (0.2 ml) and stirred at room temperature. After vacuum deaeration, the solution was cooled to 0 °C and HCl (0.1 ml) was added under nitrogen flow. Once the solution reached room temperature, it was heated and stirred for 7 hours at 80 °C. The solvent was evaporated under vacuum and the crude compound was purified by chromatograph on a ODS plate (eluent composition: MeCN /  $\text{H}_2\text{O} = 50/50$ ), affording 8-benzyl-2-(4-hydroxybenzyl)-6-(4-(4-hydroxybutoxy)phenyl)imidazo[1,2-*a*]pyrazin-3(7*H*)-one (**50**) as a yellow solid (6.96 mg, 20%).

$^1\text{H}$ -NMR (500 MHz,  $\text{CD}_3\text{OD}$ ):  $\delta$  (ppm) = 7.61 (s, 1H), 7.54 (d,  $J = 8.3$  Hz, 2H), 7.38-7.21 (m, 5H), 7.14 (d,  $J = 8.3$  Hz, 2H), 6.98 (d,  $J = 8.3$  Hz, 2H), 6.68 (d,  $J = 8.3$  Hz, 2H), 4.39 (s, 2H), 4.06 (s, 2H), 4.02 (t,  $J = 6.3$  Hz, 2H), 3.62 (t,  $J = 6.3$  Hz, 2H), 1.86-1.82 (m, 2H), 1.73-1.69 (m, 2H).  $^{13}\text{C}$ -NMR (125 MHz,  $\text{CD}_3\text{OD}$ ,  $\text{CDCl}_3$ ):  $\delta$  (ppm) = 26.86, 30.17, 33.24, 35.21, 62.61, 69.00, 108.10, 115.97, 116.19, 128.13, 129.25, 129.74, 129.77, 130.71, 130.78, 138.16, 156.97, 161.65. HR-MS: calcd for  $\text{C}_{30}\text{H}_{29}\text{N}_3\text{O}_4$ : 496.2236  $[\text{M}+\text{H}]^+$ , found:  $m/z$  496.2214.

**8-Benzyl-2-(4-hydroxybenzyl)-6-(4-((5-hydroxypentyl)oxy)phenyl)imidazo[1,2-*a*]pyrazin-3(7*H*)-one (51)**  
**(6-A15OH-CTZ)**

3-Benzyl-5-(4-((5-((*tert*-butyldimethylsilyl)oxy)pentyl)oxy)phenyl)pyrazin-2-amine (**47**) (34.5 mg, 0.07 mmol, 1 eq.) and 3-(4-((*tert*-butyldimethylsilyl)oxy)phenyl)-1,1-diethoxypropan-2-one (**11**) (55.8 mg, 0.15 mmol, 2 eq.) were dissolved in ethanol (2.0 ml) and H<sub>2</sub>O (0.2 ml) and stirred at room temperature. After vacuum deaeration, the solution was cooled to 0 °C and HCl (0.1 ml) was added under nitrogen flow. Once the solution reached room temperature, it was heated and stirred for 5 hours at 80 °C. The solvent was evaporated under vacuum and the crude compound was purified by chromatograph on a ODS plate (eluent composition: CH<sub>3</sub>OH / H<sub>2</sub>O = 50/50), affording 8-benzyl-2-(4-hydroxybenzyl)-6-(4-((5-hydroxypentyl)oxy)phenyl)imidazo[1,2-*a*]pyrazin-3(7*H*)-one (**51**) as a yellow solid (8.77 mg, 21%).

<sup>1</sup>H-NMR (500 MHz, CD<sub>3</sub>OD):  $\delta$  (ppm) = 7.61 (s, 1H), 7.53 (d, *J* = 8.5 Hz, 2H), 7.38-7.14 (m, 5H), 7.15 (d, *J* = 8.5 Hz, 2H), 6.98 (d, *J* = 8.8 Hz, 2H), 6.69 (d, *J* = 8.5 Hz, 2H), 4.39 (s, 2H), 4.06 (s, 2H), 4.00 (t, *J* = 6.5 Hz, 2H), 3.57 (t, *J* = 6.3 Hz, 2H), 1.80 (m, 2H), 1.61-1.52 (m, 6H). <sup>13</sup>C-NMR (125 MHz, CD<sub>3</sub>OD, CDCl<sub>3</sub>):  $\delta$  (ppm) = 23.52, 30.14, 33.21, 33.36, 62.82, 69.09, 108.14, 115.95, 116.18, 128.09, 129.23, 129.39, 129.71, 129.78, 130.78, 138.24, 156.95, 161.65. HR-MS: calcd for C<sub>31</sub>H<sub>31</sub>N<sub>3</sub>O<sub>4</sub>: 510.2393 [M+H]<sup>+</sup>, found: *m/z* 510.2376.

**2,8-Dibenzyl-6-(4-(2-hydroxyethoxy)phenyl)imidazo[1,2-*a*]pyrazin-3(7*H*)-one (52) (6-A12OH2H-CTZ)**

3-Benzyl-5-(4-(2-((*tert*-butyldimethylsilyl)oxy)ethoxy)phenyl)pyrazin-2-amine (**44**) (71.3 mg, 0.16 mmol, 1 eq.) and 1,1-diethoxy-3-phenylpropan-2-one (**17**) (72.7 mg, 0.32 mmol, 2 eq.) were dissolved in ethanol (4.0 ml) and H<sub>2</sub>O (0.4 ml) and stirred at room temperature. After vacuum deaeration, the solution was cooled to 0 °C and HCl (0.2 ml) was added under nitrogen flow. Once the solution reached room temperature, it was heated and stirred for 14 hours at 80 °C. The solvent was evaporated under vacuum and the crude compound was purified by chromatograph on a silicagel plate (eluent composition: CH<sub>3</sub>OH / CH<sub>2</sub>Cl<sub>2</sub> = 1/10), affording 2,8-

dibenzyl-6-(4-(2-hydroxyethoxy)phenyl)imidazo[1,2-*a*]pyrazin-3(7*H*)-one (**52**) as a yellow solid (17.9 mg, 24%).

<sup>1</sup>H-NMR (500 MHz, CD<sub>3</sub>OD):  $\delta$  (ppm) = 7.69 (s, 1H), 7.51 (d, *J* = 7.7 Hz, 2H), 7.37 (d, *J* = 7.7 Hz, 2H), 7.29-7.11 (m, 7H), 6.97 (d, *J* = 8.5 Hz, 2H), 4.38 (s, 2H), 4.13 (s, 2H), 4.04 (t, *J* = 4.5 Hz, 2H), 3.87 (t, *J* = 5.1 Hz, 2H). <sup>13</sup>C-NMR (125 MHz, CD<sub>3</sub>OD, CDCl<sub>3</sub>):  $\delta$  (ppm) = 33.78, 33.36, 35.39, 61.56, 70.72, 108.51, 116.02, 126.15, 127.44, 127.85, 128.21, 129.27, 129.48, 129.76, 129.81, 132.36, 137.87, 139.71, 161.61. HR-MS: calcd for C<sub>28</sub>H<sub>25</sub>N<sub>3</sub>O<sub>3</sub>: 452.1974 [M+H]<sup>+</sup>, found: *m/z* 452.1968.

### **2,8-Dibenzyl-6-(4-(3-hydroxypropoxy)phenyl)imidazo[1,2-*a*]pyrazin-3(7*H*)-one (**53**) (6-Al3OH2H-CTZ)**

3-Benzyl-5-(4-(3-((*tert*-butyldimethylsilyl)oxy)propoxy)phenyl)pyrazin-2-amine (**45**) (20 mg, 0.04 mmol, 1 eq.) and 1,1-diethoxy-3-phenylpropan-2-one (**17**) (19.7 mg, 0.08 mmol, 2 eq.) were dissolved in ethanol (2.0 ml) and H<sub>2</sub>O (0.2 ml) and stirred at room temperature. After vacuum deaeration, the solution was cooled to 0 °C and HCl (0.1 ml) was added under nitrogen flow. Once the solution reached room temperature, it was heated and stirred for 14 hours at 80 °C. The solvent was evaporated under vacuum and the crude compound was purified by flash chromatography (silica gel, eluent composition: n-hexane / ethyl acetate = 25/75 to ethyl acetate to CH<sub>3</sub>OH / ethyl acetate = 10/90 to 20/80), affording 2,8-dibenzyl-6-(4-(3-hydroxypropoxy)phenyl)imidazo[1,2-*a*]pyrazin-3(7*H*)-one (**53**) as a yellow solid (9.38 mg, 45%).

<sup>1</sup>H-NMR (500 MHz, CD<sub>3</sub>OD):  $\delta$  (ppm) = 7.60 (s, 1H), 7.52 (s, 2H), 7.38-7.14 (m, 10H), 6.99 (d, *J* = 8.0 Hz, 2H), 4.39 (s, 2H), 4.16 (s, 2H), 4.09 (t, *J* = 6.0 Hz, 2H), 3.73 (t, *J* = 6.3 Hz, 2H), 1.98 (q, *J* = 6.0 Hz, 2H). <sup>13</sup>C-NMR (125 MHz, CD<sub>3</sub>OD, CDCl<sub>3</sub>):  $\delta$  (ppm) = 18.36, 33.27, 116.00, 128.19, 129.30, 129.48, 129.77, 129.82, 138.04, 139.91, 161.71. HR-MS: calcd for C<sub>29</sub>H<sub>27</sub>N<sub>3</sub>O<sub>3</sub>: 466.2131 [M+H]<sup>+</sup>, found: *m/z* 466.2112.

**2,8-Dibenzyl-6-(4-(4-hydroxybutoxy)phenyl)imidazo[1,2-*a*]pyrazin-3(7*H*)-one (54) (6-AI4OH2H-CTZ)**

3-Benzyl-5-(4-(4-((*tert*-butyldimethylsilyl)oxy)butoxy)phenyl)pyrazin-2-amine (**46**) (30 mg, 0.06 mmol, 1 eq.) and 1,1-diethoxy-3-phenylpropan-2-one (**17**) (30.6 mg, 0.13 mmol, 2 eq.) were dissolved in ethanol (2.0 ml) and H<sub>2</sub>O (0.2 ml) and stirred at room temperature. After vacuum deaeration, the solution was cooled to 0 °C and HCl (0.1 ml) was added under nitrogen flow. Once the solution reached room temperature, it was heated and stirred for 13.5 hours at 80 °C. The solvent was evaporated under vacuum and the crude compound was purified by chromatograph on a silicagel plate (eluent composition: CH<sub>3</sub>OH / ethyl acetate = 1/20), affording 2,8-dibenzyl-6-(4-(4-hydroxybutoxy)phenyl)imidazo[1,2-*a*]pyrazin-3(7*H*)-one (**54**) as a yellow solid (7.73 mg, 20%).

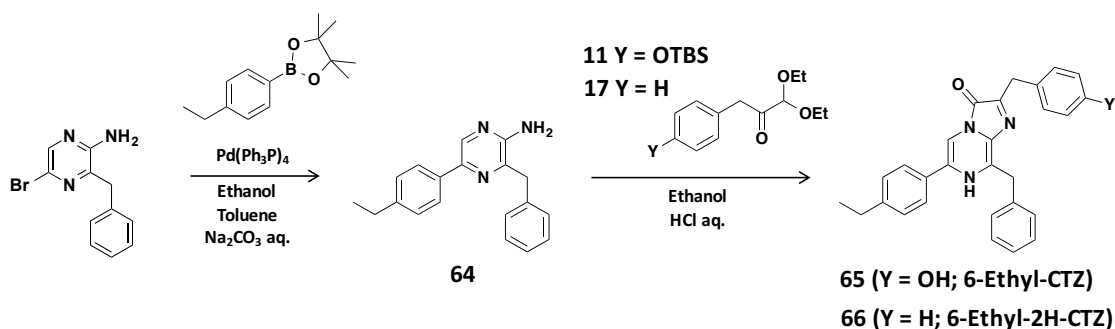
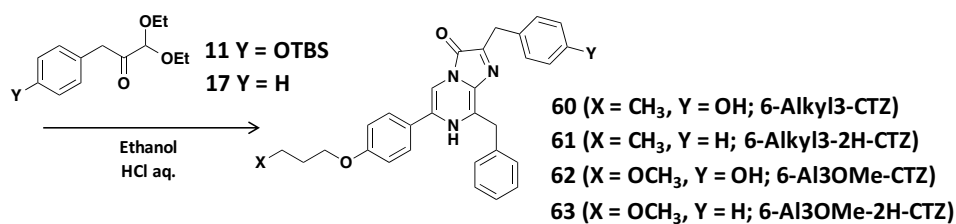
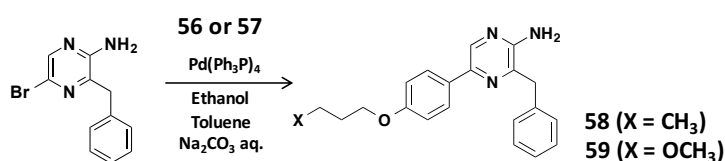
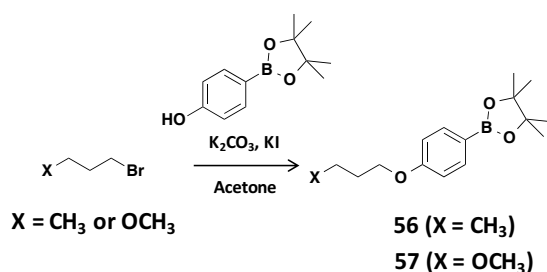
<sup>1</sup>H-NMR (500 MHz, CD<sub>3</sub>OD):  $\delta$  (ppm) = 7.61 (s, 1H), 7.51 (s, 2H), 7.38-7.14 (m, 10H), 6.97 (d,  $J$  = 7.1 Hz, 2H), 4.38 (s, 2H), 4.15 (s, 2H), 4.02 (t,  $J$  = 6.0 Hz, 2H), 3.61 (t,  $J$  = 6.3 Hz, 2H), 1.87-1.82 (m, 2H), 1.72-1.67 (m, 2H). <sup>13</sup>C-NMR (125 MHz, CD<sub>3</sub>OD, CDCl<sub>3</sub>):  $\delta$  (ppm) = 26.86, 30.17, 62.60, 69.01, 108.20, 115.98, 127.39, 128.19, 129.29, 129.48, 129.77, 129.82, 138.03, 139.91, 161.71. HR-MS: calcd for C<sub>30</sub>H<sub>29</sub>N<sub>3</sub>O<sub>3</sub>: 480.2287 [M+H]<sup>+</sup>, found:  $m/z$  480.2265.

**2,8-Dibenzyl-6-(4-((5-hydroxypentyl)phenyl)imidazo[1,2-*a*]pyrazin-3(7*H*)-one (55) (6-AI5OH2H-CTZ)**

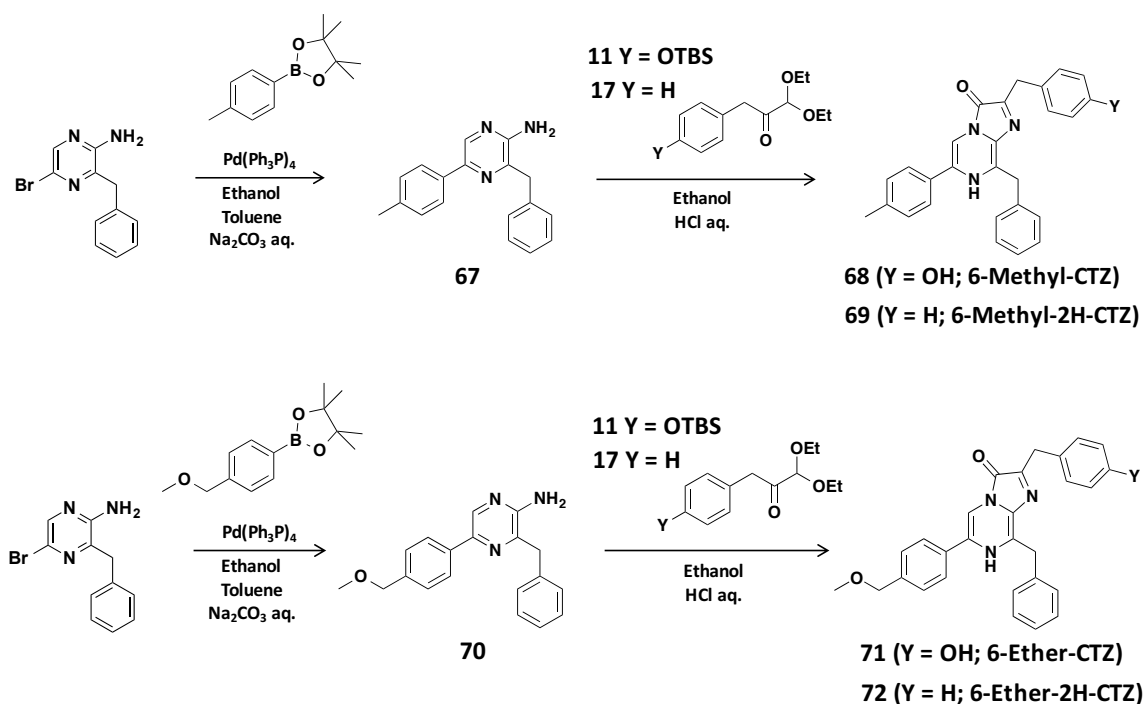
3-Benzyl-5-(4-((5-((*tert*-butyldimethylsilyl)oxy)pentyl)oxy)phenyl)pyrazin-2-amine (**47**) (30.0 mg, 0.06 mmol, 1 eq.) and 1,1-diethoxy-3-phenylpropan-2-one (**17**) (30.4 mg, 0.13 mmol, 2 eq.) were dissolved in ethanol (2.0 ml) and H<sub>2</sub>O (0.2 ml) and stirred at room temperature. After vacuum deaeration, the solution was cooled to 0 °C and HCl (0.1 ml) was added under nitrogen flow. Once the solution reached room temperature, it was heated and stirred for 13.5 hours at 80 °C. The solvent was evaporated under vacuum and the crude compound was purified by chromatograph on a silicagel plate (eluent composition: CH<sub>3</sub>OH / CH<sub>2</sub>Cl<sub>2</sub> = 1/10), affording 2,8-dibenzyl-6-(4-((5-hydroxypentyl)phenyl)imidazo[1,2-*a*]pyrazin-3(7*H*)-one (**55**) as a yellow solid

(5.81 mg, 14%).

$^1\text{H-NMR}$  (500 MHz,  $\text{CD}_3\text{OD}$ ):  $\delta$  (ppm) = 7.62 (s, 1H), 7.54 (d,  $J = 7.1$  Hz, 2H), 7.39-7.15 (m, 10H), 6.99 (d,  $J = 8.0$  Hz, 2H), 4.39 (s, 2H), 4.16 (s, 2H), 4.01 (t,  $J = 6.0$  Hz, 2H), 3.57 (t,  $J = 6.5$  Hz, 2H), 1.83-1.79 (m, 2H), 1.62-1.52 (m, 4H).  $^{13}\text{C-NMR}$  (125 MHz,  $\text{CD}_3\text{OD}$ ,  $\text{CDCl}_3$ ):  $\delta$  (ppm) = 23.53, 30.14, 33.36, 62.82, 69.12, 108.19, 116.00, 127.39, 128.19, 129.31, 129.48, 129.56, 129.77, 129.83, 131.37, 138.05, 139.93, 161.78. HR-MS: calcd for  $\text{C}_{31}\text{H}_{31}\text{N}_3\text{O}_3$ : 494.2444  $[\text{M}+\text{H}]^+$ , found:  $m/z$  494.2415.



Synthetic scheme for 6-alkylated CTZ derivatives



Synthetic scheme for 6-alkylated CTZ derivatives

### 3-Benzyl-5-(4-butoxyphenyl)pyrazin-2-amine (58)

3-Benzyl-5-bromopyrazin-2-amine (**2**) (100 mg, 0.3 mmol, 1 eq.) and 2-(4-butoxyphenyl)-4,4,5,5-tetramethyl-1,3,2-dioxaborolane (**56**) (167 mg, 0.4 mmol, 1.6 eq.) were dissolved in toluene (6 ml) and stirred at room temperature. Ethanol (1 ml) and 1 M Na<sub>2</sub>CO<sub>3</sub> aq. (2 ml) were added into the reaction mixture. After vacuum deaeration, a catalytic amount of tetrakis(triphenylphosphine)palladium(0) was added into the solution and the mixture was deaerated again and stirred for 13 hours at 100 °C. After cooling to room temperature, the solution was filtered through a Celite pad to remove the palladium catalyst. The solution was extracted with ethyl acetate, and the brown organic phase was washed with water and brine, dried over Na<sub>2</sub>SO<sub>4</sub> and evaporated. The resulting residue was purified by flash chromatography (silica gel, eluent composition: n-hexane / ethyl acetate = 80/20 to 67/33), affording 3-benzyl-5-(4-butoxyphenyl)pyrazin-2-amine (**58**) as a yellow solid (121.6 mg, 96%).

<sup>1</sup>H-NMR (500 MHz, CDCl<sub>3</sub>): δ (ppm) = 8.33 (s, 1H), 7.86 (d, *J* = 8.8 Hz, 2H), 7.33-7.23 (m, 5H), 6.98 (d, *J*

= 8.8 Hz, 2H), 4.34 (s, 2H), 4.17 (s, 2H), 4.01 (t,  $J = 6.5$  Hz, 2H), 1.79 (m, 2H), 1.52 (m, 2H), 0.99 (t,  $J = 7.4$  Hz, 2H).  $^{13}\text{C}$ -NMR (125 MHz,  $\text{CDCl}_3$ ):  $\delta$  (ppm) = 14.02, 19.39, 31.45, 41.42, 67.92, 114.95, 127.12, 127.15, 128.71, 129.10, 129.89, 136.99, 140.58, 142.87, 151.34, 159.48.

### 3-Benzyl-5-(4-(3-methoxypropoxy)phenyl)pyrazin-2-amine (59)

3-Benzyl-5-bromopyrazine-2-amine (**2**) (100 mg, 0.3 mmol, 1 eq.) and 2-(4-(3-methoxypropoxy)phenyl)-4,4,5,5-tetramethyl-1,3,2-dioxaborolane (**57**) (176.9 mg, 0.6 mmol, 2.0 eq.) were dissolved in toluene (6 ml) and stirred at room temperature. Ethanol (1 ml) and 1 M  $\text{Na}_2\text{CO}_3$  aq. (2 ml) were added into the reaction mixture. After vacuum deaeration, a catalytic amount of tetrakis(triphenylphosphine)palladium(0) was added into the solution and the mixture was deaerated again and stirred for 12 hours at 100 °C. After cooling to room temperature, the solution was filtered through a Celite pad to remove the palladium catalyst. The solution was extracted with ethyl acetate, and the brown organic phase was washed with water and brine, dried over  $\text{Na}_2\text{SO}_4$  and evaporated. The resulting residue was purified by flash chromatography (silica gel, eluent composition: n-hexane / ethyl acetate = 67/33 to 50/50), affording 3-benzyl-5-(4-(3-methoxypropoxy)phenyl)pyrazin-2-amine (**59**) as a yellow solid (127.3 mg, 96%).

$^1\text{H}$ -NMR (500 MHz,  $\text{CDCl}_3$ ):  $\delta$  (ppm) = 8.32 (s, 1H), 7.86 (d,  $J = 8.3$  Hz, 2H), 7.33-7.26 (m, 5H), 6.98 (d,  $J = 8.8$  Hz, 2H), 4.34 (s, 2H), 4.17 (s, 2H), 4.11 (t,  $J = 6.0$  Hz, 2H), 3.58 (t,  $J = 6.3$  Hz, 2H), 1.33 (m, 12H), 0.90 (s, 9H), 0.09 (s, 6H).  $^{13}\text{C}$ -NMR (125 MHz,  $\text{CDCl}_3$ ):  $\delta$  (ppm) = 29.75, 41.38, 58.87, 65.06, 69.36, 114.95, 127.11, 128.58, 128.70, 129.08, 130.04, 132.26, 136.97, 140.57, 142.77, 151.36, 139.31.

### 8-Benzyl-6-(4-butoxyphenyl)-2-(4-hydroxybenzyl)imidazo[1,2-*a*]pyrazin-3(7H)-one (60) (6-Alkyl3-CTZ)

3-Benzyl-5-(4-butoxyphenyl)pyrazin-2-amine (**58**) (30.0 mg, 0.08 mmol, 1 eq.) and 3-(4-((tert-butyl)dimethylsilyloxy)phenyl)-1,1-diethoxypropan-2-one (**11**) (63.4 mg, 0.17 mmol, 2 eq.) were dissolved in

ethanol (2.0 ml) and H<sub>2</sub>O (0.2 ml) and stirred at room temperature. After vacuum deaeration, the solution was cooled to 0 °C and HCl (0.1 ml) was added under nitrogen flow. Once the solution reached room temperature, it was heated and stirred for 6 hours at 80 °C. The solvent was evaporated under vacuum and the crude compound was purified by chromatography (silica gel, eluent composition: CH<sub>3</sub>OH / CH<sub>2</sub>Cl<sub>2</sub> = 1/20), affording 8-benzyl-6-(4-butoxyphenyl)-2-(4-hydroxybenzyl)imidazo[1,2-*a*]pyrazin-3(7*H*)-one (**60**) as a yellow solid (12.8 mg, 30%).

<sup>1</sup>H-NMR (500 MHz, CD<sub>3</sub>OD, CDCl<sub>3</sub>): δ (ppm) = 7.57 (s, 1H), 7.51 (d, *J* = 8.0 Hz, 2H), 7.41 (d, *J* = 8.3 Hz, 2H), 7.31-7.18 (m, 5H), 6.98 (d, *J* = 8.5 Hz, 2H), 6.72 (d, *J* = 8.5 Hz, 2H), 4.39 (s, 2H), 4.10 (s, 2H), 4.02 (t, *J* = 6.3 Hz, 2H), 1.81-1.75 (m, 2H), 1.54-1.49 (m, 2H), 1.00 (t, *J* = 7.4 Hz, 3H). <sup>13</sup>C-NMR (125 MHz, CD<sub>3</sub>OD, CDCl<sub>3</sub>): δ (ppm) = 14.09, 19.87, 31.95, 68.55, 107.73, 115.64, 115.90, 127.83, 128.78, 129.39, 129.43, 130.39, 137.39, 156.22, 161.15.

### 2,8-Dibenzyl-6-(4-butoxyphenyl)imidazo[1,2-*a*]pyrazin-3(7*H*)-one (**61**) (6-Alkyl3-2H-CTZ)

3-Benzyl-5-(4-butoxyphenyl)pyrazin-2-amine (**58**) (32.7 mg, 0.09 mmol, 1 eq.) and 1,1-diethoxy-3-phenylpropan-2-one (**17**) (43.7 mg, 0.19 mmol, 2 eq.) were dissolved in ethanol (2.0 ml) and H<sub>2</sub>O (0.2 ml) and stirred at room temperature. After vacuum deaeration, the solution was cooled to 0 °C and HCl (0.1 ml) was added under nitrogen flow. Once the solution reached room temperature, it was heated and stirred for 21 hours at 80 °C. The solvent was evaporated under vacuum and the crude compound was purified by chromatography (silica gel, eluent composition: CH<sub>3</sub>OH / CH<sub>2</sub>Cl<sub>2</sub> = 1/20), affording 2,8-dibenzyl-6-(4-butoxyphenyl)imidazo[1,2-*a*]pyrazin-3(7*H*)-one (**61**) as a yellow solid (27.4 mg, 60%).

<sup>1</sup>H-NMR (500 MHz, CD<sub>3</sub>OD, CDCl<sub>3</sub>): δ (ppm) = 7.45 (s, 1H), 7.48 (d, *J* = 8.3 Hz, 2H), 7.39 (d, *J* = 7.3 Hz, 2H), 7.33 (d, *J* = 7.4 Hz, 2H), 7.28-7.13 (m, 6H), 6.94 (d, *J* = 8.8 Hz, 2H), 4.38 (s, 2H), 4.16 (s, 2H), 3.96 (t, *J* = 6.5 Hz, 2H), 1.78-1.72 (m, 2H), 1.52-1.47 (m, 2H), 0.97 (t, *J* = 7.4 Hz, 3H). <sup>13</sup>C-NMR (125 MHz, CD<sub>3</sub>OD,

CDCl<sub>3</sub>):  $\delta$  (ppm) = 14.15, 20.08, 32.18, 34.08, 34.84, 68.71, 107.99, 115.79, 127.19, 128.03, 129.01, 129.27, 129.58, 129.61, 129.65, 137.69, 139.55, 161.46.

**8-Benzyl-6-(4-butoxyphenyl)-6-(4-(3-methoxypropoxy)phenyl)imidazo[1,2-*a*]pyrazin-3(7*H*)-one (62) (6-Al3OMe-CTZ)**

3-Benzyl-5-(4-(3-methoxypropoxy)phenyl)pyrazin-2-amine (**59**) (35.0 mg, 0.1 mmol, 1 eq.) and 3-(4-((tert-butyl)dimethylsilyloxy)phenyl)-1,1-diethoxypropan-2-one (**11**) (70.5 mg, 0.2 mmol, 2 eq.) were dissolved in ethanol (2.0 ml) and H<sub>2</sub>O (0.2 ml) and stirred at room temperature. After vacuum deaeration, the solution was cooled to 0 °C and HCl (0.1 ml) was added under nitrogen flow. Once the solution reached room temperature, it was heated and stirred for 6 hours at 80 °C. The solvent was evaporated under vacuum and the crude compound was purified by chromatography (silica gel, eluent composition: CH<sub>3</sub>OH / CH<sub>2</sub>Cl<sub>2</sub> = 1/20), affording 8-benzyl-6-(4-butoxyphenyl)-6-(4-(3-methoxypropoxy)phenyl)imidazo[1,2-*a*]pyrazin-3(7*H*)-one (**62**) as a yellow solid (18.2 mg, 52%).

<sup>1</sup>H-NMR (500 MHz, CD<sub>3</sub>OD):  $\delta$  (ppm) = 7.61 (s, 1H), 7.47 (d, *J* = 5.1 Hz, 2H), 7.36 (d, *J* = 7.4 Hz, 2H), 7.27-7.12 (m, 5H), 6.92 (d, *J* = 6.3 Hz, 2H), 6.67 (d, *J* = 7.1 Hz, 2H), 4.36 (s, 2H), 4.03 (s, 4H), 3.53 (t, *J* = 6.3 Hz, 2H), 3.33 (s, 3H), 2.02-1.97 (m, 2H). <sup>13</sup>C-NMR (125 MHz, CD<sub>3</sub>OD):  $\delta$  (ppm) = 30.50, 33.19, 35.16, 58.91, 66.04, 70.29, 108.15, 115.66, 115.91, 116.21, 127.84, 128.14, 129.20, 129.55, 129.74, 129.77, 130.63, 130.79, 138.08, 156.99, 161.53.

**2,8-Dibenzyl-6-(4-(3-methoxypropoxy)phenyl)imidazo[1,2-*a*]pyrazin-3(7*H*)-one (63) (6-Al3OMe-2H-CTZ)**

3-Benzyl-5-(4-(3-methoxypropoxy)phenyl)pyrazin-2-amine (**59**) (30.0 mg, 0.08 mmol, 1 eq.) and 1,1-diethoxy-3-phenylpropan-2-one (**17**) (38.0 mg, 0.17 mmol, 2 eq.) were dissolved in ethanol (2.0 ml) and H<sub>2</sub>O

(0.2 ml) and stirred at room temperature. After vacuum deaeration, the solution was cooled to 0 °C and HCl (0.1 ml) was added under nitrogen flow. Once the solution reached room temperature, it was heated and stirred for 16 hours at 80 °C. The solvent was evaporated under vacuum and the crude compound was purified by chromatography (silica gel, eluent composition: CH<sub>3</sub>OH / CH<sub>2</sub>Cl<sub>2</sub> = 1/20), affording 2,8-dibenzyl-6-(4-(3-methoxypropoxy)phenyl)imidazo[1,2-*a*]pyrazin-3(7*H*)-one (**63**) as a yellow solid (22.6 mg, 55%).

<sup>1</sup>H-NMR (500 MHz, CD<sub>3</sub>OD, CDCl<sub>3</sub>): δ (ppm) = 7.54 (s, 1H), 7.47 (d, *J* = 8.5 Hz, 2H), 7.38 (d, *J* = 7.4 Hz, 2H), 7.32 (d, *J* = 7.4 Hz, 2H), 7.27-7.12 (m, 6H), 6.93 (d, *J* = 8.8 Hz, 2H), 4.36 (s, 2H), 4.15 (s, 2H), 4.03 (t, *J* = 6.3 Hz, 2H), 3.54 (t, *J* = 6.0 Hz, 2H), 3.33 (s, 3H), 2.03-1.98 (m, 2H). <sup>13</sup>C-NMR (125 MHz, CD<sub>3</sub>OD, CDCl<sub>3</sub>): δ (ppm) = 30.36, 34.06, 34.96, 58.91, 65.90, 70.06, 108.09, 115.83, 125.75, 127.24, 127.72, 128.06, 129.32, 129.61, 129.66, 129.69, 137.76, 139.65, 152.49, 161.35.

### 3-Benzyl-5-(4-ethylphenyl)pyrazin-2-amine (**64**)

3-Benzyl-5-bromopyrazine-2-amine (**2**) (100 mg, 0.3 mmol, 1 eq.) and 2-(4-ethylphenyl)-4,4,5,5-tetramethyl-1,3,2-dioxaborolane (140.4 mg, 0.6 mmol, 1.6 eq.) were dissolved in toluene (6 ml) and stirred at room temperature. Ethanol (1 ml) and 1 M Na<sub>2</sub>CO<sub>3</sub> aq. (2 ml) were added into the reaction mixture. After vacuum deaeration, a catalytic amount of tetrakis(triphenylphosphine)palladium(0) was added into the solution and the mixture was deaerated again and stirred for 12 hours at 100 °C. After cooling to room temperature, the solution was filtered through a Celite pad to remove the palladium catalyst. The solution was extracted with ethyl acetate, and the brown organic phase was washed with water and brine, dried over Na<sub>2</sub>SO<sub>4</sub> and evaporated. The resulting residue was purified by flash chromatography (silica gel, eluent composition: n-hexane / ethyl acetate = 70/30), affording 3-benzyl-5-(4-ethylphenyl)pyrazin-2-amine (**64**) as a yellow solid (100.4 mg, 91%).

<sup>1</sup>H-NMR (500 MHz, CDCl<sub>3</sub>): δ (ppm) = 8.37 (s, 1H), 7.86 (d, *J* = 8.0 Hz, 2H), 7.33-7.25 (m, 7H), 4.37 (s, 2H), 4.18 (s, 2H), 2.70 (t, *J* = 7.4 Hz, 2H), 1.28-1.25 (m, 3H). <sup>13</sup>C-NMR (125 MHz, CDCl<sub>3</sub>): δ (ppm) = 15.78, 28.79,

41.42, 76.90, 77.16, 77.41, 125.91, 127.16, 128.48, 128.71, 129.11, 134.87, 136.95, 137.44, 140.67, 142.96, 144.47, 151.66.

**8-Benzyl-6-(4-ethylphenyl)-2-(4-hydroxybenzyl)imidazo[1,2-*a*]pyrazin-3(7*H*)-one (57) (6-Ethyl-CTZ)**

3-Benzyl-5-(4-ethylphenyl)pyrazin-2-amine (**64**) (30.0 mg, 0.1 mmol, 1 eq.) and 3-(4-((tert-butyl)dimethylsilyloxy)phenyl)-1,1-diethoxypropan-2-one (**11**) (72.6 mg, 0.20 mmol, 2 eq.) were dissolved in ethanol (2.0 ml) and H<sub>2</sub>O (0.2 ml) and stirred at room temperature. After vacuum deaeration, the solution was cooled to 0 °C and HCl (0.1 ml) was added under nitrogen flow. Once the solution reached room temperature, it was heated and stirred for 21 hours at 80 °C. The solvent was evaporated under vacuum and the crude compound was purified by chromatography (silica gel, eluent composition: CH<sub>3</sub>OH / CH<sub>2</sub>Cl<sub>2</sub> = 1/20), affording 8-benzyl-6-(4-ethylphenyl)-2-(4-hydroxybenzyl)imidazo[1,2-*a*]pyrazin-3(7*H*)-one (**65**) as a yellow solid (9.6 mg, 21%).

<sup>1</sup>H-NMR (500 MHz, CD<sub>3</sub>OD): δ (ppm) = 7.65 (s, 1H), 7.53 (d, *J* = 7.1 Hz, 2H), 7.38 (d, *J* = 7.7 Hz, 2H), 7.30-7.20 (m, 5H), 7.15 (d, *J* = 8.3 Hz, 2H), 6.69 (d, *J* = 8.3 Hz, 2H), 4.39 (s, 2H), 4.06 (2H), 2.68 (q, *J* = 7.4 Hz, 2H), 1.22 (q, *J* = 7.4 Hz, 3H). <sup>13</sup>C-NMR (125 MHz, CD<sub>3</sub>OD): δ (ppm) = 15.98, 29.58, 33.27, 108.54, 116.21, 127.87, 128.18, 129.58, 129.76, 130.59, 130.80, 138.06, 147.38, 157.01.

**2,8-Dibenzyl-6-(4-ethylphenyl)imidazo[1,2-*a*]pyrazin-3(7*H*)-one (66) (6-Ethyl-2H-CTZ)**

3-Benzyl-5-(4-ethylphenyl)pyrazin-2-amine (**64**) (35.7 mg, 0.12 mmol, 1 eq.) and 1,1-diethoxy-3-phenylpropan-2-one (**17**) (54.9 mg, 0.24 mmol, 2 eq.) were dissolved in ethanol (3.0 ml) and H<sub>2</sub>O (0.3 ml) and stirred at room temperature. After vacuum deaeration, the solution was cooled to 0 °C and HCl (0.2 ml) was added under nitrogen flow. Once the solution reached room temperature, it was heated and stirred for 14 hours at 80 °C. The solvent was evaporated under vacuum and the crude compound was purified by chromatography

(silica gel, eluent composition: CH<sub>3</sub>OH / CH<sub>2</sub>Cl<sub>2</sub> = 1/20), affording 2,8-dibenzyl-6-(4-ethylphenyl)imidazo[1,2-*a*]pyrazin-3(7*H*)-one (**66**) as a yellow solid (48.85 mg, 94%).

<sup>1</sup>H-NMR (500 MHz, CD<sub>3</sub>OD, CDCl<sub>3</sub>): δ (ppm) = 7.48 (s, 1H), 7.41 (d, *J* = 7.4 Hz, 2H), 7.35 (d, *J* = 7.1 Hz, 2H), 7.30-7.15 (m, 10H), 4.39 (s, 2H), 4.19 (s, 2H), 2.65 (q, *J* = 7.4 Hz, 2H), 1.23 (q, *J* = 7.7 Hz, 3H). <sup>13</sup>C-NMR (125 MHz, CD<sub>3</sub>OD, CDCl<sub>3</sub>): δ (ppm) = 15.68, 29.07, 34.00, 34.48, 108.07, 124.81, 126.74, 126.85, 127.14, 127.25, 127.72, 128.20, 128.42, 128.70, 128.93, 129.05, 129.24, 129.27, 129.30, 136.42, 137.00, 138.94, 146.65.

### 3-Benzyl-5-(*p*-tolyl)pyrazin-2-amine (**67**)

3-Benzyl-5-bromopyrazine-2-amine (**2**) (123.9 mg, 0.4 mmol, 1 eq.) and 4,4,5,5-tetramethyl-2-(*p*-tolyl)-1,3,2-dioxaborolane (102.0 mg, 0.7 mmol, 1.6 eq.) were dissolved in toluene (6 ml) and stirred at room temperature. Ethanol (1 ml) and 1 M Na<sub>2</sub>CO<sub>3</sub> aq. (2 ml) were added into the reaction mixture. After vacuum deaeration, a catalytic amount of tetrakis(triphenylphosphine)palladium(0) was added into the solution and the mixture was deaerated again and stirred for 19 hours at 100 °C. After cooling to room temperature, the solution was filtered through a Celite pad to remove the palladium catalyst. The solution was extracted with ethyl acetate, and the brown organic phase was washed with water and brine, dried over Na<sub>2</sub>SO<sub>4</sub> and evaporated. The resulting residue was purified by flash chromatography (silica gel, eluent composition: n-hexane / ethyl acetate = 80/20 to 70/30), affording 3-benzyl-5-(*p*-tolyl)pyrazin-2-amine (**67**) as a yellow solid (123.97 mg, 96%).

<sup>1</sup>H-NMR (500 MHz, CDCl<sub>3</sub>): δ (ppm) = 8.38 (s, 1H), 7.82 (d, *J* = 8.0 Hz, 2H), 7.32-7.23 (m, 7H), 4.53 (s, 2H), 4.17 (s, 2H), 2.39 (s, 3H). <sup>13</sup>C-NMR (125 MHz, CDCl<sub>3</sub>): δ (ppm) = 21.36, 41.34, 125.76, 127.16, 128.68, 129.09, 129.63, 134.50, 136.83, 138.07, 140.92, 142.98, 151.48.

### 8-Benzyl-2-(4-hydroxybenzyl)-6-(*p*-tolyl)imidazo[1,2-*a*]pyrazin-3(7*H*)-one (**68**) (6-Methyl-CTZ)

3-Benzyl-5-(*p*-tolyl)pyrazin-2-amine (**67**) (32.6 mg, 0.1 mmol, 1 eq.) and 3-(4-((tert-

butyldimethylsilyloxy)phenyl)-1,1-diethoxypropan-2-one (**11**) (83.6 mg, 0.2 mmol, 2 eq.) were dissolved in ethanol (2.0 ml) and H<sub>2</sub>O (0.2 ml) and stirred at room temperature. After vacuum deaeration, the solution was cooled to 0 °C and HCl (0.1 ml) was added under nitrogen flow. Once the solution reached room temperature, it was heated and stirred for 21 hours at 80 °C. The solvent was evaporated under vacuum and the crude compound was purified by chromatography (silica gel, eluent composition: CH<sub>3</sub>OH / CH<sub>2</sub>Cl<sub>2</sub> = 1/20 to 1/10), affording 8-benzyl-2-(4-hydroxybenzyl)-6-(*p*-tolyl)imidazo[1,2-*a*]pyrazin-3(7*H*)-one (**68**) as a yellow solid (23.12 mg, 50%).

<sup>1</sup>H-NMR (500 MHz, CD<sub>3</sub>OD): δ (ppm) = 7.57 (s, 1H), 7.42 (d, *J* = 7.4 Hz, 2H), 7.37 (d, *J* = 7.4 Hz, 2H), 7.27-7.13 (m, 7H), 6.68 (d, *J* = 8.3 Hz, 2H), 4.36 (s, 2H), 4.04 (s, 2H), 2.28 (s, 3H). <sup>13</sup>C-NMR (125 MHz, CD<sub>3</sub>OD): δ (ppm) = 21.24, 33.28, 35.13, 108.51, 116.22, 127.62, 127.80, 128.16, 129.74, 129.77, 130.56, 130.62, 130.80, 138.01, 140.89, 157.00.

#### **2,8-Dibenzyl-6-(*p*-tolyl)imidazo[1,2-*a*]pyrazin-3(7*H*)-one (**69**) (6-Methyl-2H-CTZ)**

3-Benzyl-5-(*p*-tolyl)pyrazin-2-amine (**67**) (32.0 mg, 0.1 mmol, 1 eq.) and 1,1-diethoxy-3-phenylpropan-2-one (**17**) (51.6 mg, 0.2 mmol, 2 eq.) were dissolved in ethanol (2.0 ml) and H<sub>2</sub>O (0.2 ml) and stirred at room temperature. After vacuum deaeration, the solution was cooled to 0 °C and HCl (0.1 ml) was added under nitrogen flow. Once the solution reached room temperature, it was heated and stirred for 21 hours at 80 °C. The solvent was evaporated under vacuum and the crude compound was purified by chromatography (silica gel, eluent composition: CH<sub>3</sub>OH / CH<sub>2</sub>Cl<sub>2</sub> = 1/40 to 1/20), affording 2,8-dibenzyl-6-(*p*-tolyl)imidazo[1,2-*a*]pyrazin-3(7*H*)-one (**69**) as a yellow solid (24.08 mg, 54%).

<sup>1</sup>H-NMR (500 MHz, CD<sub>3</sub>OD, CDCl<sub>3</sub>): δ (ppm) = 7.45 (s, 1H), 7.41 (d, *J* = 7.1 Hz, 2H), 7.36 (d, *J* = 7.4 Hz, 2H), 7.31-7.17 (m, 10H), 4.39 (s, 2H), 4.19 (s, 2H), 2.37 (s, 3H). <sup>13</sup>C-NMR (125 MHz, CD<sub>3</sub>OD): δ (ppm) = 21.35, 34.03, 34.35, 108.11, 126.94, 127.16, 127.81, 129.02, 129.34, 129.35, 129.58, 130.30, 137.15, 139.08,

140.43.

### 3-Benzyl-5-(4-(methoxymethyl)phenyl)pyrazin-2-amine (70)

3-Benzyl-5-bromopyrazine-2-amine (**2**) (166.0 mg, 0.6 mmol, 1 eq.) and 2-(4-(methoxymethyl)phenyl)-4,4,5,5-tetramethyl-1,3,2-dioxaborolane (249.5 mg, 1.0 mmol, 1.6 eq.) were dissolved in toluene (12 ml) and stirred at room temperature. Ethanol (2 ml) and 1 M Na<sub>2</sub>CO<sub>3</sub> aq. (3 ml) were added into the reaction mixture. After vacuum deaeration, a catalytic amount of tetrakis(triphenylphosphine)palladium(0) was added into the solution and the mixture was deaerated again and stirred for 13 hours at 100 °C. After cooling to room temperature, the solution was filtered through a Celite pad to remove the palladium catalyst. The solution was extracted with ethyl acetate, and the brown organic phase was washed with water and brine, dried over Na<sub>2</sub>SO<sub>4</sub> and evaporated. The resulting residue was purified by flash chromatography (silica gel, eluent composition: n-hexane / ethyl acetate = 67/33 to 50/50), affording 3-benzyl-5-(4-(methoxymethyl)phenyl)pyrazin-2-amine (**70**) as a yellow solid (169.5 mg, 88%).

<sup>1</sup>H-NMR (500 MHz, CDCl<sub>3</sub>): δ (ppm) = 8.39 (s, 1H), 7.93 (d, *J* = 8.3 Hz, 2H), 7.42 (d, *J* = 8.3 Hz, 2H), 7.43-7.25 (m, 5H), 4.51 (s, 2H), 4.42 (s, 2H), 4.19 (s, 2H), 3.4 (s, 2H). <sup>13</sup>C-NMR (125 MHz, CDCl<sub>3</sub>): δ (ppm) = 41.42, 58.18, 74.53, 76.90, 77.16, 77.41, 125.91, 127.21, 128.33, 128.71, 129.13, 136.85, 137.65, 138.17, 140.74, 142.51, 151.88.

### 8-Benzyl-2-(4-hydroxybenzyl)-6-(4-(methoxymethyl)phenyl)imidazo[1,2-*a*]pyrazin-3(7*H*)-one (71) (6-Ether-CTZ)

3-Benzyl-5-(4-(methoxymethyl)phenyl)pyrazin-2-amine (**70**) (30.0 mg, 0.09 mmol, 1 eq.) and 3-(4-((tert-butyl)dimethylsilyloxy)phenyl)-1,1-diethoxypropan-2-one (**11**) (69.2 mg, 0.19 mmol, 2 eq.) were dissolved in ethanol (2.0 ml) and H<sub>2</sub>O (0.2 ml) and stirred at room temperature. After vacuum deaeration, the solution was

cooled to 0 °C and HCl (0.1 ml) was added under nitrogen flow. Once the solution reached room temperature, it was heated and stirred for 4 hours at 80 °C. The solvent was evaporated under vacuum and the crude compound was purified by chromatography (silica gel, eluent composition: CH<sub>3</sub>OH / CH<sub>2</sub>Cl<sub>2</sub> = 1/20), affording 8-benzyl-2-(4-hydroxybenzyl)-6-(4-(methoxymethyl)phenyl)imidazo[1,2-*a*]pyrazin-3(7*H*)-one (**71**) as a yellow solid (13.8 mg, 31%).

<sup>1</sup>H-NMR (500 MHz, CD<sub>3</sub>OD): δ (ppm) = 7.70 (s, 1H), 7.59 (d, *J* = 7.4 Hz, 2H), 7.39-7.18 (m, 7H), 7.14 (d, *J* = 8.3 Hz, 2H), 6.68 (d, *J* = 8.5 Hz, 2H), 4.44 (s, 2H), 4.38 (s, 2H), 4.05 (s, 2H), 3.31-3.30 (m, 3H). <sup>13</sup>C-NMR (125 MHz, CD<sub>3</sub>OD): δ (ppm) = 33.22, 35.34, 58.47, 74.94, 108.97, 116.22, 127.80, 128.16, 129.15, 129.27, 129.75, 129.79, 129.89, 130.57, 130.78, 138.05, 141.20, 157.02.

#### **2,8-Dibenzyl-6-(4-(methoxymethyl)phenyl)imidazo[1,2-*a*]pyrazin-3(7*H*)-one (**72**) (6-Ether-2H-CTZ)**

3-Benzyl-5-(4-(methoxymethyl)phenyl)pyrazin-2-amine (**70**) (30.4 mg, 0.09 mmol, 1 eq.) and 1,1-diethoxy-3-phenylpropan-2-one (**17**) (44.2 mg, 0.19 mmol, 2 eq.) were dissolved in ethanol (2.0 ml) and H<sub>2</sub>O (0.2 ml) and stirred at room temperature. After vacuum deaeration, the solution was cooled to 0 °C and HCl (0.1 ml) was added under nitrogen flow. Once the solution reached room temperature, it was heated and stirred for 4 hours at 80 °C. The solvent was evaporated under vacuum and the crude compound was purified by chromatography (silica gel, eluent composition: CH<sub>3</sub>OH / CH<sub>2</sub>Cl<sub>2</sub> = 1/20), affording 2,8-dibenzyl-6-(4-(methoxymethyl)phenyl)imidazo[1,2-*a*]pyrazin-3(7*H*)-one (**72**) (29.35 mg, 68%).

<sup>1</sup>H-NMR (500 MHz, CD<sub>3</sub>OD, CDCl<sub>3</sub>): δ (ppm) = 8.32 (s, 1H), 7.83 (d, *J* = 6.0 Hz, 2H), 7.45-7.23 (m, 11H), 4.52 (s, 2H), 4.49 (s, 2H), 4.27 (s, 2H), 3.40 (m, 3H). <sup>13</sup>C-NMR (125 MHz, CD<sub>3</sub>OD, CDCl<sub>3</sub>): δ (ppm) = 31.67, 37.69, 58.55, 74.86, 110.68, 127.81, 127.84, 128.22, 129.19, 129.41, 129.62, 129.66, 130.01, 133.74, 136.89, 138.30, 141.41, 146.26.

### **5.2.2. Chemiluminescence assay**

In order to obtain the chemiluminescence characteristics, CH<sub>3</sub>OH solution of native CTZ or the respective CTZ derivatives (2 mM, 8  $\mu$ L) was mixed with DMSO (80  $\mu$ L) containing 0.25% (v/v) of 1 M aqueous sodium hydroxide in a 200  $\mu$ L microtube. The microtube was immediately moved into the chamber of a precision spectrophotometer (AB-1850, ATTO), equipped with a cooled charge-coupled device (CCD) camera which can detect the emission from 400 nm to 800 nm at once, and the resulting spectra were taken in 1 second. The optical spectra were normalized in percentages (%) and optical intensities were determined as the integrated value value over the from 350 to 700 nm range.

### **5.2.3. Initial bioluminescence intensities in cell lysate**

The initial bioluminescence intensities of all CTZ derivatives were determined with existing luciferases (RLuc, RLuc8, RLuc8.6-535, RLuc8SG and RLuc8.6SG). Monkey kidney fibroblasts, COS-7 cells were cultured in a 24-well plate using a TransIT-LT1 transfection reagent (Takara, Osaka, Japan). COS-7 cells were separately transfected with pcDNA3.1(+) encoding wild-type RLuc (pGL4.75), RLuc8, RLuc8.6-535, RLuc8SG, RLuc8.6SG and incubated for 44 h and then treated with a lysis buffer (E291A) (Promega, Madison, WI, USA) according to the manufacturer's protocol. An aliquot of the cell lysate (4  $\mu$ L) was mixed with phosphate buffered saline (PBS) buffer (200  $\mu$ L) containing 2  $\mu$ M native CTZ or the respective CTZ derivatives in Röhren polystyrene tubes (Sarstedt, Nümbrecht, Germany). Initial BLI of native CTZ and its derivatives were immediately measured for the first 1s with a Lumat LB 9507 luminometer (Berthold Technologies, Bad Wildbad, Germany).

### **5.2.4. Kinetic profiles in combination with RLuc8.6-535**

All CTZ derivatives were dissolved in methanol as stock solution and diluted to appropriate concentration in

PBS buffer for each measurement. The affinity column-purified RLuc8.6-535 was dissolved in PBS buffer ( $1 \mu\text{g mL}^{-1}$ ). An aliquot of the luciferase solution ( $50 \mu\text{L}$ ) was transferred into a 96-well optical bottom microplate. The BLIs were determined every 1 second with an image analyzer (Lumazone FA with PIXIS 1024, Nippon Roper) equipped with an electron multiplying charged cooled device (EM-CCD) cameras, immediately after the simultaneous injection of CTZ solutions ( $50 \mu\text{L}$ ) using an 8-channel micropipette. The 96-well optical-bottom microtiter plate was immediately set in the dark chamber of the Lumazon FA image analyzer. The first 5-second BL signal was taken as a measure of luciferase activity (the final CTZ concentrations were 0, 0.25, 0.5, 1, 2, 5, 10, 20  $\mu\text{M}$ , whereas the final concentration of RLuc8.6-535 was  $0.5 \mu\text{g mL}^{-1}$ ). The bioluminescence kinetic profiles ( $K_m$ ,  $V_{\text{max}}$  and BL half decay) were calculated using GraphPad Prism software. The overall BL intensities of CTZ derivatives were determined by long-term integration (10 min) of luminescence intensities, which were generated by complete consumption of a low concentration of luciferins ( $0.25 \mu\text{M}$ ) with excess amount of RLuc8.6-535.

### 5.2.5. Molecular dynamic simulations for free energy calculations of ligand binding

The computational docking was performed with AutoDock 4.2.6<sup>12</sup> using a crystal structure (PDB ID: 2PSJ) of an 8-mutation variant of RLuc (RLuc8)<sup>13</sup>, which includes the coelenteramide within the structure. The molecular structures of native coelenterazine (CTZ) and 6-Al3OH-CTZ were generated with Avogadro<sup>14</sup>. Each docking simulation was performed 1500 times. Ligand docking poses of CTZ and 6-Al3OH-CTZ were selected based on the binding energies  $\Delta G_{\text{docking}}$  calculated by the AutoDock internal scoring function, their relative orientation and location to the coelenteramide within the crystal structure.

Absolute binding free energies  $\Delta G_{\text{calc}}$  were calculated using the alchemical thermodynamic cycle<sup>15</sup>. All molecular dynamics simulations were performed using GROMACS 5.1.2<sup>16</sup>. The RLuc8 with a docked ligand was solvated with the TIP3P water model<sup>17</sup> in a dodecahedral box with minimum distance of 1.2 nm from the

protein (number of water molecules were about 13200) and neutralized by adding sodium ions. The missing residues of the Rluc8 structure were modeled using MODELLER<sup>18</sup>. Ligands are parameterized with the general AMBER force field<sup>19</sup> and AM1-BCC point charges<sup>20</sup> using AmberTools14<sup>21</sup>. The Amber ff99SB-ILDN force field<sup>22</sup> was used for the protein. In the thermodynamic cycle<sup>15</sup>, the van der Waals and coulombic interactions of the ligand were turned off using a linear alchemical pathway with  $\Delta\lambda = 0.05$  and  $0.1$ , respectively. A softcore potential was employed for the van der Waals interactions transformed<sup>23</sup>. Additionally, 12 non-uniformly distributed  $\lambda$  values (0.0, 0.01, 0.025, 0.05, 0.075, 0.1, 0.15, 0.2, 0.3, 0.5, 0.75, 1.0) were used for the ligand restraints to prevent the ligand leaving the binding site when the ligand-protein interactions are turned off. The relative position and orientation of the bound ligand with respect to the protein was restrained by means of one distance with force constant of  $1,000 \text{ kcal mol}^{-1} \text{ nm}^{-2}$ , two angles and three dihedral harmonic potentials with force constant of  $10 \text{ kcal mol}^{-1} \text{ rad}^{-2}$ . The contribution of the restraints to the free energy was calculated analytically<sup>24</sup>. Therefore, the complex simulations (ligand and protein in solution) with 41 windows and the ligand simulations (ligand in solution) with 31 windows were performed. Each window was first energy minimized for 5000 steps followed by 0.5 ns NVT constant and 1.0 ns NPT constant simulations for equilibration with the protein backbone particle restrained (force constant of  $1000 \text{ kJ mol}^{-1} \text{ nm}^{-2}$ ). The time step was set at 2 fs. The temperature of 298.15 K was controlled with Langevin dynamics<sup>25,26</sup>. The pressure of 1 bar was controlled with Berendsen barostat<sup>27</sup> in the equilibrium simulations. Thereafter, 10 ns unrestrained production runs were performed using Hamiltonian exchange Langevin dynamics at NPT constant, where the pressure of 1 bar was controlled with the Parrinello-Rahman barostat<sup>28</sup>. In order to enhance sampling of uncorrelated configurations, I used the Gibbs sampling scheme<sup>29</sup>, where 3 million swaps between replica pairs were attempted every 1,000 time steps. Electrostatic interactions were calculated using the particle mesh Ewald (PME) algorithm<sup>30</sup> with a real space cut-off of 1.2 nm, a spline order of 6, a relative tolerance of  $10^{-6}$ , and a Fourier spacing of 0.1 nm. The switching function was applied for the van der Waals interactions between 1.0

nm and 1.2 nm. All H-bonds were constrained using the P-LINCS method<sup>31,32</sup>. The long-range dispersion correction was applied<sup>33</sup>. For the free energy estimation, the results were analyzed using the multiple Bennet acceptance ratio (MBAR)<sup>34</sup>. The first 1 ns of each window was discarded as a non-equilibrium period. Figures were prepared with CueMol (<http://www.cuemol.org>).

### **5.2.6. Bioluminescence spectra in cell lysate**

The BL spectra of all CTZ derivatives were determined with RLuc8, RLuc8.6-535, RLuc8SG and RLuc8.6SG. An aliquot of the lysate (4  $\mu$ L) was mixed with PBS buffer (200  $\mu$ L) containing 2  $\mu$ M native CTZ or the respective CTZ derivatives in a microtube and set in the sample holder of a precision spectrophotometer (AB-1850, ATTO).

### **5.2.7. Bioluminescence intensities in living cells**

The BLI in living cells of all CTZ derivatives were determined in HeLa or COS-7 cells expressing RLuc8.6SG introduced to the cytoplasm.

HeLa cells or COS-7 cells were subcultured in a 96-well optical-bottom microtiter plate (Thermo Scientific) and transiently transfected with pcDNA3.1 (+) plasmids encoding RLuc8.6SG using a TransIT-LT1 transfection reagent (Takara, Osaka, Japan) and incubated for 24 h and 48 h, respectively. After removal of cell culture medium, the cells were incubated with Hanks' balanced salt solution (HBSS) (100  $\mu$ L) and simultaneously bathed with HBSS buffer (100  $\mu$ L) containing 20  $\mu$ M native CTZ or the respective CTZ derivatives (final CTZ concentration: 10  $\mu$ M). The 96-well optical-bottom microtiter plate was immediately set in the dark chamber of the Lumazon FA image analyzer (Nippon Roper), and the corresponding luminescence intensities from the plate were integrated every 30 seconds.

### 5.2.8. Cell membrane permeability assay of luciferins

Bioluminescence from lysate (pretreatment with promega lysis buffer for 15 min) or intact COS-7 tumor cells expressing RLuc8.6SG in cytoplasm was measured in a 96-well optical bottom microtiter plate (Thermo Scientific) using an image analyzer (Lumazone FA with PIXIS 1024 CCD camera, Nippon Roper) equipped with EM-CCD cameras. The BL measurement was started by addition of the luciferins (final concentration: 10  $\mu\text{M}$ ) and integrated for 30 min.

### 5.2.9 Bioluminescence single cell imaging

Bioluminescence imaging was performed using an Olympus DP30 Cooled Monochrome CCD Microscope Camera with a 100 $\times$  objective lens. HeLa cells in glass bottom dishes were transfected with RLuc8.6SG and incubated at 37 $^{\circ}\text{C}$  under 5%  $\text{CO}_2$  for 48 h. Cells were washed with Hank's balanced salt solution (HBSS) and suspended in HBSS (100  $\mu\text{L}$ ) (covering the central glass bottom part of dish). 6-Al3OMe-2H-CTZ in HBSS (100  $\mu\text{L}$ , 20  $\mu\text{M}$ ) was added to the glass bottom dish (final concentration of luciferin: 10  $\mu\text{M}$ ) and bioluminescence was recorded for 2 s. The reference fluorescence microscopic images were obtained by exciting Mcherry with 565 nm before addition of luciferins. The exposure time for FL images was 2 s.

### 5.2.10. Bioluminescence *in vivo* imaging

The BL intensities of two CTZ derivatives (Native-CTZ and 6-Al3OMe-2H-CTZ) with iRFP-RLuc8.6SG were compared in cos-7 tumor cells implanted in a living mouse (Figure 5-12). First, cos-7 cells grown in DMEM supplemented with 10% FBS were transiently transfected with pcDNA3.1 (+) plasmids encoding iRFP-RLuc8.6SG. After transfection for 48 h, the cells were harvested, washed once, and resuspended in HBSS buffer. The cells were counted before experiments using a cell counting chamber (Burker-Turk Deep, Erma Tokyo). An equivalent amount (50  $\mu\text{L}$ ) of cells ( $1.83 \times 10^6$  cells/mL) were subcutaneously (sc) implanted on the back of

living mice (nude mouse, female, 4 week old). The BLI measurement was started immediately after subcutaneous injection of 50  $\mu\text{L}$  of luciferin (20  $\mu\text{M}$ ) and integrated for 1 s using Lumazone FA with an electron multiplying charge-coupled device (EM-CCD) camera (Nippon Roper) (final luciferin concentration, 20  $\mu\text{M}$ ).

## 5.3 Result and Discussion

### 5.3.1 Design of novel alkylated CTZ derivatives

In the coelenterazine (CTZ)-utilizing marine luciferases, the interaction between the luciferases and CTZ is still remaining unexplained. Therefore, the design of CTZ derivatives retaining enzymatic recognition from marine luciferases such as *Gaussia* luciferase (GLuc) and *Renilla* luciferase (RLuc) and Artificial Luciferase (ALuc) is challenging. Although the crystal structure of RLuc8 (RLuc mutant) including coelenteramide (CTMD: light emitting oxidized state of CTZ) has been reported<sup>35,36</sup>, the location of CTMD in the crystal structure presented a “secondary binding” position and not the position of the CTMD/CTZ during the enzymatic recognition (Figure 5-2). So, any modification of CTZ generates a positive impact on the revealability of the mechanism of the enzymatic recognition and bioluminescence characteristics. In Chapter 2 and Chapter 3, I reported that the modification of the C-6 position of native-CTZ by comparably large substituents (Figure 5-3(C); 6-pi-X-CTZ, where “pi” indicates a styryl group and “X” indicates any functional group at the C-6 position of CTZ) displayed significant bioluminescence emission with RLuc8 and RLuc8.6-535<sup>37,38</sup>, although most of the chemical modifications of CTZ cause luminescence reduction. Therefore, among the modification of substituents at the C-2, C-5, C-6 and C-8 position of the imidazopyrazinone structure, the chemical modification of the C-6 position of CTZ holds the possibility to extend the possible bioanalytical applications of marine luciferases utilizing CTZ as substrate.

Subsequently, in contrast to 6-pi-X-CTZ series, I found that 6-et-X-CTZ (Figure. 5-3(D); “et” indicates an

ethynyl group and “X” indicate any functional group at C-6 position) result in negligibly low bioluminescence in combination with RLuc8 and RLuc8.6-535<sup>38</sup>, whereas they show effectual bioluminescence with artificial luciferases (ALuc). Therefore, I suspect that the rigidity increase in the steric bulk derived from an ethynyl group at the C-6 position of CTZ causes steric hindrance with amino acid residues of the catalytically active site consisting of D120, E144 and H285 (Figure 5-2).

In this work, in expectation of bioluminescence enhancement, I decided to develop novel CTZ derivatives, wherein the (p-hydroxy)-phenyl group in the C-6 position was alkylated (Figure 5-3(E)-(H)) to avoid steric hindrance between the luciferin and amino acid residues of the active site and to investigate the effects of the flexibility and limitation of substitution at the C-6 position on enzymatic activities. Furthermore, to explore the effect of C-2 or C-6 substitution of CTZ on BL activities exhaustively, 18 novel CTZ derivatives were synthesized (Figure 5-3). These novel CTZ derivatives besides native-CTZ (Figure 5-3(A)) and its existing blue-shifted derivative DeepBlueC<sup>TM</sup> (Figure 5-3(B)) are classified into 10 main groups according to their chemical structure. To begin with, the influence of the C-6 substituent size on enzymatic recognition was investigated. A series of 6-Al<sub>n</sub>-OH-CTZ (where “Al” indicates an alkyl chain,  $n = 2-5$ ) (Figure 5-3(E)) having different length straight alkyl linker chains at the C-6 position were synthesized. The series of 6-Al<sub>n</sub>-OH-CTZ ( $n = 2-5$ ) (Figure 5-3(E)) are characteristic for their hydroxyl group terminal at the C-2 and C-6 positions. In contrast, 6-Al<sub>n</sub>-OH-2H-CTZ derivatives (Figure 5-3(F)) have the feature of hydrogen atom substitution at the para position of the C-2 phenyl group.

In the next place, the bioluminescence behavior driven by the shape of the C-6 substituent was determined. As the CTZ derivative with 3-hydroxypropoxy substitution at the C-6 position of native CTZ (Figure 5-3(E): 6-Al3OH-CTZ) emits strong bioluminescence, I prepared a series of other functional group (e.g. methoxy or methyl group) substituted alkyl linker chains with three methylene unit length (Figures 5-3(G) and (H)). From the view point of imidazopyrazinone chemistry, the electron donating group is involved in the high

luminescence quantum yield of luciferins based on the CTZ structure. Therefore, the effects of electron donating groups (methoxy or methyl group) at the C-6 substitution on bioluminescence properties were explored by preparing other series of novel CTZ derivatives (Figures 5-3(I)-(J)).

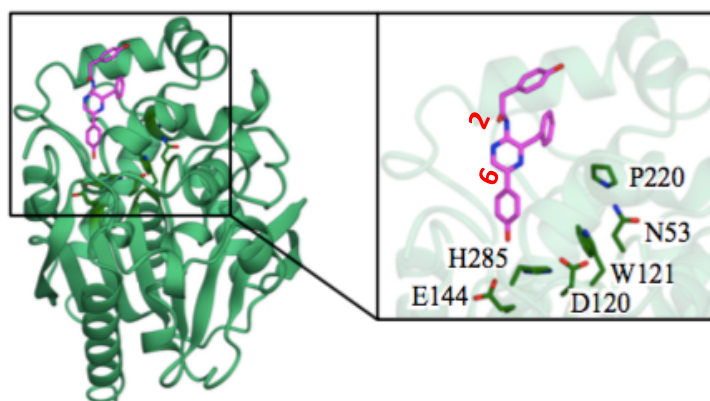


**Figure 5-2** Crystal structure of the RLuc8 with the coelenteramide (CTMD). This figure indicates a close-up view of the binding site with 6 residues (N53, D120, W121, E144, P220 and H285) which have mutagenesis affection on the enzymatic activity. (PDB ID: 2PSJ)

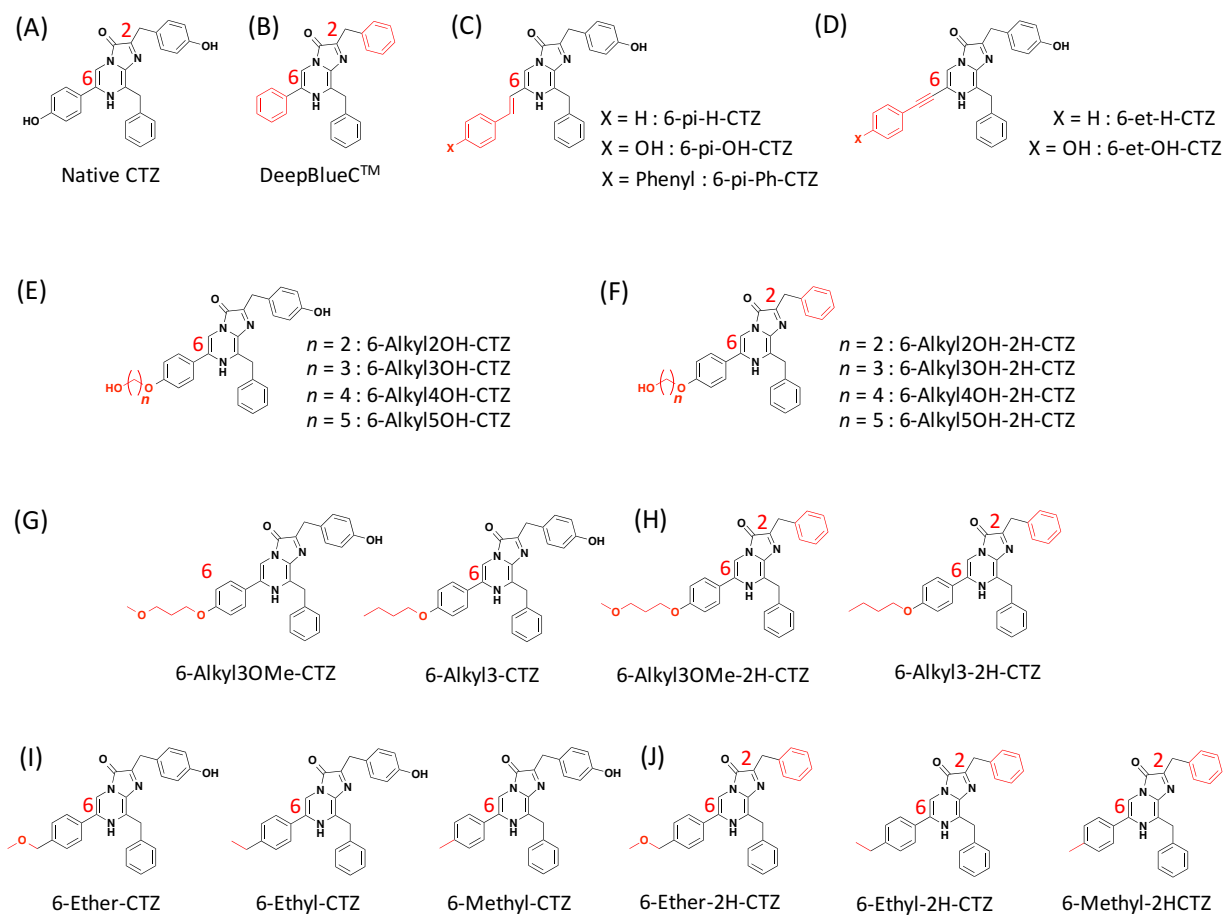


**Figure 5-3** Chemical structures of synthetic coelenterazine derivatives.

The detailed chemical structures of the synthetic coelenterazine analogues. Native-CTZ and its derivatives are categorized into 10 groups: Group (C) contains a styryl group at the C-6 position, whereas Group (D) has an ethynyl group at the C-6 position. Group (E) has a terminal hydroxyl group at the C-6 position. The distinctive feature between groups (E) and (F) is the presence or absence of the hydroxyl group at the C-2 position. Group (G) shares the terminally alkylated structure. Group (H) lacks the hydroxyl group at the C-2 position compared to Group (G). The CTZ derivatives listed as Groups (I) and (J) lack the oxygen atom at the C-6 position compared to other Groups (A), (E)-(H). The characteristic functional groups in the chemical structures are highlighted in red.

### 5.3.2. Chemiluminescence assays

To discuss any possible luciferin-luciferase mismatch, the chemiluminescence (CL) properties of luciferin should be investigated, which allows to study the chemical structure-related basic luminescent capacity. The CL

capacity of CTZ derivatives in DMSO including base was first studied. The CL characteristics of the novel CTZ derivatives are summarized in Table 5-1. The novel CTZ derivatives produced brighter light emission than DeepBlueC™. This result is not surprising, according to the imidazopyrazinone chemistry, the electron donating group at the C-6 substituent raises its fluorescence (FL) quantum yield, which influences the CL quantum yield<sup>39</sup>. Therefore, the superior light output of the novel CTZ derivatives compared to DeepBlueC™ was attributed to the existence of an electron-donating substituent at the para-position of the C-6 phenyl group of CTZ (Figure 5-3). As for the CL spectra, the spectral similarity among CTZs indicates that chemical modification at the C-6 substituent has little influence on chemiluminescence spectra, except for 6-pi-Phenyl-CTZ. I hypothesized that the red-shifted spectrum of 6-pi-Phenyl-CTZ is due to a reduction of the dihedral twisting between the C-6 substituent and the imidazopyrazinone skeleton<sup>37</sup> (See Chapter 2).

**Table 5-1** Summary of chemiluminescence (CL) characteristics: Initial chemiluminescence intensities (CLI) and CL spectra in the presence of DMSO containing 0.25% (v/v) of 1 M aqueous sodium hydroxide (chemiluminescence was determined in 1 s measurement time). Under this condition, the CLI of 6-*pi*-Phenyl-CTZ could not be obtained due to its high light output. According to CL spectra, the styryl substitution at C-6 position extends its conjugated  $\pi$ -electron system and strongly influences chemiluminescence quantum yield.

	CL intensity (CLI)	CL spectrum
	(%)	Emission max. [nm]
Native-CTZ	100	510
6-Alkyl2OH-CTZ	113	499
6-Alkyl2OH-2H-CTZ	122	499
6-Alkyl3OH-CTZ	113	500
6-Alkyl3OH-2H-CTZ	91.4	498
6-Alkyl4OH-CTZ	84.3	499
6-Alkyl4OH-2H-CTZ	105	498
6-Alkyl3OMe-CTZ	98.2	497
6-Alkyl3OMe-2H-CTZ	116	499
6-Alkyl3-CTZ	92.4	493
6-Alkyl3-2H-CTZ	124	501
6-Ethyl-CTZ	125	500
6-Ethyl-2H-CTZ	92.2	492
6-Methyl-CTZ	110	499
6-Methyl-2H-CTZ	130	500
6-Ether-CTZ	90.1	493
6-Ether-2H-CTZ	104	495
DeepBlueC™	69.0	489
6- <i>pi</i> -Phenyl-CTZ	-	528

### 5.3.3. Initial bioluminescence intensities

The initial bioluminescence intensities (BLI) of all CTZ derivatives (2  $\mu$ M) were determined from each lysate including *Renilla* luciferase (RLuc), RLuc8, RLuc8.6-535, RLuc8SG<sup>7</sup> and newly synthesized derivative RLuc8.6SG. A comparison of the initial BLI (Figure 5-4 and Table 5-1) shows that all C-6 substituted CTZ

derivatives are recognized by all RLuc mutants, RLuc8, RLuc8.6-535, RLuc8SG and RLuc8.6SG, but not by RLuc. Especially, all C-6 modified CTZ derivatives produce superior BL emission in the presence of RLuc8.6SG. Among all CTZ derivatives, the CTZ derivatives with 3-hydroxypropoxy substitution at the C-6 position of native CTZ (Figure 5-3 Group (E): 6-AI3OH-CTZ) with RLuc8.6SG show the brightest BL emission. Its intensity reaches 71 % of that of the brightest BL system, the native-CTZ/RLuc8SG pair.

In order to determine the effect of the alkyl linker chain length, the series of hydroxyl-terminated alkyl linker chains of two, three, four and five methylene units in length (Figure 5-3 Group(E)) were compared with RLuc8.6SG. The 4-hydroxybutoxy substituted derivative (6-AI4OH-CTZ) exhibits similar, but slightly decreased emission compared to that of 6-AI3OH-CTZ. 6-AI5OH-CTZ having the longest alkyl chain linker at the C-6 position of native-CTZ shows the lowest BL emission among Group (E) (Figure 5-3). Thus, a proper side alkyl chain at the C-6 position of imidazopyrazinone for high bioluminescence output is 3-hydroxypropoxy. Generally, in bioluminescent enzymatic reactions, dim bioluminescence with increasing substituent size of luciferins can be observed. However, unexpectedly, the 6-AI4OH-CTZ/RLuc8.6SG pair emitted 1.4-fold brighter BL emission than the 6-AI2OH-CTZ/RLuc8.6SG pair, while the side alkyl chain of 6-AI4OH-CTZ is two methylene units longer than 6-AI2OH-CTZ, revealing that the size at the C-6 position of CTZ is not the only factor involved in the enzymatic reaction, and the appropriate interactions between the C-6 substituent and amino acid residues may elevate the luminescence signal.

Next, a comparison of initial BLI between Group (E) and Group (F) was conducted. With much brighter emission of the series of 6-AI $n$ -OH-CTZ except for 6-AI5OH-CTZ, the comparison indicates that the lack of a hydroxyl group at the para position of the C-2 phenyl group induces luminescence decrease. Interestingly, as classic characteristic of the relatively high hydrophobicity observed in the chemical structure of 6-AI5OH-CTZ and other CTZ derivatives (Figure 5-3: Group(G) and (I)), the effects on BL brightness caused by the presence or absence of the hydroxyl group at the C-2 position was negligibly low.

In turn, according to the comparison among 6-Al3OH-CTZ, 6-Al3OMe-CTZ and 6-Alkyl3-CTZ (Figure 5-3(G)), 6-Al3OH-CTZ displayed 1.6- and 1.4-fold higher emission than 6-Al3OMe-CTZ and 6-Alkyl3-CTZ, respectively. Therefore, the comparison may indicate that the hydroxyl group at the C-6 position influences the enzymatic recognition processes at least.

Finally, the effect of the electron donating group (methoxy or methyl group) at the C-6 substituent on BL properties was evaluated by comparing the reported blue-shifted derivative DeepBlueC<sup>TM</sup> to Group (J), as shown in Figure 5-3. 6-Methyl-2H-CTZ (having a C-6 methyl group and lacking the C-2 hydroxyl group) showed 4.1-fold stronger emission than the familiar blue-shifted CTZ derivative, DeepBlueC<sup>TM</sup> (removal of both hydroxyl groups of CTZ) with RLuc8.6SG. Not only 6-methyl-2H-CTZ, but also 6-ethyl-2H-CTZ having an ethyl group at the para position of the C-6 phenyl group instead of the hydroxyl group displayed stronger BL emission than DeepBlueC<sup>TM</sup>. Although the chemiluminescence and bioluminescence characteristics of luciferins are not completely correlated, the dim bioluminescence of DeepBlueC<sup>TM</sup> may be attributed to its low chemiluminescence efficiency (Table 5-1) and enzymatic recognition from RLuc8.6 derivatives.

In bioluminescence systems, the luminescence kinetic profiles arise from the turn-over rate, and product (CTMD) inhibition and quantum yield (QY) should be carefully considered to evaluate bioluminescence intensities. Actually, DeepBlueC<sup>TM</sup> showed the brightest emission with RLuc8SG, in contrast to other C-6 CTZ derivatives preferring RLuc8.6SG as catalytic enzyme. So, the kinetic profiles of all CTZ derivatives with purified RLuc8.6-535 are discussed in Chapter5.3.4.

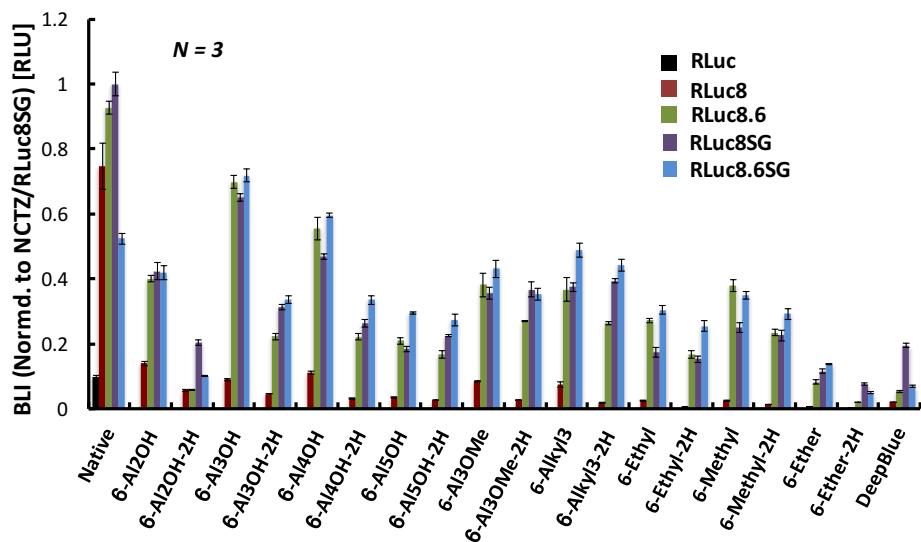


**Figure 5-4** Initial BLI from luciferin (2  $\mu$ L) incubated with 4  $\mu$ L of cell lysate containing the representative luciferases (RLuc, RLuc8, RLuc8.6-535, RLuc8SG and RLuc8.6SG) (measement time: 1s).

**Table 5-2** Initial bioluminescence intensities (BLI) with native *renilla* luciferase (RLuc), RLuc8, RLuc8.6-535, RLuc8SG and RLuc8.6SG (initial BLI is determined in 1s measurement time)

	<b>RLuc</b>	<b>RLuc8</b>	<b>RLuc8SG</b>	<b>RLuc8.6-535</b>	<b>RLuc8.6SG</b>
	<b>BLI (%)</b>	<b>BLI (%)</b>	<b>BLI (%)</b>	<b>BLI (%)</b>	<b>BLI (%)</b>
<b>Native-CTZ</b>	9.94	74.6	<b>100</b>	92.6	52.4
<b>6-Alkyl2OH-CTZ</b>	N.D.	13.9	42.4	40.0	41.9
<b>6-Alkyl2OH-2H-CTZ</b>	N.D.	5.75	20.4	5.78	10.1
<b>6-Alkyl3OH-CTZ</b>	0.10	9.03	64.9	69.8	<b>71.7</b>
<b>6-Alkyl3OH-2H-CTZ</b>	N.D.	4.66	31.4	22.2	33.6
<b>6-Alkyl4OH-CTZ</b>	N.D.	10.9	46.9	55.4	59.5
<b>6-Alkyl4OH-2H-CTZ</b>	N.D.	3.20	26.2	22.2	33.4
<b>6-Alkyl5OH-CTZ</b>	N.D.	3.48	18.3	20.9	29.5
<b>6-Alkyl5OH-2H-CTZ</b>	N.D.	2.67	22.4	16.6	27.3
<b>6-Alkyl3OMe-CTZ</b>	N.D.	8.52	35.5	38.1	43.1
<b>6-Alkyl3OMe-2H-CTZ</b>	N.D.	2.72	36.7	27.1	35.3
<b>6-Alkyl3-CTZ</b>	N.D.	7.48	37.5	36.7	48.8
<b>6-Alkyl3-2H-CTZ</b>	N.D.	1.85	39.3	26.4	44.1
<b>6-Ethyl-CTZ</b>	N.D.	2.49	17.5	27.2	30.4
<b>6-Ethyl-2H-CTZ</b>	N.D.	0.58	15.3	16.7	25.5
<b>6-Methyl-CTZ</b>	N.D.	2.53	25.0	38.0	35.0
<b>6-Methyl-2H-CTZ</b>	N.D.	1.34	22.6	23.5	29.2
<b>6-Ether-CTZ</b>	N.D.	0.79	11.5	8.29	13.7
<b>6-Ether-2H-CTZ</b>	N.D.	0.33	7.59	2.01	4.99
<b>DeepBlueC™</b>	N.D.	2.14	19.5	5.37	6.99

N.D. not detected due to low luminescent intensity

### 5.3.4. Bioluminescence kinetic profiles with RLuc8.6-535

To evaluate the detailed bioluminescence properties, the kinetic profiles of CTZ derivatives were determined with affinity column purified RLuc8.6-535 and summarized as Table 5-3. The  $K_m$  values of C-6 modified CTZ derivatives with RLuc8.6-535 are in the range of 0.2-2.0  $\mu\text{M}$ , which are on par with that of native-CTZ ( $0.69 \pm 0.07 \mu\text{M}$ ), indicating that the C-6 modification of CTZ maintains the high affinity for luciferase. And the values of maximum product formation,  $V_{\text{max}}$  values, show that 6-Al3OH-CTZ ( $(1.25 \pm 0.04) \times 10^5 \text{ s} \cdot \text{p}^{-1}$ ) achieves the highest photon emission rate, followed by native CTZ ( $(1.11 \pm 0.02) \times 10^5 \text{ s} \cdot \text{p}^{-1}$ ) and 6-Al4OH-CTZ ( $(8.26 \pm 0.34) \times 10^4 \text{ s} \cdot \text{p}^{-1}$ ), which closely correlates with results obtained by initial BLI measurements.

On the other hand, the  $K_m$  and  $V_{\text{max}}$  values of DeepBlueC<sup>TM</sup> are 0.31  $\mu\text{M}$  and  $(3.16 \pm 0.04) \times 10^3 \text{ s} \cdot \text{p}^{-1}$ , respectively. Therefore, DeepBlueC<sup>TM</sup> has high affinity for RLuc8.6-535, whereas the  $V_{\text{max}}$  value is relative low compared to other CTZs. For the explanation of changes in brightness, the  $V_{\text{max}}/K_m$  value, which is proportional to the  $k_{\text{cat}}/K_m$  value, and the relative QY values were assessed to discuss the catalytic efficiency of RLuc8.6-535.

According to a comparison of  $V_{\text{max}}/K_m$  values of native-CTZ, 6-Al3OH-CTZ, 6-Al4OH-CTZ and DeepBlueC<sup>TM</sup>, RLuc8.6-535 exhibits a higher catalytic efficiency for native-CTZ ( $160.8 \times 10^3 \text{ s} \cdot \text{p}^{-1} \cdot \mu\text{M}^{-1}$ ), followed by 6-Al3OH-CTZ ( $125.0 \times 10^3 \text{ s} \cdot \text{p}^{-1} \cdot \mu\text{M}^{-1}$ ), 6-Al4OH-CTZ ( $89.7 \times 10^3 \text{ s} \cdot \text{p}^{-1} \cdot \mu\text{M}^{-1}$ ) and DeepBlueC<sup>TM</sup> ( $10.1 \times 10^3 \text{ s} \cdot \text{p}^{-1} \cdot \mu\text{M}^{-1}$ ). In addition, the relative QY values are in the order of native-CTZ, 6-Al3OH-CTZ, 6-Al4OH-CTZ and DeepBlueC<sup>TM</sup>, which correlates with the  $V_{\text{max}}/K_m$  values.

Furthermore, the BL-half life time of native-CTZ (121 s), 6-Al3OH-CTZ (101 s) and 6-Al4OH-CTZ (109 s) is quite longer than DeepBlueC<sup>TM</sup> (15 s). Because RLuc shows flash luminescence caused by inactivation from the luminescence reaction product CTMD<sup>40</sup>, it is contemplated that the strong bioluminescence of 6-Al3OH-CTZ is contributed to its relative high catalytic turn-over rate and production efficiency of oxyluciferin in excited state compared to other CTZ derivatives.

**Table 5-3** The bioluminescence kinetic profiles of all CTZ derivatives in combination with purified RLuc8.6-535. <sup>a</sup>Michaelis-Menten constant  $K_m$  and maximum rate  $V_{max}$  were estimated with the Michaelis-Menten kinetics equation using GraphPad Prism software. The values are shown with  $\pm$  SD of three independent assays performed in triplicate. <sup>c</sup>The quantum yield was calculated by dividing the total BL signal of CTZs by the number of substrate molecules in reaction solution. The total BL signal were determined by completely consumption of a low concentration of luciferins (0.25  $\mu$ M) in the presence of excess amount of RLuc8.6-535. <sup>e</sup>Data from Chapter 2.

	Relative initial BLI [-]	$K_m^a$ [ $\mu$ M]	$V_{max}^b$ [ $s^{-1}$ ]	$V_{max}/K_m$ [ $\times 10^3 p s^{-1} \mu M^{-1}$ ]	Relative QY <sup>c</sup> [-]
Native-CTZ	100	0.69 $\pm$ 0.07	(1.11 $\pm$ 0.02) $\times 10^5$	160.8	100
6-Al2OH-CTZ	43.1	1.31 $\pm$ 0.12	(5.54 $\pm$ 0.13) $\times 10^4$	42.29	86
6-Al2OH-2H-CTZ	6	2.06 $\pm$ 0.30	(6.04 $\pm$ 0.26) $\times 10^4$	29.32	30
6-Al3OH-CTZ	75.3	1.00 $\pm$ 0.13	(1.25 $\pm$ 0.04) $\times 10^5$	125.00	84
6-Al3OH-2H-CTZ	23.9	0.85 $\pm$ 0.40	(2.65 $\pm$ 0.56) $\times 10^4$	31.17	22
6-Al4OH-CTZ	59.8	0.92 $\pm$ 0.15	(8.26 $\pm$ 0.34) $\times 10^4$	89.78	43
6-Al4OH-2H-CTZ	23.9	1.12 $\pm$ 0.29	(3.56 $\pm$ 0.24) $\times 10^4$	31.78	7
6-Al5OH-CTZ	22.5	0.42 $\pm$ 0.11	(1.86 $\pm$ 0.10) $\times 10^4$	44.28	11
6-Al5OH-2H-CTZ	17.9	1.11 $\pm$ 0.15	(1.66 $\pm$ 0.06) $\times 10^4$	14.95	5
6-Al3OMe-CTZ	41.1	1.12 $\pm$ 0.15	(5.54 $\pm$ 0.20) $\times 10^4$	49.46	34
6-Al3OMe-2H-CTZ	29.2	0.75 $\pm$ 0.20	(3.79 $\pm$ 0.24) $\times 10^4$	50.53	23
6-Alkyl3-CTZ	39.6	0.79 $\pm$ 0.18	(2.99 $\pm$ 0.19) $\times 10^4$	37.84	6
6-Alkyl3-2H-CTZ	28.5	0.33 $\pm$ 0.04	(2.30 $\pm$ 0.11) $\times 10^4$	69.69	77
6-Ethyl-CTZ	29.3	0.41 $\pm$ 0.12	(3.10 $\pm$ 0.31) $\times 10^4$	75.60	27
6-Ethyl-2H-CTZ	18.0	0.57 $\pm$ 0.12	(2.12 $\pm$ 0.17) $\times 10^4$	37.19	14
6-Methyl-CTZ	41.0	1.02 $\pm$ 0.21	(4.28 $\pm$ 0.42) $\times 10^4$	41.96	12
6-Methyl-2H-CTZ	25.3	0.92 $\pm$ 0.22	(3.88 $\pm$ 0.43) $\times 10^4$	42.17	10
6-Ether-CTZ	8.9	0.30 $\pm$ 0.03	(1.06 $\pm$ 0.02) $\times 10^4$	35.33	21
6-Ether-2H-CTZ	2.1	0.26 $\pm$ 0.02	(4.94 $\pm$ 0.08) $\times 10^3$	19.00	2
DeepBlueC <sup>TM</sup>	5.7	0.31 $\pm$ 0.009	(3.16 $\pm$ 0.04) $\times 10^3$	10.19	2
6-pi-Phenyl-CTZ	33.8 <sup>e</sup>	0.60 $\pm$ 0.09	(2.84 $\pm$ 0.13) $\times 10^4$	47.33	25

Notes: The comparison of the BL kinetic profile of each substrate is sufficient to discuss BL characteristics of CTZs. However, it is difficult to compare these values accurately because the lack of measuring equipment with both high detection sensitivity in the blue region (in case of EM-CCD camera used as a signal reader) and an injection module for flash-type bioluminescence systems.

### 5.3.5. Luminescence spectra of CTZ derivatives

To assess the luminescence spectra, the CL and BL spectra of all CTZs were investigated. The spectral characteristics are summarized as Figure 5-5 and Table 5-4. The CL emission of C-6 modified CTZ derivatives is located around 500 nm, almost identical to the native-CTZ (Figure 5-5(A) and Table 5-4). The similar emission spectra of native-CTZ and derivatives are contributed to the amide anion species of CTMD in the excited state. And the minor influence of C-6 substituents on the CL spectrum has been described in Chapter 2. During the enzymatic reaction, CTZ can form three possible light emitting excited state CTMDs in different protonation states (e.g. neutral species, phenolate anion or pyrazine anion species), which determine the emission color<sup>41</sup>. In the bioluminescence spectra of C-6 modified CTZ derivatives with RLuc derivatives, the blue-shifted emission (maximum at 401-426 nm) comes from the fact that only the neutral species of CTMD in the excited state was detected, implying that the C-6 modification prevents the deprotonation of the p-hydroxyl group on the C-6 phenyl of CTMD. Therefore, it is indicated that we successfully developed bright blue-shifted CTZ derivatives, which can be alternatives to DeepBlueC<sup>TM</sup>.

In addition, the full width at half maximum (FWHM) values of RLuc mutants with 6-A13OH-CTZ and native-CTZ are 51 nm and 89 nm, respectively (Figure 5-5(B) and Table 5-4). Because the difference of FWHM values of emission is attributed to the number of light emitters in the transition state, the broader FWHM of native-CTZ may be explained by the presence of a relatively large number of light emitters compared to C-6 modified CTZ derivatives. In addition, the comparison of the spectral behavior between BL and CL, the CL spectra result in broadening of luminescence spectra with any C-6 modified CTZ derivative, suggesting that there are some stable light emitting species in the excited state (Figure 5-5(A) and Table 5-4).

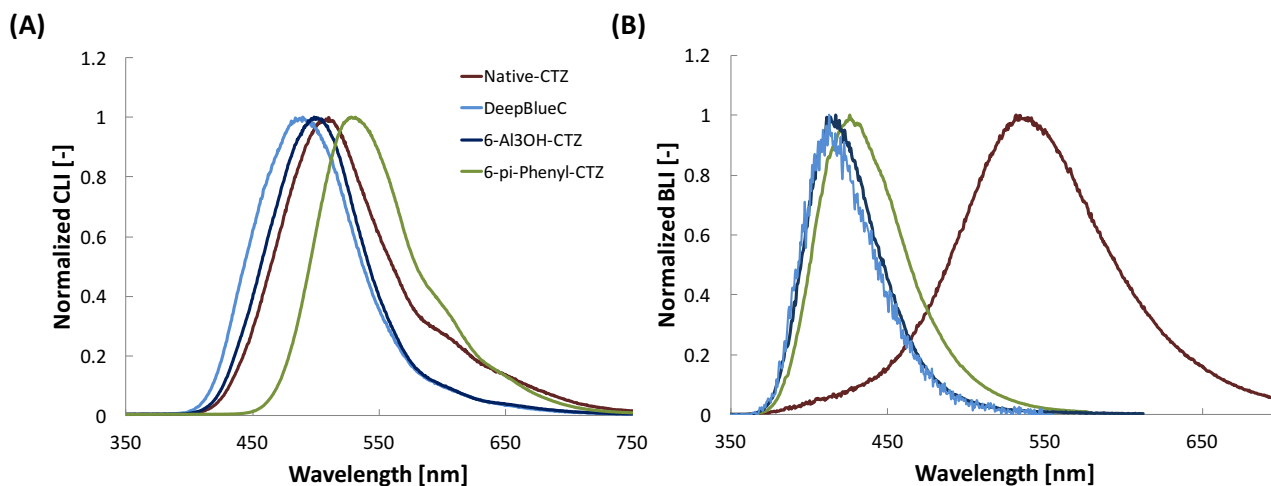


**Figure 5-5** (A) CL spectra of native-CTZ and C-6 modified CTZ derivatives (DeepBlueC<sup>TM</sup>, 6-Al3OH-CTZ and 6-pi-Phenyl-CTZ) under basic condition (B) BL spectra of native-CTZ and C-6 modified CTZ derivatives (DeepBlueC<sup>TM</sup>, 6-Al3OH-CTZ and 6-pi-Phenyl-CTZ) in combination with RLuc8.6SG.

**Table 5-4** BL spectra with native *renilla* luciferase (RLuc), RLuc8, RLuc8.6-535, RLuc8SG, RLuc8.6SG and CL spectra under basic condition

	RLuc8	RLuc8SG	RLuc8.6	RLuc8.6SG	CL
	Peak (nm)	Peak (nm)	Peak (nm)	Peak (nm)	Peak (nm)
	[FWHM (nm)]	[FWHM (nm)]	[FWHM (nm)]	[FWHM (nm)]	[FWHM (nm)]
<b>Native-CTZ</b>	<b>484</b> [98]	<b>490</b> [92]	<b>538</b> [111]	<b>530</b> [106]	<b>510</b> [96]
<b>6-Alkyl2OH-CTZ</b>	<b>411</b> [59]	<b>415</b> [54]	<b>411</b> [56]	<b>412</b> [62]	<b>499</b> [84]
<b>6-Alkyl2OH-2H-CTZ</b>	<b>413</b> [65]	<b>405</b> [70]	<b>407</b> [68]	<b>405</b> [69]	<b>499</b> [86]
<b>6-Alkyl3OH-CTZ</b>	<b>414</b> [60]	<b>412</b> [53]	<b>415</b> [56]	<b>415</b> [51]	<b>500</b> [85]
<b>6-Alkyl3OH-2H-CTZ</b>	<b>411</b> [65]	<b>405</b> [71]	<b>413</b> [56]	<b>411</b> [51]	<b>498</b> [87]
<b>6-Alkyl4OH-CTZ</b>	<b>404</b> [69]	<b>404</b> [71]	<b>412</b> [60]	<b>411</b> [62]	<b>499</b> [84]
<b>6-Alkyl4OH-2H-CTZ</b>	<b>404</b> [69]	<b>404</b> [71]	<b>405</b> [68]	<b>412</b> [52]	<b>498</b> [86]
<b>6-Alkyl5OH-CTZ</b>	<b>403</b>	<b>422</b>	<b>406</b>	<b>413</b>	<b>496</b>

	[70]	[53]	[66]	[51]	[85]
<b>6-Alkyl5OH-2H-CTZ</b>	<b>403</b>	<b>406</b>	<b>406</b>	<b>414</b>	<b>492</b>
	[70]	[71]	[68]	[49]	[87]
<b>6-Alkyl3OMe-CTZ</b>	<b>(418)</b>	<b>412</b>	<b>412</b>	<b>412</b>	<b>497</b>
	[44]	[65]	[59]	[59]	[83]
<b>6-Alkyl3OMe-2H-CTZ</b>	<b>416</b>	<b>414</b>	<b>413</b>	<b>411</b>	<b>499</b>
	[49]	[55]	[53]	[53]	[86]
<b>6-Alkyl3-CTZ</b>	<b>(413)</b>	<b>412</b>	<b>412</b>	<b>412</b>	<b>493</b>
	[46]	[65]	[60]	[62]	[87]
<b>6-Alkyl3-2H-CTZ</b>	<b>411</b>	<b>414</b>	<b>413</b>	<b>413</b>	<b>501</b>
	[50]	[56]	[53]	[54]	[86]
<b>6-Ethyl-CTZ</b>	<b>(410)</b>	<b>401</b>	<b>406</b>	<b>412</b>	<b>500</b>
	[-]	[65]	[60]	[60]	[86]
<b>6-Ethyl-2H-CTZ</b>	<b>(402)</b>	<b>414</b>	<b>411</b>	<b>411</b>	<b>492</b>
	[-]	[52]	[50]	[50]	[91]
<b>6-Methyl-CTZ</b>	<b>415</b>	<b>410</b>	<b>413</b>	<b>412</b>	<b>499</b>
	[44]	[52]	[51]	[50]	[89]
<b>6-Methyl-2H-CTZ</b>	<b>408</b>	<b>412</b>	<b>411</b>	<b>411</b>	<b>500</b>
	[45]	[53]	[49]	[50]	[92]
<b>6-Ether-CTZ</b>	<b>(420)</b>	<b>414</b>	<b>411</b>	<b>410</b>	<b>493</b>
	[-]	[53]	[49]	[51]	[91]
<b>6-Ether-2H-CTZ</b>	<b>(393)</b>	<b>412</b>	<b>406</b>	<b>412</b>	<b>495</b>
	[-]	[56]	[53]	[50]	[96]
<b>DeepBlueC™</b>	<b>416</b>	<b>416</b>	<b>410</b>	<b>412</b>	<b>489</b>
	[57]	[59]	[51]	[49]	[94]
<b>6-pi-Phenyl-CTZ</b>	<b>434</b>	<b>434</b>	<b>426</b>	<b>426</b>	<b>528</b>
	[61]	[66]	[64]	[63]	[84]

FWHM: full width at half maximum

### 5.3.6. Docking simulation study

A previous docking simulation of native-CTZ to the lower portion of the RLuc8 active site including the putative catalytic amino residue, indicated that the hydroxyl group at the C-6 position binds to these residues (H285, E144 and D120) via hydrogen bonding and it might strongly affect the enzyme activity<sup>35,36</sup>. In order to elucidate the enzymatic recognition mechanism of native-CTZ and 6-Al3OH-CTZ by *renilla* luciferase derivatives, a computational docking simulation of luciferin with RLuc8 was conducted using Autodock4.2.6.

As mentioned before, the position of CTMD in the RLuc8 crystal structure presented a “secondary binding” position and not the position of the CTMD/CTZ during the enzymatic recognition. Therefore, the current work also conducted docking simulation of substrates in a “secondary binding” position to investigate the most stable conformation of 6-Al3OH-CTZ in the enzyme (Figure 5-6(C)). First, I estimated the absolute binding free energies of CTMD ( $-6.64 \pm 0.12$  kcal/mol) and native-CTZ ( $-6.50 \pm 0.10$  kcal/mol). The obtained results are very similar, indicating that this docking simulation result of native-CTZ-RLuc8 complex is valuable (Figure 5-6(A)(B) and Table 5-5). Then, the relative orientation of the bound native-CTZ with respect to RLuc8 was calculated. The most stable conformation regarding the orientation (Figure 5-6(B): Site-1-up and Site-1-down) of native-CTZ indicates that native-CTZ can advantageously insert into the catalytic active site as binding pose site-1-down formation ( $-7.67 \pm 0.11$  kcal/mol), in other words, the C-6 phenyl group of native-CTZ may protrude from the active site pocket. However, it is also possible that the C-6 phenyl group of native-CTZ can insert into the active site pocket as binding pose site-1-up ( $-6.50 \pm 0.10$  kcal/mol), because the accuracy of this ligand-protein complex associated calculation is  $1.0 \text{ kcal mol}^{-1}$ <sup>15</sup>. Actually, native-CTZ with familiar RLuc derivatives (RLuc8 and RLuc8.6-535) showed two emission peaks (Figure 5-7), a red-shifted major shoulder around 500-550 nm and a blue-shifted shoulder at 390 nm, which indicates that the excited state CTMD can form at least three light emitters during the enzymatic reaction. The formation of the phenolate anion and the pyrazine anion CTMD gives rise to the red-shifted emission around 480 nm and 530 nm, respectively. On

the other hand, the blue-shifted emission originates from the neutral CTMD form, due to the incomplete deprotonation of the p-hydroxyl group at the C-6 phenyl group of native-CTZ. Because the emission color depends to a large extent on its interaction with amino acid residues in the catalytic active site, native-CTZ is perhaps captured by RLuc derivatives in both orientation binding poses (the configuration of site1-up and site-1-down) inside the enzyme pocket illustrated in Figure 5-6(B), resulting in two emission peaks. Interestingly, native-CTZ shows differences in the BL emission wavelength between RLuc and RLucSG mutant (Figure 5-8(A)-(B)). Therefore, it can be assumed that the C-6 hydroxyl group interacts with different amino acid residues depending on the variety of luciferase.

Next, I calculated the relative orientation of the bound 6-Al3OH-CTZ with respect to RLuc8 and the results are shown in Figure 5-6(C). As a result, the configuration of site-1-up ( $-7.65 \pm 0.14$  kcal/mol) is preferred for 6-Al3OH-CTZ inside the enzyme pocket, which implies that in the most stable conformation, the alkyl linker moiety at the C-6 position of 6-Al3OH-CTZ may insert into the catalytically active site of RLuc8 and interacts with amino acid residues via hydrophobic and hydrogen bond interaction. Therefore, the docking simulation results may sustain the assumption that the size or shape of the C-6 substituent of native-CTZ is strongly involved in bioluminescence activities.

**Table 5-5** Summary of ligand binding energies; absolute binding free energies  $\Delta G_{calc}$  and binding energies with AutoDock internal scoring function  $\Delta G_{docking}$ . The unit of all values is kcal/mol. The site1 is near the binding site of coelenteramide within the crystal structure, while site2 is near the amino acids (N53, D120, W121, E144, P220, and H285) which have mutagenesis affection on the enzymatic activity<sup>24,25</sup>. In the up pose, the five-membered ring faces the inside of the binding site, while in the down pose outward. Snapshots of the binding poses are shown in Figure 5-6.

Ligand	Site-1-up	Site-1-down
NCTZ ( $\Delta G_{calc}$ )	$-6.50 \pm 0.10$	$-7.67 \pm 0.11$
6-Al3OH-CTZ ( $\Delta G_{calc}$ )	$-7.65 \pm 0.14$	$-5.58 \pm 0.11$
Coelenteramide ( $\Delta G_{calc}$ )	$-6.64 \pm 0.12$	-

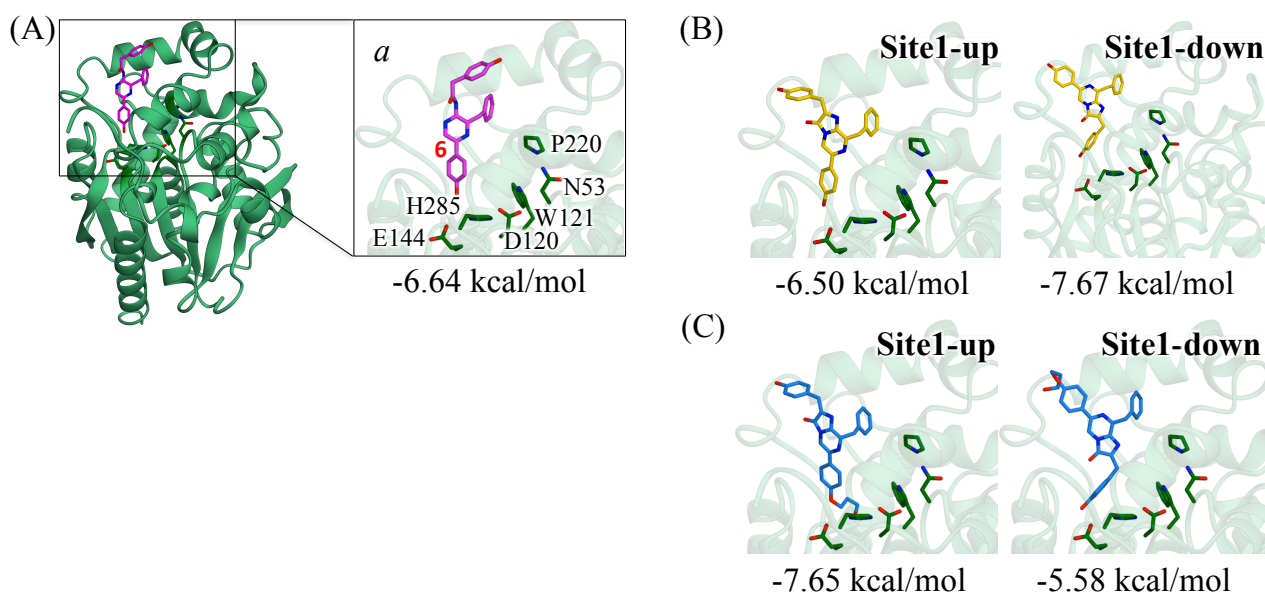


**Figure 5-6** Binding poses predicted with the docking simulation (A) Crystal structure of the RLuc8 with the coelenteramide (CTMD). Inset *a* is a close-up view of the binding site with 6 residues, which have mutagenesis affection on the enzymatic activity. Binding poses of (B) the native and (C) the 6-Al3OH-CTZ. The absolute binding free energies are shown as reference.

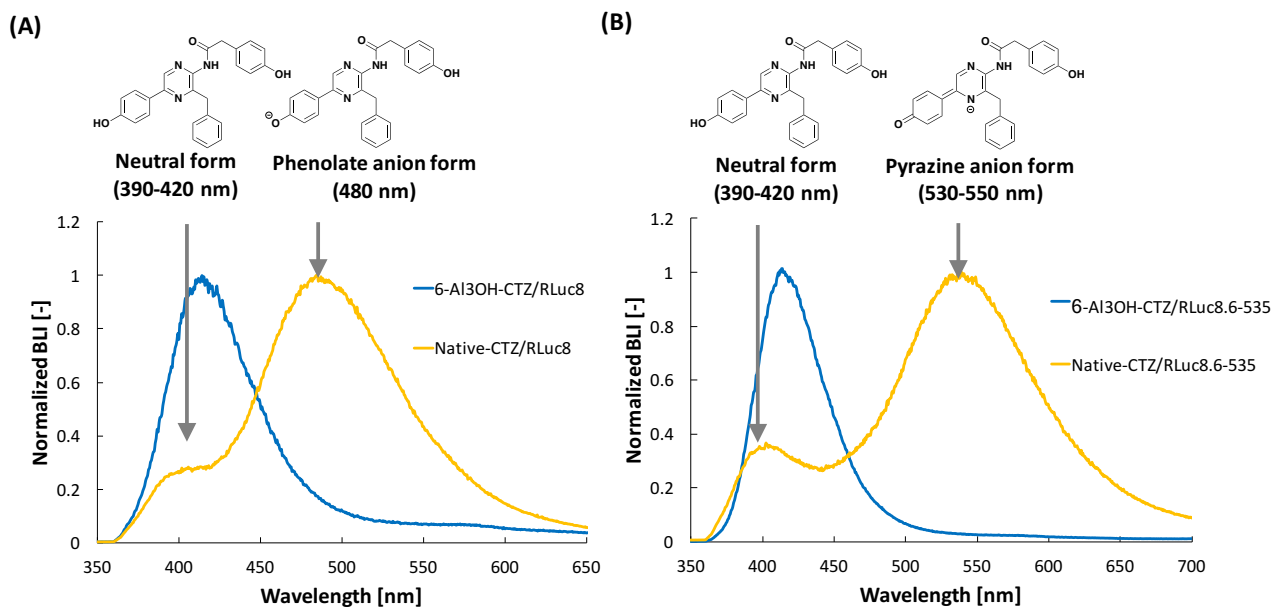


**Figure 5-7** (A) BL spectra of native-CTZ and 6-Al<sub>3</sub>OH-CTZ with RLuc8, (B) BL spectra of native-CTZ and 6-Al<sub>3</sub>OH-CTZ with RLuc8.6-535. In contrast to native-CTZ, 6-Al<sub>3</sub>OH-CTZ protects the p-hydroxyl group at the C-6 position, which prevents the deprotonation of the p-hydroxyl group at the C-6 position, resulting in blue-shifted emission.

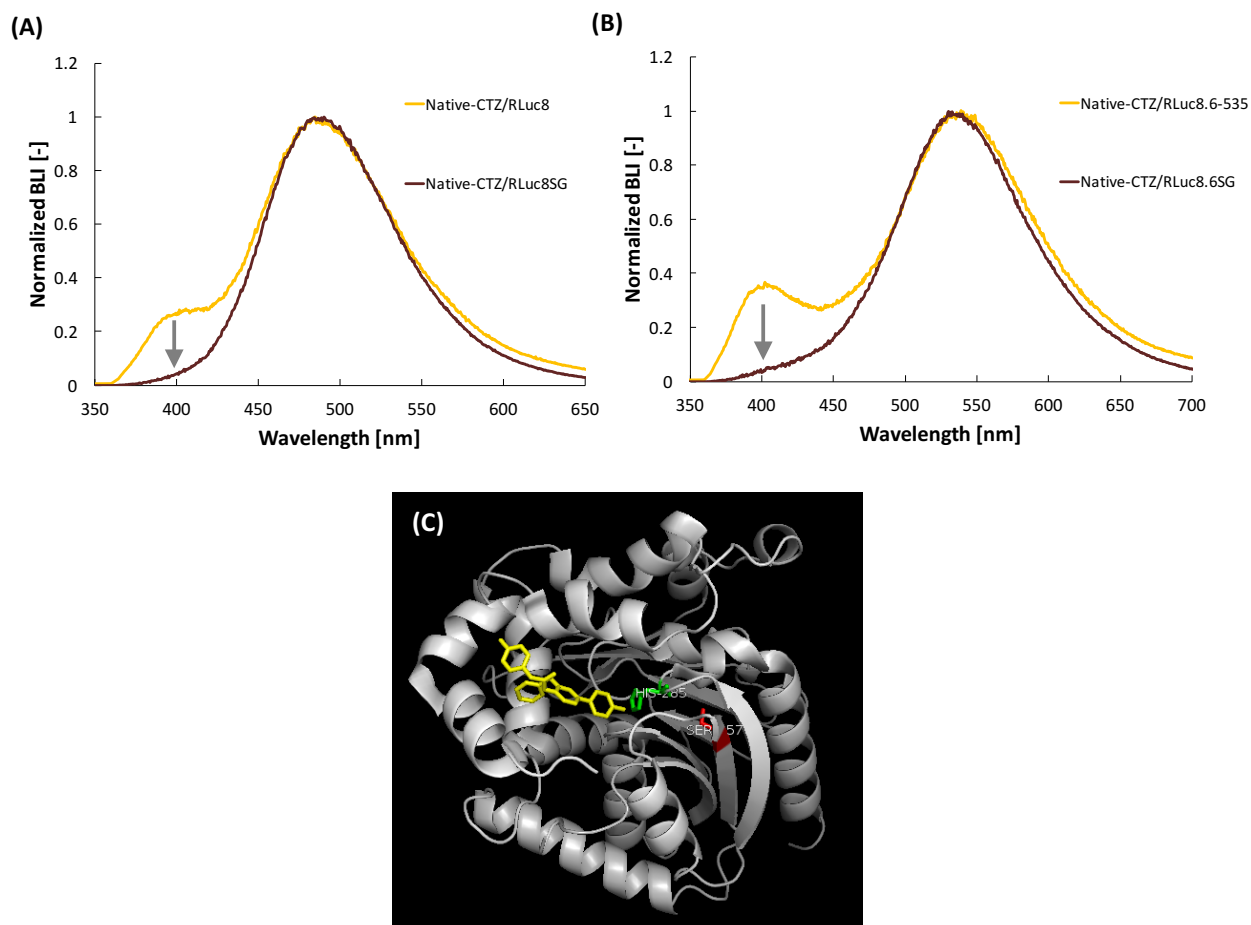


**Figure 5-8** (A) BL spectra with RLuc8 and RLuc8SG, (B) BL spectra with RLuc8.6-535 and RLuc8.6SG. (C) Crystal structure of RLuc8 (PDB 2PSD). CTMD, His285 and Ser257 (mutation site) are colored yellow, green and red, respectively.

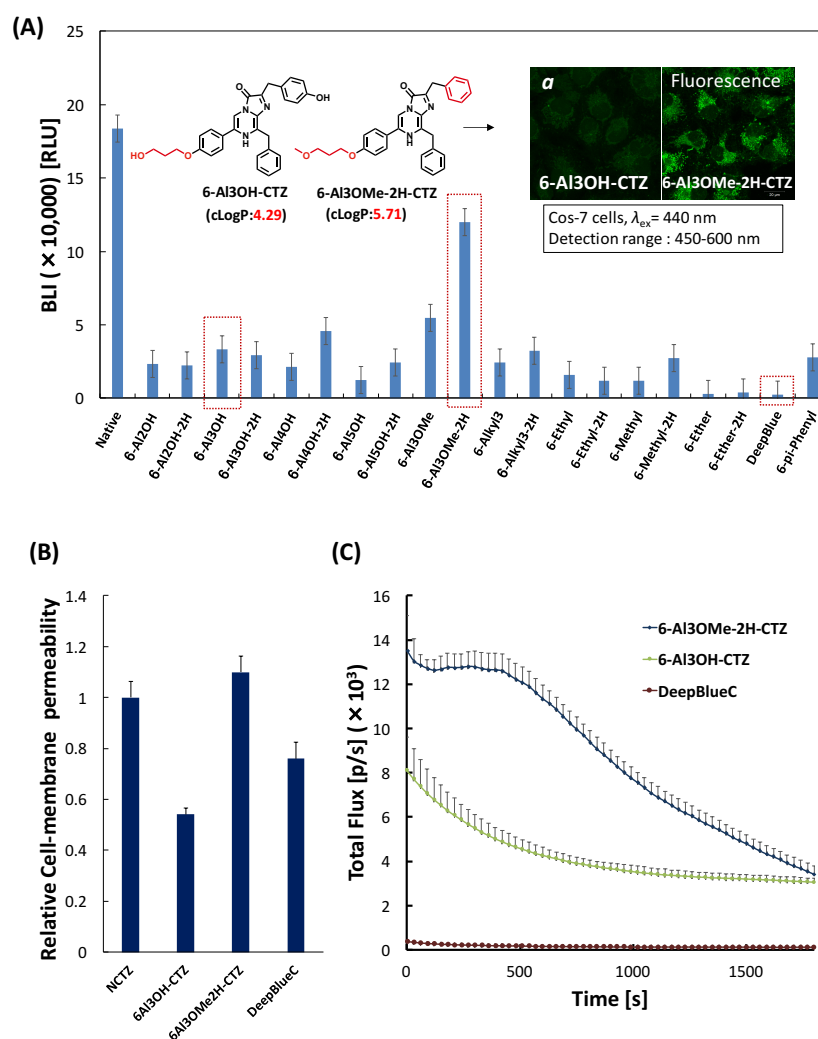
### 5.3.7. Bioluminescence intensities in living mammalian cells

Bioluminescence characteristics of all CTZ derivatives were identified in COS-7 tumor cells expressing RLuc8.6SG introduced to the cytosol. It is generally accepted that native-CTZ can penetrate the mammalian cell membrane and diffuse throughout the cytosol<sup>42</sup>. The BL characteristics of all CTZ derivatives in living mammalian cells were summarized as Figure 5-9 and Table 5-6. Surprisingly, the results show that 6-Al3OMe-2H-CTZ with RLuc8.6SG (Figure 5-3 Group (H)) emitted approximately 2-fold and 54-fold stronger bioluminescence than 6-Al3OH-CTZ and DeepBlueC<sup>TM</sup>, respectively. The BLI of 6-Al3OMe-2H-CTZ is 46% of that of native-CTZ. The time-dependent bioluminescence in living cells shows that the best optical stability is found in 6-Al3OMe-2H-CTZ (BL-half decay: 18.5 min), whereas DeepBlueC<sup>TM</sup> showed relative flash luminescence (BL-half decay: 7 min) (Figure 5-9(B) and Table 5-6). Similar results could be obtained in another mammalian cell, HeLa cells (data not shown). The relatively high BL signal of 6-Al3OMe-2H-CTZ is considered to be due to its high cell membrane permeability. Then, in order to evaluate cell membrane permeability of several CTZs (NCTZ, 6-Al3OH-CTZ, 6-Al3OMe-2H-CTZ and DeepBlueC<sup>TM</sup>), I calculated the ratio of the total BL signal from intact cells to lysed cell solutions with the indicated luciferin at 10  $\mu$ M. The test result shows that 6-Al3OMe-2H-CTZ has approximately twice higher membrane penetrating ability compared to 6-Al3OH-CTZ.

In order to design luciferin analogues having superior optical characteristics in living cells, several factors such as lipid-water partition coefficient, subcellular localization of luciferins and efflux from cells are considerable. For example, the cLogP values of native-CTZ (4.42) and 6-Al3OH-CTZ (4.29) are very similar, indicating that these two substrates have similar hydrophobic character. However, contrary to expectation, the cell membrane permeability of native-CTZ is much higher than 6-Al3OH-CTZ (Figure 5-9(B)). In addition, luciferins can be transported out of cells by membrane transport proteins. Previously, the two membrane transport proteins, ABCB1 and P-glycoprotein (Pgp), have been reported as mediating the efflux of CTZs<sup>43</sup>.

Interestingly, Pgp has substrate specificity for native-CTZ, CTZ-*f*, CTZ-*h* and CTZ-*hcp*, but not for CTZ-*n* and CTZ-*cp*. Thus, the effects of membrane transport proteins on luciferin efflux are considerable.

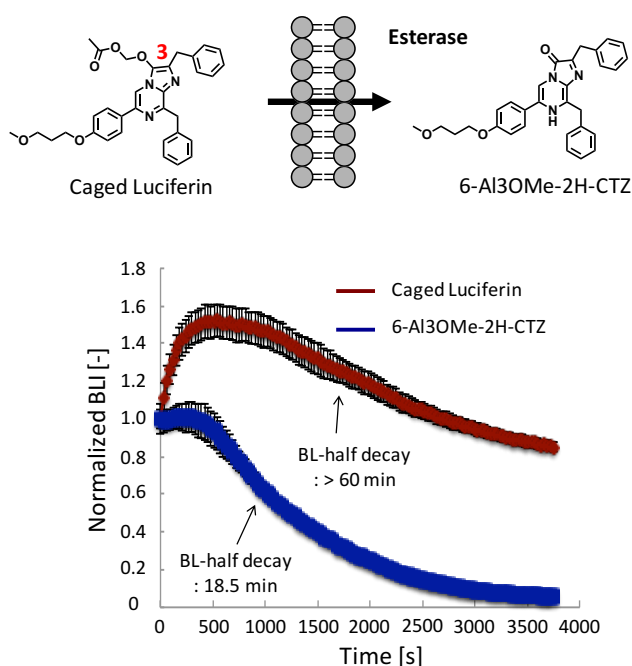
In conclusion, in order to obtain bioluminescence from physiological tissue, an appropriate amount of luciferin should be taken up by cells expressing the corresponding luciferase. With bright blue and prolonged emission, I applied 6-Al3OMe-2H-CTZ for some BL-imaging (see Chapter 5.3.8).



**Figure 5-9** (A) Total BLI with RLuc8.6SG for 30 min in living cells. Inset *a* indicates the FL imaging of COS-7 cells incubated with luciferins (B) Cell membrane permeability test of luciferins. The cell membrane permeability was calculated by dividing the BL signals of CTZs in mammalian cells by the BL signal obtained from cell lysate solution. The cell membrane permeability values are normalized to native-CTZ and RLuc8.6SG was used as luciferase, (C) BL kinetic profile of 6-Al3OMe-2H-CTZ, 6-Al3OH-CTZ and DeepBlueC<sup>TM</sup> in combination with RLuc8.6SG expressing COS-7 cells.

**Table 5-6** BL characteristics in living COS-7 tumor cells expressing RLuc8.6SG

	Total BLI [p/s]	BL-half life time (10 $\mu$ M) [min]
<b>6-Al3OH-CTZ</b>	$2.5 \times 10^5$	11
<b>6-Al3OMe-2-CTZ</b>	$5.2 \times 10^5$	18.5
<b>DeepBlueC™</b>	$9.7 \times 10^3$	7

**Figure 5-10** Bioluminescence emission decay of acetoxymethyl-6-Al3OMe-2H-CTZ (Caged Luciferin) and 6-Al3OMe-2H-CTZ.

Considering the application of CTZ for BL imaging, the required BL-half life time depends on the measuring objects (e.g. protein-protein interactions rate varies among species). For this purpose, I also confirmed that the BL-half decay of 6-Al3OMe-2H-CTZ can be prolonged by introducing an acetoxymethyl group into the reaction site of the imidazopyrazinone core (C-3 carbonyl moiety). The deprotection of the acetoxymethyl group is gradually occurring by cellular enzymes such as esterases, which allow the originally caged luciferin to react with luciferase inside cells.

### 5.3.8. Novel CTZ derivatives for highly sensitive bioluminescence imaging

#### 5.3.8.1. Single cell imaging

As one of the most useful BL applications, single cell imaging by 6-Al3OMe-2H-CTZ-RLuc8.6SG pair was firstly undertaken in HeLa cells. The 6-Al3OMe-2H-CTZ-RLuc8.6SG pair allows single cell imaging with high resolution similar to fluorescence imaging (Figure 5-11). By introducing RLuc8.6SG into organelles (e.g. cytosol, plasma membrane and nucleus) using the respective localization tag, I successfully brighten cell organelles. In addition, these results imply that 6-Al3OMe-2H-CTZ can diffuse throughout the cell.

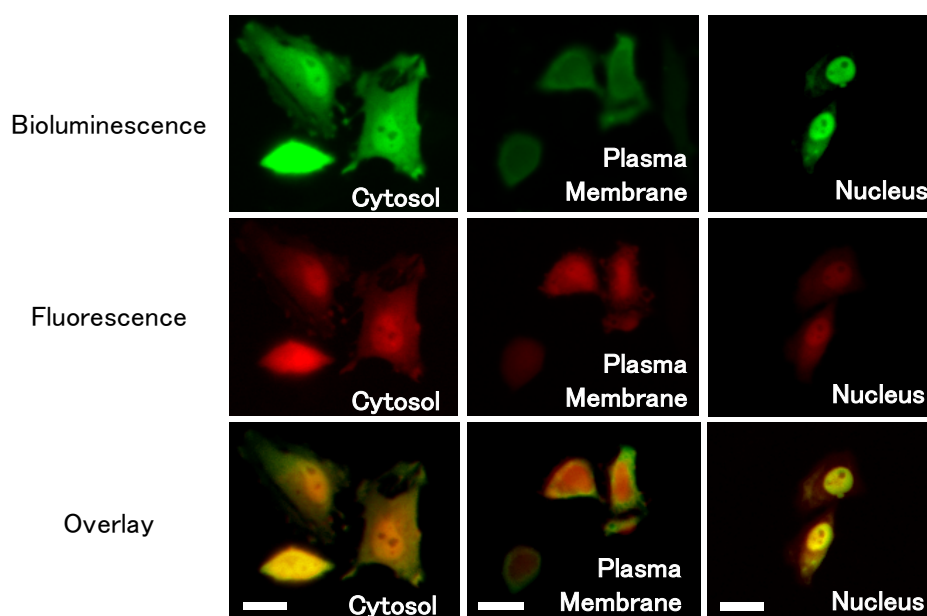


**Figure 5-11** BL (upper) and FL (middle) imaging of HeLa cells expressing RLuc8.6SG introduced to cytoplasm, plasma membrane and nucleus. The exposure time for BL and FL imaging were 2 s and 1 s, respectively. The reference FL signal was captured by exciting Mcherry with light 565 nm. Scale bars, 25  $\mu\text{m}$ .

#### 5.3.8.2. *in vivo* imaging of cancer cells

Furthermore, the usability of 6-Al3OMe-2H-CTZ was evaluated with a red fluorescent protein (iRFP) fused BRET luciferase. Fabrication of a BRET protein is an efficient strategy for the extension of bioluminescence emission maxima. However, the emission maxima of existing marine luciferase-based BRET proteins is limited

to the range from 460 nm to 600 nm. Further red-shifting the emission of fluorescent proteins (FPs) fused marine luciferases is challenging, because the spectral overlap between the absorption spectrum of FPs and the emission spectrum of marine luciferases (more or less 500 nm emission maximum) is considerable to design BRET proteins. Then, I focused on a series of near-infrared fluorescent proteins (iRFPs),<sup>10</sup> which are commonly used in *in vivo* studies, because their maximum emission is over 700 nm, whereas their second absorption peak is located around 380 nm attributed to a Soret band of the biliverdin (BV) chromophore (Figure 5-12(A) inset *a*). Therefore, it was assumed that the Soret band enables iRFPs to be a sufficient BRET acceptor of the blue-shifted BL system 6-AI3OMe-2H-CTZ-iRFPRLuc8.6SG pair, due to the large spectral overlap (Figure 5-12(A)).

In turn, I measured the *in vitro* BRET spectrum by using COS-7 cells expressing iRFP-RLuc8.6SG after treatment with BV. As expected, iRFP-RLuc8.6SG displayed a far red-shift of the emission and the spectral shifting between the emission maximum of iRFP and the 6-AI3OMe-2H-CTZ pair is down to 300 nm. Therefore, the physiological tissue penetration of marine luciferase bioluminescence is expected to be improved by the iRFP-RLuc8.6SG-6-AI3OMe-2H-CTZ pair. For comparison between 6-AI3OMe-2H-CTZ and native-CTZ, the same amounts of COS-7 cancer cells ( $1.83 \times 10^6$  cells/mL) expressing iRFP-RLuc8.6SG fusion protein previously treated with BV chromophore and the respective CTZs (6-AI3OMe-2H-CTZ and native-CTZ) were simultaneously injected into the subcutaneous layer on the back of a nude mouse. The comparison indicated that the implanted COS-7 cells including the 6-AI3OMe-2H-CTZ-iRFPRLuc8.6SG pair showed much brighter bioluminescence emission than native-CTZ.

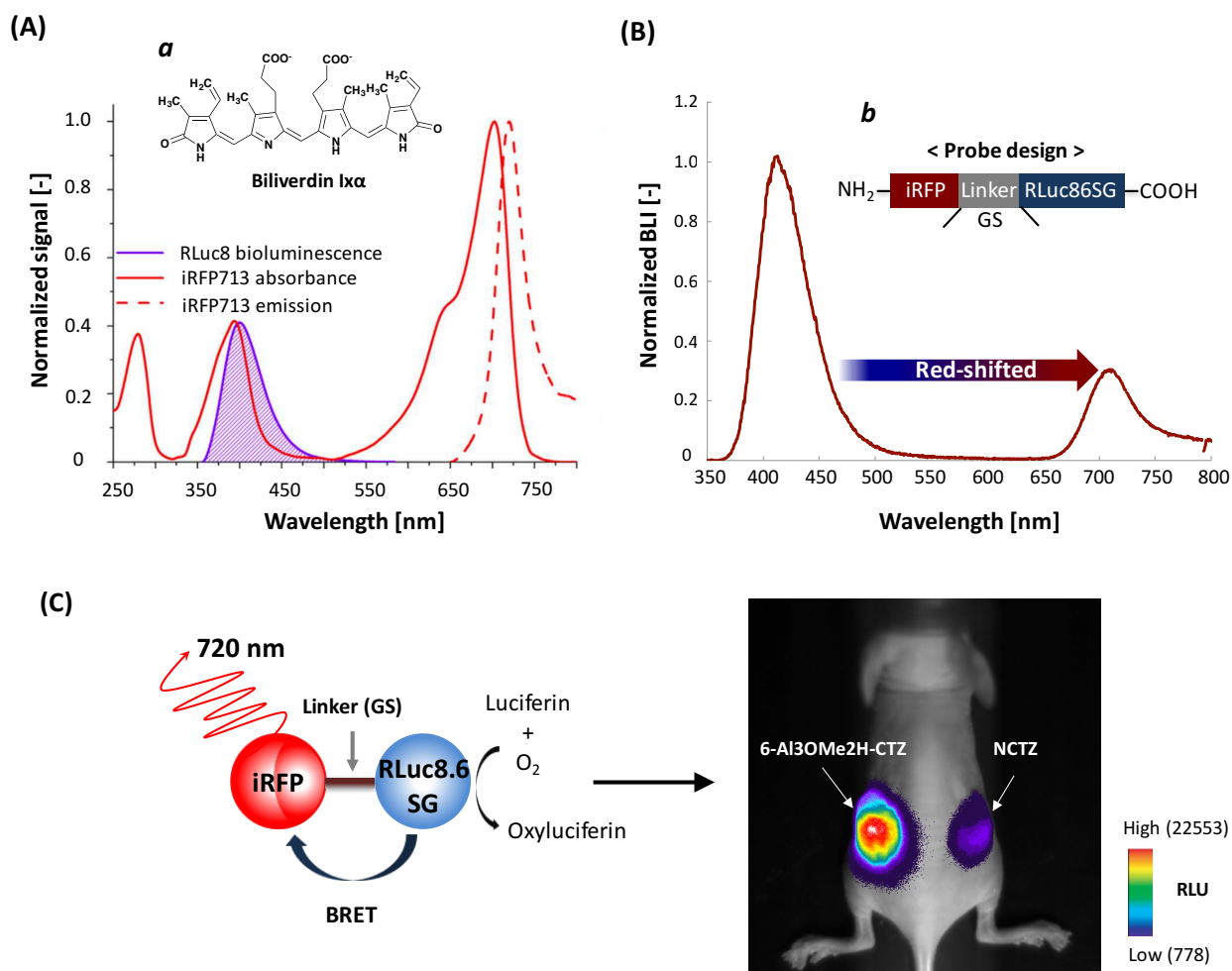


**Figure 5-12** (A) Overlap of normalized absorption spectrum driven from Biliverdin IX $\alpha$  chromophore of iRFP (Inset a) and normalized emission spectrum of RLuc8 with blue-shifted CTZ derivative<sup>44</sup> (B) Bioluminescence spectrum of iRFP-RLuc8.6SG fusion protein with 6-Al3OMe-2H-CTZ in cos-7 cells. Inset b illustrates the schematic of iRFP-RLuc8.6SG. The fusion protein with a linker consisting of two amino acid residues (G, S) displays the highest BRET efficiency. (C) The bioluminescence image was obtained using nude mice subcutaneously (sc) injected with the same amounts of COS-7 cells ( $1.83 \times 10^6$  cells/mL) expressing iRFP-RLuc8.6SG and CTZs {6-Al3OMe-2H-CTZ (left dorsal) and native-CTZ (right dorsal)}. The luminescence image was taken at 1 s exposure time.

**Note:** In general, the BRET efficiency is greatly influenced by energy transfer rate constant ( $k_T(r)$ ), which can be calculated by following equation<sup>7</sup>.

$$k_T(r) = \frac{q_D \kappa^2 9000 (\ln 10)}{\tau_D r^6 128 \pi^5 N n^4} J(\lambda)$$

where the  $\varrho_D$  value is the luminescence quantum yield of the BRET donor,  $n$  is the refractive index of the medium,  $N$  is the Avogadro number,  $r$  is the distance between BRET donor and acceptor,  $\tau_D$  is the life-time of the excited BRET donor,  $J(\lambda)$  is the overlap integral representing the degree of overlap of the donor emission spectrum with the acceptor absorption spectrum, and  $\kappa^2$  is the orientation factor. The  $J(\lambda)$ ,  $\varrho_D$  and  $\kappa^2$  values are crucial factors when it comes to select a luminescent protein for BRET. According to the relative QY values from Chapter 5.3.4 Table 5-3, 6-*Al3OMe-2H-CTZ* displays an approximately 10-fold larger luminescence quantum yield than reported blue-shifted CTZ derivatives, DeepBlueC<sup>TM</sup>. As for the  $\kappa^2$  value, we found the appropriate linker (two amino acid residues, G and S) by evaluating the 713 nm/413 nm ratio, which expresses BRET efficiency. Therefore, among all parameters indicated in the above equation, the optical property of the BRET acceptor most strongly influences the  $J(\lambda)$  value.

$$J(\lambda) = \frac{\int_0^{\infty} F_D(\lambda) \varepsilon_A(\lambda) \lambda^4 d\lambda}{\int_0^{\infty} F_D(\lambda) d\lambda}$$

Where  $F_D(\lambda)$  is the donor emission at the emission wavelength ( $\lambda$ ), and  $\varepsilon_A$  is the acceptor's molar absorption coefficient expressed in  $M^{-1}cm^{-1}$ . From these equations, the relatively low BRET efficiency compared to existing BRET proteins is explained by the relatively low molar absorption coefficient of the acceptor. But the BRET spectra illustrated in Figure 5-12(B) were taken in living cells. Therefore, the expression and folding yield of BRET proteins are important elements to consider.

## 5.4. Conclusions

In summary, I successfully developed novel CTZ derivatives, wherein the (p-hydroxy)-phenyl group in the C-6 position was alkylated. The effect of flexibility and limitation of the C-6 substituent on enzymatic recognition by *Renilla* luciferase (RLuc) and its mutants was used to explore bright-blue CTZ derivatives and the motivation for elucidation of the enzymatic recognition of luciferin analogues. As a result, the CTZ

derivatives with 3-hydroxypropoxy substitution at the C-6 position of native CTZ (6- $\text{Al}3\text{OH-CTZ}$ ) showed the brightest BL emission as blue-shifted derivatives in cell lysate. The results of docking simulation and bioluminescence measurement in solution suggested that the size or shape of the C-6 substituent strongly affects the turn-over number and luminescence quantum yield of marine luciferase systems. However, in order to find out the binding interaction between CTZ and luciferase, the crystal structure of luciferase including its luciferin instead of oxyluciferin is still required, which convinces us to superior luciferin analogues for marine luciferases. However, as a result, with 50-fold stronger emission at comparable wavelength in mammalian living cells, one of the C-6 alkylated CTZ derivatives, 6- $\text{Al}3\text{OMe-2H-CTZ}$  can be a useful bright blue-shifted alternative to commercially available DeepBlueC<sup>TM</sup>, which enables single cell imaging with high-resolution and *in vivo* imaging of mice in combination with the iRFP-RLuc8.6SG fusion protein.

## References

- (1) Close, D. M., Xu, T., Sayler, G. S. and Ripp, S., *Sensors.*, **2011**, *11*, 180-206.
- (2) Thorne, N., Inglese, J. and Auld, D. S., *Chemistry and Biology.*, **2010**, *17*, 646-657.
- (3) Prescher, J. A. and Contag, C. H., *Curr. Opin in Chem. Bio.*, **2010**, *14*, 80-89.
- (4) Kim, S. B., Yoshimura, H., and Tao, H., *Anal. Chem.*, **2013**, *85*, 590-609.
- (5) Bade, C. E., *Bioluminescent Imaging*, Springer Science Business Medea, New York, **2016**.
- (6) Hoshino, H., Nakajima, Y. and Ohmiya, Y., *Nature Method.*, **2007**, *4*, 637-639.
- (7) Saito, K., Chang, Y. F., Horikawa, K., Hatsugai, N., Higuchi, Y., Hashida, M., Yoshida, Y., Matsuda, T., Arai, Y. and Nagai, T., *Nat. Commun.*, **2012**, *3*, 1-9.
- (8) Suzuki, K., Kimura, T., Shinoda, H., Bai, G., Daniels, M. J., Arai, Y., Nakano, M. and Nagai, T., *Nat. Commun.*, **2016**, *7*, 1-10.

- (9) Takai, A., Nakano, M., Saito, K., Haruko, R., Watanabe, T. M., Ohyanagi, T., Jin, T., Okada, Y. and Nagai, T., *PNAS*, **2015**, *112*, 4352-4356.
- (10) Yu, D., Gustafson, W. C., Han, C., Lafaye, C., Noirclerc-Savoie, M., Ge, W. P., Thayer, D. A., Huang, H., Kornberg, T. B., Royant, A., Jan, L. Y., Jan, Y. N., Weiss, W. A. and Shu, X., *Nat. Commun.*, **2014**, *5*, 3626.
- (11) Kojima, R., Takakura, H., Ozawa, T., Tada, Y., Nagano, T. and Urano, Y., *Angew. Chem., Int. Ed.*, **2013**, *52*, 1175–1179.
- (12) Morris, G. M. et al., *J. Comput. Chem.*, **2009**, *30*, 2785–2791.
- (13) Loening, A. M., Fenn, T. D. and Gambhir, S. S., *J. Mol. Biol.*, **2007**, *374*, 1017–1028.
- (14) Hanwell, M. D., *J. Cheminf.*, **2012**, *4*, 1.
- (15) Aldeghi, M., Heifetz, A., Bodkin, M. J., Knapp, S. and Biggin, P. C., *Chem. Sci.*, **2016**, *7*, 207–218.
- (16) Abraham, M. J. et al., *Gromacs, SoftwareX*, **2015**, *1*, 19–25.
- (17) Jorgensen, W. L., Chandrasekhar, J., Madura, J. D., Impey, R. W. and Klein, M. L., *J. Chem. Phys.*, **1983**, *79*, 926.
- (18) Fiser, A., Sali, A., and Modeller, *Methods Enzymol.*, **2003**, *374*, 461–491.
- (19) Wang, J., Wolf, R. M., Caldwell, J. W., Kollman, P. A. and Case, D. A., *J. Comput. Chem.*, **2004**, *25*, 1157–1174.
- (20) Jakalian, A., Jack, D. B. and Bayly, C. I., *J. Comput. Chem.*, **2002**, *23*, 1623–1641.
- (21) Case, D. A., et al., **2014**, Amber 14.
- (22) Larsen, K. L. et al., *Proteins*, **2010**, *78*, 1950–1958.
- (23) Beutler, T. C., Mark, A. E., Schaik, R. C. V., Gerber, P. R., Gunsteren and W. F. V., *Chem. Phys. Lett.*, **1994**, *222*, 529–539.
- (24) Boresch, S., Tettinger, F., Leitgeb, M. and Karplus, M., *J. Phys. Chem. B*, **2003**, *107*, 9535–9551.
- (25) Gunsteren, W. F. V. and Berendsen, H. J. C., *Mol. Sim.*, **1988**, *1*, 173–185.

- (26) Goga, N., Rzepiela, A. J., Vries, A. H. D., Marrink, S. J. and Berendsen, H. J. C., *J. Chem. Theory Comput.*, **2012**, *8*, 3637–3649.
- (27) Berendsen, H. J. C., Postma, J. P. M., Gunsteren, W. F. V., DiNola, A. and Haak, J. R., *J. Chem. Phys.*, **1984**, *81*, 3684.
- (28) Parrinello, M. and Rahman, A., *J. Appl. Phys.*, **1981**, *52*, 7182.
- (29) Chodera, J. D. and Shirts, M. R., *J. Chem. Phys.*, **2011**, *135*, 194110.
- (30) Darden, T., York, D., Pedersen, L. and Ewald, P. M., *J. Chem. Phys.*, **1993**, *98*, 10089.
- (31) Hess, B., Bekker, H., Berendsen, H. J. C. and Fraaije, J. G. E. M., *J. Comput. Chem.*, **1997**, *18*, 1463.
- (32) Hess, B. and Lincs, P., *J. Chem. Theory Comput.*, **2008**, *4*, 116.
- (33) Shirts, M. R., Mobley, D. L., Chodera, J. D. and Pande, V. S., *J. Phys. Chem. B*, **2007**, *111*, 13052–13063.
- (34) Shirts, M. R. and Chodera, J. D., *J. Chem. Phys.*, **2008**, *129*, 124105.
- (35) Loening, A. M., Fenn, T. D., Wu, A. M. and Gambhir, S. S., *Protein Eng., Des. Sel.*, **2006**, *19*, 391–400.
- (36) Loening, A. M., Wu, A. M. and Gambhir, S. S., *Nat. Methods*, **2007**, *4*, 641.
- (37) Nishihara, R., Suzuki, H., Hoshino, E., Suganuma, S., Sato, M., Saitoh, T., Nishiyama, S., Iwasawa, N., Citterio, D., and Suzuki, K., *Chem. Commun.*, **2014**, *51*, 391-394.
- (38) Nishihara, R., Abe, M., Nishiyama, S., Citterio, D., Suzuki, K., and Kim, S. B., *Scientific Reports*, **2017**, *7*, 908.
- (39) Saito, R., Hirano, T., Maki, S., Niwa, H. and Ohashi, M., *Bull. Chem. Soc. Jpn.*, **2011**, *84*, 90–99.
- (40) Arnim, A. G. V. and Woo, J., *Plant Methods*, **2008**, *4*, 23.
- (41) Giuliani, G., Molinari, P., Ferretti, G., Cappelli, A., Anzini, M., Vomero, S. and Costa, T., *Tetrahedron Letters*, **2012**, *53*, 5114-5118.
- (42) Zhao, H., Doyle, T. C., Wong, R. J., Cao, Y., Stevenson, D. K., Piwnica-Worms, D. and Contag, C. H., *Molecular Imaging*, *3*, 43-54.

(43) Pichler, A., Prior, J. L. and Piwnica, W. D., *Proc Natl Acad Sci USA.*, **2004**, *101*, 1702-1707.

(44) Rumyantsev, K. A., Turoverov, K. K. and Verkhusha, V. V., *Sci.Rep.*, **2016**, *6*, 36588.

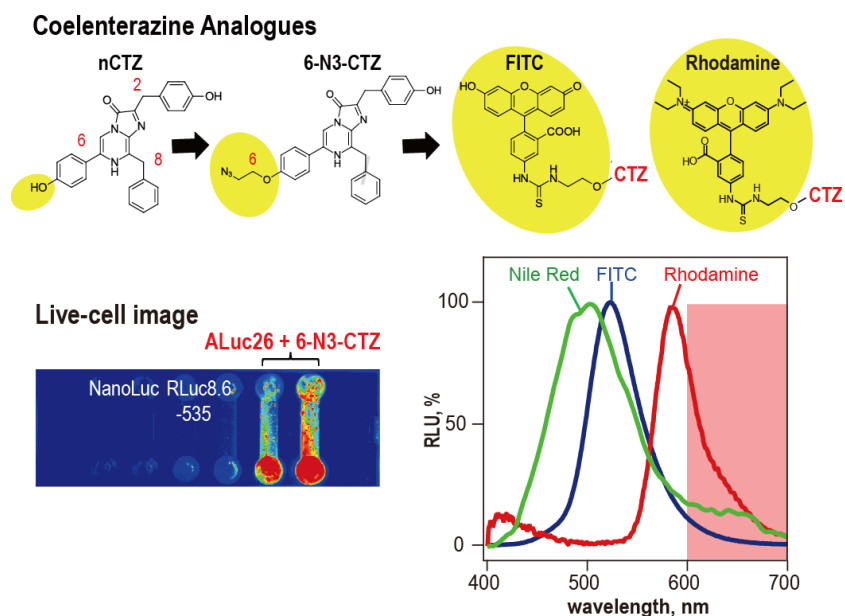


## **Chapter6**

# **Fabrication of Red-shifted Coelenterazine Analogues for Bioluminescent Applications**

### **Summary**

Native coelenterazine (nCTZ) is the common substrate to most marine luciferases and photoproteins. In this study, ten novel azide- and dye-conjugated CTZ analogues were synthesized by conjugating a series of organic dyes or an azide group to the C-2 or C-6 position of CTZ backbone to obtain (i) improved optical intensity and sustainability, (ii) steric hindrance-driven substrate selectivity, and (iii) chemiluminescence/ bioluminescence resonance energy transfer (C/ BRET). The advantages of the newly synthesized CTZ analogues were investigated with various marine luciferases. The results demonstrate that azide group-conjugated CTZ analogues selectively activate artificial luciferases (ALucs) over the other marine luciferases: for instance, 6-N3-CTZ specifically illuminates ALuc26, which does not luminesce with furimazine, convincing two luminescent systems with fully independent and non-interfering reporters each other. Further, some of the dye-conjugated CTZ analogues exerted characteristic optical peaks in the CRET and BRET spectra, a large portion of which is found to be with red or near infrared region longer than 600 nm, which is highly tissue-permeable. Although many attempts to modify CTZ have been tried, this study is the first example that dye-conjugation to CTZ is systematically investigated. This is unique bioluminescence system appends a new toolbox to bioassays and molecular imaging.



## 6.1. Introduction

Fluorescent proteins (FPs) and luciferases are widely used optical readouts for monitoring various biological processes in living subjects. These optical readouts are utilized independently or cooperatively for illuminating many intracellular molecular events, for example, bioluminescence resonance energy transfer, (BRET) between luciferase, and determination of protein–protein interactions (PPIs) in mammalian cells<sup>1-4</sup>.

Compared to FP, luciferase can be considered a better optical readout in bioassays by virtue of its sensitivity and versatility, but it commonly has the drawbacks of relatively poor optical intensity and limited colorimetric variety. These drawbacks have been partly addressed by improved and engineered variants of luciferases<sup>5, 6</sup>. *Renilla reniformis* luciferase (RLuc), derived from sea pansy, has been genetically modified to improve its optical stability and red-shifted property<sup>7, 8</sup>. A series of artificial luciferases (ALucs) were also established by extracting frequently occurring amino acid sequences from the public database of copepod luciferases<sup>9, 10</sup>. ALucs, emitting greatly bright and glowing bioluminescence, have also been newly established<sup>11</sup>.

Simultaneously, great efforts have been made to synthesize the specific substrate that potentially provides better optical performance<sup>12, 13</sup> and colorimetric variety of luciferases<sup>14, 15</sup>, since native coelenterazine (CTZ) was isolated from coelenterate *Aequorea victoria*<sup>16</sup>. many CTZ analogues have been organically synthesized

and conjugated with other heterogeneous components like cages<sup>17</sup> or alkyne/triazole groups<sup>18</sup>, or a fluorescent dye<sup>19</sup>.

I previously demonstrated that optical performance of ALucs is greatly dominated by the substrates<sup>11, 13</sup>; for example, an existing coelenterazine (CTZ) analogue, CTZi, enabled dramatically biased bioluminescence to ALucs, compared to RLuc8.6-535. Independently, I investigated the advantages of C-6 extended modification of CTZ, in terms of bioluminescence, allowing a large spectral blue shift of the bioluminescence spectra, but causing little influence on the enzymatic recognition of RLucs<sup>12</sup>. Further, the C-6 and C-2 positions of CTZ were found to be the specificity core for marine luciferases<sup>13</sup>. The above studies strongly suggest that the luciferase–luciferin reactions adhere basically to the traditional host–guest docking models. The reaction may be controllable by modifying the functional groups in the luciferin.

These achievements encouraged me to create an efficient luciferin–luciferase assay system with enhanced optical intensities and/or resonance energy transfer (RET) of bioluminescence by pairing dye- /azide-conjugated CTZ analogues and luciferases including newly established ALucs. To our knowledge, azide- and organic dye-conjugated luciferins have not been systemically investigated to date.

I first reviewed an earlier crystallographic study on a RLuc8—coelenteramide binding model, where the C-6 hydroxyphenyl group of coelenteramide makes a rigid catalytic triad, in conjunction with Asp120 of RLuc8<sup>20</sup>, which means no space for bulk in the binding. By increasing the steric bulk at C-6 position, I predicted that steric hindrance would inhibit the binding to RLuc, and that, due to the low sequence identity between RLuc and ALucs, ca. 17%, ALucs might be able to accommodate a bulkier moiety if they contain variant residues in their active site pockets. In contrast, the C-2 hydroxyphenyl group of the bound coelenteramide protrudes from the active site pocket and forms hydrophobic interactions with Leu165, and Phe180.

Based on the knowledge, I synthesized a series of CTZ analogues, carrying various fluorescent dyes or azide group (N<sub>3</sub>). The optical performance was examined with existing marine luciferases and newly fabricated ALucs.

The azide group-conjugated CTZ analogues selectively activate artificial luciferases (ALucs) over the other marine luciferases, which may be driven by their unique host guest–chemistry. Additionally, some of the dye-conjugated CTZ analogues exerted characteristic CRET and BRET spectra with red region RET emission, which is highly tissue-permeable.

Although many attempts to modify CTZ have been tried, this study is the first example that dye-conjugation to CTZ is systematically investigated. The present bioluminescence-based imaging system provides a useful toolbox to current bioassay and molecular imaging studies.

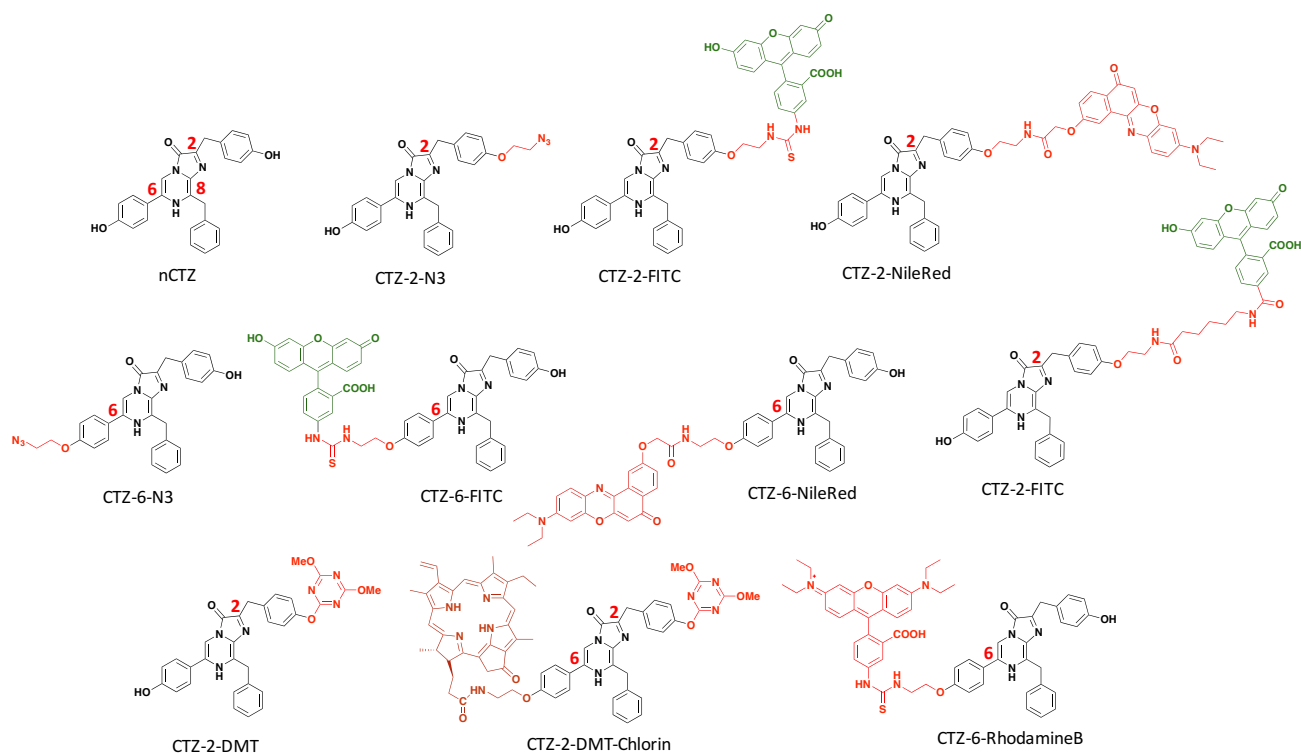
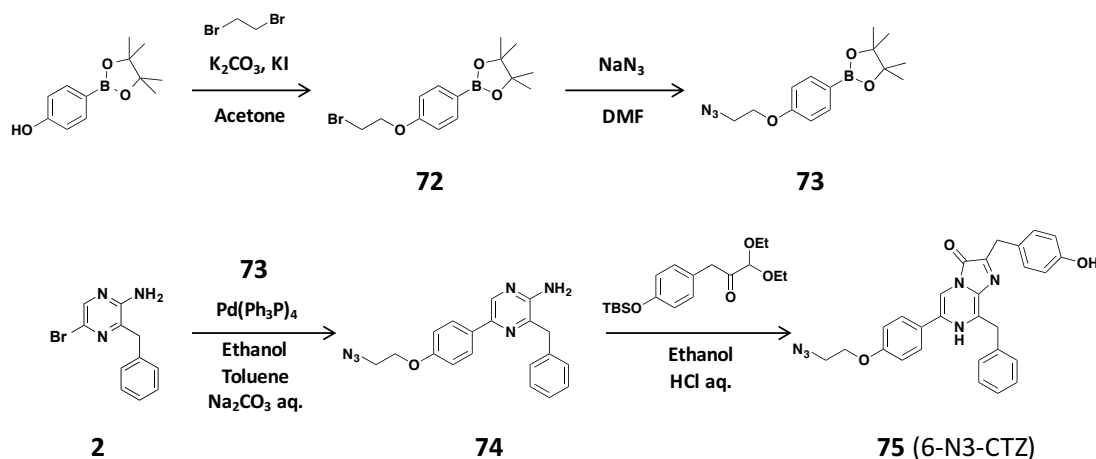


**Figure 6-1** Chemical structures of 10 novel coelenterazine analogues, synthesized for marine luciferases in the present study. The CTZ analogues were dye-bridged at C-2 or C-6 positions. Abbreviations: nCTZ, native coelenterazine; N3, an azide group; FITC, fluorescein isothiocyanate; SFX, fluorescein succinimidyl ester; DMT, 4,6-dimethoxy-1,3,5-triazin-2-yl.

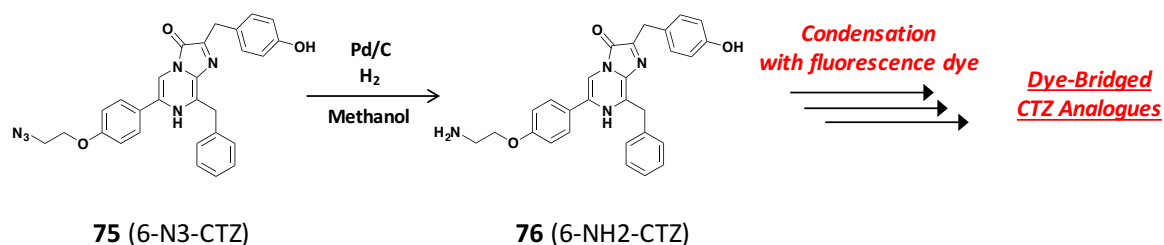
## 6.2. Experimental section

### 6.2.1. Synthesis of novel CTZ derivatives

The ten novel CTZ derivatives were newly synthesized according to the synthesis routes reported in literatures<sup>21,22</sup>. The major synthetic schemes of selected CTZ analogues are as follows:



Synthetic scheme for 6-N3-CTZ (compound **2**, **72** and **73** are reported<sup>9</sup>)



Synthetic strategy for dye-bridged CTZ analogues

#### 5-(4-(2-Azidoethoxy)phenyl)-3-benzylpyrazin-2-amine (**74**)

3-Benzyl-5-bromopyrazin-2-amine (**2**) (660 mg, 2.50 mmol, 1.0 eq.) and 2-(4-(2-azidoethoxy)phenyl)-4,4,5,5-tetramethyl-1,3,2-dioxaborolane (**73**) (1.0 g, 3.46 mmol, 1.6 eq.) were dissolved in toluene (15 ml) and stirred at room temperature. Ethanol (5 ml) and 1 M sodium carbonate aq. (7 ml) were added into the reaction mixture. After vacuum deaeration, a catalytic amount of tetrakis(triphenylphosphine)palladium(0) was added

into the solution and the mixture was deaerated again and stirred for 20 hours at 100 °C. After cooling to room temperature, the solution was filtered through a Celite pad to remove the palladium catalyst. The solution was extracted with ethyl acetate, and the brown organic phase was washed with water, sat. sodium hydrogen carbonate aq. and brine, dried over sodium sulfate and evaporated. The resulting residue was purified by means of silica gel column chromatography (eluent composition: chloroform/ethyl acetate = 19/1 to 9/1) to afford 5-(4-(2-azidoethoxy)phenyl)-3-benzylpyrazin-2-amine (**74**) as a yellow solid (0.590 g, 68%):

<sup>1</sup>H-NMR (300 MHz, CDCl<sub>3</sub>) δ= 8.33 (s, 1H), 7.89 (d, *J* = 9 Hz, 2H), 7.19-7.38 (m, 5H), 7.01 (d, *J* = 8.7 Hz, 2H), 4.37 (s, 2H), 4.18-4.22 (m, 4H), 3.63 (t, *J* = 4.8 Hz, 2H). <sup>13</sup>C-NMR (125 MHz, CDCl<sub>3</sub>): δ (ppm) = 41.37, 50.29, 67.14, 115.02, 127.16, 127.21, 128.69, 129.10, 130.82, 136.91, 137.04, 140.61, 142.48, 151.49, 158.47. HR-MS: calcd for C<sub>19</sub>H<sub>19</sub>N<sub>6</sub>O<sub>1</sub>: 347.1616 [M+H]<sup>+</sup>, found: *m/z* 347.1620.

**6-(4-(2-Azidoethoxy)phenyl)-8-benzyl-2-(4-hydroxybenzyl)imidazo[1,2-*a*]pyrazin-3(7*H*)-one (75) (6-N3-CTZ)**

5-(4-(2-Azidoethoxy)phenyl)-3-benzylpyrazin-2-amine (**74**) (500 mg, 1.44 mmol, 1.0 eq.) and 3-(4-((tert-butyl)dimethylsilyloxy)phenyl)-1,1-diethoxypropan-2-one (814 mg, 2.31 mmol, 1.6 eq.) were dissolved in ethanol (25 ml) and water (8 ml) and stirred at room temperature. After vacuum deaeration, the solution was cooled to 0 °C and HCl (4 ml) was added under nitrogen flow. Once the solution reached room temperature, it was heated and stirred for 15 hours at 80 °C. The reaction solvent was evaporated and the crude compound was purified by means of silica gel column chromatography (eluent composition: ethyl acetate/methanol = 20/1) to afford 6-(4-(2-azidoethoxy)phenyl)-8-benzyl-2-(4-hydroxybenzyl)imidazo[1,2-*a*]pyrazin-3(7*H*)-one (**75**) (287 mg, 40%) as a yellow solid:

<sup>1</sup>H-NMR (500 MHz, CD<sub>3</sub>OD) δ= 7.55 (s, 1H), 7.41 (d, *J* = 7.5 Hz, 2H), 7.31 (t, *J* = 7.0 Hz, 2H), 7.23 (m, 5H), 7.04 (d, *J* = 9.0 Hz, 2H), 6.74 (d, *J* = 8.5 Hz, 2H), 4.39 (s, 2H), 4.22 (t, *J* = 5.0 Hz, 2H), 4.11 (s, 2H), 3.64 (t, *J*

= 4.5 Hz, 2H).  $^{13}\text{C}$ -NMR (125 MHz,  $\text{CD}_3\text{OD}$ ,  $\text{CDCl}_3$ ):  $\delta$  (ppm) = 33.14, 35.08, 51.05, 68.24, 108.24, 127.63, 127.97, 129.13, 129.25, 129.55, 129.62, 129.74, 130.39, 130.47, 130.62, 137.75, 156.56, 160.59. HR-MS: calcd for  $\text{C}_{28}\text{H}_{25}\text{N}_6\text{O}_3$ : 493.1970  $[\text{M}+\text{H}]^+$ , found:  $m/z$  493.1988.

**6-(4-(2-Aminoethoxy)phenyl)-8-benzyl-2-(4-hydroxybenzyl)imidazo[1,2-a]pyrazin-3(7H)-one (76) (6-NH<sub>2</sub>-CTZ)**

6-N3-CTZ (**75**) (20 mg, 0.04 mmol, 1.0 eq.) was dissolved in methanol (5 ml). After vacuum deaeration, a catalytic amount of 5% Pd/C was added into the solution and the mixture was deaerated again and stirred for 5 hours at 40 °C under H<sub>2</sub> atmosphere. The solution was filtered through a Celite pad to remove the catalyst. The solution was evaporated to afford crude 6-(4-(2-aminoethoxy)phenyl)-8-benzyl-2-(4-hydroxybenzyl)imidazo[1,2-a]pyrazin-3(7H)-one (**76**), which was used directly for the next reaction: HR-MS: calcd for  $\text{C}_{28}\text{H}_{27}\text{N}_4\text{O}_3$ : 467.2083  $[\text{M}+\text{H}]^+$ , found:  $m/z$  467.2095.

**5-(3-(2-(4-(8-Benzyl-2-(4-hydroxybenzyl)-3-oxo-3,7-dihydroimidazo[1,2-a]pyrazin-6-yl)phenoxy)ethyl)thioureido)-2-(6-hydroxy-3-oxo-3H-xanthen-9-yl)benzoic acid (77) (6-FITC-CTZ)**

Fluorescein isothiocyanate (7.8 mg, 0.02 mmol, 1.0 eq.) and 6-NH<sub>2</sub>-CTZ (**76**) (20 mg, 0.04 mmol, 2.0 eq.) were dissolved in ethanol (5 ml) and tetrahydrofuran (3 ml) and stirred for 3 hours at 40 °C. The reaction solvent was evaporated and the crude compound was purified by means of preparative HPLC (eluent composition: acetonitrile/water = 2/1) to afford 5-(3-(2-(4-(8-benzyl-2-(4-hydroxybenzyl)-3-oxo-3,7-dihydroimidazo[1,2-a]pyrazin-6-yl)phenoxy)ethyl)thioureido)-2-(6-hydroxy-3-oxo-3H-xanthen-9-yl)benzoic acid (**77**) (2.2 mg, 13%) as a yellow solid:

$^1\text{H}$ -NMR (500 MHz,  $\text{CD}_3\text{OD}$ )  $\delta$  = 8.11 (d,  $J$  = 2.0 Hz, 1H), 7.71 (d,  $J$  = 7.0 Hz, 1H), 7.59 (s, 2H), 7.38 (d,  $J$  = 7.5 Hz, 2H), 7.28 (t,  $J$  = 7.0 Hz, 2H), 7.22 (t,  $J$  = 7.5 Hz, 1H), 7.14 (m, 5H), 6.68 (m, 6H), 6.54 (q,  $J$  = 8.5 Hz,

2H), 4.40 (s, 2H), 4.30 (t,  $J = 5.5$  Hz, 2H), 4.60 (m, 4H). HR-MS: calcd for  $C_{49}H_{38}N_5O_8S$ : 856.2441  $[M+H]^+$ , found:  $m/z$  856.2430.

**N-(2-(4-(8-benzyl-2-(4-hydroxybenzyl)-3-oxo-3,7-dihydroimidazo[1,2-a]pyrazin-6-yl)phenoxy)ethyl)-2-((9-(diethylamino)-5-oxo-5H-benzo[a]phenoxazin-2-yl)oxy)acetamide (78) (6-Nile-Red-CTZ)**

2,5-Dioxopyrrolidin-1-yl-2-((9-(diethylamino)-5-oxo-5H-benzo[a]phenoxazin-2-yl)oxy)acetate (24.0 mg, 0.04 mmol, 1.0 eq.) and 6-NH<sub>2</sub>-CTZ (**76**) (45.7 mg, 0.09 mmol, 2.0 eq.) were dissolved in methanol (0.5 ml) and tetrahydrofuran (3 ml) and stirred for 30 minutes at 60 °C. The reaction solvent was evaporated and the crude compound was purified by means of silica column chromatography (eluent composition: chloroform/methanol = 19/1) to afford N-(2-(4-(8-benzyl-2-(4-hydroxybenzyl)-3-oxo-3,7-dihydroimidazo[1,2-a]pyrazin-6-yl)phenoxy)ethyl)-2-((9-(diethylamino)-5-oxo-5H-benzo[a]phenoxazin-2-yl)oxy)acetamide (**78**) (17.8 mg, 43%) as a purple solid:

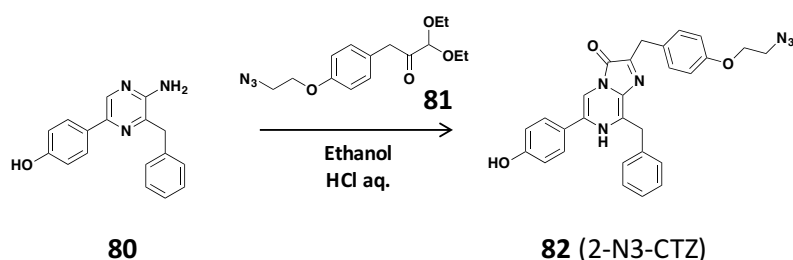
<sup>1</sup>H-NMR (300 MHz, DMSO-*d*<sub>6</sub>)  $\delta$ =8.08 (d  $J$ =8.8 Hz, 1H), 7.95 (d,  $J$ =2.4 Hz, 1H), 7.46 (d,  $J$ =7.2 Hz, 2H), 7.39 (d,  $J$ =9.2 Hz, 2H), 7.33 (t,  $J$ =6.8 Hz, 3H), 7.24 (m, 6H), 6.74 (d,  $J$ =8.8 Hz, 2H), 6.66 (dd,  $J$ =2.4 Hz, 8.8 Hz, 1H), 6.60 (d,  $J$ =8.8 Hz, 2H), 6.17 (s, 1H), 6.12 (s, 1H), 4.72 (s, 2H), 4.38 (s, 2H), 4.09 (s, 2H), 4.02 (t,  $J$ =6.4 Hz, 1H), 3.65 (t,  $J$ =6.4 Hz, 3H), 3.21 (q,  $J$ =7.2 Hz, 4H), 1.07 (t,  $J$ =7.2 Hz, 6H). HR-MS: calcd for  $C_{50}H_{45}N_6O_7$ : 841.3350  $[M+H]^+$ , found:  $m/z$  841.3351.

**6-Chlorin-2-DMT-CTZ (79)**

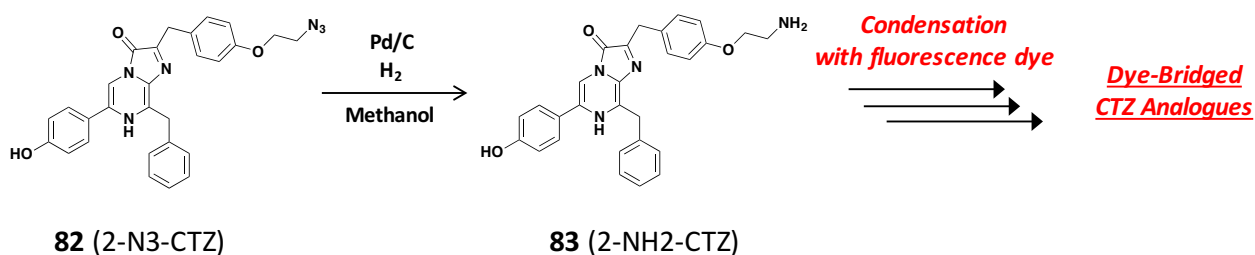
Pyropheophorbide (10.9 mg, 0.02 mol, 1.0 eq.) and 4-(4,6-dimethoxy-1,3,5-triazin-2-yl)-4-methylmorpholinium chloride n-hydrate (11.0 mg, 0.04 mmol, 2.0 eq.) were dissolved in THF (0.5 mL) stirred for 30 minutes at 60 °C. 6-NH<sub>2</sub>-CTZ (**76**) (9.3 mg, 0.02 mmol, 1.0 equiv) dissolved in methanol (1 mL) was added into the reaction mixture and stirred at 60 °C overnight. The reaction solvent was evaporated and the

crude compound was purified by chromatograph on a silicagel plate (eluent composition: ethyl acetate/methanol = 9/1) to afford 6-Chlorin-2-DMT-CTZ (**79**) (10.0 mg, 51%) as a brown solid:

$^1\text{H-NMR}$  (400 MHz,  $\text{CDCl}_3$ )  $\delta$ = 9.39 (s, 1H), 9.35 (s, 1H), 8.53 (s, 1H), 7.97 (dd,  $J$ =11.6 Hz, 18 Hz, 1H), 7.71 (s, 1H), 7.62 (d,  $J$ = 8.8 Hz, 2H), 7.53 (d,  $J$ =7.2 Hz, 2H), 7.22 (m, 5H), 7.00 (d,  $J$ =8.4 Hz, 2H), 6.62 (d,  $J$ =8.4 Hz, 2H), 6.57 (d,  $J$ =8.4 Hz, 2H), 6.26 (d,  $J$ =17.6 Hz, 1H), 6.14 (d,  $J$ =11.6 Hz, 1H), 5.50 (t,  $J$ =5.5 Hz, 1H), 5.22 (d,  $J$ =20 Hz, 1H), 5.06 (d,  $J$ =20 Hz, 1H), 4.54 (s, 2H), 4.88 (q,  $J$ =7.5 Hz, 1H), 4.33 (s, 1H), 4.01 (m, 2H), 3.95 (s, 6H), 3.81 (s, 1H), 3.51 (s, 3H), 3.38 (s, 4H), 3.21 (s, 3H), 2.64 (m, 3H), 2.45 (m, 1H), 2.24 (m, 1H), 1.90 (m, 1H) 1.80 (d,  $J$ =7.2 Hz, 3H), 1.66 (t,  $J$ =8.0 Hz, 6H). HR-MS: calcd for  $\text{C}_{66}\text{H}_{64}\text{N}_{11}\text{O}_7$ : 1122.4990  $[\text{M}+\text{H}]^+$ , found:  $m/z$  1122.4983.



Synthetic scheme for 2-N<sub>3</sub>-CTZ (compound **80** is reported<sup>9</sup>)



Synthetic strategy for dye-bridged CTZ analogues

**2-(4-(2-Azidoethoxy)benzyl)-8-benzyl-6-(4-hydroxyphenyl)imidazo[1,2-*a*]pyrazin-3(7*H*)-one (82) (2-N<sub>3</sub>-CTZ)**

4-(5-amino-6-benzylpyrazin-2-yl)phenol (**80**) (24.3 mg, 0.99 mmol, 1.0 eq.) and 3-(4-(2-azidoethoxy)phenyl)-1,1-diethoxypropan-2-one (**81**) (53.8 mg, 0.18 mmol, 2.0 eq.) were dissolved in ethanol (1.5 ml) and water (0.2 ml) and stirred at room temperature. After vacuum deaeration, the solution was cooled to 0 °C and HCl (0.1 ml) was added under nitrogen flow. Once the solution reached room temperature, it was heated and stirred for 18 hours at 80 °C. The reaction solvent was evaporated and the crude compound was purified by means of preparative HPLC (eluent composition: acetonitrile/water = 1/1) to afford 2-(4-(2-azidoethoxy)phenyl)-8-benzyl-6-(4-hydroxybenzyl)imidazo[1,2-*a*]pyrazin-3(7*H*)-one (**82**) (41 mg, 48%) as a yellow solid:

<sup>1</sup>H-NMR (300 MHz, CDCl<sub>3</sub>) δ= 7.44-7.35 (m, 4H), 7.29-7.19 (m, 5H), 6.87-6.83 (m, 4H), 4.38 (s, 2H), 4.11-4.09 (m, 4H), 3.53 (t, *J* = 4.9 Hz, 2H).

**2-(4-(2-Aminoethoxy)benzyl)-8-benzyl-6-(4-hydroxyphenyl)imidazo[1,2-*a*]pyrazin-3(7*H*)-one (83) (2-NH<sub>2</sub>-CTZ)**

2-N<sub>3</sub>-CTZ (**82**) (106.0 mg, 0.21 mmol, 1.0 eq.) was dissolved in methanol (8 ml). After vacuum deaeration, a catalytic amount of 5% Pd/C was added into the solution and the mixture was deaerated again and stirred for 15 hours at 40 °C under H<sub>2</sub> atmosphere. The solution was filtered through a Celite pad to remove the catalyst. The solution was evaporated to afford crude 2-(4-(2-aminoethoxy)benzyl)-8-benzyl-6-(4-hydroxyphenyl)imidazo[1,2-*a*]pyrazin-3(7*H*)-one (**83**), which was used directly for the next reaction.

**5-(3-(2-(4-(8-Benzyl-6-(4-hydroxyphenyl)-3-oxo-3,7-dihydroimidazo[1,2-a]pyrazin-6-yl)methyl)phenoxy)ethyl)thioureido)-2-(6-hydroxy-3-oxo-3H-xanthen-9-yl)benzoic acid (84) (2-FITC-CTZ)**

Fluorescein isothiocyanate (9.8 mg, 0.02 mmol, 0.8 eq.) and 2-NH<sub>2</sub>-CTZ (**83**) (14.2 mg, 0.03 mmol, 1.0 eq.) were dissolved in tetrahydrofuran (5 ml) and stirred for 2 hours at room temperature. The reaction solvent was evaporated and the crude compound was purified by means of preparative HPLC (eluent composition: acetonitrile/water = 1/1) to afford 5-(3-(2-(4-(8-benzyl-6-(4-hydroxyphenyl)-3-oxo-3,7-dihydroimidazo[1,2-a]pyrazin-6-yl)methyl)phenoxy)ethyl)thioureido)-2-(6-hydroxy-3-oxo-3H-xanthen-9-yl)benzoic acid (**84**) (4.3 mg, 17%) as a yellow solid:

<sup>1</sup>H-NMR (500 MHz, CD<sub>3</sub>OD) δ= 8.13 (d, *J* = 1.8 Hz, 1H), 7.72 (dd, *J* = 8.3 Hz, 2.0 Hz, 1H), 7.44-7.36 (m, 4H), 7.29-7.20 (m, 5H), 7.12 (d, *J* = 8.3 Hz, 1H), 6.92-6.87 (m, 4H), 6.66-6.64 (m, 4H), 6.52 (dd, *J* = 8.7 Hz, 2.3 Hz, 2H), 4.38 (s, 2H), 4.20 (t, *J* = 5.2 Hz, 2H), 4.10 (s, 2H), 4.00 (t, *J* = 4.9 Hz, 2H).

**5-(((6-((2-(4-((8-Benzyl-6-(4-hydroxyphenyl)-3-oxo-3,7-dihydroimidazo[1,2-a]pyrazin-2-yl)methyl)phenoxy)ethyl)amino)-6-oxohexyl)carbonyl)-2-(6-hydroxy-3-oxo-3H-xanthen-9-yl)benzoic acid (85) (2-SFX-CTZ)**

5-Fluorescein succinimidyl ester (5.0 mg, 0.008 mmol, 1.0 eq.) and 2-NH<sub>2</sub>-CTZ (**83**) (30.1 mg, 0.06 mmol, 7.5 eq.) were dissolved in methanol (2 ml) and tetrahydrofuran (2 ml) and stirred for 2 hours at 40 °C. The reaction solvent was evaporated and the crude compound was purified by means of preparative HPLC (eluent composition: acetonitrile/water = 1/1) to afford 5-(((6-((2-(4-((8-Benzyl-6-(4-hydroxyphenyl)-3-oxo-3,7-dihydroimidazo[1,2-a]pyrazin-2-yl)methyl)phenoxy)ethyl)amino)-6-oxohexyl)carbonyl)-2-(6-hydroxy-3-oxo-3H-xanthen-9-yl)benzoic acid (**85**) (1.7 mg, 21%) as an orange-brown solid:

<sup>1</sup>H-NMR (500 MHz, CD<sub>3</sub>OD) δ= 8.40 (d, *J* = 1.2 Hz, 1H), 8.25 (bs, 2H), 8.15 (dd, *J* = 8.0 Hz, 1.7 Hz, 1H),

7.44-7.35 (m, 4H), 7.29-7.21 (m, 6H), 6.87 (d,  $J = 8.6$  Hz, 2H), 6.82 (d,  $J = 8.6$  Hz, 2H), 6.66 (d,  $J = 2.3$  Hz, 2H), 6.54-6.48 (m, 4H), 4.37 (s, 2H), 4.07 (s, 2H), 3.99 (t,  $J = 5.2$  Hz, 2H), 3.53 (t,  $J = 5.2$  Hz, 2H), 3.36 (t,  $J = 6.9$  Hz, 2H), 2.23 (t,  $J = 7.2$  Hz, 2H), 1.64 (sep,  $J = 7.5$  Hz, 2H), 1.39 (m, 2H).

***N*-(2-(4-((8-benzyl-6-(4-hydroxyphenyl)-3-oxo-3,7-dihydroimidazo[1,2-*a*]pyrazin-2-yl)methyl)phenoxy)ethyl)-2-((9-(diethylamino)-5-oxo-5*H*-benzo[*a*]phenoxazin-2-yl)oxy)acetamide (86)**  
**(2-Nile-Red-CTZ)**

2,5-Dioxopyrrolidin-1-yl-2-((9-(diethylamino)-5-oxo-5*H*-benzo[*a*]phenoxazin-2-yl)oxy)acetate (30.8 mg, 0.06 mmol, 1.8 eq.) and 2-NH<sub>2</sub>-CTZ (**83**) (16.1 mg, 0.03 mmol, 1.0 eq.) were dissolved in methanol (3.0 ml) and stirred for 30 minutes at 40 °C. The reaction solvent was evaporated and the crude compound was purified by means of silica column chromatography (eluent composition: chloroform/methanol = 19/1 to 9/1) to afford *N*-(2-(4-((8-benzyl-6-(4-hydroxyphenyl)-3-oxo-3,7-dihydroimidazo[1,2-*a*]pyrazin-2-yl)methyl)phenoxy)ethyl)-2-((9-(diethylamino)-5-oxo-5*H*-benzo[*a*]phenoxazin-2-yl)oxy)acetamide (**86**) (4.7 mg, 16%) as a purple solid:

<sup>1</sup>H-NMR (500 MHz, CD<sub>3</sub>OD, CDCl<sub>3</sub>)  $\delta$ = 8.34 (s, 1H), 8.09 (d,  $J = 8.6$  Hz, 1H), 7.95 (d,  $J = 2.6$  Hz, 1H), 6.81 (d,  $J = 9.2$  Hz, 1H), 7.37-7.20 (m, 8H), 7.07 (d,  $J = 7.7$  Hz, 2H), 6.85 (d,  $J = 8.6$  Hz, 2H), 6.77 (dd,  $J = 9.2$  Hz, 2.6 Hz, 1H), 6.59 (d,  $J = 8.6$  Hz, 2H), 6.55 (s, 1H), 6.17 (s, 1H), 4.69 (s, 2H), 4.34 (s, 2H), 4.02 (s, 2H), 4.00 (t,  $J = 4.9$  Hz, 2H), 3.67 (t,  $J = 4.9$  Hz, 2H), 3.52 (q,  $J = 7.2$  Hz, 4H), 1.26 (t,  $J = 7.3$  Hz, 6H).

### 6.2.2. Determination of relative bioluminescence intensities of dye-conjugated CTZ analogues with existing marine luciferases

The relative bioluminescence intensities of the dye- and azide-conjugated CTZ analogues were determined with various marine luciferases in mammalian cells (Figure 6-3(B)).

The pcDNA3.1(+) vectors encoding each copepod luciferase were obtained from our previous studies<sup>9, 23</sup>, where each copepod luciferase was tagged with a “KEDL” sequence for the intracellular retention. The pcDNA3.1(+) vector encoding *Renilla reniformis* luciferase 8.6-535 (RLuc8.6-535) was also obtained from our previous study<sup>9</sup>.

COS-7 cells, derived from the kidney of African green monkey, were grown in Dulbecco’s minimal essential medium (high glucose, DMEM) (Gibco), supplemented with 10% heat-inactivated fetal bovine serum (FBS) (Gibco) and 1% penicillin/straptomycin (P/S) (Gibco). The COS-7 cells were subcultured in a 96-well optical-bottom microtiter plate (Nunc) and transiently transfected with the pcDNA3.1(+) vectors encoding each marine luciferase using TransIT-LT1 (Mirus), as shown along the X-axis of Figure 6-3(B). The marine luciferases include *Gaussia princeps* luciferase (GLuc; GenBank AAG54095.1)<sup>23</sup> or RLuc8.6-535<sup>7</sup>, and Aluc16–34<sup>9</sup>. 16 hours after the transfection, the cells in each well were lysed with 50  $\mu$ L of a lysis buffer (E291A; Promega), and an aliquot of the lysates (10  $\mu$ L) was transferred into a fresh 96-well optical bottom microplate (Thermo Scientific), using an 8-channel micropipette. 40  $\mu$ L of RLuc assay buffer, carrying nCTZ (E2820; Promega), was injected into the aliquot, using a 12-channel micropipette, and immediately after that, the relative optical intensities of the lysates in the microplate were determined every 5 minutes, using an image analyzer (LAS-4000, FujiFilm), equipped with a cooled CCD camera. The bioluminescence intensities were normalized by integration time (second) and light-emitting area ( $\text{mm}^2$ ). The unit of the normalized bioluminescence intensity was subsequently expressed in terms of relative luminescence unit per second–area (RLU/sec/ $\text{mm}^2$ ).

The absolute optical intensities were listed in Table 6-1 to demonstrate the optical stability of the substrate–luciferase pairs (Table 6-1).

Regarding evaluation of the expression levels of the luciferases, it is inadequate to conduct a western blotting analysis, because multiple primary antibodies have to be applied at once. Furthermore, because of the poor folding efficiency caused by a large amount of cysteine, it is not suitable to purify the expressed luciferases

from bacterial cell lines. Alternatively, I referred to our western blot analysis for investigating the total protein amounts with the same cell line, plasmids, luciferases, and protocol as those of the present study<sup>13</sup>. The results show that no variance occurs in the applied protein amounts.

I further investigated the variance in the expression levels of a luciferase (ALuc30) with varying plasmids and substrates in mammalian COS-7 cells (Table 6-3). This study was conducted on the premise that the protein expression levels are equivalent with the bioluminescence intensities. The results show that the expression levels of ALuc30 can be variable up to 2-fold by changing the expression vectors.

Considering that the expression levels are practically unable to be normalized in living mammalian cells, the results in Figures 6-3 and 6-3 were noted as “relative” optical intensities.

### **6.2.3. Determination of the optical spectra of azide-modified CTZ analogues**

As the azide-modified CTZ analogues emit strong bioluminescence with ALucs, I further investigated the corresponding bioluminescence spectra (Figure 6-3(C)).

The cell lysates were made following the same method as that shown in Figure 6-3(B). An aliquot of the lysates (20  $\mu$ L) was transferred into a 200  $\mu$ L microtube and mixed with 80  $\mu$ L of the RLuc assay buffer (E2820; Promega), carrying nCTZ, 2-N3-CTZ, or 6-N3-CTZ. The microtube was immediately moved into the chamber of a precision spectrophotometer (AB-1850, ATTO), equipped with a cooled charge-coupled device (CCD) camera that can capture the entire light in one shot, and the resulting spectra were taken in an integration of 30 seconds. The optical spectra were normalized in percentages (%).

### **6.2.4. Fabrication of new ALuc variants for selected CTZ analogues**

As azide-modified CTZs luminesce strongly with ALuc16, 25, and 34, I expanded the experimental boundary to the other ALucs, newly fabricated from ALuc 25, and ALuc 34 in the hope of improved optical properties

(Figure 6-2 and Figure 6-4).

The new ALuc variant sequences were made by our previously suggested method as follows<sup>9, 11</sup>: Briefly, the sequence of ALuc25 or ALuc30 was fragmented and aligned to make three lanes with CLUSTALW ver2.1 to investigate their internal sequential homology (named Single-Sequence Alignment (SSA))<sup>9</sup>. This alignment specified characteristic three-repeated lanes, whose second and third lanes were highly conserved. The new ALuc sequences were generated by replacing the original amino acids in the alignment with new candidates to enhance the homology between the second and third lanes sequences. The new ALuc sequences derived from ALuc25 and ALuc30 were named ALuc26–28, and ALuc36–39, respectively (Figure 6-2).

Based on the sequential information above, the murine codon-optimized cDNA constructs, encoding the artificially designed amino acid sequences (ALuc26–28 and ALuc36–39), were custom-synthesized, on order, by Eurofins Genomics (Tokyo, Japan). The synthesized cDNAs encoding each luciferase and a “KDEL” tag were subcloned into pcDNA3.1(+) (Invitrogen), using the specific restriction sites, *HindIII* and *XhoI*, for expression in mammalian cells, where the KDEL was added to the end of the sequence of each luciferase for the cell retention. The overall sequence fidelity was confirmed with a sequencing service provided by Eurofins Genomics (Tokyo, Japan).

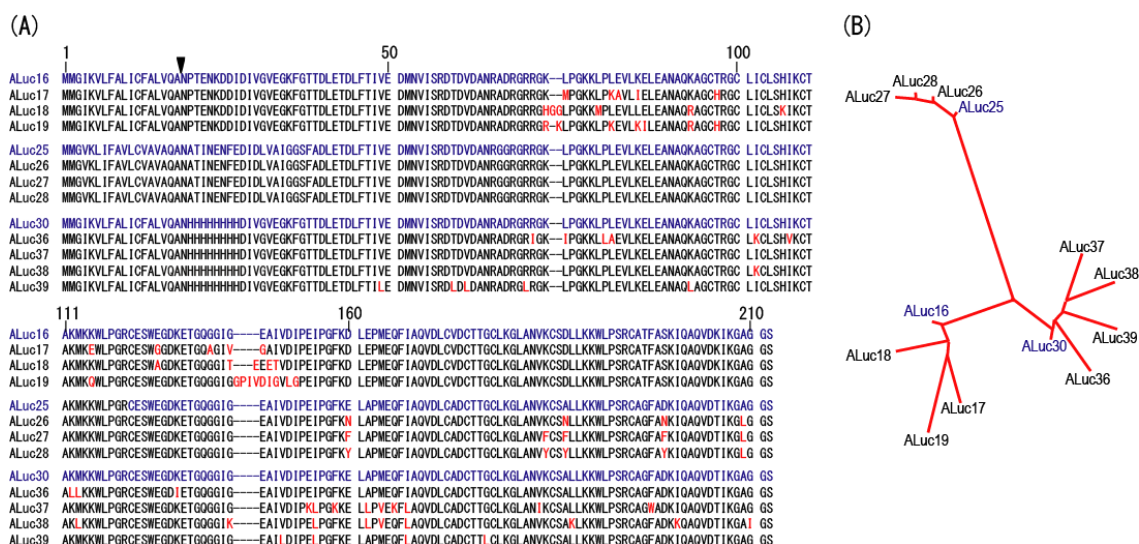


**Figure 6-2** (A) The sequences of ALucs, newly synthesized in this study. The sequences in blue and black indicate, respectively, the prototypes and the sibling sequences. Letters in red highlight the amino acids that are different from others. (B) The phylogenetic tree of newly fabricated ALucs. The new ALucs were derived from ALuc25, ALuc16, or ALuc30, respectively. The original ALucs were marked in blue.

### 6.2.5. Relative bioluminescence intensity matrix of selected CTZ analogues with new ALuc variants

The relative bioluminescence intensities of selected CTZ analogues, with different ALuc variants, were addressed in matrix (Figure 6-4(B)).

The COS-7 cells were prepared following the same method as that shown in Figure 6-3(B). The COS-7 Cells, in each well of a 96-well optical bottom microplate, were transiently transfected with pcDNA3.1 vector (Invitrogen), encoding GLuc, RLuc8.6-535, or one of the new variants of ALucs, using TransIT-LT1 (Mirus). 16 hours after the transfection, the cells were lysed and an aliquot of the lysates transferred into a fresh 96-well optical bottom microplate. The corresponding optical intensities, developed with the same protocol as that in Figure 6-3(B), were determined by LAS-4000 and finally analyzed with the specific software, Multi Gauge v3.2 (FujiFilm). The specific optical intensity and stability were summarized in Table 6-2.

### 6.2.6 Cell-based assays on the basis of the new ALuc-luciferin systems

The live-cell images and optical profiles of 6-N3-CTZ were compared with those of Furimazine and nCTZ (Figure 6-5). The amino acid sequence of NanoLuc was previously reported. The cDNA construct encoding NanoLuc and a “KDEL” tag was custom-synthesized by the help of Eurofins Genomics (Tokyo), and subcloned into pcDNA3.1 vector (Invitrogen) for mammalian cell expression, where the “KDEL” tag was added for cell retention.

COS-7 cells were first grown over 6-channel microslides ( $\mu$ -Slide VI<sup>0.4</sup>, ibidi) and transiently transfected with NanoLuc, RLuc8.6-535, or ALuc26. 16 hours after incubation, the cells on each microslide were rinsed with HBSS buffer (Gibco) and immediately bathed with 60  $\mu$ L of Furimazine, nCTZ, or 6-N3-CTZ dissolved in an HBSS buffer (final concentration:  $10^{-4}$  M), using a multichannel pipet (Gilson). The microslides were immediately transferred to the dark chamber of the LAS-4000 (FujiFilm) and their optical intensities integrated every 5 minutes. The optical images of the microslides were adjusted according to the optical intensity scales. The optical image of 6-N3-CTZ on the microslide was displayed, additionally, in terms of RLU per distance (mm).

### 6.2.7. Measurement of the BRET and CRET spectra of azide- or dye-conjugated CTZ analogues

The corresponding bioluminescence spectra were obtained with affinity column-purified ALuc16 (Figure 6-6).

In brief, the affinity column-purified ALuc16 was prepared beforehand as follows: I first generated the DNA construct of ALuc16, carrying a Strep-II tag at the C-terminus *via* PCR. The construct was then cloned into a pOPTHM vector (providing a cleavable N-terminal His<sub>6</sub>-MBP tag) and expressed in the bacterial strain SHuffle T7 Express *lysS* (New England Biolabs) with 0.3 mM IPTG induction. The cells were resuspended and sonicated in ice-cold lysis buffer {50 mM Tris-HCl pH 8.0, 500 mM KCl, 5 mM imidazole, 0.2 mg/mL hen egg white

lysozyme (HEWL), and 1 tablet of EDTA-free Protease Inhibitor Cocktail (Roche Diagnostics)} was added. The lysate was centrifuged at 18,000 rpm for 40 min, and the resulting supernatant liquid was passed over a 5 mL HisTrap HP column (GE Healthcare). An ÄKTA Purifier system (GE Healthcare) was used to wash and elute the ALuc16 fusion protein as follows: The column was washed with 100 mL of wash buffer (20 mM Tris-HCl pH 8.0, 50 mM potassium phosphate pH 8.0, 100 mM NaCl, and 15 mM imidazole pH 8.0) and then eluted in an imidazole gradient (15–300 mM) over 80 mL. The eluted sample was dialyzed to a metal-cation-free Tris-HCl buffer (0.05 M, pH 8.2) at 4°C for 24 h and finally adjusted by dilution to a concentration of 1 mg/mL.

The CRET spectra were determined as follows (Figure 6-6(A)): The CH<sub>3</sub>OH solution of respective dye-conjugated CTZ analogues were mixed with PBS buffer (final concentration: 0.5 mM, 8 μL) and transferred to a 200 μL microtube. The microtube was set in a dark chamber of a high precision spectrophotometer (AB-1850, ATTO). The corresponding chemiluminescence spectra were measured by integrating all the wavelengths of light for 5 seconds, immediately after injecting 80 μL of DMSO. Separately, the CRET spectrum of the 6-Rh-CTZ was determined immediately after injection of 100 μL DMSO solution dissolving 10% (v/v) of 2.5 M aqueous sodium hydroxide into a CH<sub>3</sub>OH solution of 6-Rh-CTZ (2 mM, 100 μL) (final concentration: 1 mM).

The BL spectra were also determined as follows (Figures 6-3(C) and 6-6(B)): The purified ALuc16 stock was diluted 500-fold to 2 μg/mL with a universal or an assay buffer before experiments. 20 μL of the diluted ALuc16 was transferred into a 200 μL PCR microtube and mixed with 80 μL of azide or dye-conjugated CTZ analogues. The microtube was immediately moved into the chamber of the precision spectrophotometer (AB-1850, ATTO) and the resulting spectra were taken in an integration of 30 seconds.

The spectrum of the 6-Rh-CTZ–RLuc8.6-535 pair was determined separately as follows: COS-7 cells expressing RLuc8.6-535 were lysed with a lysis buffer (Promega) and an aliquot of the lysate (4 μL) was transferred to a 200 μL microtube. The lysate in the microtube was mixed with 200 μL of 6-Rh-CTZ dissolved in PBS buffer (2 μM), and the resulting BRET spectra were immediately determined using precision

spectrophotometer (AB-1850, ATTO).

### 6.2.8 Plasmid-driven optical intensity and stability of selected CTZ analogues with ALuc30

The plasmid-driven optical intensities and stabilities of selected CTZ analogues were determined with ALuc30 (Table 6-3). cDNA encoding ALuc30-KDEL or ALuc30PA was subcloned into the mammalian expression plasmids, pEBpuro vector (Wako Purechemicals), pEB\_hyg vector (Wako Purechemicals), pEBneo vector (Wako Purechemicals), pCAGhyg vector (Wako Purechemicals), and pCAGneo vector (Wako Purechemicals), respectively, where “KDEL” and “PA” mean an endoplasmic reticulum (ER) retention signal and a PA-tag at the C-terminal end of ALuc30, respectively. The corresponding plasmids were named as pEBpuro-ALuc30KD and pCAGhyg-ALuc30PA. As a reference, cDNA encoding RLuc8.6-535 was subcloned into pEBpuro vector and named pEBpuro-RLuc8.6-535.

The relative optical intensities of the above plasmids were determined following the protocol shown in Figure 6-3(B). The optical intensities were integrated every 5 minutes, and the intensities at 0 and 20 minutes were summarized in Table 6-1.

## 6.3. Results and discussion

Native coelenterazine (nCTZ), in an imidazopyrazinone backbone, is the common substrate of most marine luciferases, including *Renilla reniformis* luciferase (RLuc) and *copepoda* luciferases<sup>1</sup>.

In this study, the C-2 and C-6 positions of the structure were bridged with organic dyes or an azide group to achieve (i) improvement of optical intensity and stability, (ii) bulkiness-driven size effects, and (iii) bioluminescence or chemiluminescence resonance energy transfer (B/CRET).

### 6.3.1. Azide-modified CTZ analogues showed greatly improved optical intensities and red-shifted bioluminescence spectra

I previously investigated the advantages of C-6 extended modification of CTZ in the bioluminescence capacity, allowing a large spectral shift of the bioluminescence spectra and little influence on the enzymatic recognition of RLucs<sup>12</sup>. As a more specific approach, I examined in this study if C-2 or C-6 position of the imidazopyrazinone backbone can be extended by conjugating dyes or an ethyl azide group (Figure 6-3).

The resulting relative optical intensities in Figure 6-3(B) show that (i) the optical intensities of azide group (N3)-modified CTZs are generally superior to other dye-conjugated CTZs with ALucs, and (ii) ALucs generally produce brighter bioluminescence with azide-conjugated CTZs than with conventional marine luciferases, like GLuc and RLuc8.6-535.

The results show that azide-conjugated CTZ analogues with ALucs exerted approximately 2 or 4-fold brighter bioluminescence than nCTZ. Between the CTZ analogues, azide-modified at C-6 and C-2 positions, 6-N3-CTZ showed approximately 2-fold brighter bioluminescence than 2-N3-CTZ with ALucs. Similarly, between the CTZ analogues, FITC-conjugated at C-6 and C-2 positions, 6-FITC-CTZ exerted approximately 5-fold brighter bioluminescence than 2-FITC-CTZ with ALucs. These two cases suggest that ALucs prefers C-6 position-modified CTZ analogues.

Excepting the azide-modified cases, the dye-conjugated CTZ analogues generally emitted weaker bioluminescence intensities than did nCTZ. As the azide group is compact, compared to others, the size of the dyes works as a burden to the bioluminescence reaction. The suppressed optical intensities were not improved even by 10-times higher concentrations of 2-SFX-CTZ and 6-Nile-Red-CTZ (Figure 6-3(B)).

As the azide-conjugated CTZ analogues emitted excellent bioluminescence intensities (see Figure 6-3(B)), the corresponding bioluminescence spectra were determined with ALuc16, 23, and 34. For simplicity, Figure 6-3(C) demonstrates spectra with only ALuc34.

The results show that the optical maxima ( $\lambda_{\max}$ ) of 2-N3-CTZ and 6-N3-CTZ are ca. 513 and 505 nm with ALuc34, respectively. These  $\lambda_{\max}$  values represent 16 nm and 8 nm red-shifted spectra of the azide-modified CTZ analogues, compared with nCTZ. The intensity ratios of the wavelengths greater than 600 nm by 2-N3-CTZ and 6-N3-CTZ were found to be 6% and 5%, respectively.

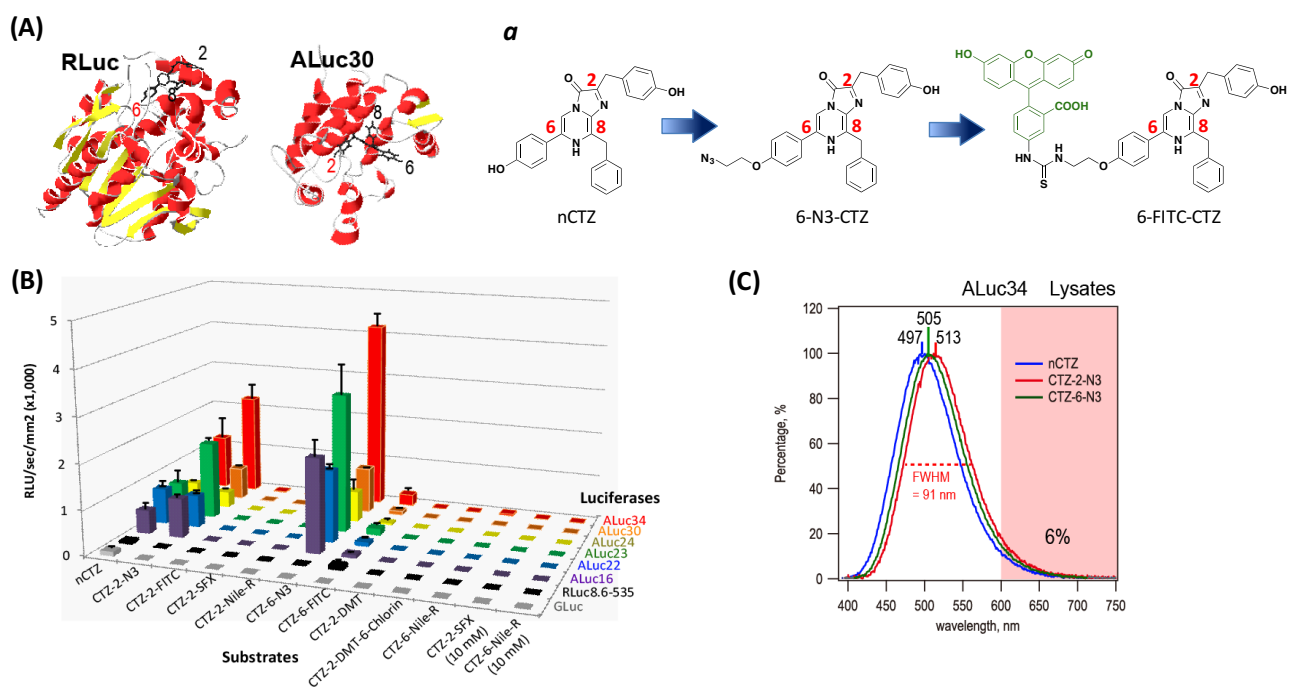


**Figure 6-3** (A) The molecular structures of two marine luciferases, *Renilla reniformis* luciferase 8 (RLuc8) (PDB: 2PSJ) and artificial luciferase 30 (ALuc30)<sup>11</sup> and their binding with coelenteramide and native coelenterazine (nCTZ), respectively. The molecular structure of ALuc30 is a supersecondary model, which was calculated with respect to the X-ray crystallographic information of the coelenterazine-binding protein (CBP)<sup>11</sup>. Inset *a* exemplifies synthetic luciferins, carrying a bulky side chain at C-6 position.

(B) Relative substrate-specific optical intensities of marine luciferases ( $n = 3$ ). Because copepod-derived luciferases (GLuc and ALucs) secret, they were retained in the cells with an ER retention signal (KDEL), as explained in the experimental section. The X- and Y-axes specify newly synthesized CTZ analogues and conventional marine luciferases, respectively. The Z-axis shows the corresponding optical intensities, normalized by measurement time (s) and area (mm<sup>2</sup>). The percentages on the bars indicate the optical intensities that remained after 20 minutes. The inset shows the bioluminescence spectra of ALuc34 with 6-N3-CTZ and 6-FITC-CTZ. Abbreviations: GLuc, *Gussia princeps* luciferase; RLuc8.6-535, *Renilla reniformis* luciferase 8.6-535; ALuc16, artificial luciferase 16. The asterisk denotes the maximal optical intensity of each luciferase with newly synthesized CTZ analogs. The specific optical intensity and stability were summarized in Table 6-1. (C) Bioluminescence spectra of the newly synthesized azide-modified CTZ analogues with ALuc34. All the spectra were normalized as percentages (%) of maximal intensity. FWHM means the full width at half maximal intensity in wavelength. The percentage in black denotes the portion of red light emission longer than 600 nm over the total light emission.

**Table 6-1** Relative optical intensities (RLU/sec/mm<sup>2</sup>) and sustainability (%) of the newly synthesized azide- or dye-conjugated CTZ analogues with conventional luciferases, shown in Figure 6-3(B) ( $n=3$ ). Two concentrations of the substrates were applied for the light measurement: i.e., 1 mM and 10 mM. Accordingly, the results were grouped into 1 and 10 mM areas. Light- and dark-colored spots show the optical intensities higher than 15 and 1,500 RLU/sec/mm<sup>2</sup>, respectively.

	1 mM															10 mM								
	nCTZ		2-N3-CTZ		2-FITC-CTZ		2-SFX-CTZ		2-Nile-R-CTZ		6-N3-CTZ		6-FITC-CTZ		2-DMT-CTZ		2-DMT-6-Chlorin-CTZ		6-Nile-R-CTZ		2-SFX-CTZ		6-Nile-R-CTZ	
	ave	SD	ave	SD	ave	SD	ave	SD	ave	SD	ave	SD	ave	SD	ave	SD	ave	SD	ave	SD	ave	SD	ave	SD
GLuc	102 ± 36		7 ± 1		2 ± 0		2 ± 1		0 ± 1		1 ± 0		1 ± 0		1 ± 1		0 ± 1		2 ± 1		3 ± 0		1 ± 1	
RLuc8.6-535	71 ± 5		3 ± 1		3 ± 0		2 ± 1		0 ± 1		15 ± 3		96 ± 20		2 ± 1		1 ± 1		1 ± 1		3 ± 0		2 ± 1	
ALuc16	529 ± 128		876 ± 67		4 ± 4		3 ± 1		1 ± 1		2,097 ± 326		74 ± 5		2 ± 1		1 ± 1		0 ± 2		3 ± 0		2 ± 0	
ALuc22	797 ± 91		723 ± 52		4 ± 1		3 ± 0		1 ± 0		1,612 ± 87		96 ± 16		2 ± 0		2 ± 1		2 ± 0		4 ± 0		2 ± 1	
ALuc23	711 ± 230		1,718 ± 49		6 ± 3		2 ± 1		1 ± 0		3,092 ± 612		154 ± 37		2 ± 1		1 ± 1		1 ± 1		3 ± 0		2 ± 1	
ALuc24	498 ± 166		359 ± 30		0 ± 1		3 ± 1		1 ± 1		690 ± 188		35 ± 2		2 ± 0		1 ± 1		3 ± 0		3 ± 1		2 ± 1	
ALuc30	351 ± 91		716 ± 68		2 ± 2		2 ± 1		0 ± 1		1,019 ± 36		84 ± 5		2 ± 0		1 ± 1		2 ± 0		3 ± 0		2 ± 0	
ALuc34	1,218 ± 386		2,256 ± 277		10 ± 4		2 ± 1		0 ± 1		4,205 ± 246		249 ± 39		1 ± 1		1 ± 1		38 ± 16		3 ± 0		2 ± 1	

RLU/sec/mm<sup>2</sup>

### 6.3.2. Selected coelenterazine analogues showed unique luciferase preference

As ALuc16, ALuc23, and ALuc34 emit relatively strong optical intensities with 2-N3-CTZ and 6-N3-CTZ, sibling luciferases from ALucs were newly created and examined with 2-N3-CTZ and 6-N3-CTZ. In other words, ALucs26-28 were created from ALuc23 and ALuc25, and ALucs36-39 from ALuc30 and ALuc34. On the other hand, ALucs17-19 were previously reported in our study<sup>9</sup>, wherein they were made by modifying ALuc16 (Figure 6-2 and Figure 6-4).

The newly synthesized ALucs showed unique phylogenetic positions, which are distinctly different from those of conventional marine luciferases, like MpLuc1, and MLuc (Figure 6-4(A), Table 6-2). The results reveal that nCTZ commonly luminesces with a broad range of marine luciferases, including GLuc, RLuc8.6-535, ALucs17-19, and ALuc26. Particularly, nCTZ strongly luminesces with both ALuc18 and ALuc26, whereas azide-conjugated CTZ analogues, biased to ALuc26 rather than ALuc18, did not luminesce with RLuc8.6-535 and GLuc. In contrast, 6-pi-OH-CTZ emitted strong bioluminescence only with RLuc8.6-535.

The above results show that every substrate has its preferred marine luciferases: e.g., only [6-N3-CTZ-

ALuc26], [nCTZ–ALuc18], and [6-pi-OH-CTZ–Rluc8.6-535] pairs luminesce. These matched pairs may be utilized in a multiplex assay system, which simultaneously determines ligands with multiple optical readouts.

The best optical sustainability was found with ALuc26 (Table 6-2), which sustained 64 % and 52% of its optical intensity, till 20 minutes after injection of nCTZ and 6piOH-CTZ, respectively. Optical sustainability of 6-N3-CTZ was found to be generally poor with the tested marine luciferases: e.g., ALuc19 sustained 54% of optical intensity with 2-N3-CTZ for 20 minutes, but 6-N3-CTZ in the same condition sustained only 8%.

Considering that 6-N3-CTZ generally emits bustling optical intensities with ALucs, its rapid turnover rates could be a reason for the quick decrease in the optical intensities with ALuc19 or ALuc26.

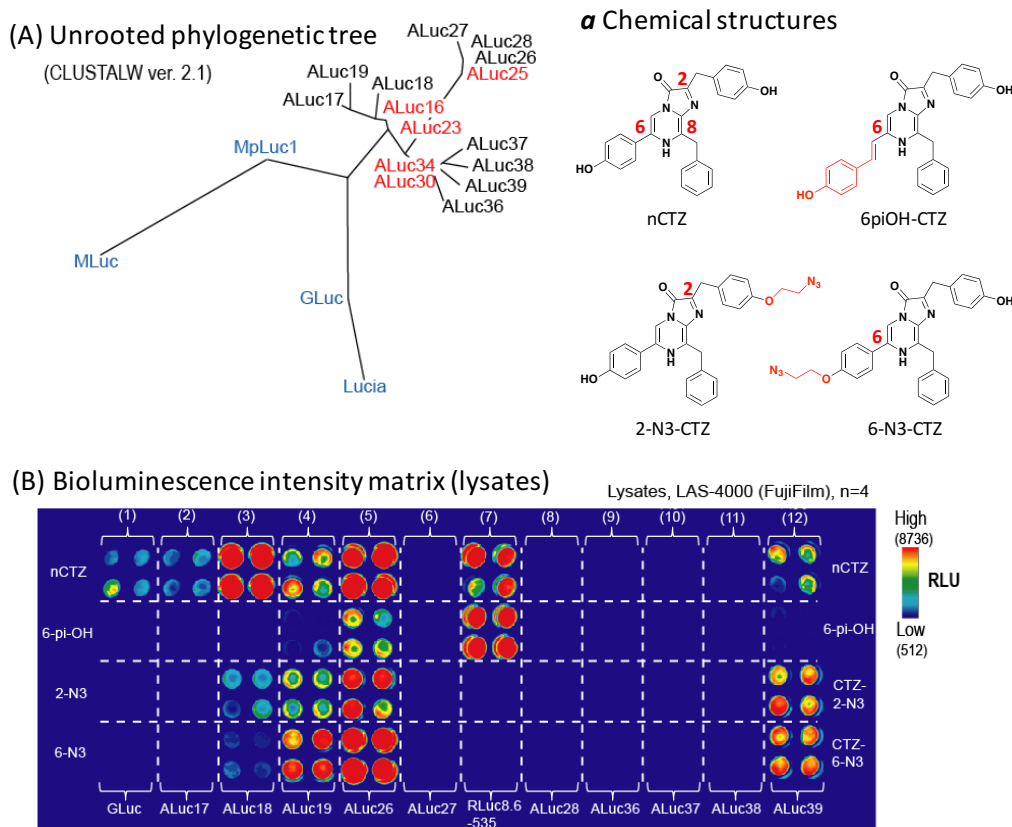


**Figure 6-4** (A) The unrooted phylogenetic tree of newly fabricated artificial luciferases and conventional marine luciferases. The new ALucs (black) were fabricated by modifying the brightest luciferases, ALuc16, ALuc23, ALuc30, in Figure 6-2(red). Conventional marine luciferases (blue) are phylogenetically distinctive from the ALucs. Inset **a** shows chemical structures of the selected CTZ analogues for bioluminescence imaging studies. (B) Relative optical intensities of the most potent CTZ analogues in Figure 6-3 with newly fabricated ALucs. The optical image represents the integrated photon flux during the initial 5 minutes. Because copepod-derived luciferases (GLuc and ALucs) secret, they were retained in the cells with an ER retention signal (KDEL), as explained in the experimental section. The newly synthesized CTZ analogues have their own unique optical specificities with marine luciferases ( $n=4$ ). The specific values were listed in Table 6-2.

**Table 6-2** Absolute optical intensities (RLU/sec/mm<sup>2</sup>) and sustainability of the newly synthesized azide-modified CTZ analogues with new ALucs, shown in Figure 6-4(B) ( $n=3$ ). The percentage (%) indicates the optical intensity that remained at 20 minutes after substrate injection, compared to what emitted at 0 minute after substrate injection. The dotted line in red highlights the zone of poor optical intensity.

		nCTZ			6piOH-CTZ			CTZ-2-N3			CTZ-6-N3			RLU/sec/mm <sup>2</sup>
GLuc	min	ave	SD	%										
	0	8,979	2,459	32	35	6	17	608	127	8	172	33	16	
	20	2,906	716		6	2		48	9		28	6		
RLuc8.6	0	6,757	4,021	63	<b>10,113</b>	1,340	57	<b>269</b>	28	52	364	73	33	
-535	20	4,245	2,569		5,813	829		139	12		119	27		
ALuc17	0	8,416	874	38	198	23	41	2,205	130	62	2,517	339	11	
	20	3,227	425		81	11		1,360	97		285	32		
ALuc18	0	<b>55,593</b>	1,836	16	<b>477</b>	40	24	<b>9,623</b>	1,800	23	6,721	675	1	
	20	8,957	436		117	8		2,230	446		46	3		
ALuc19	0	14,740	2,968	41	5,838	1,134	29	13,245	772	54	22,893	3,429	8	
	20	5,997	1,098		1,710	280		7,136	443		1,732	222		
<b>ALuc26</b>	0	<b>53,263</b>	7,413	<b>64</b>	<b>14,399</b>	2,284	<b>52</b>	<b>23,002</b>	5,325	<b>47</b>	<b>57,578</b>	1,602	<b>27</b>	
	20	33,844	9,100		7,458	997		10,792	2,256		15,572	2,058		
ALuc27	0	68	28	31	22	10	36	28	16	21	94	38	15	
	20	21	10		8	4		6	4		14	6		
ALuc28	0	496	67	59	43	15	49	31	6	65	265	35	15	
	20	292	47		21	8		20	4		41	4		
ALuc36	0	262	19	93	4	1	75	47	7	40	75	16	40	
	20	243	26		3	1		19	3		30	10		
ALuc37	0	229	37	61	0	0	0	2	1	50	11	3	55	
	20	140	35		0	0		1	1		6	2		
ALuc38	0	199	33	1	0	1	0	1	3	1	14	3	1	
	20	2	52		0	1		0	1		0	2		
ALuc39	0	2,788	964	46	949	161	23	4,237	661	43	4,175	236	21	
	20	1,287	473		216	33		1,841	269		861	72		

### 6.3.3. 6-N3-CTZ selectively luminesces with ALuc26 in living mammalian cells

As the [6-N3-CTZ–ALuc26] pair showed excellent optical properties in lysates, they were further examined in living mammalian cells (Figure 6-5).

Besides 6-N3-CTZ, I simultaneously examined nCTZ and Furimazine, as nCTZ is the most commonly used substrate in many laboratories, and Furimazine is known to strongly luminesce with NanoLuc.

Furimazine emitted strong bioluminescence only with NanoLuc in COS-7 cells, whereas 6-N3-CTZ selectively luminesced with ALuc26. There were no cross reactions between [Furimazine–NanoLuc] and [6-N3-CTZ–ALuc26], convincing that these two luminescent systems are fully independent and non-interfering reporters each other. In contrast, nCTZ allowed bioluminescence with all the tested luciferases. The

corresponding optical profile highlights that 6-N3-CTZ specifically illuminates ALuc26 in living COS-7 cells. The overall absolute optical intensities were in the order of [Furimazine–NanoLuc] > [6-N3-CTZ–ALuc26] > [nCTZ–NanoLuc] = [nCTZ–ALuc26] > [nCTZ–Rluc8.6-535].

The time course of bioluminescence in live cells shows that the best optical stability is found in the order of [Furimazine–NanoLuc] > [6-N3-CTZ–ALuc26] > [nCTZ–Rluc8.6-535].

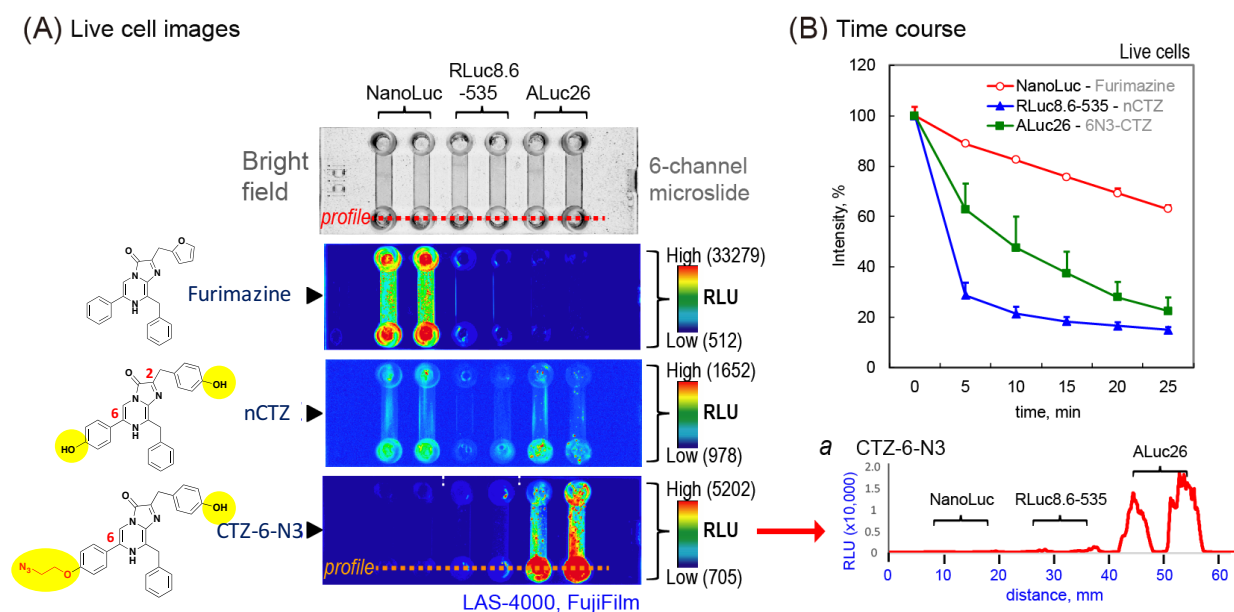


**Figure 6-5** Live cell-based bioluminescence imaging and time course. (A) Comparison of substrate-driven live cell images on 6-channel microslides. The optical intensities of 6-N3-CTZ were compared with those of Furimazine and nCTZ. Inset *a* shows the optical profile of 6-N3-CTZ according to marine luciferases. The optical image represents the integrated photon flux for the initial 5 minutes. (B) Time course of the bioluminescence intensities activated by Furimazine, nCTZ, and 6-N3-CTZ. The optical intensities were determined every 5 minutes.

### 6.3.4. CRET and BRET spectra of dye-bridged CTZ analogues

Spectra of chemiluminescence and bioluminescence, showing their resonance energy transfer (RET), were determined (Figure 6-6).

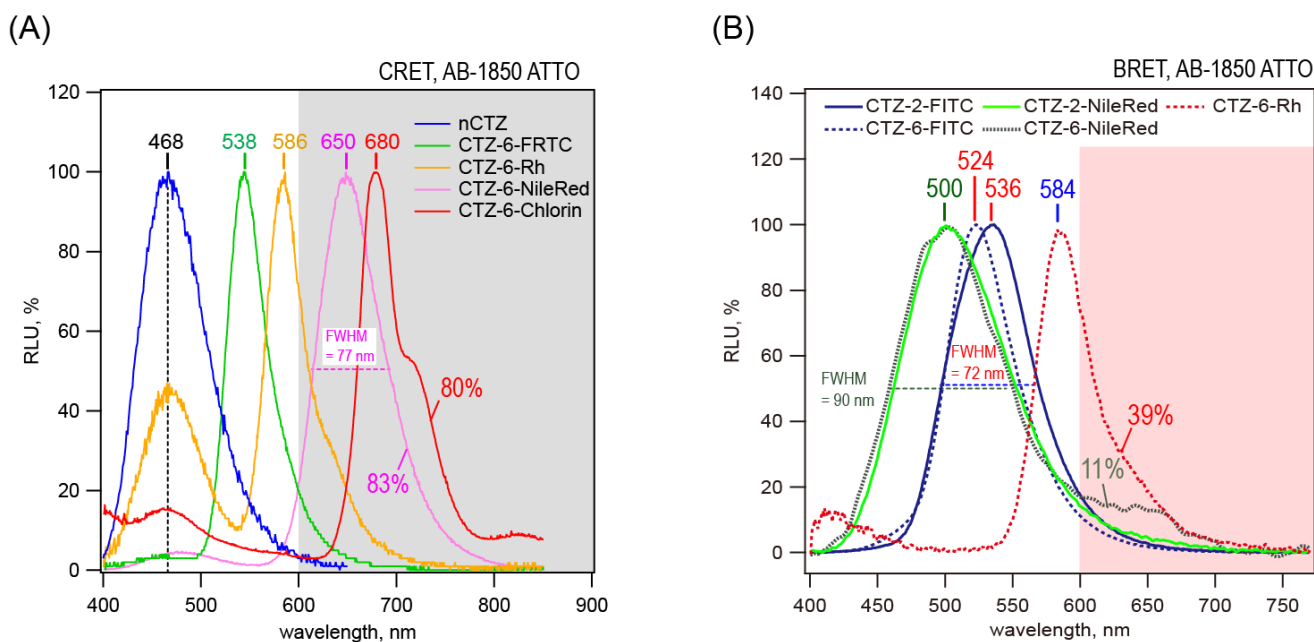


**Figure 6-6** (A) The chemiluminescence resonance energy transfer (CRET) spectra of CTZ analogues dye-bridged at the C-6 position. The spectra were normalized as percentages (%) of maximal intensity. The percentage in red denotes the portion of red light emission longer than 600 nm over the total light emission. Among tested, spectra with poor optical intensities were omitted in the figure. (B) Bioluminescence resonance energy transfer (BRET) spectra of the representative dye-bridged coelenterazine analogues with ALuc16 and RLuc8.6-535. The spectra of 2-FITC-CTZ, 6-FITC-CTZ, 2-NileRed-CTZ, and 6-NileRed-CTZ were determined with ALuc16, while that of 6-Rh-CTZ with RLuc8.6-535. All the spectra were normalized as percentages (%) of maximal intensity. FWHM means the full width at half maximal intensity in wavelength (nm). The percentage in red indicates the portion of red light emission longer than 600 nm over the total light emission. Among tested, spectra with poor optical intensities were omitted in the figure.

The chemiluminescence spectrum of nCTZ was determined as a reference and its maximal peak ( $\lambda_{\max}$ ) was found at 468 nm. The spectra of 6-FITC-CTZ, 6-Rh-CTZ, 6-Nile Red-CTZ, and 6-Chlorin-CTZ commonly showed small chemiluminescence peaks near 468 nm. The maximal peaks of 6-FITC-CTZ, 6-Rh-CTZ, 6-Nile Red-CTZ, and 6-Chlorin-CTZ were found at ca. 545 nm, 586 nm, 650 nm, and 680 nm, respectively<sup>24-28</sup>. These peak positions are almost the same as the predicted emission peak positions of each bridged dye after resonance energy transfer.

These two characteristic peaks in the spectra indicate that the resonance energy of chemiluminescence, generated by degradation of coelenterazine, was transferred to the conjugated dye.

The authors further examined the BRET spectra of dye-conjugated CTZ analogues with affinity column-purified ALuc16 or a cell lysate, carrying RLuc8.6-535 (Figure 6-6(B)). Among the synthesized CTZ analogues, Rhodamine-conjugated CTZ analogue showed a greatly red-shifted RET spectrum, where 39% of the total photons were emitted in the red and infra-red region longer than 600 nm, which is highly tissue-permeable and commonly referred to as “optical window”. The  $\lambda_{\text{max}}$  was found at 584 nm, which is generally accepted as the optical peak of Rhodamines<sup>25</sup>. On the other hand, Nile Red-conjugated CTZ showed a relatively weak RET spectrum. From a comparison of C-2 and C-6 position-modified CTZs, it was noticed that 6-Nile Red-CTZ had a weak peak at 650 nm, which is the predicted emission peak position of the Nile red, after resonance energy transfer<sup>24</sup>. About 11% of the overall light emission by 6-Nile Red CTZ was located in the region longer than 600 nm.

The above results in the BRET efficiency among Rhodamine-, Nile Red- and FITC-conjugated CTZs may be explained with the dye’s polarity sensitivity: for example, the fluorescein and rhodamine in the CTZ analogues are less sensitive to solvent polarity allowing high RET efficiency, whereas Nile Red is known to be strongly influenced by solvent polarity causing poor RET efficiency<sup>19</sup>. Further, the orientation of the dyes to the conjugated CTZ could also be suboptimal for the RET inside the pocket of ALuc16. CRET spectra of the dye-conjugated CTZs are also explained with their polarity sensitivity: for example, 6-Nile Red-CTZ shows a clear RET peak because the Nile Red exerts fluorescence in polar organic solvents such as DMSO and DMF, but not in aqueous solution<sup>29</sup> (Figure 6-6(A)).

In the spectra of FITC-conjugated CTZ analogues, no distinctly separate excitation and emission peaks were found around 500–520 nm; instead, strong optical peaks were found at 524 nm and 536 nm, which look reasonable as the RET emission, considering that reference studies reporting that (i) the emission of FITC is between 516-525 nm<sup>26</sup>, (ii) a FITC-conjugated CTZ analogue showed chemiluminescence at 532 nm<sup>19</sup>. The results suggest that the weak peaks at 500 nm may have been superimposed by emission peaks at 524 nm and

536 nm.

Further comparison of the FWHMs of the spectra revealed that the largest widths were with Nile Red-conjugated CTZs, and the narrowest widths with 6-FITC-CTZ. The overall order of the widths was as follows:

6-Nile Red-CTZ = 2-Nile Red-CTZ > 2-FITC-CTZ > 6-FITC-CTZ.

### 6.3.5. Expression vector-driven optical intensity and stabilities of ALuc30

The optical properties of azide-conjugated CTZ analogues were further evaluated, with respect to mammalian expression vectors encoding ALuc30 (Table 6-3).

The overall optical intensity of KDEL-tagged ALuc30 was approximately 2-fold more than that of PA-tagged ALuc30, which may be interpreted (i) to have a better ER retention effect with KDEL tag than with PA tag or (ii) to have higher folding efficiency with KDEL tag than with PA tag. No significant variance was noticed in optical intensity and sustainability by changing the expression vectors. The optical properties were rather greatly influenced by the substrates applied. 6-N<sub>3</sub>-CTZ showed a rapid drop in optical intensity, 20 minutes after the injection. This result corresponds with that of the same substrate in Table 6-1.

As a reference, the optical intensity and stability of RLuc8.6-535 in pEBpuro vector (Wako) were determined simultaneously. RLuc8.6-535 emitted considerable bioluminescence with 6-piOH-CTZ and nCTZ, whereas it could not activate CTZ-2-N<sub>3</sub> and CTZ-6-N<sub>3</sub>. This sharp contrast suggests that 6-piOH-CTZ may be useful as a pinpoint imaging agent in a multi-luciferase-based bioassay system.

**Table 6-3** Plasmid-driven optical intensities (RLU/sec/mm<sup>2</sup>) and sustainability of ALuc30–substrate pairs (*n*=3). Abbreviations: KDEL, an endoplasmic reticulum (ER) retention signal meaning KDEL; PA, a PA-tag; *puro*, puromycin; *hyg*, hygromycin; *neo*, neomycin. The percentage (%) denotes the optical intensity that remained at 20 minutes after substrate injection, compared to what remained at 0 minutes after substrate injection. The dotted line in red highlights the zone of poor optical intensity to RLuc8.6-535.

		RLU/sec/mm <sup>2</sup>											
		nCTZ			6piOH-CTZ			CTZ-2-N3			CTZ-6-N3		
	min	ave	SD	%	ave	SD	%	ave	SD	%	ave	SD	%
pEBpuro RLuc8.6	0	289	78	58	305	112	58	5	1	80	9	3	33
	20	168	42		178	65		4	2		3	1	
pEBpuro A30KDEL	0	<b>2,514</b>	191	36	468	6	26	893	82	42	<b>2,265</b>	122	8
	20	913	47		122	2		374	33		180	30	
pCAGhyg A30PA	0	<b>2,204</b>	404	35	469	127	23	1,212	476	29	<b>1,746</b>	443	7
	20	773	182		107	29		346	129		121	37	
pCAGneo A30PA	0	668	193	32	216	64	23	576	108	29	1,153	137	7
	20	217	57		50	15		167	34		80	9	
pEBpuro A30PA	0	842	430	34	197	63	23	679	381	29	987	279	7
	20	287	145		46	14		195	114		66	21	
pEBhyg A30PA	0	1394	191	33	423	28	23	1051	231	30	<b>2130</b>	273	7
	20	455	61		99	8		319	67		145	18	
pEBneo A30PA	0	859	213	32	220	44	24	684	116	29	1197	212	7
	20	275	53		52	12		200	44		80	15	

## 6.4. Conclusions

With the available data, I synthesized a new series of dye- or azide-conjugated CTZ analogues, by conjugating a series of organic dyes or an azide group to the C-2 or C-6 position of CTZ backbone.

Our accomplishments may be summarized as follows: (i) greatly enhanced optical intensities were found with the azide-conjugated CTZ analogues, which interestingly provide highly ALuc-specific optical intensities. Some of the unique pairs like [6-N3-CTZ–ALuc26] have no cross-reactions with other conventional bioluminescence systems like [Furimazine–NanoLuc] and [6pi-OH-CTZ–RLuc8.6-535] pairs. This result is convincing that the present bioluminescent system is fully independent and non-crossreacting reporters with the others. These pairs may be applicable for multiplex assay systems; (ii) I achieved unique red-shifted chemi- and bioluminescence spectra, which was via the CRET and BRET between the dye-conjugated CTZ analogues and luciferases. The optical signature longer than 600 nm greatly improves the tissue permeability in living subjects.

Although many attempts to modify CTZ have been applied to date, this study is the first systemic approach

to conjugate many organic dyes to CTZ. This unique bioluminescence system appends a new toolbox to bioassays and molecular imaging. This study provides new insights into how dye- or azide-conjugated CTZ analogues luminesce with marine luciferases, and how their unique optical selectivity and functionality can become an important addition to the bioluminescence toolbox for bioassays and molecular imaging.

## **6.5. Appendix**

### **6.5.1. BL investigation of C-2 or C-6 modified CTZ derivatives with RLuc8.6-535**

In order to determine the effect of C-2 or C-6 substitution on BL intensities, I further measured the BLI in the presence of RLuc8.6-535 at high concentration. To determine BL of the CTZ derivatives (nCTZ, plasmids encoding RLuc8.6-535 were separately transfected into COS-7 cells cultured in a 24-well plate using a TransIT-LT1 transfection reagent (Takara, Osaka, Japan). The cells were incubated for 48 h (longer incubation time compared to chapter 4.22 to express large number of luciferases) and then treated with a lysis buffer (E291A) (Promega, Madison, WI, USA) according to the manufacturer's protocol.

As shown as Figure 6-7, in bioluminescence, C-2 modified with organic fluorescent dyes (2-FITC-CTZ and 2-SFX-CTZ) showed extremely weak or no luminescence, while C-6 modified with same organic fluorescent dye (6-FITC-CTZ) showed comparable luminescence to native system in the combination with RLuc8.6-535. From these results, the suitability of the C-6 modification is appropriate for novel BL emission system.

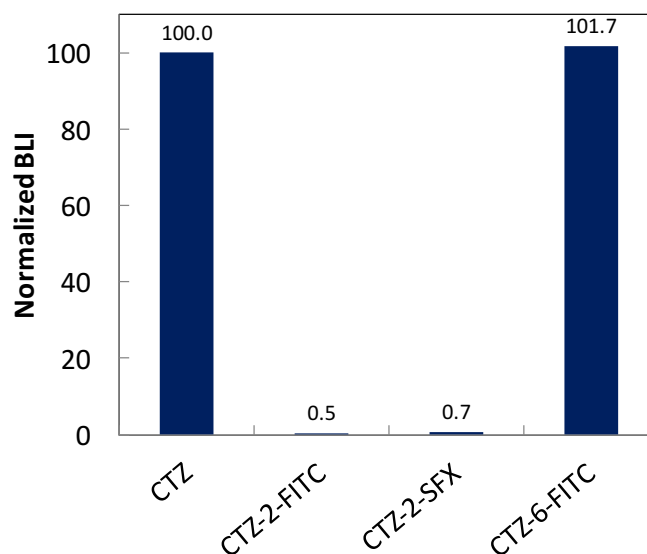


**Figure 6-7** Relative optical intensities of the synthetic CTZ derivatives in the presence of RLuc8.6-535.

## References

- (1) Shimomura, O., *Bioluminescence*, World Scientific Publishing Co. Pte. Ltd, Singapore, **2006**.
- (2) Fields, S., Interactive learning: Lessons from two hybrids over two decades. *Proteomics*, **2009**, *9*, 5209-5213.
- (3) Sun, S. H., Yang, X. B., Wang, Y., and Shen, X. H., *Int. J. Mol. Sci.*, **2016**, *17*.
- (4) Ozawa, T., Yoshimura, H., and Kim, S. B., *Anal. Chem.*, **2013**, *85*, 590-609.
- (5) Hall, M. P., Unch, J., Binkowski, B. F., Valley, M. P., Butler, B. L., Wood, M. G., Otto, P., Zimmerman, K., Vidugiris, G., Machleidt, T., Robers, M. B., Benink, H. A., Eggers, C. T., Slater, M. R., Meisenheimer, P. L., Klaubert, D. H., Fan, F., Encell, L. P., and Wood, K. V. *ACS Chem. Biol.*, **2012**, *7*, 1848-1857.
- (6) Wang, Y., Akiyama, H., Terakado, K., and Nakatsu, T., *Sci. Rep.*, **2013**, *3*.
- (7) Loening, A. M., Wu, A. M., and Gambhir, S. S., *Nat. Methods*, **2007**, *4*, 641-643.
- (8) Loening, A. M., Dragulescu-Andrasi, A., and Gambhir, S. S., *Nat. Methods*, **2010**, *7*, 5-6.
- (9) Kim, S. B., Torimura, M., and Tao, H., *Bioconjugate Chem.*, **2013**, DOI: 10.1021/bc400411h.
- (10) Kim, S. B., Nishihara, R., Citterio, D., and Suzuki, K., **2017**, *ACS Comb. Sci.*, Just Accepted.
- (11) Kim, S. B., and Izumi, H. *Biochemical and Biophysical Research Communications*, **2014**, *448*, 418-423.

- (12) Nishihara, R., Suzuki, H., Hoshino, E., Suganuma, S., Sato, M., Saitoh, T., Nishiyama, S., Iwasawa, N., Citterio, D., and Suzuki, K., **2014**, *Chem. Commun.* *51*, 391-394.
- (13) Nishihara, R., Abe, M., Nishiyama, S., Citterio, D., Suzuki, K., and Kim, S. B., **2017**, *Sci. Rep.*, *7*, 908.
- (14) Kuchimaru, T., Iwano, S., Kiyama, M., Mitsumata, S., Kadonosono, T., Niwa, H., Maki, S., and Kizaka-Kondoh, S., *Nature Communications*, 2016, *7*.
- (15) Inouye, S., and Shimomura, O., *Biochemical and Biophysical Research Communications*, **1997**, *233*, 349-353.
- (16) Shimomura, O., and Johnson, F. H., *Proc. Natl. Acad. Sci. U. S. A.*, **1975**, *72*, 1546-1549.
- (17) Lindberg, E., Mizukami, S., Ibata, K., Miyawaki, A., and Kikuchi, K., *Chem-Eur J*, **2013**, *19*, 14970-14976.
- (18) Jiang, T. Y., Yang, X. F., Yang, X. Y., Yuan, M. L., Zhang, T. C., Zhang, H. T., and Li, M. Y., *Org Biomol Chem*, **2016**, *14*, 5272-5281.
- (19) Lakowicz, J. R. *Principles of Fluorescence Spectroscopy, 3rd edition* Plenum Publishers, New York., **2006**.
- (20) Woo, J. C., Howell, M. H., and Von Arnim, A. G., *Protein Sci.*, **2008**, *17*, 725-735.
- (21) Inouye, S., Iimori, R., Sahara, Y., Hisada, S., and Hosoya, T., *Anal Biochem*, **2010**, *407*, 247-252.
- (22) Lindberg, E., Mizukami, S., Ibata, K., Fukano, T., Miyawaki, A., and Kikuchi, K. *Chem Sci*, **2013**, *4*, 4395-4400.
- (23) Tannous, B. A., Kim, D. E., Fernandez, J. L., Weissleder, R., and Breakefield, X. O., *Mol. Ther.*, **2005**, *11*, 435-443.
- (24) Dsouza, R. N., Pischel, U., and Nau, W. M. *Chem Rev*, **2011**, *111*, 7941-7980.
- (25) Sameiro, M., and Goncalves, T., *Chem Rev*, **2009**, *109*, 190-212.
- (26) Saito, R., Ohno, A., and Ito, E., *Tetrahedron*, **2010**, *66*, 583-590.
- (27) Sackett, D. L., and Wolff, J., *Anal Biochem*, **1987**, *167*, 228-234.
- (28) Sasaki, S., Mizutani, K., Kunieda, M., and Tamiaki, H., *Tetrahedron*, **2013**, *69*, 9772-9778.

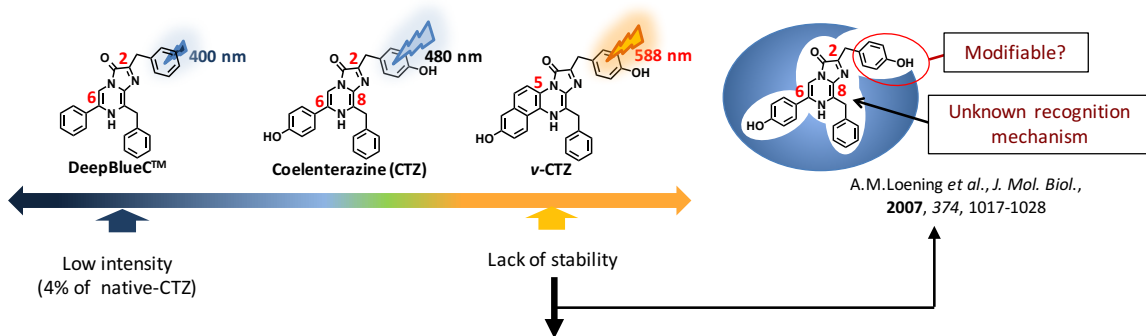
(29) Ghoneim, N. *Spectrochim Acta A*, **2000**, 56, 1003-1010.



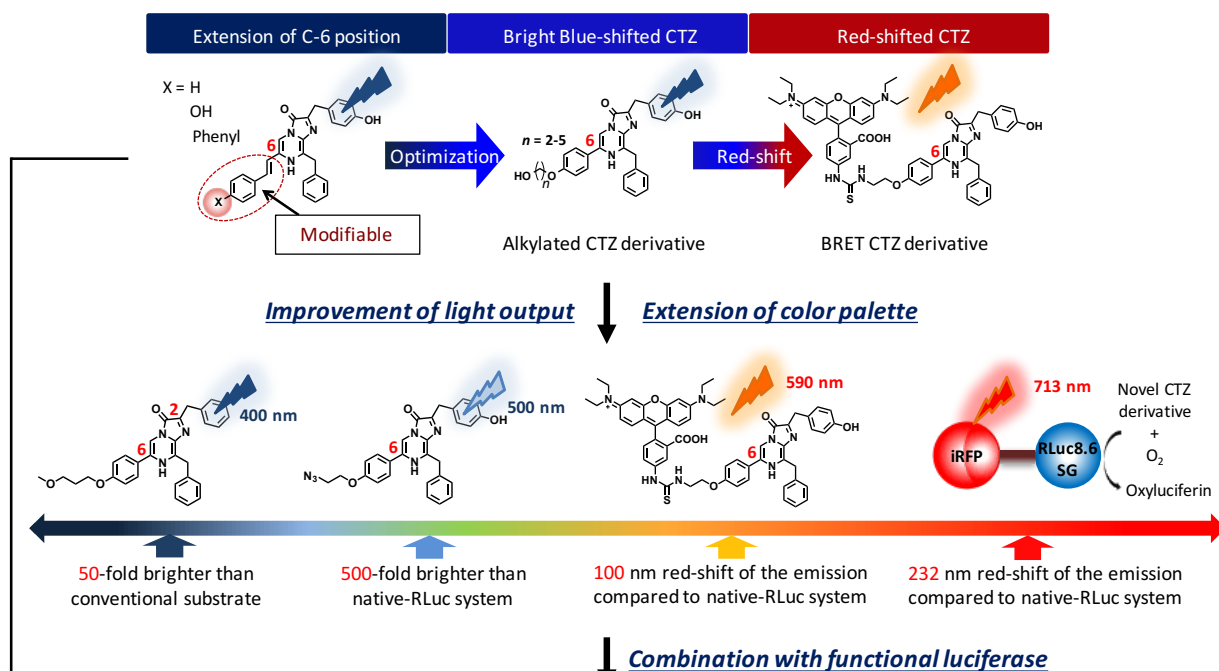
# Chapter 7

## General Conclusion and Perspective

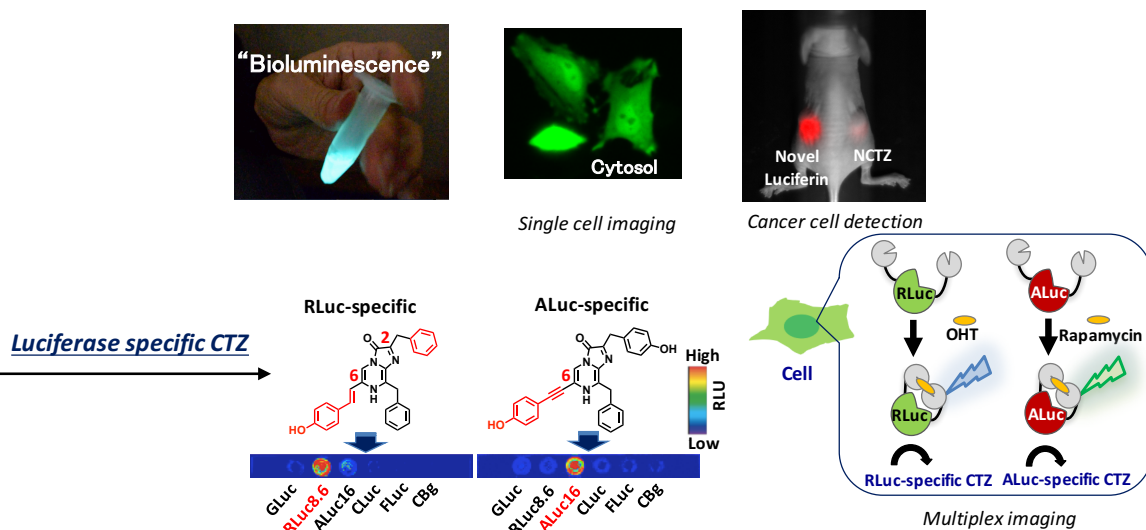
### Native-CTZ and reported CTZ derivatives



### Current work: Development of C-6 modified CTZ derivatives



### Extension of BL application



Bioluminescence is emitted by an enzymatic oxidation reaction involving a bioluminescent substrate (luciferin) and an enzyme (luciferase). Marine luciferases such as *Renilla* luciferase (RLuc) and artificial luciferase (ALuc) generate cofactor-free bioluminescence with native coelenterazine (nCTZ). There is a lot of interest in developing new CTZ derivatives. However, the design of novel CTZ derivatives resulting in enhanced optical intensity with prolonged bioluminescence is challenging, because the detailed enzymatic recognition mechanism of the RLuc/CTZ reaction is still mostly unknown. In fact, most of the reported CTZ analogues fail to emit bioluminescence, since their structural modifications prevent their enzymatic recognition. As the bioluminescence capacity of CTZ is due to its imidazopyrazinone backbone, precedent studies have focused on the effect of substitution at the C-2, C-5, C-6, and C-8 positions of the backbone. Although the substitution effect at the C-2 position on enzymatic recognition is relatively low, most of the CTZ analogues substituted at the C-2 position cannot show bioluminescence properties superior to those of native CTZ. In contrast to the C-2 position, the substitution at the C-8 position resulted in negligibly low bioluminescence in combination with RLuc. Formation of a bridge between C-5 and C-6 positions leads to more planar and rigid molecular structures and sacrifices chemical stability. Although the C-6 position is an alternative site for substitution, most of the studies have focused on the chemiluminescence properties.

In this work, I introduced the creation of efficient CTZ derivatives optimized for RLuc derivatives and ALucs, which are the most widely used marine luciferases.

To begin with, I present three types of CTZ derivatives with styryl substituents at the C-6 position. All of them show strong bioluminescence emission in combination with the Rluc8 and Rluc8.6 *renilla* luciferase variants, with brightest emission observed in the case of the 6-pi-Ph-CTZ/Rluc8.6 pair. With its 11- and 25-fold stronger emission at comparable wavelength, 6-pi-H-CTZ and 6-pi-Ph-CTZ are useful bright blue-shifted alternatives to DeepBlueC<sup>TM</sup>, which is commonly applied in BRET-based assays in combination with GFP. These results encouraged me to develop further C-6 modified CTZ derivatives.

Then, I successfully developed luciferase-specific coelenterazine analogues, which were combined with our molecular tension probes enabling very high specificity via a two-switch system that utilizes both a substrate and a bioactive small molecule. I believe this work represents breakthroughs in several key areas: 1) By specifically activating a single-target luciferase in a mixture of multiple luciferases, spectral overlap, which usually contaminates the optical signal in bioassays, is avoided; 2) I combined specific analogues with luciferases sandwiched between two proteins that undergo a protein-to-protein interaction upon the addition of a small-molecule activator. Bioluminescence was only produced in the presence of both the specific small molecule and the specific substrate; 3) I have shown that our system inhibits spectral overlap in bioassays by preventing the concurrent activation of two luciferases in the same reaction mixture; 4) My specific analogues have great potential in structural studies of luciferases with substrates bound in the active site. I believe the work represents a significant step forward in the development of high-throughput bioassays and molecular imaging *in vivo*. To the best of my knowledge, my synthesized coelenterazine analogues are the first analogues to display such high selectivity, and thus inhibit optical contamination.

Furthermore, I newly developed blue-shifted CTZ derivatives, wherein the (p-hydroxy)-phenyl group in the C-6 position was alkylated to enhance light output. As expected, the modification at the C-6 position of CTZ with a flexible alkyl chain linker elevates the turn-over rate of the substrate and results in strong bioluminescence emission. With 50-fold stronger emission at comparable wavelength, C-6 alkylated CTZ derivatives are useful bright blue-shifted alternatives to DeepBlueC™, which enable single cell analysis with high-resolution and *in vivo* imaging of cancer cells in combination with a NIR fluorescent protein (iRFP) fused RLuc8.6-535 variant.

To expand the color variation of marine-luciferases, ten novel dye-conjugated CTZ analogues were organically synthesized by bridging a series of fluorescent dyes or an azide group to the CTZ backbone. With these unique CTZ analogues, I accomplished (i) an improved optical intensity and sustainability, (ii) a greatly

biased luciferase specificity by bulkiness-driven steric hindrance, and/or (iii) red-shifted chemiluminescence/bioluminescence resonance energy transfer (C/ BRET). Especially, one of the alkylated CTZ derivatives, 6-N3-CTZ with ALuc emits approximately 500-fold brighter emission than the native RLuc bioluminescence system. As described above, the change in optical properties by luciferin modification helps expanding the application of bioluminescence imaging. Furthermore, I believe that the knowledge gained through this study is useful for the continued elucidation of the enzymatic recognition mechanism and contributes to the development of novel CTZ derivatives with superior optical properties, in particular regarding C-6 substituted derivatives, which have been mostly out of focus, so far.

Recently, optogenetic technologies are developed for use in understanding life phenomena such as nerve circuit function. However, this technique also needs an external light to excite the light-sensitive optogenetic probe. Therefore, it can be foreseen that bioluminescence phenomena are utilized as excitation light of optogenetic probes to control the life phenomena in deep physiological tissue in the future. Thus, the development of novel bioluminescent probes can accelerate other imaging technologies.

For this reason, it is also expected that the knowledge obtained through this study is of high interest to scientists in many (bio)chemistry-oriented fields such as chemical biology and others.

## List of publications

- (1) Ryo Nishihara, Hideyuki Suzuki, Emi Hoshino, Sakura Suganuma, Moritoshi Sato, Tsuyoshi Saitoh, Shigeru Nishiyama, Naoko Iwasawa, Daniel Citterio, Koji Suzuki, Bioluminescence coelenterazine derivatives with imidazopyrazinone C-6 extended substitution, *Chemical Communications*, **2015**, Vol.51, No.2, pp.391-394.
- (2) Sung Bae Kim, Simon Miller, Toshiya Senda, Ryo Nishihara, Koji Suzuki, Cation-Driven Optical Properties of Artificial Luciferases, *Analytical Sciences*, **2015**, Vol.31, pp.955-960, selected as Hot Article.
- (3) Sung Bae Kim, Ryo Nishihara, Daniel Citterio, Koji Suzuki, A Genetically Encoded Molecular Tension Probe for Tracing Protein-Protein Interactions in Mammalian Cells, *Bioconjugate Chemistry*, **2016**, Vol.27, pp.354-362.
- (4) Ryo Nishihara, Simon Miller, Masahiro Abe, Toshiya Senda, Shigeru Nishiyama, Daniel Citterio, Koji Suzuki, Sung Bae Kim, Luciferase-Specific Coelenterazine Analogues for Optical Contamination-Free Bioassays, *Scientific Reports*, **2017**, 7, 908.
- (5) Sung Bae Kim, Ryo Nishihara, Daniel Citterio, Koji Suzuki, Fabrication of New Lineage of Artificial Luciferases from Natural Luciferase Pools, *ACS Combinatorial Science*, Just Accepted.
- (6) Ryo Nishihara, Takahiro Nakajima, Eiji Yamamoto, Sung Bae Kim, Shigeru Nishiyama, Naoko Iwasawa, Daniel Citterio, Moritoshi Sato, Koji Suzuki, Blue Coelenterazine Derivatives for Highly Sensitive Bioluminescent Imaging (**Manuscript in preparation**)
- (7) Ryo Nishihara, Satoshi Kishigami, Yoshiki Kakudate, Simon Miller, Toshiya Senda, Shigeru, Nishiyama, Daniel Citterio, Koji Suzuki, Sung Bae Kim, Dye-Bridged Coelenterazine Analogues for Marine Luciferases, **submitted**.

## **Acknowledgement**

I would like to express my sincere thanks to my academic supervisor, Prof. Koji Suzuki for his continuous guidance, support and encouragement during the progress of this study. And his vast knowledge of analytical chemistry has helped me to perform this thesis.

I would like to acknowledge Prof. Yasuaki Einaga and Prof. Yukari Fujimoto for their constructive suggestions and careful reviewing of this dissertation.

I would like to thank Prof. Daniel Citterio for his kind assistance, encouragement and advice throughout the present work. I would like to thank Prof. Shigeru Nishiyama and Dr. Naoko Iwasawa for valuable advice concerning organic synthesis.

I especially appreciate Dr. Sung-Bae Kim, Dr. Takahiro Nakajima and Prof. Moritoshi Sato for their enormous efforts in this bioluminescence study. Without their dedicated assistance and effort, this study could have never been achieved.

I also appreciate Ms. Emi Hoshino, Mr. Yoshiki Kakudate, Mr. Masahiro Abe, Mr. Yuma Ikeda, Mr. Masanobu Tanaka, Mr. Satoshi Kishigami and Ms. Nanako Nomura for their dedicated assistance and effort during their tough research. I am looking forward to the publication of their works in the future.

I am indebted to the Research Fellowship of the Japan Society for the Promotion of Science for Young Scientists for its full support of my academic activity.

Finally, I would like to thank my family for their kind support and understanding.